ARCHITECTURAL ELEMENT ANALYSIS OF GLACIATED TERRAINS

ARCHITECTURAL ELEMENT ANALYSIS OF GLACIATED TERRAINS

By

JESSICA MARIE SLOMKA, B.Sc. (Hons), M.Sc.

A Thesis

Submitted to the School of Graduate Studies

in Partial Fulfillment of the Requirements

for the Degree

Doctor of Philosophy

McMaster University

Doctor of Philosophy (2014) McMaster University

(Geography and Earth Sciences) Hamilton, Ontario, Canada

TITLE: **ARCHITECTURAL ELEMENT ANALYSIS OF GLACIATED TERRAINS**

AUTHOR: Jessica Marie Slomka B.Sc. (Hons.)

(McMaster University, Hamilton, 2009)

M.Sc.

(McMaster University, Hamilton, 2011)

SUPERVISOR: Professor Dr. Carolyn H. Eyles

NUMBER OF PAGES: xviii, 347

ABSTRACT

This thesis investigates how architectural element analysis (AE) can be utilized to deconstruct the sedimentary architecture of glacial sedimentary successions, and its significance for paleoenvironmental reconstruction, understanding depositional histories, and providing insight to the hydrostratigraphy of glaciated terrains. The first component of this thesis explores the applicability of AEA to the local-scale analysis of a till succession exposed in outcrop sections in order to understand the significance of the bounding surface hierarchy and architectural elements in sediments deposited in a subglacial depositional environment. Fieldwork was conducted at two outcrop sites in north-central Illinois, U.S.A., which expose Late Wisconsin-age till of the Tiskilwa Formation, in order to test the local-scale applicability of AEA to the architectural analysis of a subglacial succession (Chapter 2). A major finding of this study was that fifth-order bounding surfaces delineate ‘element associations’ which can be mapped across the local study area, and utilized for detailed paleoenvironmental reconstruction of the ‘subglacial bed mosaic’ and local-scale reconstruction of the depositional history of the till sheet, including periods of separation and reattachment of the ice and its bed.

The second part of this research explores AEA at Sólheimajökull (Iceland), specifically to test the validity of AEA for the analysis of glacial successions, and to better understand the environmental significance of unit contacts (bounding surfaces) and sedimentary geometries in a modern glacial landscape. Fieldwork was conducted at Sólheimajökull and basic principles of AEA and landsystems analysis were integrated in

order to facilitate delineation of the sedimentary architecture and allostratigraphy of the Sólheimajökull landsystem (Chapter 3). Fifth-order surfaces delineate landsystem tract components, which can be utilized to characterize the heterogeneity and sedimentary architecture, delineate allostratigraphic units, and reconstruct the depositional history of the Sólheimajökull landsystem.

Data from Sólheimajökull (Chapter 3) and Illinois (Chapter 2) were utilized as a modern and outcrop analogue, respectively, to provide insight to the sedimentary architecture of subsurface Quaternary glacial deposits in Georgetown, southern Ontario (Canada; Chapter 4). Basic concepts of AEA were applied to the analysis of sediments recovered from fully-cored boreholes. A major finding of this study is that AEA can be effectively utilized for delineation of subsurface architectures from the analysis of core, and the hierarchies of bounding surfaces and units of AEA can be utilized to organize the sedimentary heterogeneity into a 'nested' architectural framework. The geometry and spatial relationship of architectural units (sixth-order surfaces) and architectural components (fifth-order surfaces) provides insight to the hydrostratigraphy of Georgetown.

AEA, as utilized in this thesis, provides a systematic methodology with which to deconstruct glacial successions into their basic architectural building blocks at various scales of resolution. AEA enhances traditional facies models by facilitating site-specific delineation, visualization, and characterisation of the sedimentary geometry of facies associations, which in turn, allows direct comparison of sedimentary architectures at different study sites; this has significant implications for analogue selection for the purpose of reservoir analysis. The architectural framework of glacial deposits and its potential significance to hydrostratigraphic models (as discussed in this thesis) may help to facilitate communication and translation of data between the disciplines of ‘geology’ and ‘hydrogeology’. The results of this project can be utilized as a framework to better understand the sedimentary geometry and hydrostratigraphy of modern and Quaternary glacial deposits in southern Ontario, previously glaciated terrains elsewhere, and other modern glacial landsystems, and provide insight into other applications such as civial engineering projects, aggregate resources, placer mining exploration, and land use planning.

TABLE OF CONTENTS

ACKNOWLEDGEMENTS

This thesis could not have been possible without the collaboration, assistance, insight, and generosity offered by many different people. The 'kick off' point of this research was the Georgetown project, and so I first thank Tim Lotimer and the Region of Halton (including Tom Renic and Jon Clark) for reaching out to my supervisor and lab group to be part of this project, always being so supportive of our work, and providing funding. Ever since my undergraduate thesis work, Tim Lotimer has been a true mentor, great teacher, and provided invaluable insight into 'real-world' applications of scientific problems (always asking 'OK, so why should we care?'). This project provided me with many exciting new experiences, three thesis projects, and the opportunity to collaborate with different students and professionals including Steve Davies (AECOM) and Steve Usher and John Gordon (SLR Consulting), who were extremely helpful and generous with providing data and core storage. Core logging was made very comfortable, convenient, and enjoyable with the help of the MacCormack family (Kelsey and Mike), who graciously offered their family garage as a core storage and logging facility, provided lemonade (Tyler), showed me how to drive a tractor (Carter), and taught me how to properly jump off a diving board (Ashley).

I want to thank my McMaster family, the Glacial Sedimentology Lab (BSB 312), for all of those hot, humid, long, buggy, extremely dry, extremely wet, sandy boots, muddy everything field days. I especially thank Rodrigo Narro, Prateek Gupta, and Riley Mulligan for providing field assistance, and although they earned the Rubber Hammer award (you're welcome), this research would not have been possible without their help, hard work, and support. I am indebted to Riley Mulligan for providing countless hours of help in the field, driving and flying all over the place to reach field sites, insightful and helpful discussion, and a sort of 'side-kick' in any lab-related activity, from iSci-ing to IBA-ing. I want to thank our newest Glacial Lab member, Leslea Lotimer, for helping me sort out the tills, having great discussions and lots of laughs (tickle breaks!), and sharing a great friendship.

I would like to thank Dr. Helgi Björnsson (University of Iceland) for deciding to approach me one day as I was fervently sketching channels and bars at Sólheimajökull, and asked me what I was doing. Thank you, Helgi, for inviting us to visit you at the University, and for welcoming us with open arms (and thanks to your graduate students for offering us cake and coffee!). I would like to thank the people of Iceland for being so welcoming and accommodating (including the mechanic that we called on Saturday morning at his house!), and I am truly grateful for the experience of conducting research in their beautiful country. I must also give thanks to Café Sólheimajökull for providing first-hand accounts of changes at the ice margin and jökulhaups, hot coffee when it was needed the most, and running water (i.e. bathroom). The Iceland work was greatly enhanced by the LiDAR imagery provided by the University of Iceland, assistance with ArcScene provided by Jay Brodeur, and MobileMapper equipment organized by Pat DeLuca (I'm sorry the charger was lost in a crevasse but based on the rate of ice marginal retreat, I expect it to be recovered in about 2 years!). Thank you to Riley Mulligan and my brother, Andrew, for having incredible patience and being great field assistants.

The Illinois work would not have been possible without the support and enthusiasm of Don McKay, Dick Berg, and Olivier Caron at the Illinois State Geological Survey, who provided financial support for our work and brute force with shoveling and climbing outcrop in the hottest weather. Thank you for teaching me (through experience) to never again attempt to do field work in Illinois in July, and for opening up my eyes to Illinois cuisine (Greek, Chinese, Mexican, Barbeque!). I am truly grateful for your kindness and hospitality, open-mindedness and willingness to explore different approaches, and providing such an enjoyable and rewarding experience.

My committee (Tim Lotimer, Dr. Joe Boyce, and Dr. Jim Smith) provided encouragement, advice, and mentorship along the way, and I am truly appreciative of their help and involvement. I would like to thank Dr. Andrew Miall for taking the time to review my final thesis as an external examiner and providing kind and helpful comments, and for a lifetime of innovative and inspiring work, part of which this thesis is based. I must thank all the sources funding for this work, including my supervisor, Dr. Carolyn H. Eyles, *Halton Region, Illinois State Geological Survey, McMaster Graduate Studies, Canadian Quaternary Association, Ontario Graduate Scholarship program, Natural Sciences and Engineering Research Council, and the Geological Society of America. I would also like to thank the Alberta Energy Regulator for being so supportive and understanding as I completed the final stages of this thesis.*

To my husband, Kevin Elmer, thank you for your patience and understanding throughout my graduate work, putting up with stacks of papers on every surface in our apartment, courageously climbing outcrop and being scale for photos, driving hours to visit me, and joining the army so I could actually finish my thesis! To my family, thank you for encouraging my rock collection and Lowville park adventures when I was young, embracing my rock talk, muddy shovels, drives to airports (drives everywhere), the Friday morning 'J. Slomka' breakfast club, laundry facilities, sacrificing the dining room table (look, this is what I've been doing on the computer all these years!), and fully supporting me in everything that I do. Joey and Andrew, thank you for trying to explain to other people what I do ('look at dirt') and helping me move furniture here and there. I am incredibly fortunate and grateful to have amazing friends in my life, who are true inspirations and have enriched my life immensely. I especially thank Natalie Szponar, Laura Wright, Tori Madejski, Steph Nardilli, Tara MacBournie, Leslea Lotimer, Aaron Mickle, Sarah Dickin, and Sanya Rana for giving me much needed breaks, great laughs, good times, all those wonderful coffees, and a social life to keep me sane and get me out of my own head from time to time!

My academic career and success is, without a doubt, owed to my supervisor, Dr. Carolyn H. Eyles. Carolyn, you opened my eyes to the world and awakened my love of Earth Science right from your first year course 1G03. You are a true teacher and friend, and have always believed in me and encouraged me to be innovative, creative, and thorough in my work, and pushed me to mine data for all its worth, look at things from new perspectives, consider all options and possibilities, question everything, have confidence to put myself out there, and collaborate with others. You have been an incredible mentor, and strive to foster the culture of a 'family' in our lab (proud of our strengths and patient with our shortcomings), which I am so grateful to have experienced. You have been an insirping role model to me, as someone I will always try to live up to (even though I know I will never quite match…there's only one Carolyn!). Words cannot express the immense gratitude I have for all the teaching opportunities, conferences, field experiences, celebrations, support of all types, and invaluable advice that you have given me. I am so incredibly fortunate and thankful to have crossed paths with you (and early on I decided to linger for a while…7 years!). I can say with certainty that you were the 'tipping point' of my adult life and the catalyst that set me on the incredible journey I am now on, for which I am forever grateful.

Sincerely,

JSlomka

Jess

September 2014

LIST OF FIGURES AND TABLES

CHAPTER 1: INTRODUCTION

Architectural element analysis (AEA) is an emerging methodology in the fields of sedimentology and stratigraphy, and is recognised as a powerful tool for the analysis of fluvial and deep-marine deposits (Miall, 1996; 2010; 2014). AEA provides a tool to systematically delineate sedimentary geometries at different scales of resolution, based on careful analysis of facies associations and facies contacts, which allows paleoenvironmental reconstruction at local and regional scales. AEA is based on earlier ideas relating to bedform hierarchies (Allen, 1968), the geometry of facies contacts (Allen, 1963), and an understanding of the components of fluvial systems, including their geometry and allo- and autogenic controls (Beerbower, 1964; Allen, 1983). AEA advances traditional facies models (e.g. James and Dalrymple, 2010) by integrating the above mentioned concepts to facilitate delineation and characterization of the 2- and 3-dimensional sedimentary architecture of a depositional system. AEA has been utilized and modified to describe and interpret the sedimentary geometry of deposits formed in fluvial (Allen, 1983; Miall, 1985, 1988, 1994; Hjellbakk, 1997; Miall and Jones, 2003; Opluštil et al., 2005; Yangquan et al., 2005; Best et al., 2006; Kostic and Aigner, 2007; Ghazi and Mountney, 2009; Slomka and Eyles, 2013), shallow marine (Yuvaraj, 2011), deep marine (Miall, 1989; Clark and Pickering, 1996; Drinkwater and Pickering, 2001; Labourdette and Jones, 2007; Pyles et al., 2007, 2008; Hubbard et al., 2008; Funk et al., 2012; Terlaky et al., *accepted manuscript*), deltaic (Eriksson et al. 1995), jökulhlaup (Marren et al., 2009), and subglacial (Boyce and Eyles, 2000) depositional environments. AEA has also been applied to the analysis of sediments recovered from boreholes and integrated with geophysical (Hornung and Aigner, 1999; Boyce and Eyles, 2000; Heinz and Aigner, 2003; Bersezio et al., 2007) and hydrogeological (Gerber et al., 2001) data, and utilized for computer-based modeling (Dreyer et al., 1993; Deutsch and Tran, 2002). It should be noted here that several studies make use of the terms '*architectural element*', *'depositional element'*, and *'element hierarchies'*, and do so either without the intention of implying the use of AEA or, more commonly, by utilizing concepts of AEA but neglecting to demonstrate the fundamental principles of AEA, such as the delineation of a bounding surface hierarchy and systematic characterization of the geometry of facies associations (Miall 1985; 1988).

1.1 INTRODUCTION TO AEA

A rudimentary form of AEA was introduced by Allen (1983) for the analysis of braided river sandstones of the Brownstones exposed in outcrop sections in Wales, and Miall (1985; 1988) refined AEA as a systematic methodology to characterize the sedimentary architecture of fluvial deposits and interpret their depositional history. Prior to the introduction and more widespread utilization of AEA, detailed analyses of sedimentary successions were based on end member vertical profiles and facies models (e.g. Miall, 1977; Eyles et al., 1985; McPherson et al., 1987; Shanmugam and Moiola, 1988), and quantitative prediction of facies successions was tested using a Markov Chain approach (e.g. Miall, 1973). Facies models are advantageous for understanding the suite of facies types and depositional processes associated with a particular depositional environment; however, end member facies models do not represent all the natural spatiotemporal variability in facies types and depositional and erosional processes in a depositional environment, which makes direct comparison of site-specific sedimentary successions difficult (Dalrymple, 2010). Comparison of the sedimentary architecture recorded from different local study sites is important for interpretation and paleoenvironmental reconstruction of a regional-scale study area (see Chapter 4, this thesis), characterization and identification of appropriate outcrop analogues for the interpretation of deeper subsurface deposits (e.g. Dreyer et al., 1993), and to inform and enhance existing facies models and establish new facies models for depositional settings that warrant distinction from existing generalized models (Dalrymple, 2010).

The fundamental principle of AEA is the bounding surface hierarchy, which serves to define the framework of a sedimentary deposit. Bounding surfaces, as utilized in AEA, are facies contacts that can be delineated from outcrop, and assigned a numerical order based on the degree of environmental change recorded by that surface (Miall, 1988; 2010). Bounding surfaces record environmental change at various scales of resolution, such as the supply of sand grains to a ripple crest preserved as a foreset (delineated by a zeroth-order surface that may record diurnal fluctuations in current energy) or a major climatic change such as the onset of glaciation (delineated by a seventh-order surface that may record a major unconformity between glacial basin fill and bedrock; Miall, 1988; Boyce and Eyles, 2000). The bounding surface hierarchy defines the geometry of time-stratigraphic facies packages at different scales of resolution, which allows optimization of sedimentary complexity at a local scale while maintaining the ‘big picture’ geologic framework. In abstract terms, the bounding surface hierarchy of AEA is loosely analogous to the frame of a house, in which rooms are defined and other building materials are anchored. The composition (facies types) and dimensions (geometry) of building materials used to construct different houses (sedimentary deposits) may be similar, but the orientation and arrangement of the materials, and the abundance of certain building materials over others, gives each room and house a unique *architecture*. Delineation and characterization of the architecture of a sedimentary deposit at different scales of resolution is the main objective of AEA.

The underlying roots of AEA can be traced to the early stages of the classification of types of bedforms, bedding contacts, and cross-stratification in fluvial deposits (McKee and Weir, 1953; Allen, 1963, 1968), the development of facies and facies models (Miall, 1977; Dalrymple, 2010), and the characterization of features comprising alluvial depositional environments (Beerbower, 1964; Allen, 1983). A comprehensive review of the underlying ideas and concepts of AEA would unduly lengthen this thesis (see Miall, 1985, 1996); however, it is appropriate to include a brief discussion on the specific advances in sedimentology and stratigraphy which influenced and directly contributed to the development of AEA.

1.1.1 Foundational concepts of AEA

The fundamental components of AEA include the description and interpretation of facies types and associations, delineation of a bounding surface hierarchy, and characterization of the ‘building blocks’ of a sedimentary deposit (facies associations with a characteristic geometry); all of which are derived from important pioneer studies of depositional processes and environments.

An early descriptive classification scheme of sedimentary stratification was proposed by McKee and Weir (1953), which emphasizes the geometry, scale, and internal structure of stratified units and the nature of set bounding surfaces (Fig. 1.1). The most significant contribution of this classification scheme to AEA is recognition of the variability in the nature and geometry of the lower bounding surface (e.g. erosional and non-erosional, curved/trough and planar) and the geometry of layered sedimentary deposits (e.g. lenticular, tabular, wedge-shaped; Fig 1.1.; McKee and Weir 1953). A revised classification scheme of cross-stratification was later proposed by Allen (1963), which emphasizes the utilization of objective, descriptive terminology for the classification of cross-stratification and its relationship to the lower set or coset bounding surface (Fig. 1.2). The descriptors used to classify cross-stratification were combined in different ways and resulted in fifteen different architectures of cross-stratification (Fig. 1.3A), which can be utilized for paleoenvironmental interpretation (Fig. 1.3B; Allen, 1963). Allen (1963)'s classification scheme expands on earlier ideas put forth by McKee and Weir (1953), and emphasises the significance of the scale (e.g. cross stratification within ripples versus dunes), unit complexity (grouping, lithology, and shape), and paleoenvironmental significance of cross-stratification architecture. Utilization of sedimentary architecture (i.e. scale and unit complexity) for paleoenvironmental reconstruction is a key component of AEA.

1.1.1.1 Hierarchies

The concept of '*hierarchy*' is a recurring theme in AEA, including a hierarchy of internal sedimentary components of a depositional system (relating to their scale; e.g. range of bedforms in a fluvial system), bounding surfaces (relating to the degree of environmental

Fig. 1.1 Classification scheme of stratification of McKee and Weir (1953). A. Classification of stratified units. B. Classification of cross-stratified units. C. Cartoon of cross-stratified units in B (modified from McKee and Weir, 1953).

A

Character of lower surface of stratified unit	Apparent shape of stratified unit	Internal (primary) structure of stratified unit
erosional	lenticular wedge-shaped	structureless irregular
nonerosional	tabular irregular	ripple-laminated horizontally stratified cross-stratified

B

Basic criterion	**Subordinate criterion**					
Set of cross-strata				***Cross-strata***		
Character of lower bounding surface	**Shape**	**Attitude of axis**	**Symmetry**	**Arching**	**Dip**	**Length**
nonerosional surfaces (simple cross-stratification)	lenticular	plunging	symmetric	concave	high angle (>20 degrees)	small scale (tens of cm)
planar surfaces of erosion (planar cross-stratification)	tabular	nonplunging	asymmetric	straight		medium scale (tens of cm to 6 m)
curved surfaces of erosion (trough cross-stratification)	wedge-shaped			convex	low angle (<20 degrees)	large scale (>6 m)

C

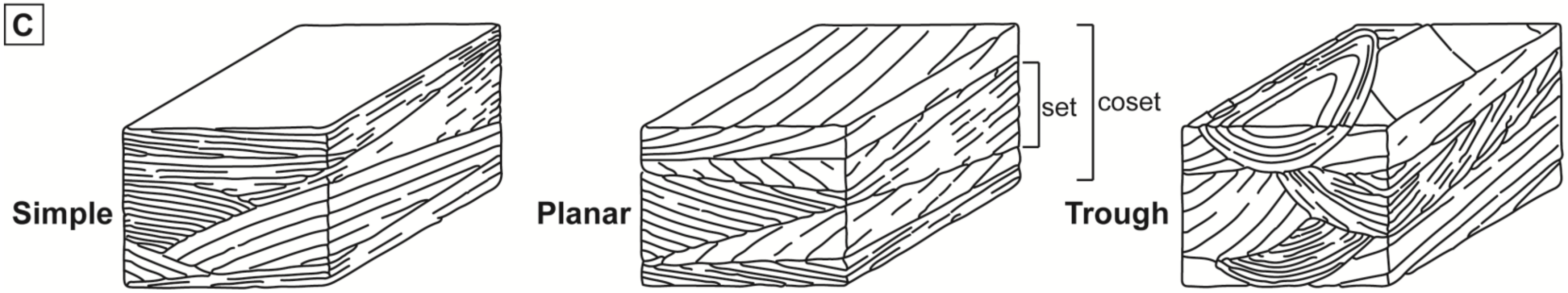

Fig. 1.2 Classification scheme of cross-stratification of Allen (1963). A. Cartoons illustrating descriptive criteria for classifying cross-stratification. B. Relationship of descriptive criteria utilized for the classification of cross-stratification (modified from Allen, 1963).

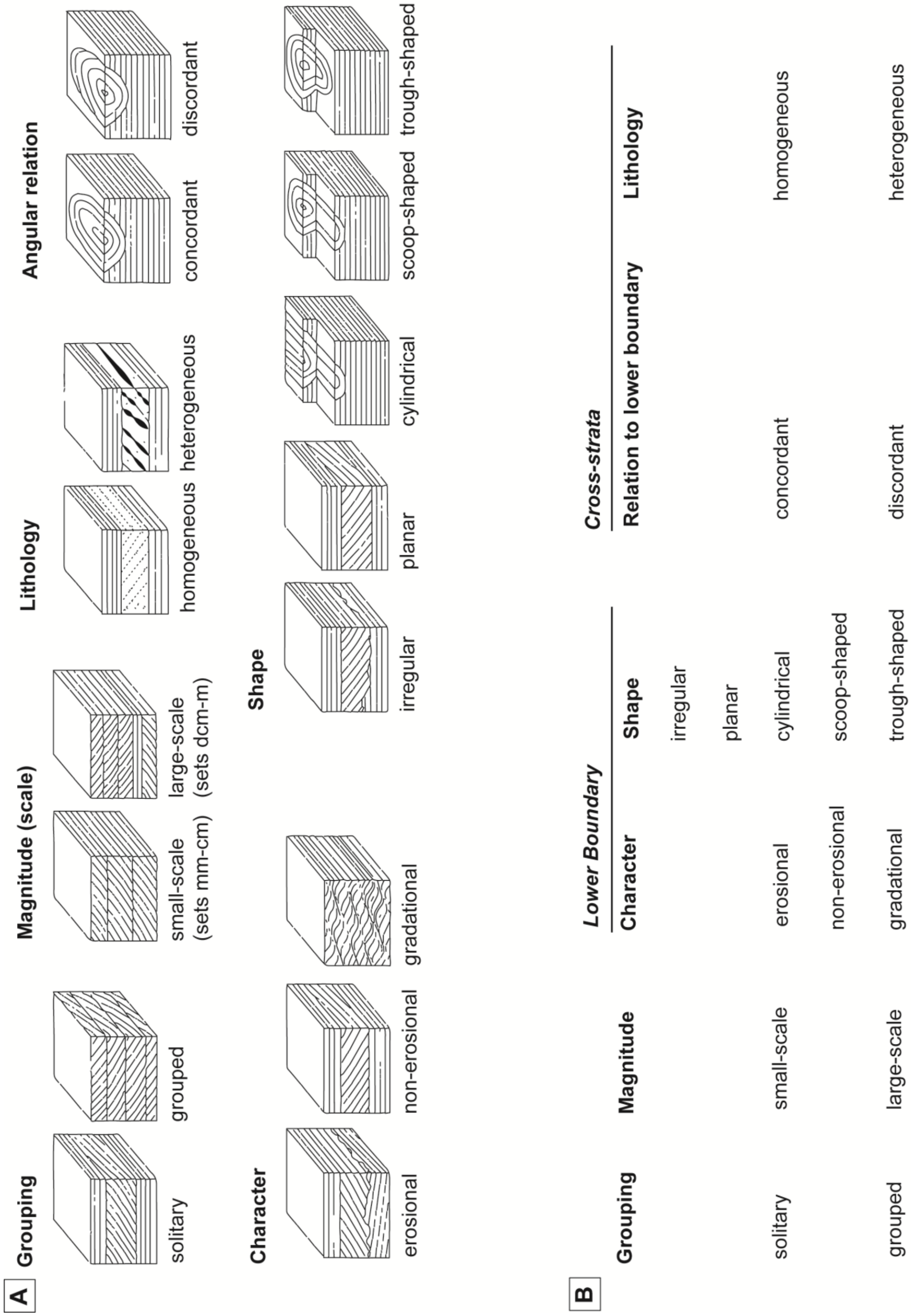
A
Grouping
solitary
grouped
Magnitude (scale)
small-scale
(sets mm-cm)
large-scale
(sets dcm-m)
Lithology
homogeneous
heterogeneous
Angular relation
concordant
discordant
Character
erosional
non-erosional
gradational
Shape
irregular
planar
cylindrical
scoop-shaped
trough-shaped
B
Lower Boundary
Cross-strata
Grouping
Magnitude
Character
Shape
Relation to lower boundary
Lithology
irregular
planar
solitary
small-scale
erosional
cylindrical
concordant
homogeneous
non-erosional
scoop-shaped
grouped
large-scale
gradational
trough-shaped
discordant
heterogeneous

Fig. 1.3 Types of cross-stratification by Allen (1963). A. Cartoons representing types of cross-stratification. B. Genetic interpretation and relative assemblages of types of cross-stratification (modified from Allen, 1963).

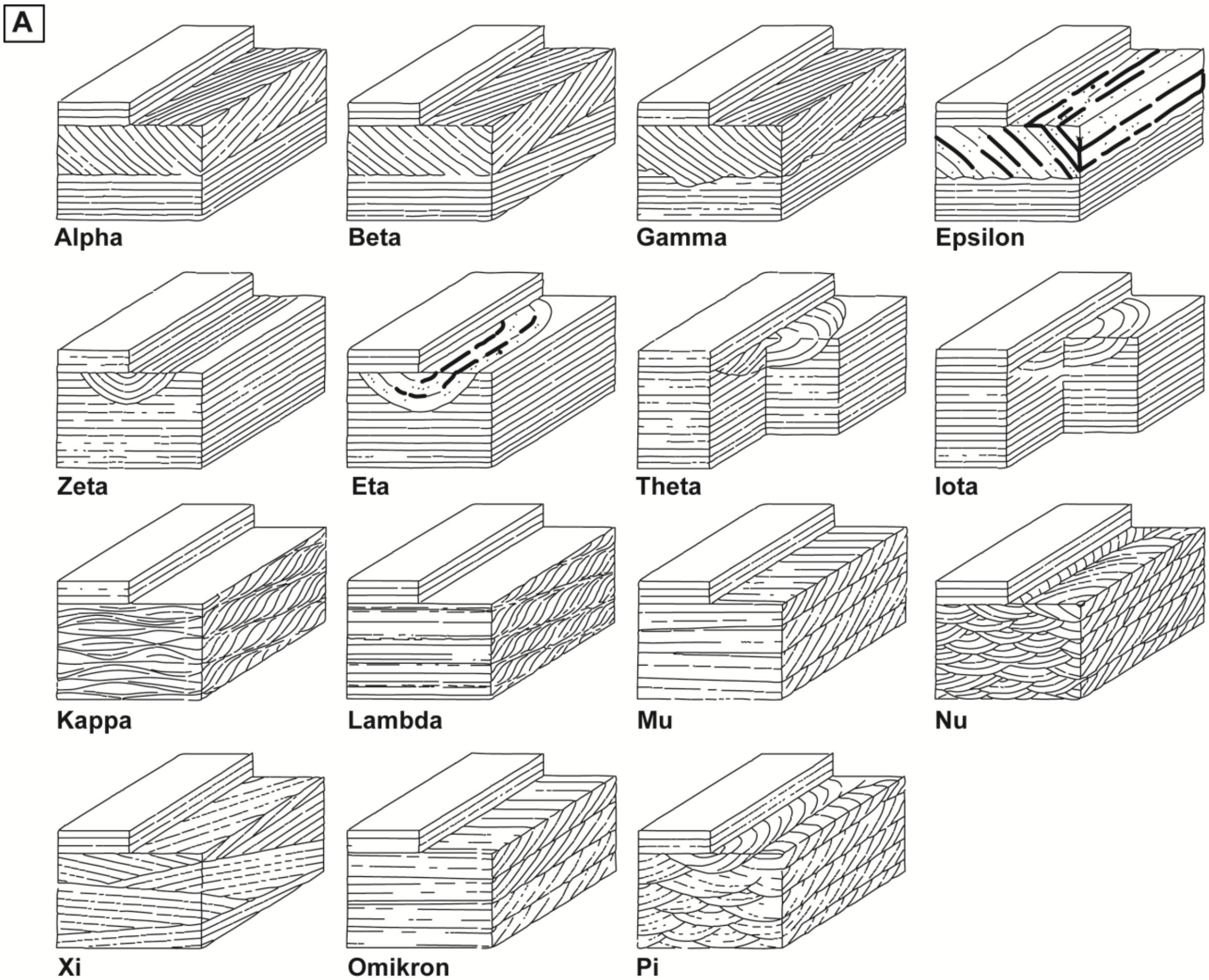

B

	Group I	Group II	Group III	
Description	solitary mostly large-scale planar or irregular surfaces *Interpretation:* migration (subaqeuous or aeolian) of solitary banks with curving or linear fronts that are commonly slip-off faces	solitary mostly large-scale filling lows in the form of cylinders, scoops, or troughs *Interpretation:* cutting and filling of isolated channels, pits, or hollows. Cutting and filling may or may not be simultaneous.	grouped small- or large-scale *Interpretation:* migration of trains of different forms of small- or large-scale asymmetrical ripple marks, depending on the size and shape of the sets forming the coset.	
Types	Alpha Beta Gamma Epsilon Xi	Zeta Eta Theta Iota	Small-scale: Kappa Lambda Mu Nu	Large-scale: Omikron Pi

change), and sedimentary units (relating to their scale, length of time they record, and degree of environmental change they represent; e.g. a single bedform in a channel versus a valley fill succession; Miall 1985; Miall 2010).

Hierarchy relating to bedforms

Allen (1968) identified a hierarchy of bedforms in the fluvial environment based on the flow energy, flow depth, and sediment availability at the time of their formation (Fig. 1.4). Although Allen (1968)'s hierarchy relates directly to sediments of fluvial origin, a brief but important comment regarding 'bedform hierarchy' was made by Allen (1968), stating,

> "the conceptions embodied in this definition can also be extended, with but little extra effort, to sand accumulations shaped by wind in the desert and to the wholly erosional flutings and groovings of cohesive mud, ice and rock beds." (Allen 1963, pg. 162).

Allen (1968) recognized the applicability of bedform hierarchies to sediments deposited in a range of depositional environments, and related the development of the bedform hierarchy to the scale of the depositional system and autogenic controls (such as grain size, flow velocity, and geometry of instabilities between the fluid and bed). The magnitude and types of external and internal controls acting on the fluvial system were hypothesized to result in different assemblages of bedforms (Fig. 1.4C). Wilson (1972) identified a bedform hierarchy of aeolian sand deposits, termed 'aeolian bedform elements', and ranked the bedforms from 1st- to 4th-order (loosely based on the fluvial bedform hierarchy of Allen, 1968; Figs. 1.4A, 1.5A). The hierarchical order of aeolian bedform elements is consistent with the scale and genetic interpretation of the bedform

(Fig. 1.5A). Friend et al. (1979) expanded the concept to include a bedform assemblage through the grouping of bedforms into sand bodies with a specific external geometry, comprising sheet and ribbon (including simple and complex or multi-storey forms). Identification of an assemblage of superimposed bedforms of various scales, with a characteristic external geometry, and formed under different environmental conditions, forms the basis of AEA (Allen, 1983).

Hierarchy relating to bounding surfaces

A hierarchical classification not only applies to the physical scale of bedforms and elements of a depositional system, but also to bounding surfaces separating sedimentary units of different types and scales. The delineation of a bounding surface hierarchy is the foundation of AEA (Miall, 1988). Brookfield (1977) identified a bounding surface hierarchy (based on Wilson, 1972) consisting of 1st- to 3rd- order surfaces in modern and ancient aeolian sand units (Fig. 1.5B), whereby bounding surfaces of various scales are generated by the superimposition of aeolian bedforms, and represent various degrees of environmental change. For example, 3rd-order surfaces delineate cross-stratified sets and represent local changes in wind direction and velocity, and 1st-order surfaces cross-cut lower-order surfaces and record the migration of draas (Brookfield, 1977). Sequence stratigraphy, which was introduced by Exxon in the same year as Brookfield (1977)'s paper on aeolian bounding surfaces, relies strongly on the identification and delineation of bounding surfaces of various degrees of environmental significance separating sedimentary units (Vail et al., 1977); however, the primary objective of sequence stratigraphy is to understand the control of sea level change on large-scale basin-fill successions in order to predict lithologies and to delineate the continuity and geometry of sand bodies (primarily for hydrocarbon exploration purposes). Sequence stratigraphy does not require the hierarchical ranking of bounding surfaces at various scales (local to regional) which is a fundamental component of AEA (Miall, 1988; Bhattacharya and Posamentier, 1994).

Hierarchy relating to sedimentary units

AEA uses hierarchies of bedforms and bounding surfaces, their form, and their genetic interpretation, as the basis for paleoenvironmental reconstruction; hence, a hierarchy is also utilized to characterize the degree of environmental change resulting in different assemblages of bedforms and bounding surfaces. The degree of environmental change is recorded by sedimentary units and bounding surfaces of different physical scale which likely formed over different temporal scales, from facies (small-scale sediment packages; first- to third-order surfaces), facies associations (‘architectural elements’; fourth-order surfaces), large-scale channel fill (fifth-order), and valley and basin fill (sixth- and seventh-order; Miall, 1985). Beerbower (1964) identified and classified five main ‘environmental elements’ of the fluvial depositional system, including a channel, abandoned channel, crevasse, levee, and floodplain. According to Beerbower (1964), different types and magnitudes of external (‘allocyclic’; e.g. subsidence, compaction, topography, slope, discharge, and load) and internal (‘autocyclic’; e.g. diversion, crevasse, neck and chute cutoff, and meander migration) controls acting on an alluvial depositional system influence the type, geometry, lithologic composition, and lithologic cycles (e.g. cyclothems) of environmental elements (Beerbower, 1964). The ‘environmental element’ is a crude precursor to the ‘architectural element’ of AEA (Allen 1983; Miall 1985).

Arguably the most important advance in sedimentology during the 20th century was the advent of the concept of facies and facies models (Miall 1977; Walker, 1984, 1990; Eyles et al. 1985; James and Dalrymple, 2010), as this has contributed significantly to the description, classification, and interpretation of sedimentary deposits, and understanding of the depositional processes that formed them. Although facies models provide a summary of facies and processes in a given depositional environment, they do not provide the flexibility required to capture the variability in facies types and associations, the geometry of deposits, and range of depositional processes at a specific study site at various spatial scales, which makes direct comparison between study areas, difficult. Facies codes, first developed for the description of fluvial sediments (Miall, 1977) and types of diamict (Eyles et al., 1983; Fig. 1.6), provide sedimentologists with a tool for standardized, objective facies classification, which, accompanied by site-specific detailed facies descriptions and a facies model, allows detailed paleoenvironmental analysis and objective comparison to other study areas. The diamict facies code developed by Eyles et al. (1983) includes careful description of diamict facies contacts and provides glacial sedimentologists with a powerful tool to describe, identify, and interpret diamicts deposited by in different depositional environments (e.g. subglacial versus glaciolacustrine).

Fig. 1.4 Bedform hierarchy and assemblages of Allen (1968). A. Bedforms generated under different flow velocities (modified from Allen, 1968; Ashley, 1990). B. Bedform hierarchy relationship to flow depth (modified from Allen, 1968). C. Bedform hierarchy assemblages formed under different depositional conditions (modified from Allen, 1968).

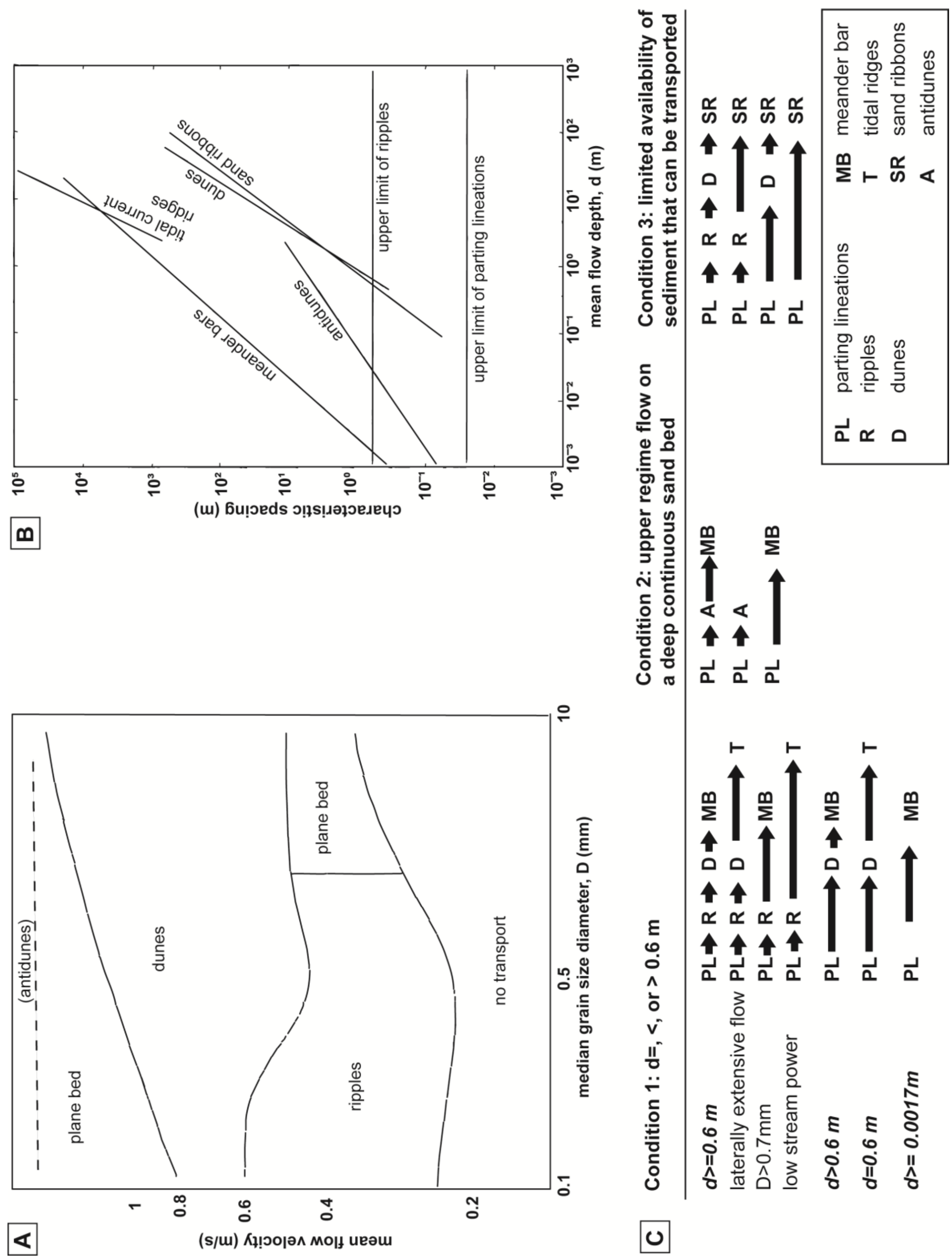
A
mean flow velocity (m/s)
median grain size diameter, D (mm)
(antidunes)
plane bed
dunes
ripples
plane bed
no transport
B
characteristic spacing (m)
mean flow depth, d (m)
sand ribbons
dunes
tidal current ridges
meander bars
antidunes
upper limit of ripples
upper limit of parting lineations
C
Condition 1: d=, <, or > 0.6 m
Condition 2: upper regime flow on a deep continuous sand bed
Condition 3: limited availability of sediment that can be transported
d>=0.6 m
laterally extensive flow
D>0.7mm
low stream power
d>0.6 m
d=0.6 m
d>= 0.0017m
PL parting lineations
R ripples
D dunes
MB meander bar
T tidal ridges
SR sand ribbons
A antidunes

Fig. 1.5 Bedform and bounding surface hierarchy in aeolian deposits. A. Hierarchy and genetic origin of aeolian bedforms (modified from Wilson, 1972). B. Hierarchy of bounding surfaces in aeolian deposits exposed in outcrop (modified from Brookfield, 1977).

A

Order	Wavelength	Height	Orientation	Possible origin	Suggested name
1st	300-5500 m	20-450 m	longitudinal or transverse	primary aerodynamic instability	draas
2nd	3-600 m	10 cm-100 m	longitudinal or transverse	primary aerodynamic instability	dunes
3rd	0.15-2.5 m	0.2-5 cm	longitudinal or transverse	primary aerodynamic instability	aerodynamic ripples
4th	0.5 cm-20 m	0.05 cm-1 m	transverse	impact mechanism	impact ripples
	1 cm-30 m	0.05 cm-1 m	longitudinal	secondary Taylor-Görtler vortices	secondary ripple sinuosity

B

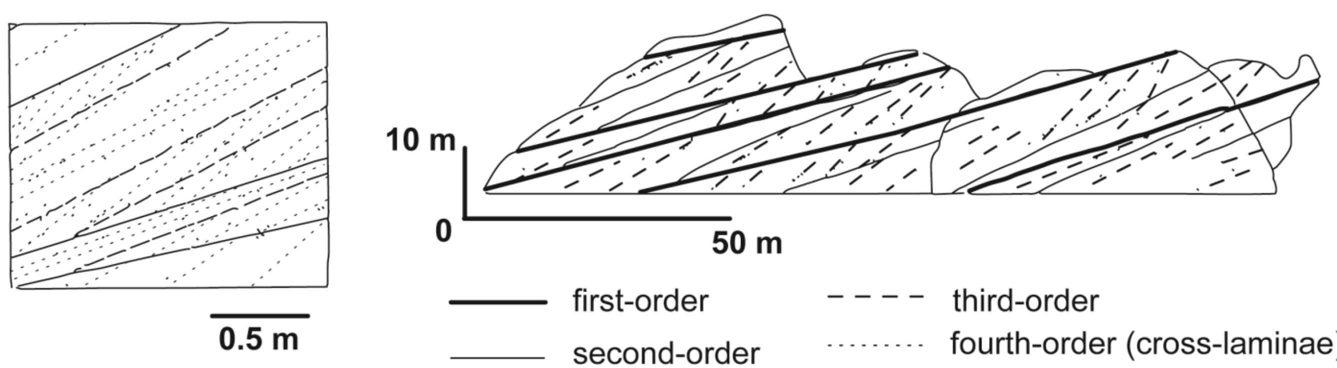

Fig. 1.6 Facies codes developed for A. braided river deposits (modified from Miall, 1977) and B. diamict (modified from Eyles et al., 1983)

A

Code	Lithofacies	Sedimentary structure	Interpretation
Gm	gravel, massive or crudely bedded (rare sand and fines)	ripples, crossbeds, imbricated gravel	longitudinal bars, channel-lag deposits
Gt	stratified gravel	trough crossbeds	minor channel fill
Gp	stratified gravel	planar crossbeds	lingoid bars, deltaic growths
St	sand (medium to coarse), may be pebbly	solitary (theta), grouped (pi) crossbeds	dunes
Sp	sand (medium to coarse), may be pebbly	solitary (alpha), grouped (omikron) planar crossbeds	lingoid bars, sand waves
Sr	sand (very fine to coarse)	ripples	ripples
Sh	sand (very fine to coarse), may be pebbly	horizontal, parting, or streaming lineation	planar bed
Ss	sand (fine to coarse), may be pebbly	broad shallow scours (and eta cross-stratification)	minor channels or scour hollows
Fl	sand (very fine), silt, mud	ripples, undulatory bedding, bioturbation, rootlets, caliche	waning flood or overbank deposits
Fm	mud, silt	rootlets, dessication cracks	drape deposits (ponded water)

B

Diamict, D

Dm	matrix-supported
Dc	clast-supported
D-m	massive
D-s	stratified
D-g	graded

Interpretation

D--(r)	resedimented
D--(c)	current reworked
D--(s)	sheared

Contacts

erosional
conformable
loaded
interbedded

Fine-grained (mud), F

Fl	laminated
Fm	massive
F-d	with dropstones

Sand, S

Sr	rippled
St	trough cross bedded
Sh	horizontal lamination
Sm	massive
Sg	graded
Sd	soft sediment deformation

The integration of data regarding different types and geometries of facies contacts (and their genetic interpretation), bedform hierarchies and geometries of facies associations (and their paleoenvironmental significance), an understanding of autogenic and allogenic controls on sedimentary geometries, and facies codes and models, serves as the underlying foundation of AEA, and has allowed the development of AEA as powerful methodology for the analysis of sedimentary geometry in different depositional environments.

1.2 ESTABLISHED METHODOLOGY OF AEA

Allen (1983) documented the internal geometry of braided river fluvial deposits of the Late Devonian Brownstones in Wales from sandstone exposed in outcrop (Fig. 1.7) in order to reconstruct channel style, and differentiate between low-sinuosity (lenticular and multi-storey geometry) and high-sinuosity (displaying lateral accretion bedding) stream deposits. Building on previous work establishing bounding surface and bedform geometry and hierarchies, Allen (1983) identified four types of bedding contact (concordant/discordant, erosional/non-erosional) in the fluvial sandstones which, together with facies composition, form a hierarchy of bedding contacts that delineate laminae (zeroth-order), set boundaries (first-order), groups of genetically-related facies called ‘complexes’ (second-order), and groups of complexes (third-order; Fig. 1.7A). Delineation of the internal geometry of cross-stratified sandstone bodies allows reconstruction of bar types (cross- and plane-bedded simple, compound, and compound-composite types) and dunes recorded in the Brownstones. A series of detailed hand sketches of cross-stratification and bounding surfaces allowed the identification of 'depositional features' with distinct internal geometries which make up the internal architecture of the sandstone sheets (Fig. 1.7B; Allen, 1983). The sand body geometries recorded from outcrop, combined with facies models of fluvial systems, lead to the establishment of site-specific facies models for the low-sinuosity fluvial system recorded in the Brownstones (Allen, 1983).

Miall (1985) recognized the significance of sedimentary architecture for paleoenvironmental reconstruction, and refined the earlier concepts of Allen (1983) to develop the methodology of AEA. Miall (1985) proposed a hierarchy consisting of first- to fourth-order surfaces (similar to that of Allen, 1983), which was later refined to include first- to sixth-order surfaces (Miall, 1988; Fig. 1.8). Fourth-order surfaces delineate architectural elements, the basic building blocks of the sedimentary architecture of a system, and fifth-order bounding surfaces mark the base of channel complexes. The bounding surface scheme of Miall (1985) also designates a sixth-order bounding surface to demarcate the base of a paleovalley complex (Fig. 1.8).

Miall (1985) emphasized the importance of describing the nature of the upper and lower bounding surfaces, external and internal geometry, and scale of the architectural elements. In Miall's original paper (Miall, 1985), eight different architectural elements were identified, including channel (CH), lateral accretion (LA), sandy bedform (SB), gravel bars and bedforms (GB), laminated sand sheet (LS), overbank fines (OF), sediment gravity flows (SG), and foreset macroforms (FM; Fig. 1.8A). These architectural elements vary in scale and internal complexity, and the CH element is particularly complex in that it is comprised of other architectural elements. In a later revision of AEA,

Fig. 1.7 Sedimentary architecture of the Brownstones (Wales) braided river sandstone. A. Facies contact hierarchy of zeroth- to third-order surfaces. B. Depositional features recording different architectures of sandstone bodies (black circles indicate gravel; modified from Allen, 1983).

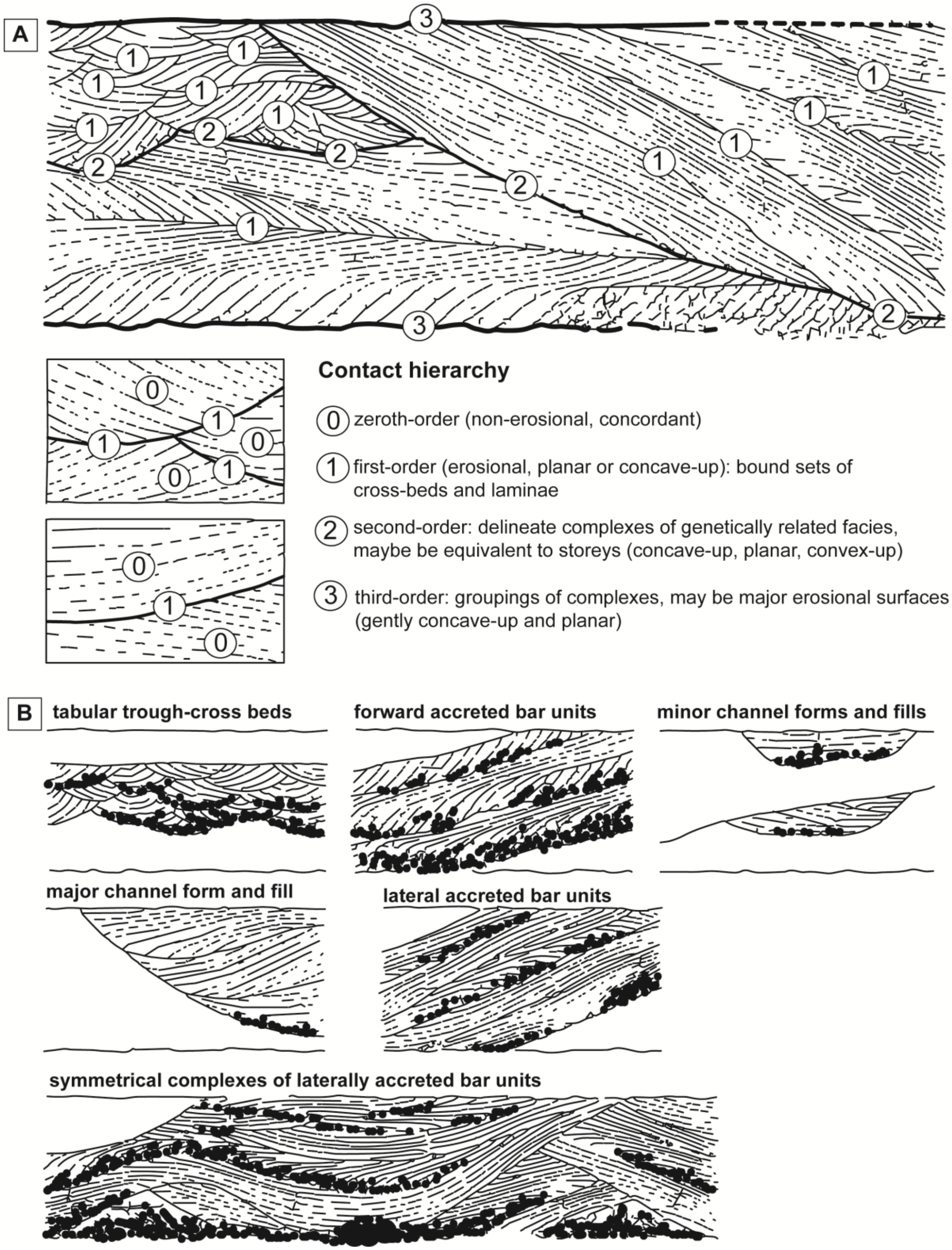
A
3
1
2
0
Contact hierarchy
0 zeroth-order (non-erosional, concordant)
1 first-order (erosional, planar or concave-up): bound sets of cross-beds and laminae
2 second-order: delineate complexes of genetically related facies, maybe be equivalent to storeys (concave-up, planar, convex-up)
3 third-order: groupings of complexes, may be major erosional surfaces (gently concave-up and planar)
B
tabular trough-cross beds
forward accreted bar units
minor channel forms and fills
major channel form and fill
lateral accreted bar units
symmetrical complexes of laterally accreted bar units

Fig. 1.8 Architectural element analysis of fluvial deposits characterized by Miall (1985). A. Cartoon illustrating architectural elements of fluvial deposits and B. The internal facies composition and geometry of elements (modified from Miall, 1985). C. Revised bounding surface hierarchy (modified from Miall, 1988). D. Bounding surface hierarchy of fluvial deposits (modified from Miall, 1988).

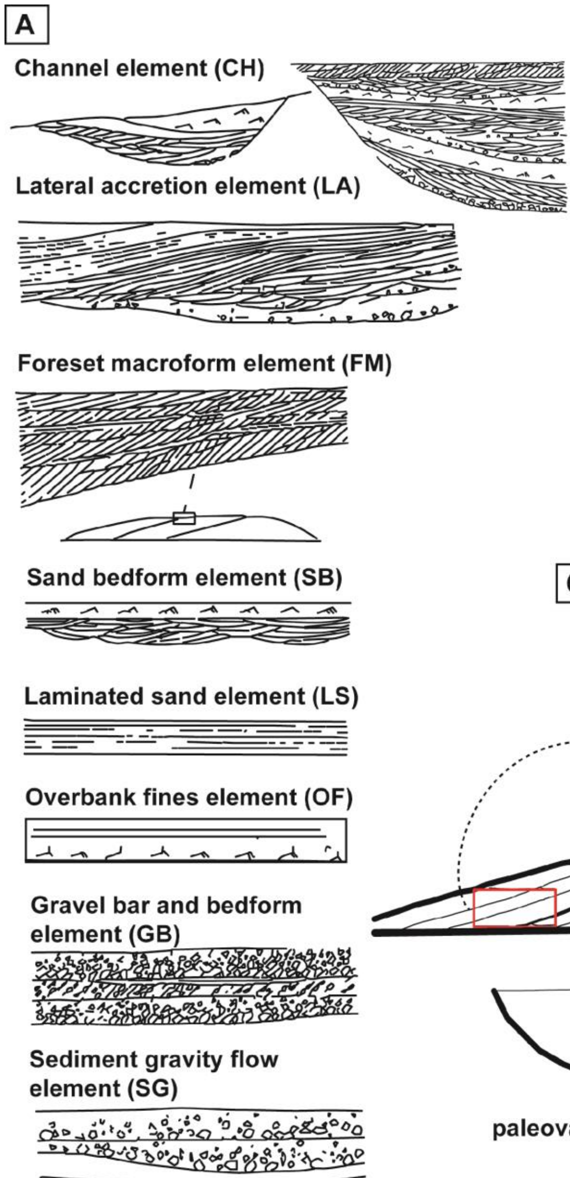

B

Element	Lithofacies assemblage	Geometry
CH	any combination	finger, lens, sheet; concave-up erosional base
GB	Gm, Gp, Gt	lens, blanket; tabular bodies
SB	St, Sp, Sh, Sl, Sr, Se, Ss	lens, sheet, blanket, wedge
FM	St, Sp, Sh, Sl, Sr, Se, Ss	lens resting on flat or channelled base
LA	St, Sp, Sh, Sl, Sr, Se, Ss; rare Gm, Gt, Gp	wedge, sheet, lobe; internal lateral accretion surfaces
SG	Gm, Gms	lobe, sheet
LS	Sh, Sl; rare St, Sp, Sr	blanket, sheet
OF	Fm, Fl	thin to thick blankets

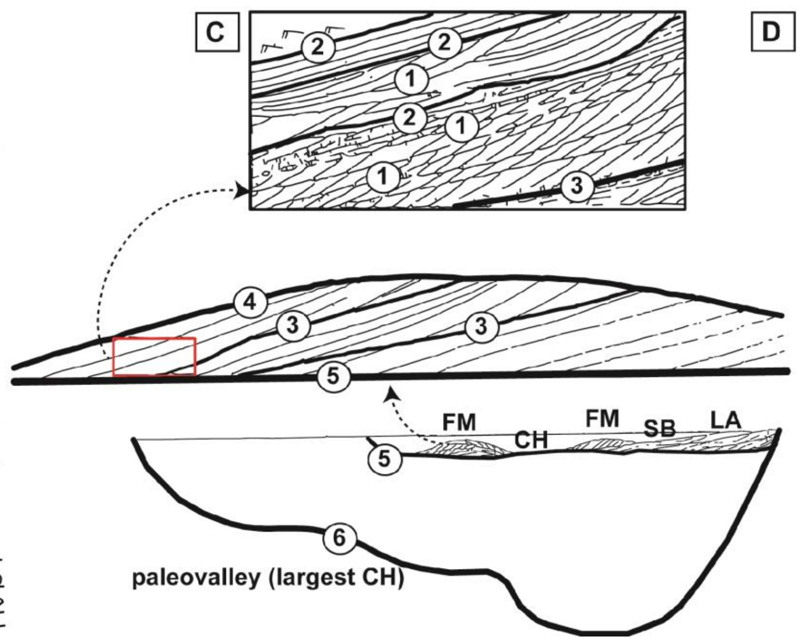

D

Order	Description
1	set boundary
2	coset boundary
3	erosional surface separating similar facies assemblages
4	delineate elements (macroforms)
5	major sand sheets and channel-fill complexes
6	define mappable stratigraphic subdivisions (members or submembers)

Fig. 1.9 Conceptual architectural models representing different fluvial styles based on the assemblage and spatial relationship of architectural elements. A. Proximal alluvial fan. B. Deep, low sinuosity river. C. Fine-grained meandering river (modified from Miall, 1985). Refer to Fig. 1.8 for architectural element codes and description.

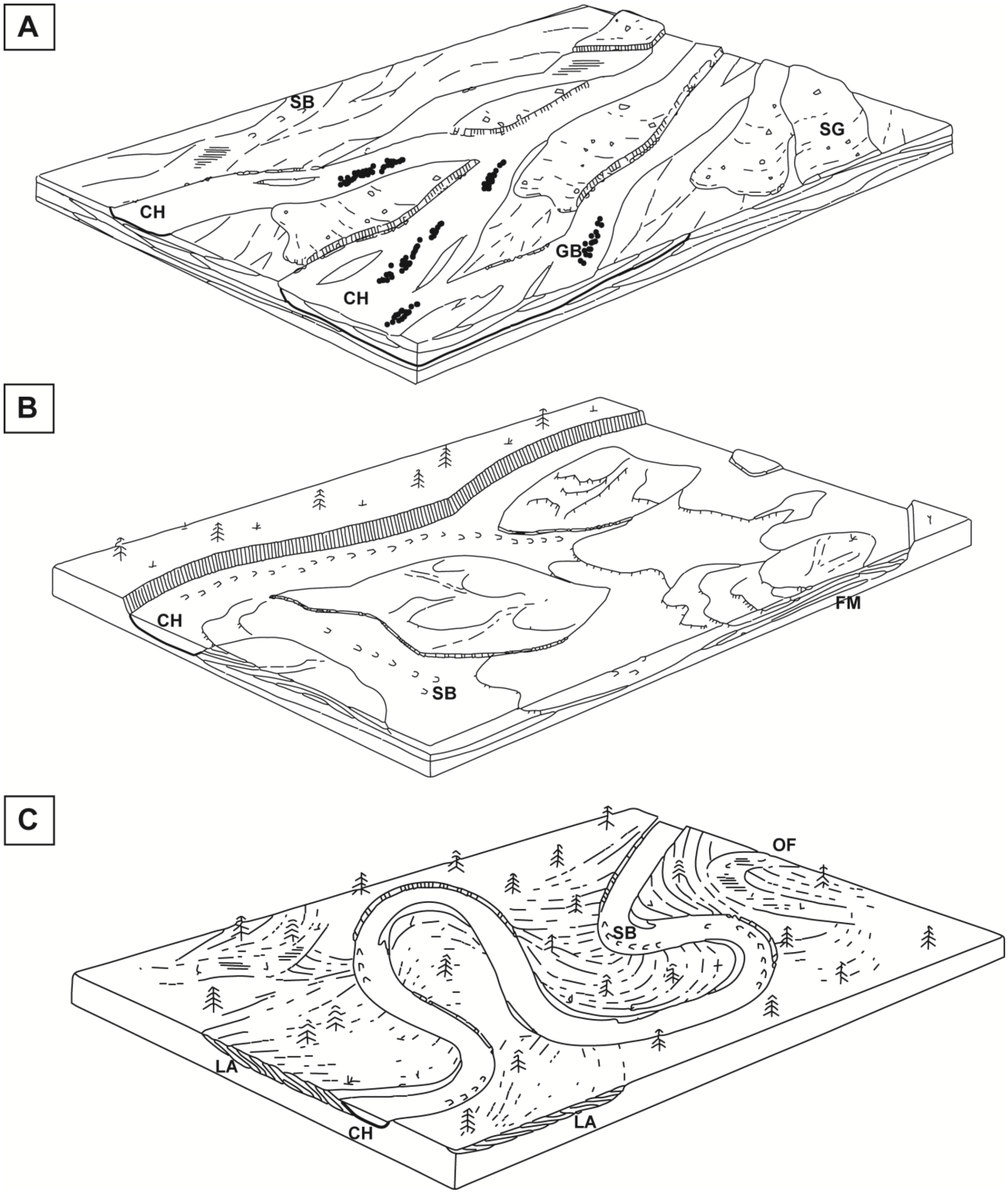
A
SB
SG
CH
GB
CH
B
CH
FM
SB
C
OF
SB
LA
CH
LA

the FM element was subdivided into the lateral accretion (LA) and downstream accretion (DA) elements (Miall, 1988). The assemblage and spatial arrangement of architectural elements allowed Miall (1985) to develop a series of facies models, from proximal alluvial fans dominated by sediment gravity flows to sheetflood river plains dominated by flash floods (Fig. 1.9).

Recognition of the significance of facies contacts at small-scales of resolution (below that of a set boundary, recording individual ripple foresets) and larger-scale contacts demarcating a high degree of environmental change (the base of a basin-fill succession) prompted yet another revision of the bounding surface hierarchy to include zeroth- to seventh-order surfaces (Miall, 2010). Architectural element analysis of fluvial deposits by other workers has resulted in the characterization of several different architectural elements including levee, crevasse splay, and shallow lake elements (e.g. Hornung and Aigner, 1999; Ghazi and Mountney, 2009).

1.2.1 Limitations of AEA

AEA is a powerful tool for the analysis of sedimentary architecture; however, it is limited in certain aspects. Four main limitations of AEA include: 1) difficulty in precise predictive mapping utilizing AEA, 2) uncertainty in regional correlations and the significance of site-specific and local-scale sedimentary architecture delineated by AEA, 3) the restriction of AEA to sediments exposed in outcrop sections that are laterally and vertically extensive, and the paucity of outcrop sections that allow for full 3-dimensional reconstruction of sedimentary geometry of large-scale elements, and 4) terminology and bounding surface definitions are ambiguous, and genetic interpretations may be used for descriptive purposes (e.g. Fig. 1.8), which hinders objective and systematic description of observations and data. This makes comparison of sedimentary geometries delineated at different sites difficult. The limitations of AEA are discussed below, mainly with reference to comments made by Walker (1990) and Bridge (1993).

1.2.1.1 Limitation 1: Predictive mapping of elements

AEA facilitates delineation of the geometry of genetically-related facies associations which are packaged at different spatial scales (Fig. 1.8C). The geometry of architectural elements (fourth-order surfaces; Fig. 1.8) is delineated from outcrop sections, and the spatial arrangement and relationship of architectural elements allowed Miall, (1985) to construct a series of twelve conceptual architectural models representing different fluvial styles in which an assemblage of different architectural elements may be included (of which three models are depicted in Fig. 1.9). The spatial arrangement and relationship of architectural elements delineated from outcrop sections may allow paleoenvironmental reconstruction of units with similar fluvial styles to those illustrated in these architectural models (Fig. 1.9); however, Walker (1990) aptly pointed out that,

> "if the combinations of elements are 'almost infinitely variable', and the elements have become the basis for prediction, it follows that prediction can only be attempted *within* an element…but it is impossible to predict where to look for channels, gravel bars and bedforms, or lateral accretion deposits" (Walker, 1990).

The combination of architectural elements within a deposit is, in fact, not infinitely variable because depositional environments have a specific suite of transport and depositional processes, and are influenced by certain autogenic and allogenic controls;

hence, the sedimentary architecture of a depositional environment likely contains a finite suite of facies associations and architectural elements (e.g. fluvial versus subglacial architectures). Understanding of the potential autogenic and allogenic controls (e.g. tectonics, climate, sediment availability, topography) of an area may provide insight into the types and assemblages of architectural elements that are likely to compose the sedimentary architecture (Fig. 1.9; Miall, 1985). The spatial arrangement and relationship of architectural elements and the bounding surface hierarchy can therefore allow mapping of 'architectural units' across a local-scale study area (Fig. 1.10) and the types and spatial arrangement of architectural elements may be predicted at a local scale.

1.2.1.2 Limitation 2: Type-models for sedimentary architectures

The architectural models of Miall (1985; Fig. 1.9) are not intended as type-models of the sedimentary architecture of different fluvial styles (as noted by Miall, 1985) because the precise spatial arrangement, contiguity, interconnectedness, and geometry of architectural elements formed within a depositional environment are probably highly variable; hence, a single 'type-site architectural model' for a depositional environment is improbable. The lack of a 'type-site model' for paleoenvironmental interpretation of local-scale sedimentary architectures is pointed out by Walker (1990), stating,

> "AEA offers no overall point of reference *(norm)* for a depositional system as a whole….and in the absence of a norm there is no way of knowing whether the individual example is similar to, or greatly different from, other examples".

Facies models provide a 'norm' or 'type-model' of facies assemblages for a depositional environment; however, it has long since been recognized that facies models do not

Fig. 1.10 Architectural units ('Element Associations', EAs) delineated in Limehouse, Ontario, Canada. A. Study area location in Limehouse pit (grey box represents the orientation and location of B.). B. Conceptual block diagram of Element Associations (EAs1-6) bounded by fifth-order surfaces (based on data recorded from outcrop sections; from Slomka and Eyles, 2013).

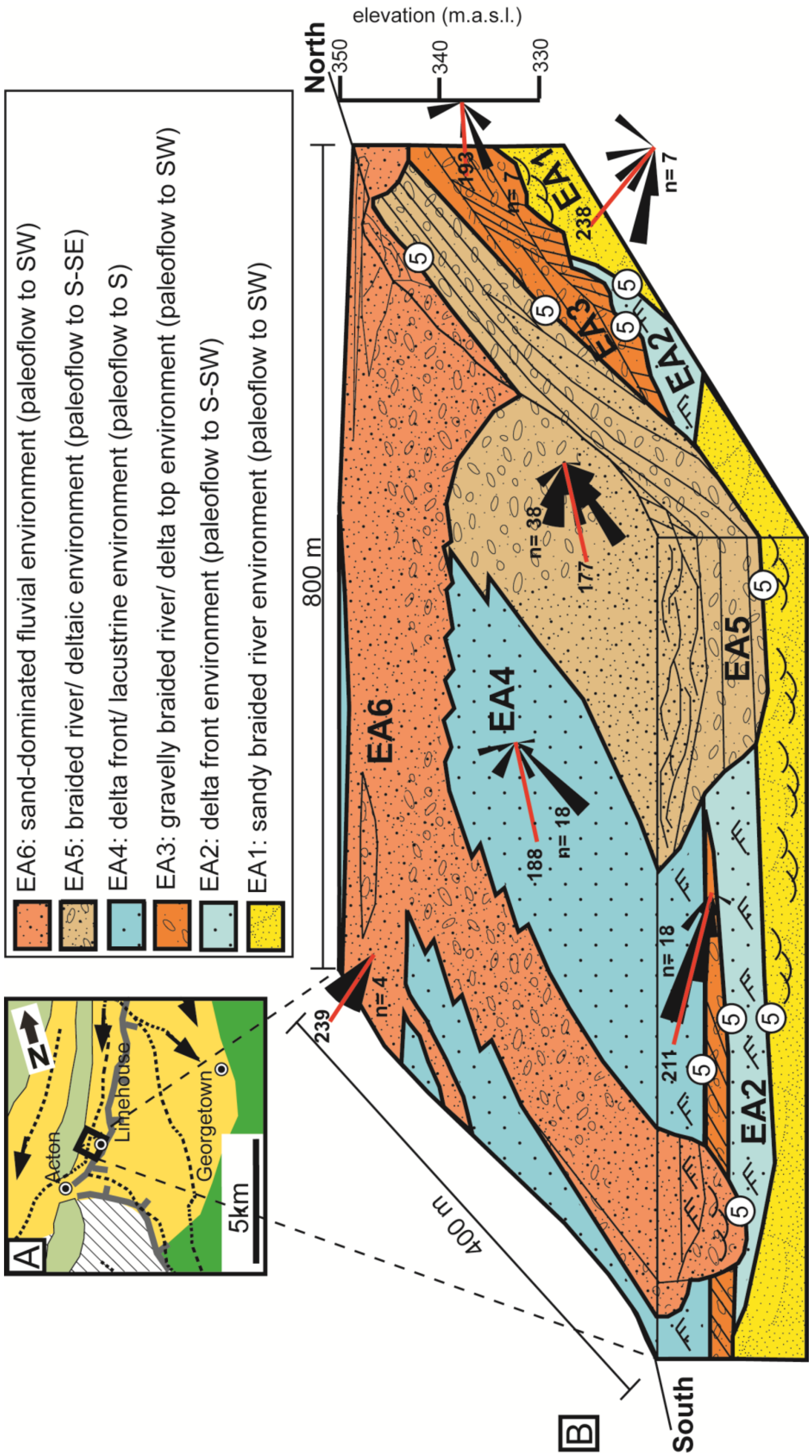
A
N
Acton
Limehouse
Georgetown
5km
EA6: sand-dominated fluvial environment (paleoflow to SW)
EA5: braided river/ deltaic environment (paleoflow to S-SE)
EA4: delta front/ lacustrine environment (paleoflow to S)
EA3: gravelly braided river/ delta top environment (paleoflow to SW)
EA2: delta front environment (paleoflow to S-SW)
EA1: sandy braided river environment (paleoflow to SW)
elevation (m.a.s.l.)
350
340
330
North
South
800 m
400 m
B
EA6
EA5
EA4
EA3
EA2
EA1
n= 4
239
n= 7
193
n= 7
238
n= 38
177
n= 18
188
n= 18
211

account for all variability in facies types, associations, and processes in a depositional environment, and new facies models are constructed to represent depositional environments that do not 'fit' to existing generalized facies models (James and Dalrymple, 2010; Miall, 2014). The sedimentary architecture of a deposit delineated utilizing AEA is likely to be site-specific (due to the spatiotemporal variability of depositional processes); however, the application of AEA is still in its infancy for many depositional environments, and, similar to facies models, additional future studies utilizing AEA may provide a database of sedimentary architectures applicable to different depositional environments and allow patterns of architectural element assemblages to be utilized as 'type-assemblages' (likely similar to the fluvial-sites architectural models of Miall, 1985; Fig. 1.9). Future studies utilizing AEA for the analysis of deposits formed in different depositional environments, and in different geographic locations, may provide insight to the distinction between 'norm' and 'outlier' architectures.

1.2.1.3 Limitation 3: Scale and accessibility

The third limitation of AEA identified here is the scale of, and accessibility to, exposed outcrop sections. AEA is commonly utilized for delineation of sedimentary architecture from exposed outcrop sections, which are finite in their vertical and lateral extent, and on which facies and sedimentary geometries can be traced laterally for some distance; however, Walker (1990) points out that,

> "it is obvious that AEA requires three-dimensional outcrop of a kind rarely encountered; it is almost impossible to do in the subsurface where bounding surfaces are hard or impossible to define in cores." (Walker, 1990).

The delineation of the geometry of architectural elements is dependent on the scale of the element; whereby if the width or length of an element exceeds the lateral extent of the outcrop exposure, or the thickness of an element is greater than the vertical extent of the outcrop, the geometry of the architectural element (or architectural unit, element association; Fig. 1.10) cannot be defined. This is the greatest drawback of AEA because: 1) elements (e.g. channels and gravel bars; CH and GB elements; Fig. 1.8) are commonly tens to hundreds of metres long or wide, and several tens of metres in thickness, greater than the scale of most outcrop exposures; 2) outcrop sections are commonly 2-dimensional faces that rarely orthogonally intersect; and 3) outcrop sections rarely dissect elements orthogonal or perpendicular to paleoflow direction (Bridge, 1993). In order to overcome the limitation of scale and accessibility, detailed paleocurrent data collected from cross-bedded sand and gravel facies, rippled sand facies, and bedding surfaces, in combination with data on the nature of facies contacts, may be utilized to reconstruct the 3-dimensional geometry of architectural elements (e.g. the Castlegate Sandstone architecture delineated by Miall, 1994). Geophysical data (e.g. ground penetrating radar, GPR) can be used to provide a three-dimensional reconstruction of sedimentary geometry (e.g. Hornung and Aigner, 1999; Boyce and Eyles, 2000; Heinz and Aigner, 2003; Bersezio et al., 2007); however, geophysical methods are commonly dependant on site conditions (e.g. GPR is most successful in areas with coarse-grained sediment above the water table) and geometries imaged by geophysical methods are again limited by the scale of the architectural elements and dimensions of the geophysical survey. The limitation of scale makes application of AEA to analysis of core data difficult; however, detailed attention to facies types and contacts, careful grouping of facies associations, systematic characterization of unit hierarchies, and utilization of modern analogues allows delineation of sedimentary geometries (as demonstrated in this thesis; Chapter 4) Outcrop analogues and geophysical and hydrogeological data are commonly utilized to provide additional information for subsurface architectural models (e.g. Boyce and Eyles, 2000; Bridge and Tye, 2000; Gerber et al., 2001; Hansen et al., 2009). Alternatively, pits are excavated and outcrop sections are cleared to expose faces orientated orthogonal to each other (e.g. Kessler et al., 2012); however, only small-scale (several tens of centimetres to a few metres) sedimentary geometries are typically delineated from such excavations.

1.2.1.4 Limitation 4: Terminology and ambiguity

The importance of objective terminology for the description of sedimentary deposits was highlighted by Allen (1963) and utilized to refine the classification scheme of cross-stratification (Fig. 1.3). Bridge (1993) noted that the nomenclature utilized to classify architectural elements (Fig 1.8) is interpretative, and suggested the use of descriptive and unambiguous terminology, and mutually exclusive parameters, to classify and communicate data on bounding surfaces and sediment geometries. Bridge (1993) also noted that the bounding surface hierarchy of AEA is difficult to apply in the field because surfaces delineating different sedimentary bodies (e.g. ripples versus cross-beds) may have formed in a similar time-scale and bounding surfaces may transition between hierarchical levels (Bridge, 1993). As a result, Bridge (1993) suggested a hierarchical order of sediment bodies (e.g. microforms, mesoforms, and macroforms) rather than bounding surfaces.

1.3 SEDIMENTARY ARCHITECTURE OF GLACIAL DEPOSITS

Quaternary-age glacial deposits commonly host groundwater reservoirs that serve as significant aquifers for municipal water supply. There is also increasing interest in the potential of glacial deposits to form hydrocarbon reservoirs, particularly in regions of North and South America (França and Potter, 1991; Eyles et al., 1995, Bachu, 1997; Huuse et al., 2012). Locating and delineating groundwater and/or hydrocarbon reservoirs in glacial deposits requires information regarding the geometry and architecture, and internal heterogeneity, of the reservoirs and their hosting deposits. Characterizing the sedimentary heterogeneity of glacial deposits is challenging, and is due, in part, to the dynamic nature of glacial depositional environments and the lack of a systematic methodology to record multi-scale heterogeneity and geometry directly in the field. Effective translation of these data to create comprehensive stratigraphic models is also an issue.

The architecture of glacial deposits is most commonly recorded using a landsystem approach (Evans, 2005), both at modern ice margins and in previously glaciated regions (discussed in Chapter 3 of this thesis), and is documented by analysis of glacial sediments exposed in outcrop utilizing facies analysis and lithostratigraphy (e.g. Meyer and Eyles, 2007), tectonostratigraphy, including the analysis of deformation structures (e.g. Phillips et al., 2002; Arnaud, 2012; Kessler et al., 2012), basin analysis (e.g. Eyles et al., 1985), geophysical imaging (e.g. Eyles et al., 2003), allostratigraphy (e.g. Eyles et al., 1998), sequence stratigraphy (e.g. Brookfield and Martini, 1999), and microfabric analysis (e.g. Menzies et al., 2006). Lithostratigraphy, sequence stratigraphy, and allostratigraphy are all formal stratigraphic methodologies for the delineation of sedimentary units and architecture; however, utilization of these approaches for architectural analysis of glacial successions, which are commonly non-marine, may not be appropriate, for reasons discussed in later chapters of this thesis (Chapters 2-4). Analysis of glacial deposits utilizing tectonostratigraphy and microfabric analysis provide insight into the physical stresses exerted on glacial sediments (commonly of subglacial origin) and the style of deformation (strain) in response to that stress, which is commonly recorded by secondary structures and deformed sediment bodies (Arnaud, 2012). However, these approaches do not provide a systematic methodology for delineating and interpreting the detailed sedimentary geometry of facies associations (i.e. sediment bodies) for paleoenvironmental analysis at various scales of resolution. Recently, AEA has been applied to the architectural analysis of glacial deposits, specifically those of jökulhlaup (Marren et al., 2009) and subglacial (Boyce and Eyles, 2000) origin (Fig. 1.11). Understanding the internal heterogeneity and architecture of glacial deposits is timely, specifically as it relates to recent issues concerning bitumen flow to surface in the previously glaciated terrain of the Primrose/Wolf Lake oil sands area in Alberta, Canada (Alberta Energy Regulator, 2014).

Fig. 1.11 Architectural element analysis (AEA) applied to the analysis of subglacial sediments. A. Architectural elements identified in the Northern Till (Ontario) exposed in outcrop sections, including diamict elements, interbeds, and deformed zone elements (modified from Boyce and Eyles, 2000). B. Fence diagram of architectural elements delineated in boreholes drilled in the Whitevale area (north of Toronto; modified from Boyce and Eyles, 2000).

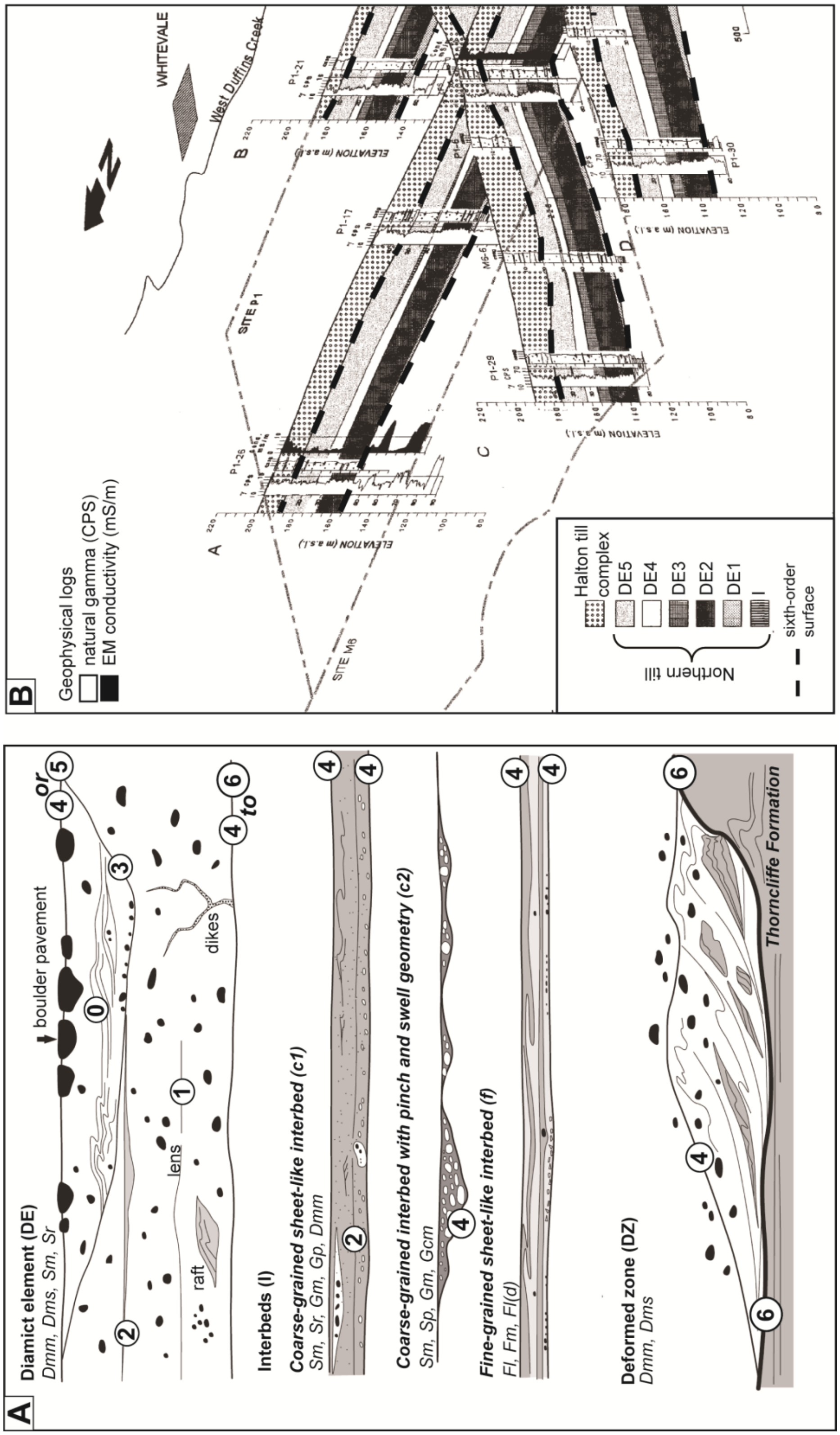
A
Diamict element (DE)
Dmm, Dms, Sm, Sr
boulder pavement
lens
raft
dikes
or
to
Interbeds (I)
Coarse-grained sheet-like interbed (c1)
Sm, Sr, Gm, Gp, Dmm
Coarse-grained interbed with pinch and swell geometry (c2)
Sm, Sp, Gm, Gcm
Fine-grained sheet-like interbed (f)
Fl, Fm, Fl(d)
Deformed zone (DZ)
Dmm, Dms
Thorncliffe Formation
B
Geophysical logs
natural gamma (CPS)
EM conductivity (mS/m)
Halton till complex
DE5
DE4
DE3
DE2
DE1
I
Northern till
sixth-order surface
WHITEVALE
West Duffins Creek
SITE P1
SITE M8
ELEVATION (m a.s.l.)

1.4 OBJECTIVES OF THIS RESEARCH

This thesis utilizes AEA as a descriptive and interpretive tool to systematically record the sedimentary heterogeneity and geometry of modern and Quaternary-age glacial successions and is based on detailed observation of facies types, facies associations, their geometry, and the nature and spatial arrangement of bounding surfaces between facies. This thesis explores the full capacity of AEA in order to answer three main research questions:

1) How can AEA be utilized to deconstruct glacial successions (exposed in outcrop, boreholes, and at modern ice margins) into their component building blocks that make up the sedimentary architecture?;

2) How does AEA enhance paleoenvironmental reconstruction and further our understanding of the depositional history of glaciated regions?; and

3) *How can the architectural framework of a glacial succession (delineated utilizing AEA) provide insight to predictive mapping of subsurface glacial deposits and inform hydrogeologic models in glaciated terrains?*

This project involves detailed examination of late-Wisconsin-age glacial deposits exposed in outcrop sections in Illinois (Chapter 2), investigation of sedimentary architecture delineated from glacial deposits at a modern ice margin (Sólheimajökull, southern Iceland; Chapter 3), and analysis of Quaternary-age sediment recovered from fully-cored boreholes drilled in Georgetown, Ontario (Chapter 4; Fig. 1.12).

Chapter 2 of this thesis explores how AEA can be utilized to organize and characterize the detailed sedimentary heterogeneity of a till succession. Fieldwork was conducted at two outcrop sites in north-central Illinois, U.S.A. (Fig. 1.12), which expose Late Wisconsin-age till of the Tiskilwa Formation. Detailed facies analysis requires close and careful inspection of sediments and their bounding discontinuities (including measurements such as paleocurrent directions, gravel clast size and orientations, and dip direction of bedding planes), and delineation of sedimentary geometries from outcrop requires laterally and vertically extensive exposures; however, subglacial deposits are rarely well-exposed in section, partly due to their susceptibility to slumping and surface desiccation (and cementation) and the angle of the exposed outcrop face which is commonly near-vertical where tills are exposed in stream cuts (e.g. Rouge River near Toronto), making clearing of debris and access to clean outcrop faces difficult. The Rattlesnake Hollow study area in Illinois was selected based on the lateral and vertical extent of well-exposed and easily accessible outcrop sections of till, which allowed detailed field collection of data to be used for AEA. Fieldwork at Rattlesnake Hollow allowed the identification of five architectural elements (fourth-order surfaces) which comprise the internal architecture of the Tiskilwa Formation till. The grouping of genetically-related architectural elements and their relationship to fifth-order bounding surfaces facilitated the characterization of larger-scale architectural packages, called element associations, which can be mapped across the local study area. The results of this study demonstrate the applicability of AEA to the systematic documentation and interpretation of local-scale till sheet heterogeneity at different scales of resolution (Research question 1). The fifth-order bounding surfaces delineated in the till (in this study) record allogenic controls on the subglacial bed mosaic, which generate periods of separation and reattachment of the ice and its bed and allow deposition of sands in subglacial canals (Research question 2). The heterogeneity within the Tiskilwa Formation till, as recorded in this study, may be utilized to inform local-scale groundwater investigations in areas where the till is more deeply buried (Research question 3).

The third chapter of this thesis explores the validity of AEA for delineation of the sedimentary architecture of a modern glacial landscape. Fieldwork was conducted at Sólheimajökull glacier in southern Iceland (Fig. 1.12). Sólheimajökull is an outlet glacier of the Mýrdalsjökull icecap (Fig. 1.12), which overlies the Katla volcano, and has experienced several jökulhlaup (catastrophic flood) events triggered by volcanic eruptions, geothermal activity, ice-dammed lakes, and storm events. The Sólheimajökull landscape was selected to test AEA based on its accessibility (including a gravel road accessible to vehicles and short walking distance to the ice margin and proglacial area), availability of vertical outcrop sections which expose tills and glaciofluvial sediments along the proglacial river and on abandoned terraces, and the rich collection of previously conducted and ongoing research, historical accounts, and visual documentation (satellite imagery, air photos, hand-drawn sketch maps dating back to 1705 AD) at Sólheimajökull, which allowed verification of the recent depositional history and evolution of the glacial landscape. Fieldwork was conducted at Sólheimajökull and basic principles of AEA and landsystems analysis were integrated in order to facilitate delineation of the sedimentary architecture of the Sólheimajökull landsystem. Sixth-order surfaces delineate landsystem tracts, which are deconstructed into smaller-scale architectural units called landsystem components (fifth-order surfaces) made of genetically-related surface features (fourth-order surfaces; Research question 1). The spatial arrangement of landsystem components, together with data regarding previously reconstructed ice margin positions, jökulhlaup events and their effect on the geomorphology of the glacial landscape, and historical imagery and accounts of geomorphic changes such as the location of proglacial streams, allowed the characterization of allostratigraphic units and reconstruction of the depositional history and evolution of the Sólheimajökull landsystem (Research question 2). The internal sedimentary architecture of landsystem tracts in ice marginal, proglacial, and ice distal locations, as delineated in this study, can be utilized as a guide for the characterization of the subsurface architectures of Quaternary glacial deposits in previously glaciated terrain. The geometry of the glaciofluvial landsystem tract may also provide insight into the geometry and heterogeneity of coarse-grained units that may host prospective aquifers in previously glaciated areas (Research question 3).

Data from Sólheimajökull and Illinois were utilized as modern and outcrop analogues, respectively, to provide insight into the sedimentary architecture of subsurface Quaternary glacial deposits in Georgetown, southern Ontario (Canada; Chapter 4; Fig. 1.12). The Georgetown area was selected for study because of concerns related to the sustainability of new and existing municipal groundwater supplies in the area, and the need to understand the subsurface heterogeneity as it relates to the connectivity and effectiveness of aquifers and aquitards. The thick succession of Quaternary glacial deposits, that commonly infill buried bedrock valleys in the Georgetown area, have complex spatial relationships and have been the focus of several previous studies (Meyer and Eyles, 2007; Brennan, 2011; Slomka, 2011; Slomka and Eyles, 2013). The availability of 24 fully-cored boreholes in the Georgetown area allowed basic concepts of AEA to be applied to the analysis of subsurface sediments and the delineation of fourth- to seventh-order surfaces and a hierarchy of units including architectural elements, architectural components, and architectural units (Research question 1). The spatial arrangement and relationship of architectural components identified in core facilitated reconstruction of the detailed depositional history of the Georgetown area, including at least six 'incision events' by glaciofluvial erosional processes (Research question 2), and may provide insight to the hydrogeology of aquifer systems in the Georgetown area. A major finding of this study is that AEA can be effectively utilized for delineation of subsurface architectures from the analysis of core, and the hierarchies of bounding surfaces and units of AEA can be utilized to organize the sedimentary heterogeneity into a 'nested' architectural framework. This framework preserves the high-resolution sedimentary complexity in areas with closely spaced boreholes and detailed architectural information and maintains the 'big picture' geologic framework for application in areas with a higher degree of uncertainty in the delineation of unit geometries. The nested architectural framework may be utilized to inform hydrostratigraphic models of the Georgetown area, and the methods applied in this study can be applied to subsurface investigations in other previously glaciated areas (Research question 3).

AEA, as utilized in this thesis, provides a tool to construct an architectural framework in glacial successions, and may help to facilitate communication and translation of data between the disciplines of 'geology' and 'hydrogeology'. The results

Fig. 1.12 Field site locations. A. Locations of field sites in North America including Rattlesnake Hollow, Illinois (Chapter 2) and Georgetown, Ontario (Chapter 4; imagery from Google Earth, 2014). B. Field site location at Sólheimajökull in southern Iceland (Chapter 3; imagery from Google Earth, 2013).

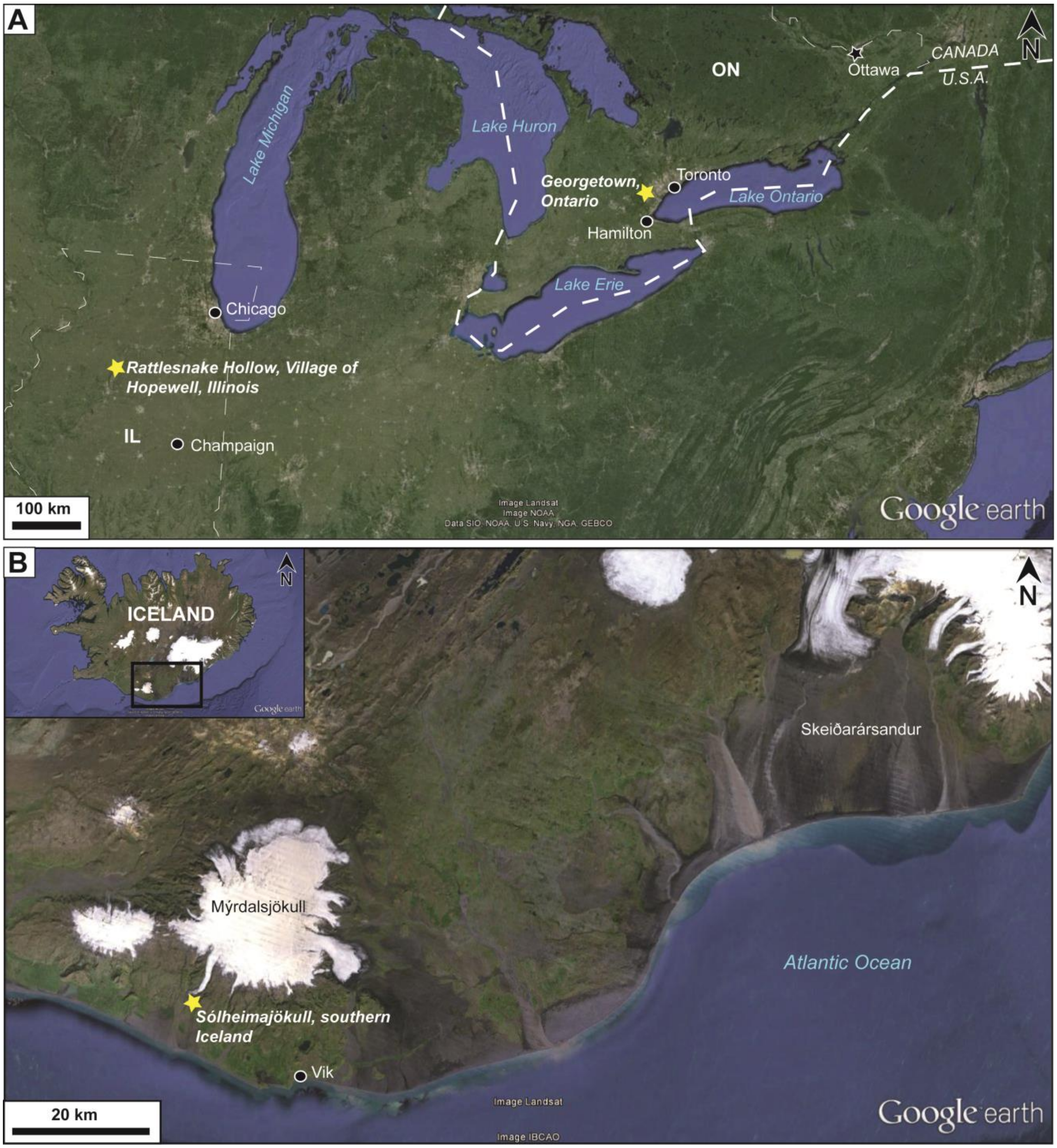
A
N
ON
Ottawa
CANADA
U.S.A.
Lake Michigan
Lake Huron
Georgetown, Ontario
Toronto
Lake Ontario
Hamilton
Lake Erie
Chicago
Rattlesnake Hollow, Village of Hopewell, Illinois
IL
Champaign
100 km
Google earth
B
ICELAND
N
Skeiðarársandur
Mýrdalsjökull
Atlantic Ocean
Sólheimajökull, southern Iceland
Vik
20 km
Image Landsat
Image IBCAO
Google earth

of this project can be utilized as a framework to better understand the sedimentary geometry and hydrostratigraphy of modern glacial landscapes and Quaternary glacial deposits elsewhere.

1.5 THESIS STRUCTURE

This thesis is a ‘sandwich’-style thesis composed of five chapters, including:

(i) Chapter 1: Introduction

This chapter introduces the fundamental concepts and ideas underlying AEA, provides an overview of the methodology of AEA and its limitations, and very briefly summarizes other methodologies utilized to delineate the sedimentary architecture of glacial deposits.

(ii) Chapter 2: Internal architecture of a till sheet, Tiskilwa Formation, north-central Illinois, U.S.A.

The detailed internal architecture of the Tiskilwa Formation till sheet is delineated from two outcrop sections. Facies types and the nature of facies contacts (bounding surfaces) are recorded in five sedimentary logs. The nature of facies contacts and change in facies type and association on either side of the contact allowed the delineation of a bounding surface hierarchy. Facies associations with a characteristic geometry (bounded by fourth-order surfaces) allowed the characterization of five architectural elements. The assemblage of genetically-related architectural elements and the stratigraphic position of major erosional surfaces (fifth-order) allowed the identification of five element associations (EAs1-5), which provide insight to the depositional history of the Tiskilwa

Formation till, and its significance to hydrogeological investigations, in the local study area.

(iii) Chapter 3: Architectural-landsystem analysis of a modern glacial landscape, Sólheimajökull, southern Iceland

This chapter explores the applicability of AEA to the analysis of glacial sediments at a modern ice margin in southern Iceland. Concepts of architectural element analysis and landsystem analysis are integrated in order to delineate the sedimentary architecture of the Solheimajokull landsystem. The architectural-landsystem approach, as utilized here, allowed the characterization of four landsystem tracts composed of smaller-scale architectural units ('landsystem components'), which in turn, allowed the identification of eight different allostratigraphic units and reconstruction of the evolution of Sólheimajökull landsystem.

(iv) Chapter 4: Deconstructing the sedimentary architecture of Quaternary glacial sediments recovered from fully-cored boreholes, Georgetown, Ontario using architectural element analysis

This paper examines 24 fully-cored boreholes drilled in the Georgetown area of southern Ontario in order to delineate the sedimentary architecture of subsurface glacial deposits in an area with a paucity of outcrop sections. The core was logged in detailed, including facies types and the nature of facies contacts, which were recorded in 24 vertical profile logs. The nature of facies contacts, genetic interpretation of facies types, and the change in facies associations on either side of facies contacts facilitated the delineation of a bounding surface hierarchy (fifth- to seventh-order). The genetic interpretation of facies types, and their stratigraphic position in vertical succession, allowed the delineation of eleven architectural units (AU1-11; sixth-order surfaces). Detailed analysis of smaller-scale packages of genetically-related facies within each AU and the nature of facies contacts, allowed the delineation of smaller-scale units, called architectural components (delineated by fifth-order surfaces), which define the architecture of the AUs and allow for paleoenvironmental reconstruction in the Georgetown area.

(*v) Chapter 5: Conclusions and Recommendations for Future Work*

This chapter provides a brief summary and discussion of the significance of the research findings in Chapters 2-4 of this thesis, and areas of future research are suggested.

1.6 PREFACE

The chapters (Chapters 2-4) composing the body of this thesis are formatted and prepared for submission to peer-reviewed scientific journals. The Illinois paper in Chapter 2 has several authors, of which J. Slomka is the primary author. The research, writing, and figure drafting was conducted by J. Slomka, editing of the manuscript and figures and discussion was provided by C.H. Eyles (Supervisor), fieldwork assistance, editing, and data access were provided by the co-authors (R. Mulligan, D. McKay, and R. Berg), and additional fieldwork assistance was provided by others mentioned in the

Acknowledgements section of Chapter 2. This paper is accepted for publication in Sedimentology (manuscript number SED-2014-OM-045).

The Iceland paper (Chapter 3) is submitted to Geomorphology (manuscript number GEOMOR-4972) and is undergoing the peer-review process. The primary author is J. Slomka, who was responsible for fieldwork, data collection and analysis, review of the literature, writing of the manuscript, and drafting of figures, and the second author is C.H. Eyles (Supervisor) who provided significant editing of the manuscript and figures and insightful discussion on the ideas presented in the manuscript.

The third paper composing the body of this thesis (Chapter 4) has two authors. J.Slomka (primary author) and C.H. Eyles (Supervisor). J.Slomka was responsible for field reconnaissance, core analysis, data collection and analysis, literature review, writing of the manuscript, and drafting figures. C.H. Eyles contributed to editing of the manuscript and figures and helpful discussion of ideas contained within the manuscript. This paper is formatted to submit to Canadian Journal of Earth Sciences, and is not yet in review.

REFERENCES

Alberta Energy Regulator 2014. CNRL Primrose. Available online: http://aer.ca/compliance-and-enforcement/cnrl-primrose (Accessed on 18-08 2014).

Allen, J.R.L. 1963. Classification of cross-stratified units, with notes on their origin. Sedimentology, 2: 93-14.

Allen, J.R.L. 1968. The nature and origin of bedform hierarchies. Sedimentology, 10: 161-182.

Allen, J.R.L 1983. Studies in fluvialite sedimentation bars, bar-complexes and sandstone sheets (low-sinuosity braided streams) in the brownstones (L. Devonian), Welsh Borders. Sedimentary Geology, 33: 237-293

Arnaud, E. 2012. The paleoclimatic significance of deformation structures in Neoproterozoic successions. Sedimentary Geology, 243-244: 33-56.

Bachu, S. 1997. Flow of formation waters, aquifer characteristics, and their relation to hydrocarbon accumulations, Northern Alberta Basin, AAPG Bulletin, 81(5): 712 733.

Beerbower, J. R. 1964. Cyclothems and cyclic depositional mechanisms in alluvial plain sedimentation. Symposium on cyclic sedimentation, Kansas Geology Survey, Bulletin 169: 31- 42.

Bersezio, R., Giudici, M., and Mele, M. 2007. Combining sedimentological and geophysical data for high-resolution 3-D mapping of fluvial architectural elements in the Quaternary Po Plain (Italy). Sedimentary Geology, 202: 230-248.

Best, J., Woodward, J., Ashworth, P., Smith, G.S., and Simpson, C. 2006. Bar-top hollows: a new element in the architecture of sandy braided rivers. Sedimentary Geology, 190: 241-255.

Bhattacharya, J.P. and Posamentier, H.W. 1994. Sequence stratigraphy and allostratigraphic applications in the Alberta Foreland basin. *In* Geological Atlas of the Western Canada Sedimentary basin. (Eds. G.D. Mossop and I. Shetsen).

Online version: http://www.ags.gov.ab.ca/AGS_PUB/ATLAS_WWW/A_CH25/CH_25_F.HTM (accessed 2014-06-01).

Boyce, J.I. and Eyles, N. 2000. Architectural element analysis applied to glacial deposits: Internal geometry of a late Pleistocene till sheet, Ontario, Canada. Geological Society of America Bulletin, 112: 98-118.

Brennan, A. 2011. Characterizing the Quaternary hydrostratigraphy of buried valleys using multi-parameter borehole geophysics, Georgetown, Ontario. M.Sc. thesis, School of Geography and Earth Sciences, McMaster University, Hamilton, Ontario, Canada.

Bridge, J.S. 1993. Description and interpretation of fluvial deposits: a critical perspective. Sedimentology, 40: 801- 810.

Bridge, J.S. and Tye, R.S. 2000. Interpreting the dimensions of ancient fluvial channel bars, channels, and channel belts from wireline-logs and cores. AAPG Bulletin, 84(8): 1205-1228.

Brookfield, M.E. 1977. The origin of bounding surfaces in ancient aeolian sandstones. Sedimentology, 24: 303-332.

Brookfield, M.E. and Martini, I.P. 1999. Facies architecture and sequence stratigraphy in glacially influenced basins: basic problems and water-level/ glacier input-point controls (with an example from the Quaternary of Ontario, Canada). Sedimentary Geology, 123: 183- 197.

Clark, J.D. and Pickering, K.T. 1996. Architectural elements and growth patterns of submarine channels: application to hydrocarbon exploration. AAPG Bulletin, 80(2): 194-221.

Dalrymple, R. W. (2010). Interpreting sedimentary successions: facies, facies analysis and facies models. *In* Facies Models, *Edited by* R. W. Dalrymple. Geological Association of Canada, pp. 3-18.

Deutsch, C.V. and Tran, T.T. 2002. FLUVSIM: a program for object-based stochastic modeling of fluvial depositional systems. Computers & Geosciences, **28**: 525-535.

Dreyer, T., Falt, L.M., Hoy, T., Knarud, R., Steel, R., and Cuevas, J.L. (1993). Sedimentary architecture of field analogues for reservoir information (SAFARI): a case study of the fluvial Escanilla Formation, Spanish Pyrenees. *In* The geological modeling of hydrocarbon reservoirs and outcrop analogues. *Edited by* S.S. Flint and I.D. Bryant. International Association of Sedimentologists special publication, Number 15. Blackwell Scientific Publications, Oxford, UK.

Drinkwater, N.J. and Pickering, K.T. 2001. Architectural elements in a high-continuity sand-prone turbidite system, late Precambrian Kongsfjord Formation, northern Norway: Application to hydrocarbon reservoir characterization. AAPB Bulletin, 85(10): 1731-1757.

Eriksson, P.G., Reczko, B.F.F., Boshoff, A.J., Schreiber, U.M., Van der Neut, M., Snyman, C.P. 1995. Architectural elements from Lower Proterozoic braid-delta and high-energy tidal flat deposits in the Magaliesberg Formation, Transvaal Superground, South Africa. Sedimentary Geology, 97: 99- 117.

Evans, D.J.A. 2005. Glacial landsystems. *Edited by* D.J.A. Evans. Arnold: London, 544 pp.

Eyles, N., Eyles C.H., and Miall, A.D. 1983. Lithofacies types and vertical profile models; an alternative approach to the description and environmental interpretation of glacial diamict and diamictite sequences. Sedimentology, 30: 393- 410

Eyles, N., Clark, B.M., Kaye, B.G., Howard, K.W.F., and Eyles, C.H. 1985. The application of basin analysis techniques to glaciated terrains: an example from the Lake Ontario basin, Canada. Geosciences Canada, 12(1): 22-32.

Eyles, N., França, A.B., Bonorino, G.G., Eyles, C.H., and Paulsen, O.L. 1995. Hydrocarbon-bearing Late Paleozoic glaciated basins of southern and central South America. *In* A. J. Tankard, R. Suárez S., and H. J. Welsink, Petroleum basins of South America: AAPG Memoir 62, p. 165–183.

Eyles, C.H., Eyles, N., and Gostin, V.A. 1998. Facies and allostratigraphy of high-latitude, glacially influenced marine strata of the Early Permian southern Sydney Basin, Australia. Sedimentology, 45: 121-161.

Eyles, N., Doughty, M., Boyce, J.I., Mullins, H.T., Halfman, J.D., Koseoglu, B. 2003. Acoustic architecture of glaciolacustrine sediments deformed during zonal stagnation of the Laurentide Ice Sheet; Mazinaw Lake, Ontario, Canada. Sedimentary Geology, 157: 133-151.

França, A.B. and Potter, P.E. 1991. Stratigraphy and reservoir potential of glacial deposits of the Itararé Group (Carboniferous-Permian), Parana Basin, Brazil. AAPG Bulletin, 75(1): 62-85.

Friend, P.F., Slater, M.J., and Williams, R.C. 1979. Vertical and lateral building of river sandstone bodies, Ebro Basin, Spain. Journal of the Geological Society of Londay, 136: 39-46.

Funk, J.E., Slatt, R.M., and Pyles, D.R. Quantification of static connectivity between deep-water channels and stratigraphically adjacent architectural elements using outcrop analogs. AAPG Bulletin, 96(2), 277-300.

Gerber, R.E., Boyce, J.I. and Howard, K.W.F. 2001. Evaluation of heterogeneity and field-scale groundwater flow regime in a leaky till aquitard. Hydrogeology Journal, 9: 60-78.

Ghazi, S., and Mountney, N.P. 2009. Facies and architectural element analysis of a meandering fluvial succession: the Permian Warchha Sandstone, Salt Range, Pakison. Sedimentary Geology, 221: 99- 126.

Hansen, L., Beylich, A., Burki, V., Eilertsen, R.S., Fredin, O., Larsen, E., Lyså, A., Nesje, A., Stalsberg, K., and Tonnesen, J.D. 2009. Stratigraphic architecture and infill history of a deglaciated bedrock valley based on georadar, seismic profiling and drilling. Sedimentology, 56: 1751-1773.

Heinz, J., and Aigner, T. 2003. Hierarchical dynamic stratigraphy in various Quaternary gravel deposits, Rhine glacier area (SW Germany): implications for hydrostratigraphy. International Journal of Earth Science, 92: 923- 938.

Hjellbakk, A. 1997. Facies and fluvial architecture of a high-energy braided river: the Upper Proterozoic Seglodden Member, Varanger Peninsula, northern Norway. Sedimentary Geology, 114: 131- 161.

Hornung, J. and Aigner, T., 1999. Reservoir and aquifer characterization of fluvial architectural elements: Stubensandstein, Upper Triassic, southwest Germany. Sedimentary Geology, 129: 215- 280.

Hubbard, S.M., Romans, B.W., Graham, S.A. 2008. Deep-water foreland basin deposits of the Cerro Toro Formation, Magallanes basin, Chile: architectural elements of a sinuous basin axial channel belt. Sedimentology, 55: 1333-1359.

Huuse, M., Le Heron, D. P., Dixon, R., Redfern, J., Moscariello, A., and Craig, J. 2012. Glaciogenic reservoirs and hydrocarbon systems: an introduction. Geological Society of London, Special Publications, 368: 1-28.

James, N.P. and Dalrymple, R.W. 2010. Facies models. Geological Association of Canada, St. John's, Newfoundland

Kessler, T.C., Klint, K.E.S., Nilsson, B., and Bjerg, P.L. 2012. Characterization of sand lenses embedded in tills. Quaternary Science Reviews, 53: 55-71.

Kostic, B., and Aigner, T. 2007. Sedimentary architecture and 3D ground-penetrating radar analysis of gravelly meandering river deposits (Neckar Valley, SW Germany). Sedimentology, 54: 789- 808.

Labourdette, R. and Jones, R.R. 2007. Characterization of fluvial architectural elements using a three-dimensional outcrop data set: Escanilla braided system, South Central Pyrenees, Spain. Geosphere, 3: 422-434.

Marren, P. M., Russell, A. J., and Ruschmer, E.L. (2009). Sedimentology of a sandur formed by multiple jökulhlaups, Kverkfjöll, Iceland. Sedimentary Geology, 213: 77-88.

McKee, E.D. and Weir, G.W. 1953. Terminology for stratification and cross-stratification in sedimentary rocks. Bulletin of the Geological Society of America, 64: 381-390.

McPherson, J.G., Shanmugam, G., and Moiola, R.J. 1987. Fan-deltas and braid deltas: varieties of coarse-grained deltas. Geological Society of America, 99: 331-340.

Menzies, J., van der Meer, J.J.M., and Rose, J. 2006. Till- as a glacial "tectomict", its internal architecture, and the development of a "typing" method for till differentiation. Geomorphology, 75: 172-200.

Meyer, P.A. and Eyles, C. H. 2007. Nature and origin of sediments infilling poorly defined buried bedrock valleys adjacent to the Niagara Escarpment, southern Ontario, Canadian Journal of Earth Sciences, 44: 89- 105.

Miall, A.D. 1973. Markov chain analysis applied to an ancient alluvial plain succession. Sedimentology, 20: 347-364.

Miall, A.D. 1977. A review of the braided-river depositional environment. Earth-Science Reviews, 13: 1-62

Miall, A.D. 1985. Architectural-element analysis: A new method of facies analysis applied to fluvial deposits. Earth-Science Reviews, 22: 261-308.

Miall, A.D. 1988. Architectural elements and bounding surfaces in fluvial deposits: anatomy of the Kayenta Formation (Lower Jurassic), southwest Colorado. Sedimentary Geology, 55: 233-262.

Miall, A.D. 1989. Architectural elements and bounding surfaces in channelized clastic deposits: notes on comparisons between fluvial and turbidite systems. *In* Sedimentary Facies on the Active Plate Margin. *Edited by* A. Taira and F. Masuda. Terra Scientific Publishing Company (TERRAPUB), Tokyo.

Miall, A.D. 1994. Reconstructing fluvial macroform architecture from two-dimensional outcrops: examples from the Castlegate sandstone, Book Cliffs, Utah.

Miall, A.D. 1996. The geology of fluvial deposits. Berlin: Springer Verlag, p. 582.

Miall, A.D. and Jones, B.G. 2003. Fluvial architecture of the Hawkesbury Sandstone (Triassic), near Sydney, Australia. Journal of Sedimentary Research, 73(4), 531-545.

Miall, A.D., 2010. Alluvial Deposits. *In* Facies Models 4. *Edited* by N. P. James and R.W. Dalrymple. Geological Association of Canada, St. Johns, Newfoundland.

Miall, A.D. 2014. Fluvial depositional systems. Springer International Publishing, Switzerland, 316 p.

Opluštil, S., Martínek, K., and Tasáryová, A. 2005. Facies and architectural analysis of fluvial deposits of the Nýřany Member and the Týnec Formation (Westphalian D-Barruelian) in the Kladno-Rakovník and Pilsen basins. Bulletin of Geosciences, 80(1): 45-66.

Phillips, E.R., Evans, D.J.A., and Auton, C.A. 2002. Polyphase deformation at an oscillating ice margin folling the Loch Lomond Readvance, central Scotland, UK. Sedimentary Geology, 149: 157-182.

Pyles, D. R., 2007. Architectural elements in a ponded submarine fan, Carboniferous Ross Sandstone, western Ireland, in T. H. Nilsen, R.D. Shew, G. S. Steffens, and J. R. J. Studlick, eds., Atlas of deep-water outcrops: AAPG Studies in Geology 56, p. 206–209.

Slomka, J. 2011. Sedimentary architecture of shallow and deep subsurface Quaternary sediments, southern Ontario. M.Sc. thesis, School of Geography and Earth Sciences, McMaster University, Hamilton, Ontario, Canada.

Slomka, J.M. and Eyles, C.H. (2013). Characterizing heterogeneity in a glaciofluvial deposit using architectural elements, Limehouse, Ontario, Canada. Canadian Journal of Earth Sciences, 50: 911-929.

Terlaky, V., Rocheleau, J. and Arnott, R.W.C. (accepted) Stratal composition and component architectural elements of an ancient deep-marine basin-floor succession, Neoproterozoic Windermere Supergroup, British Columbia, Canada. Journal of Sedimentary Research, Online source: http://www.windermere.uottawa.ca/sites/default/files/secure/publications/Basin%20floor%20elements.pdf (2014-07-03)

Vail, P.R., Mitchum, R.M., Jr., and Thompson, S., III 1977. Seismic stratigraphy and global changes of seal level, Part 3: relative changes of sea level from coastal onlap. In M26: Seismic Stratigraphy- Applications to Hydrocarbon Exploration, American Association of Petroleum Geologists Special Volumes, A165: 63-81.

Walker, R.G. 1990. Perspective, facies modeling and sequence stratigraphy. Journal of Sedimentary Petrology, 60(5): 777-786.

Wilson, I. G. 1972. Aeolian bedforms- their development and origins. Sedimentology, 19: 173-210.

Yangquan, J., Jiaxin, Y., Sitian, L., Ruiqi, Y., Fengjiang, L., Shengke, Y. 2005. Architectural units and heterogeneity of channel reservoirs in the Karamay Formation, outcrop area of Karamay oil field, Junggar basin, northwest China. AAPG Bulletin, 89(4): 529-545.

Yuvaraj, S.V. 2011. Use of architectural-element analysis to interpret the depositional environment and reservoir characteristics of the Pictures Cliffs Sandstone, northern San Juan Basin, Colorado. M.Sc. Thesis. Bowling Green State University, U.S.A.

CHAPTER 2: INTERNAL ARCHITECTURE OF A TILL SHEET, TISKILWA FORMATION, NORTH-CENTRAL ILLINOIS, U.S.A.

Abstract

Thick till sheets deposited during the Quaternary form significant aquitards in many areas of North America. However, the detailed heterogeneity, architecture, and depositional history of till units are not well understood. This study utilizes architectural element analysis (AEA) to facilitate delineation of the internal architecture of the Tiskilwa Formation exposed at two outcrop sections in north-central Illinois, U.S.A. AEA is based on physical characteristics (nature of facies contacts and change in facies associations), delineation of sedimentary geometry, and understanding depositional processes at different scales of resolution. This allows for modification of AEA for analysis of sedimentary architecture in other depositional environments, including subglacial deposits. Eleven facies types are identified in this study, including sand, gravel, and diamict facies that record a suite of subglacial depositional processes. Detailed analysis of the nature and geometry of facies contacts (bounding surface hierarchy) and change in facies associations allows the delineation of five architectural elements, including coarse-grained lens, coarse-grained sheet, mixed zone, diamict lens, and diamict sheet elements. The spatial arrangement and genetic interpretation of elements and their spatial relationship to fifth-order bounding surfaces facilitates the delineation of five larger-scale architectural units ('element associations'), which can be mapped in the local study area and in turn record at least three stacked successions of meltwater accumulation and till deposition. The results of this study can be utilized for architectural analysis and paleoenvironmental reconstruction of till sheets in the study area and elsewhere.

2.1 INTRODUCTION

Thick successions of subglacial till deposited in North America by the Laurentide Ice Sheet during the Late Quaternary (Benn and Evans, 2010) form significant aquitards, and can also serve as a source of potable water due to the presence of coarse-grained interbeds (e.g. Rodvang and Simpkins, 2001). However, the heterogeneity, internal architecture, and precise mechanics of till are not well understood, and this results in inaccurate prediction of their three-dimensional facies geometry and control on water and contaminant migration to often deeper subsurface coarse-grained units (Boyce and Eyles, 2000; Gerber et al., 2001; Evans et al., 2006).

This study involves the analysis of a till unit (Tiskilwa Formation) exposed in two stream cuts in north-central Illinois (Fig. 2.1). The Tiskilwa Formation (Fm.) is a Late Quaternary-age (Michigan sub-episode of the Wisconsin Episode) till unit within the Wedron Group (Fig. 2.2) that was deposited by the Michigan Lobe of the LIS as it advanced southwestward out of the Michigan Basin (Hansel and Johnson, 1996; Hansel and McKay, 2010). The Tiskilwa Fm. is a major constituent of the Bloomington-Shelbyville Moraine complex (Fig. 2.1A, D) and overlies (and is interstratified with) several thick coarse-grained units (e.g. Henry Fm.) which form important aquifers for several communities in Illinois (Figs. 2.1, 2.2; Kempton et al., 1982). The sedimentological characteristics of the Tiskilwa Fm. have been described in outcrop studies (e.g. Johnson and Hansel, 1990; Carlson et al., 2004) and regional geological reports (e.g. Willman and Frye, 1970; Wickham and Johnson 1981; Wickham et al., 1988; Hansel and Johnson, 1996) as a homogeneous and massive till with a sandy texture, illite-

Fig. 2.1 Regional study area in north-central Illinois, U.S.A. (A) Significant geomorphic features and terrains (modified from Hansel and McKay, 2010). (B) Hillshade digital terrain model (DTM) draped with surficial geology and major geomorphic features (location of C shown in the box) in the Rattlesnake Hollow area. (C) Hillshade DTM with surficial geology showing the location of the two outcrop sections, Stop 1-3 (A-A') and Stop 1-5 (B-B'), in Rattlesnake Hollow near the Village of Hopewell (data from McKay et al., 2007 and ISGS et al., 2011). (D) Conceptual cross-section of till sheets of the Wedron Group, including end moraines formed during ice stagnation, and outwash deposits of the Mason Group from Shelbyville to Chicago (the geometry of diamict units is based on subsurface geological records analysed by the ISGS; modified from Hansel and McKay, 2010).

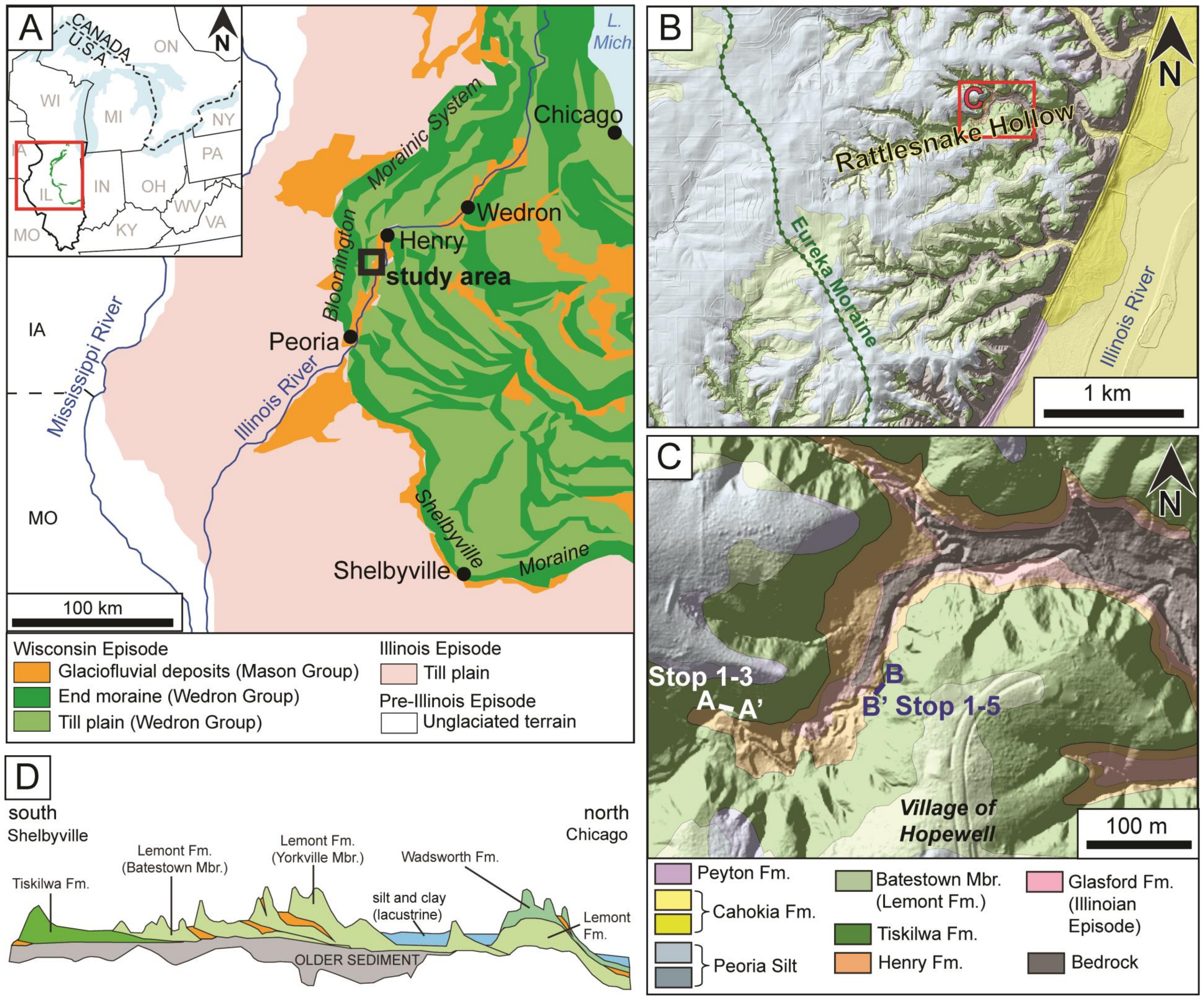
A
CANADA
U.S.A.
ON
N
WI
MI
NY
PA
IL
IN
OH
WV
VA
KY
MO
L. Mich
Chicago
Bloomington Morainic System
Wedron
Henry
study area
IA
Mississippi River
Peoria
Illinois River
MO
Shelbyville Moraine
Shelbyville
100 km
Wisconsin Episode
Glaciofluvial deposits (Mason Group)
End moraine (Wedron Group)
Till plain (Wedron Group)
Illinois Episode
Till plain
Pre-Illinois Episode
Unglaciated terrain
B
N
C
Rattlesnake Hollow
Eureka Moraine
Illinois River
1 km
C
N
Stop 1-3
A A'
B
B' Stop 1-5
Village of Hopewell
100 m
Peyton Fm.
Cahokia Fm.
Peoria Silt
Batestown Mbr. (Lemont Fm.)
Tiskilwa Fm.
Henry Fm.
Glasford Fm. (Illinoian Episode)
Bedrock
D
south
Shelbyville
north
Chicago
Tiskilwa Fm.
Lemont Fm. (Batestown Mbr.)
Lemont Fm. (Yorkville Mbr.)
Wadsworth Fm.
silt and clay (lacustrine)
Lemont Fm.
OLDER SEDIMENT

Fig. 2.2 Time-distance diagram of north-central Illinois during the Late Quaternary (Michigan Subepisode of the Wisconsinan Episode). (A) Approximate ice marginal position and corresponding glacial landforms and stratigraphic units from Peoria to Chicago (shading indicates deposition of Fms.). (B) Conceptual idealized log of the stratigraphy (assuming preservation of all units) near Wedron comprising the Wedron and Mason Groups (the full succession of units here may not be present at all locations; based on data from Johnson and Hansel, 1990; Hansel and Johnson, 1996; Carlson et al., 2004; Hansel and McKay, 2010).

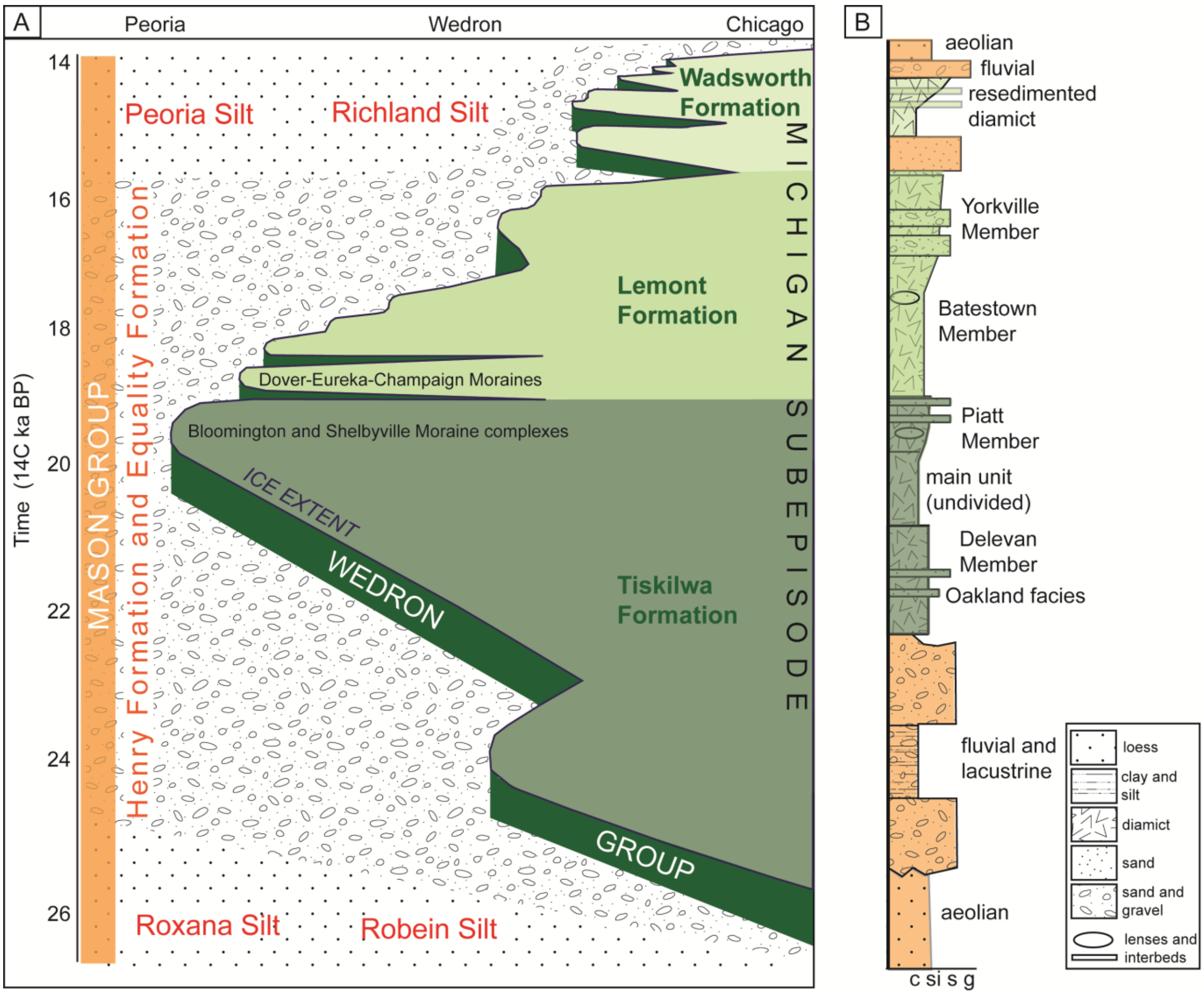
A
Peoria
Wedron
Chicago
Time (14C ka BP)
14
16
18
20
22
24
26
MASON GROUP
Henry Formation and Equality Formation
Peoria Silt
Richland Silt
Wadsworth Formation
Lemont Formation
Dover-Eureka-Champaign Moraines
Bloomington and Shelbyville Moraine complexes
ICE EXTENT
WEDRON
GROUP
Tiskilwa Formation
MICHIGAN SUBEPISODE
Roxana Silt
Robein Silt
B
aeolian
fluvial
resedimented diamict
Yorkville Member
Batestown Member
Piatt Member
main unit (undivided)
Delevan Member
Oakland facies
fluvial and lacustrine
aeolian
c si s g
loess
clay and silt
diamict
sand
sand and gravel
lenses and interbeds

rich mineral content, and rare coarse-grained interbeds. It comprises four subunits, including (from the bottom upward) the Oakland facies of the Delevan Member (grey diamict with abundant wood fragments), the main Delevan Member (a silt-rich heterogeneous grey diamict), the ‘main’ unit (previously described as massive and homogeneous diamict with a distinctive reddish colour), and the Piatt Member (a stratified heterogeneous grey diamict; Fig. 2; Willman and Frye, 1970; Johnson and Hansel, 1990; Hansel and Johnson, 1996; Carlson et al., 2004). Diamict facies of the Tiskilwa Fm. in Illinois have previously been interpreted as subglacial in origin because of their strong fabric direction that is consistent with ice paleoflow direction (Johnson and Hansel, 1990; Carlson et al., 2004), the presence of bullet-shaped clasts, boulder pavements, and shear planes (Johnson and Hansel, 1990), a regional spatial relationship to (and greatest thickness in) the Bloomington-Shelbyville Morainic System (Wickham et al., 1988), overconsolidated and structureless diamict facies characteristics, sharp and erosional facies contacts between diamict beds (Johnson and Hansel, 1990), and deformation and incorporation of underlying sand facies and wood fragments (Wickham et al., 1988; Johnson and Hansel, 1990; Carlson et al., 2004).

The objective of this paper is to delineate, describe, and visualize the internal architecture of the Tiskilwa Fm. using architectural element analysis (AEA). AEA facilitates understanding of the spatial relationship of system components (e.g. different types of bedforms in a fluvial system, or submarine fans and channels in a deep-water setting; Miall, 1985; Hubbard et al., 2008), the sedimentary architecture constructed as a result of shifting components over spatiotemporal scales, and the auto- and allogenic controls on the sedimentary architecture. The basic principles of AEA (packaging of facies associations and the hierarchy of bounding surfaces) are defined and utilized based on physical and visible sedimentological evidence; hence, they can be modified for the analysis of sediments deposited in different depositional environments. The vertical succession and spatial arrangement of facies associations and the nature of facies contacts are fundamental to the delineation of the bounding surface hierarchy of AEA, which is not reliant on relative base level change (sequence stratigraphic approach) and does not require identification of chronostratigraphic units or surfaces between different depositional environments (allostratigraphic approach); making AEA suitable for the analysis of complex glacial successions in non-marine settings.This analysis will facilitate a detailed interpretation of the depositional history of the Tiskilwa Fm. in the local study area and enhance understanding of its heterogeneity at a local-scale. The detailed internal sedimentary architecture of the Tiskilwa Fm. has not been previously documented; this study provides insight to the detailed architecture of the Tiskilwa Fm. in the local study area, and the paleoenvironmental and hydrostratigraphic significance of subunits within the till.

2.2 STUDY AREA AND METHODS

The study area is located in the Village of Hopewell, Illinois (roughly 150 km southwest of Chicago) within a forested ravine called Rattlesnake Hollow (Fig. 2.1; McKay et al., 2008). Two outcrop exposures (named ‘Stop 1-3’ and ‘Stop 1-5’) of the Tiskilwa Fm. were studied, located along the valley walls of an underfit ephemeral tributary stream to the modern Illinois River (Fig. 2.1). The outcrop exposure at Stop 1-3 is orientated orthogonal to ice paleoflow direction, and the exposure at Stop 1-5 is orientated parallel to ice paleoflow direction (Fig. 2.1; Carlson et al., 2004). The succession at Stop 1-3 is composed of a paleosol, the Sangamon Geosol (oldest), which is in turn overlain by a loess unit (>4 m thick), the Roxana Silt. These units are directly overlain by the glaciofluvial sand and gravel facies of the Henry Fm. and the Tiskilwa Fm. at the top of the succession (youngest) exposed at this site. At Stop 1-5, the lowermost unit comprises an Illinoian-age till, overlain by the Roxana Silt, Henry Fm., and Tiskilwa Fm. (Figs. 2.1, 2.2; McKay et al., 2008).

The outcrop faces were cleaned of debris with shovels, photographed from the base of the exposure, and logged where accessible. Five detailed sedimentological logs were recorded (RH1-RH5), which include data on grain size (x-axis), thickness (y-axis), primary and secondary sedimentary structure, clast shape, size, and lithology, and the nature of facies contacts (Fig. 2.3). A total of eleven facies types are recorded from outcrop in the sedimentological logs (Fig. 2.3), and include: matrix-supported diamict facies (massive/structureless, Dmm; deformed, Dmd; laminated, Dml; and stratified, Dms), sand facies (massive/structureless, Sm; deformed, Sd; and stratified sand, Ss), gravel facies (massive/structureless, Gm; deformed, Gd; and stratified, Gs), and fine-grained facies (massive/structureless and deformed, Fmd; Figs. 2.4-2.7).

Architectural element analysis (AEA) is a methodology that was developed for the delineation of sedimentary heterogeneity in fluvial sandstones exposed in outcrop (Allen, 1983; Miall, 1985). AEA is based on the concept of facies models (facies associations)

Fig. 2.3 Sedimentary logs recorded from outcrop exposures in Rattlesnake Hollow (the tops of logs are hung from the top of the exposed section and elevations are given in metres above mean sea level, m a.s.l.). (A) Outcrop Stop 1-3 (logs RH1-3). (B) Outcrop Stop 1-5 (logs RH4, 5). Facies codes indicate diamict facies (laminated, Dml; massive Dmm; deformed, Dmd; and stratified, Dms), sand facies (stratified, Ss; deformed, Sd; massive, Sm), gravel facies (stratified, Gs; massive, Gm; deformed, Gs), and fine-grained facies (Fmd). See Fig. 2.1 for outcrop locations and Figs. 2.4-2.7 for descriptions and photographs of facies types and contacts.

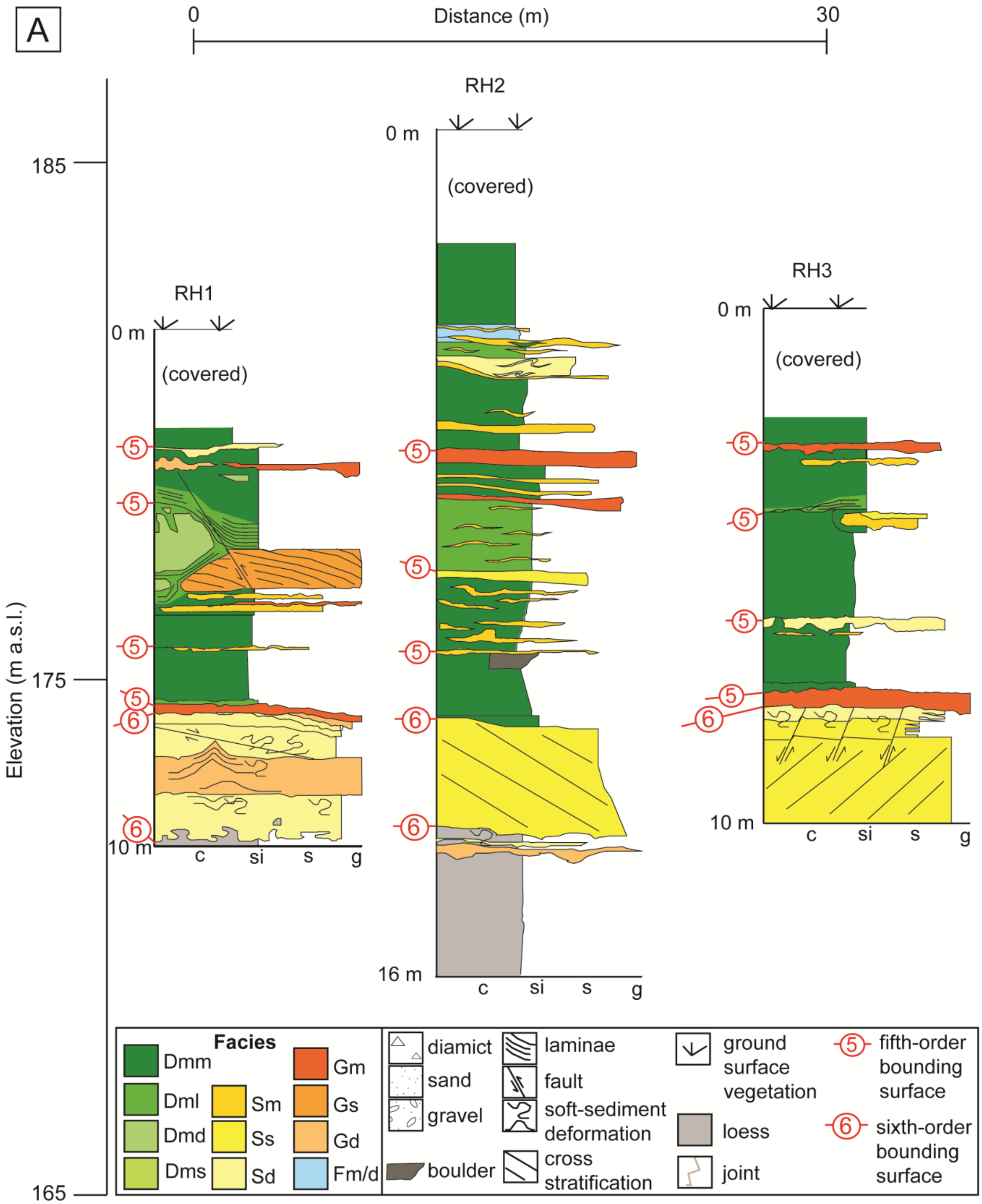
A
0
Distance (m)
30
Elevation (m a.s.l.)
185
175
165
RH1
RH2
RH3
0 m
(covered)
10 m
16 m
c si s g
5
6
Facies
Dmm
Dml
Dmd
Dms
Sm
Ss
Sd
Gm
Gs
Gd
Fm/d
diamict
sand
gravel
boulder
laminae
fault
soft-sediment deformation
cross stratification
ground surface vegetation
loess
joint
fifth-order bounding surface
sixth-order bounding surface

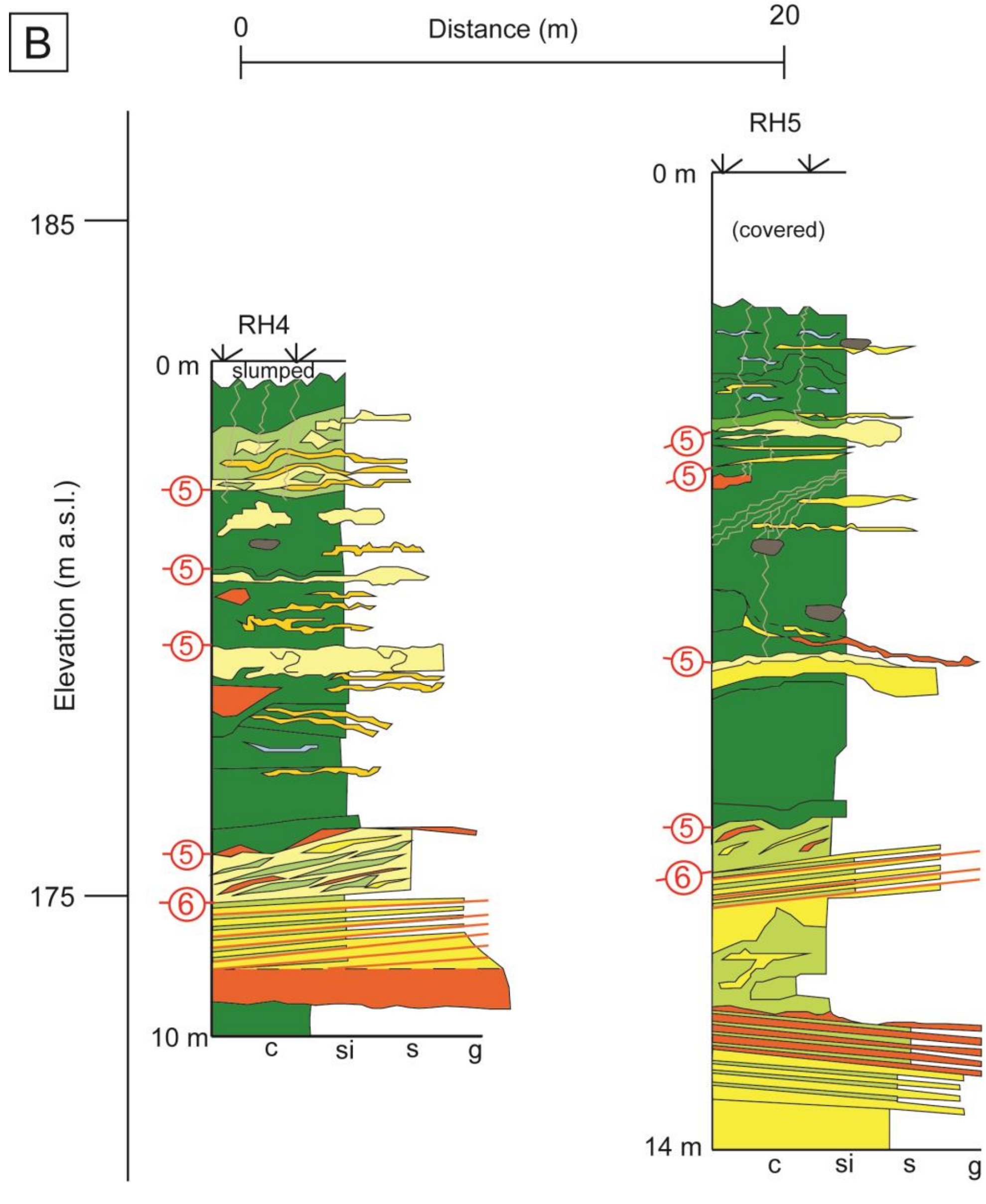
B
0
Distance (m)
20
RH5
0 m
(covered)
185
RH4
0 m
slumped
Elevation (m a.s.l.)
5
5
5
5
5
5
5
5
6
6
175
10 m
c
si
s
g
14 m
c
si
s
g

Table 2.1 Facies description and interpretation. Facies codes indicate diamict facies (matrix-supported laminated, Dml; massive Dmm; deformed, Dmd; and stratified, Dms), sand facies (stratified, Ss; deformed, Sd; massive, Sm), gravel facies (stratified, Gs; massive, Gm; deformed, Gs), and fine-grained facies (Fmd). See Figs. 2.4-2.6 for photographs of facies types (Miall, 1977, 2010; Eyles et al., 1983).

Facies	Grain size	Sedimentary structure	Interpretation
Dmm	Diamict. Grey to reddish brown clayey silt and silt matrix with gravel clasts throughout. Clasts are sub cm to 15 cm (rarely 20 cm) in diameter, angular to subrounded, and of local and far traveled litholgy	Matrix-supported, massive, blocky appearance, near vertical joints, laterally continuous beds up to 2 m thick and lenses	Interpreted to record complete homogenizaton of sediment during subglacial transport, and deposition of subglacial till by lodgement and meltout processes.
Dml	Diamict. Grey to reddish brown clayey silt and silt matrix with gravel clasts throughout. Clasts are sub cm to 15 cm (rarely 20 cm) in diameter, angular to subrounded, and of local and far traveled litholgy	Matrix-supported, apparently fissile and laminated (sub cm layers) with near parallel and bifurcating lineations, discontinuous beds up to 20 cm thick. Long axes of gravel clasts are crudely orientated along the lineations.	Laminae are interpreted to have been produced by shearing of diamict as a result of ice overburden pressure, low shear resistance of diamict, and subglacial transport (displacement).
Dms	Diamict. Light brown clayey silty matrix with gravel clasts throughout. Clasts are sub cm to 3 cm in diameter, angular to subrounded, and of local and far traveled litholgy	Matrix-supported diamict (dipping beds 1-3 cm thick) interbedded with poorly sorted sand and gravel facies	Interpreted to record subglacial or ice-marginal resedimentation of diamict by meltout and gravity flow, and glaciotectonization by shearing.
Dmd	Diamict. Red, grey, and reddish brown silty matrix with gravel clasts throughout. Clasts are sub cm to 10 cm in diameter, angular to subrounded, and of local and far traveled litholgy	Matrix-supported with evidence of deformation such as brecciation, folding, rotation, shear, and loading at facies contacts. Commonly interstratified with diamict and sand facies, laterally discontinuous	Interpreted to record erosion, entrainment, and deformation of previously deposited diamict during subglacial transport and density loading of diamict into underlying substrate material.
Sm	Sand. Fine- to very coarse-grained. Well to poorly sorted. Rare pebbly sand	Massive. Forms discontinuous lenses and pockets. Commonly enclosed in diamict facies	Penetrative glaciotectonization or rapid sedimentation of sand facies in a subglacial setting.
Sd	Sand. Fine- to very coarse-grained. Poorly sorted. Rare pebbly sand	Various deformation such as faulting (normal), folding, and shearing. Forms laterally continuous beds (up to 50 cm thick), discontuous and partially interconnected lenses, and isolated pods. Commonly enclosed in diamict facies	Glaciotectonization, deformation by water escape, and shear strain of sand facies in a subglacial setting.
Ss	Sand. Coarse- to very coarse-grained and pebbly sand.	Crude cross stratification. Forms discontinuous lenses within diamict facies and thin (up to 20 cm thick) beds within a larger pod of sand facies.	Interpeted to record sorting and deposition in a subaqueous environment, proabaly in a subglacial conduit or proglacial setting.
Gm	Gravel. Poorly sorted, granule- to cobble-sized clasts (round to subangular, various lithology), commonly contains a coarse- to very coarse-grained sand (and rare silt) matrix	Clast supported. Massive, no sedimentary structures nor stratification apparent. Forms laterally continuous beds up to 30 cm thick and isolated pods encased in diamict facies	Interpreted to record rapid sedimentation or sheet flow of gravel facies in a subaqueous setting, or penetrative glaciotectonization of gravel facies in a subglacial setting.
Gd	Gravel. Poorly sorted, granule-sized (rare cobble) clasts (subround to angular, various lithology), commonly contains a coarse- to very coarse-grained sand (and rare silt) matrix	Clast supported. Deformation of crudely stratified gravel, including shearing, folding, faulting (reverse), and rotation. No primary sedimentary structures apparent. Forms discontinuous beds up to 10 cm thick and isolated pods encased in diamict facies	Interpreted to record glaciotectonization of gravel facies in a subglacial depositional environment.
Gs	Gravel. Poorly sorted, granule- to cobble- sized clasts (round to subangular, various lithology), commonly contains a coarse- to very coarse-grained sand matrix	Clast-supported. Crude cross stratification. Forms isolated pods within diamict facies	Interpreted to record avalanching, rolling, and deposition of gravel clasts along foresets of a subaqueous bedform.
Fmd	Clay, silt and rare very fine-grained sand.	Micro- and macrofaults (normal faults are common), which cross-cut folds, shear planes, and loaded facies contacts. Form discontinuous stringers and lenses. Commonly interbedded with sand facies and enclosed in diamict facies.	Interpreted to record deposition of fine-grained facies by meltwater during ice stagnation, and subsequent deformation by glaciotectonization, water escape, and shear strain in a subglacial to ice-marginal depositional setting.

Fig. 2.4 Diamict facies (matrix-supported). (A) Laminated (Dml) diamict facies (laminations are millimetre-scale lineaments orientated subhorizontally across the photo). (B) Massive (Dmm) with near vertical joints. (C) Deformed (Dmd) diamict facies associated with massive sand facies (refer to Fig. 2.11H for Dmd facies associated with massive diamict facies). (D) Horizons of stratified (Dms) diamict facies interbedded with sand and gravel facies. See Table 2.1 for facies descriptions.

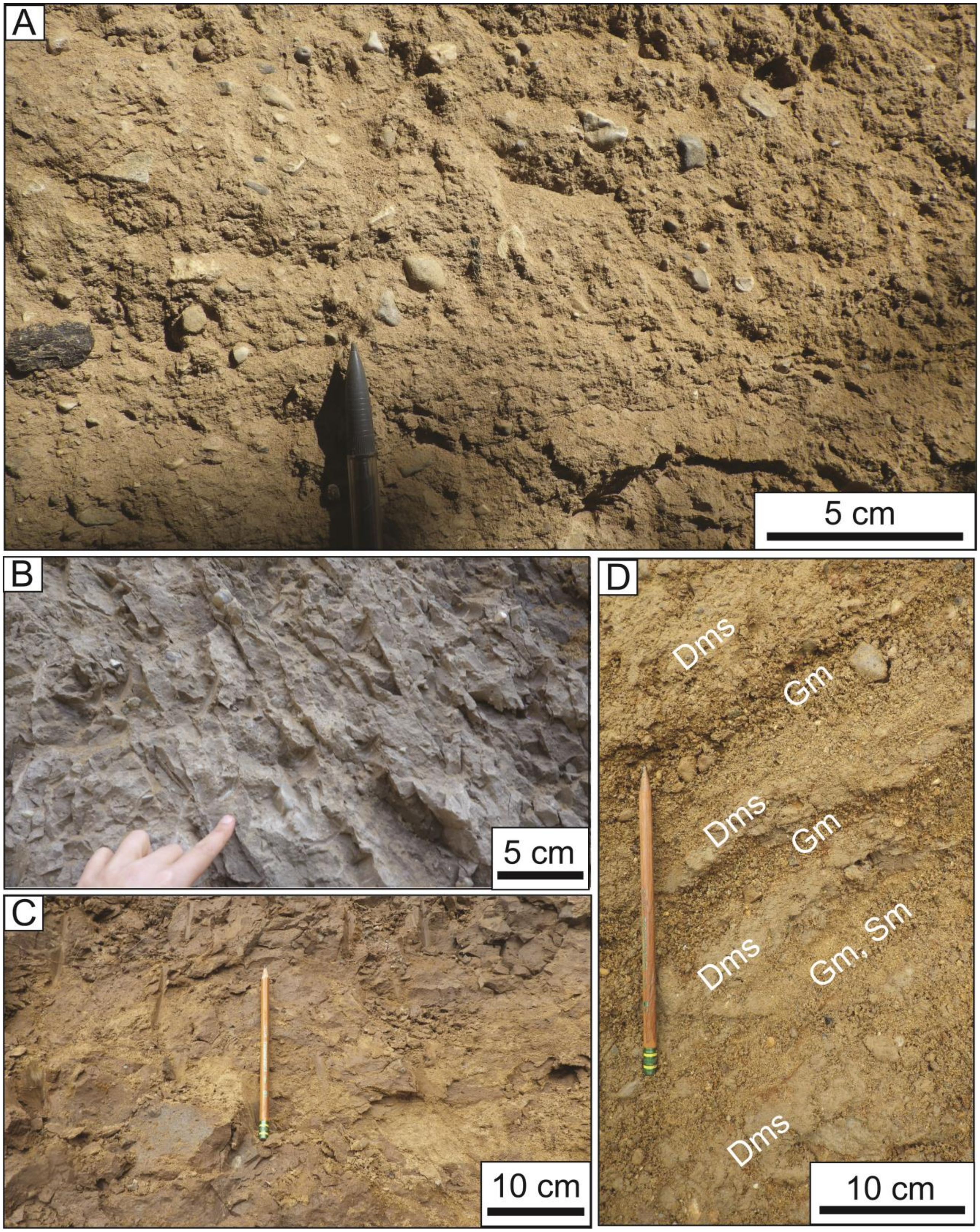
A
5 cm
B
5 cm
C
10 cm
D
Dms
Gm
Dms
Gm
Dms
Gm, Sm
Dms
10 cm

Fig. 2.5 Sand and fine-grained facies. (A) Stratified (Ss) sand facies. (B) Massive (Sm) sand facies underlying crudely stratified and deformed sand facies. (C) Fine-grained facies (Fmd) interbedded with massive and deformed diamict facies. (D) Deformed sand (Sd) and fine-grained (Fmd) facies. See Table 2.1 for facies descriptions.

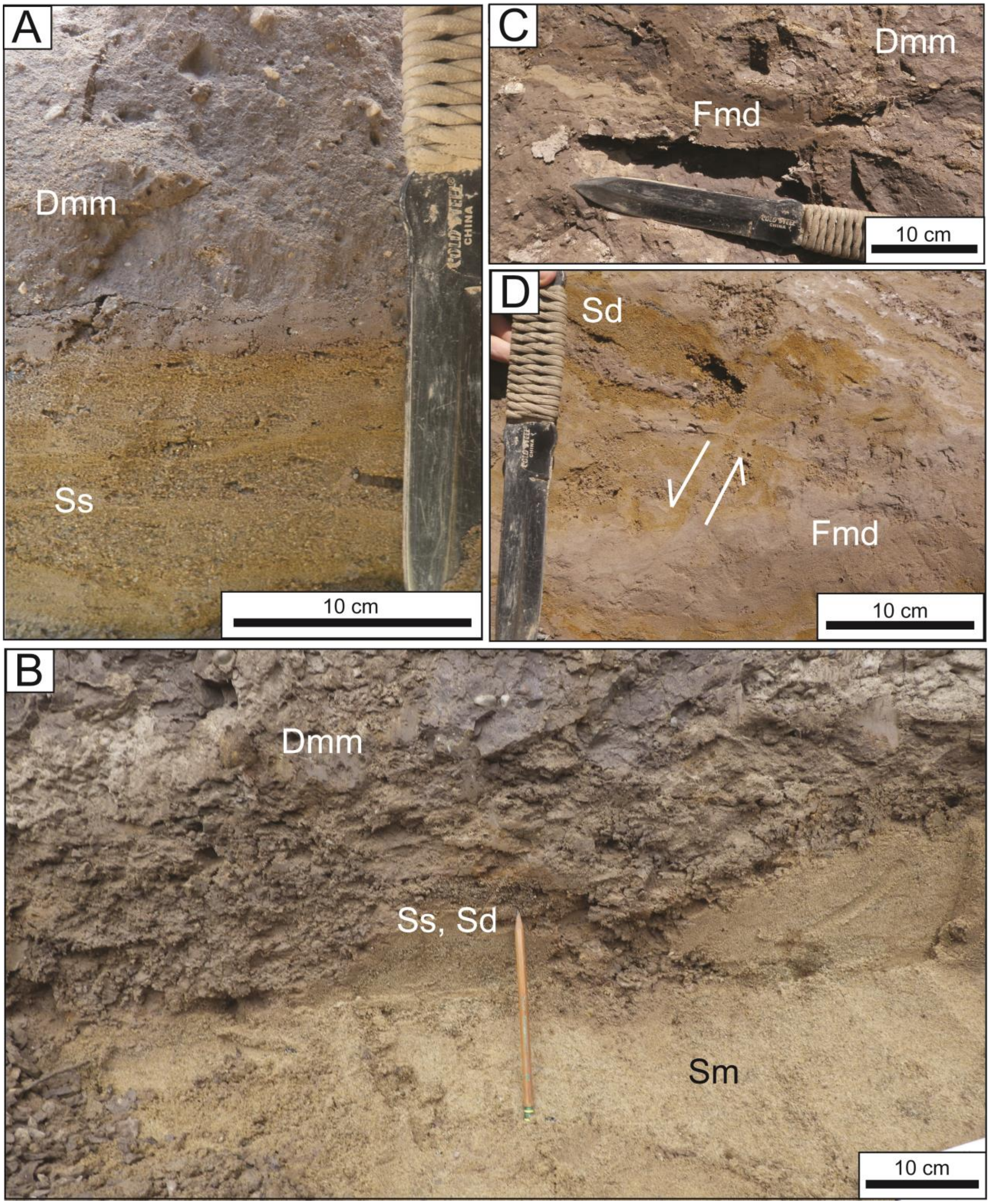
A
Dmm
Ss
10 cm
C
Dmm
Fmd
10 cm
D
Sd
Fmd
10 cm
B
Dmm
Ss, Sd
Sm
10 cm

Fig. 2.6 Gravel facies. (A) Stratified (Gm) gravel facies with crudely imbricated clasts along foresets dipping from the upper right to lower left of the photo. (B) Massive (Gm) gravel facies encased in diamict facies. (C) Deformed (Gd) gravel facies associated with deformed sand and diamict facies. (D) Deformed (Gd) gravel facies encased in diamict facies. See Table 2.1 for facies descriptions.

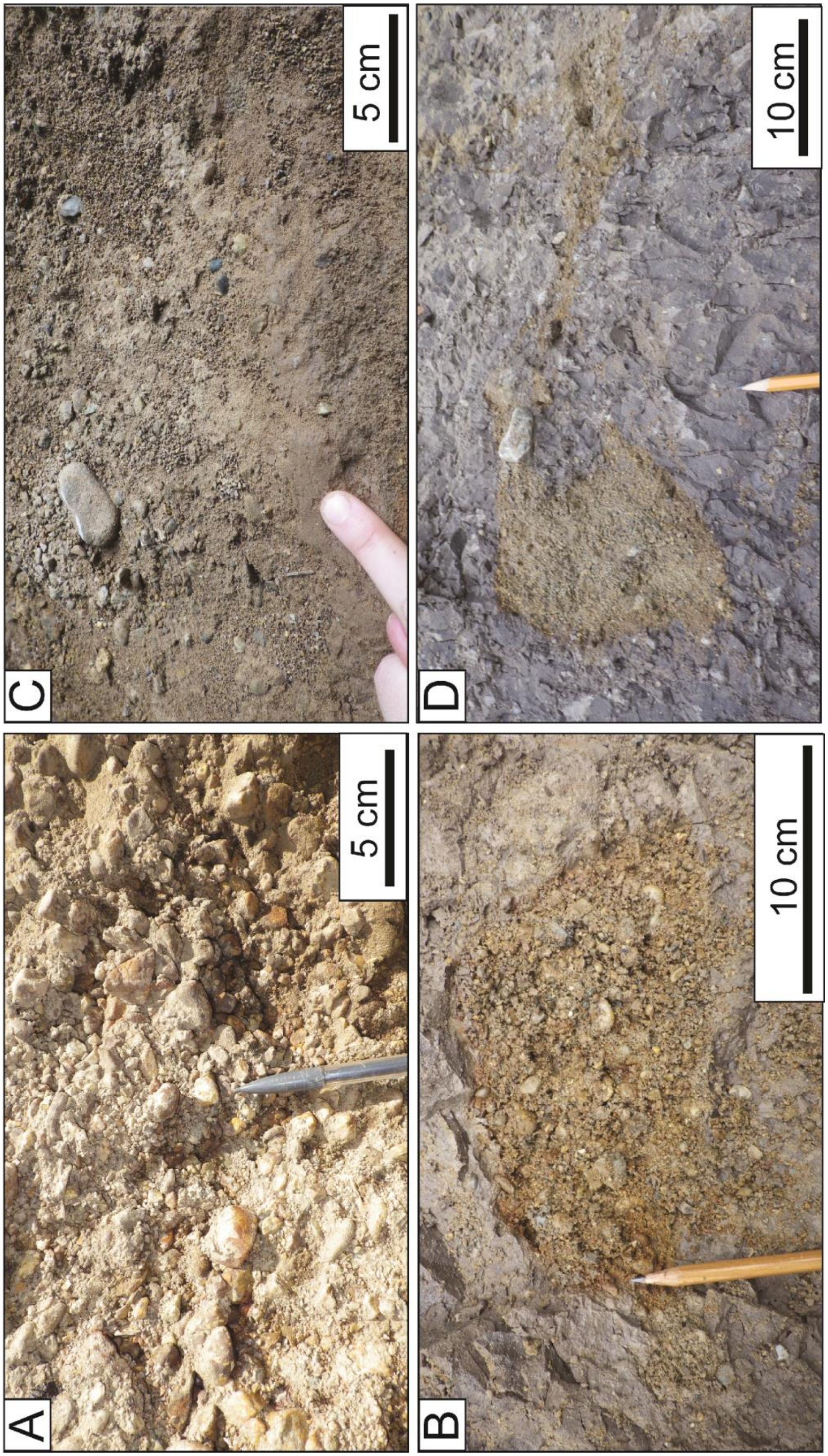
A
5 cm
B
10 cm
C
5 cm
D
10 cm

and early ideas of facies contacts and bedform hierarchies (Allen, 1963, 1968). It advances the facies model by including a geometric component; whereby AEA facilitates delineation of the 2- and 3-dimensional geometry and spatial relationship of facies associations at different scales of resolution within a hierarchical framework of bounding surfaces (Allen, 1983; Miall, 1985). This is a powerful methodology because it provides insight to the spatial configuration and relationship of facies associations, the evolution of a depositional system at different scales (e.g. individual beds and bedforms, to channels and valley trains), facilitates site-specific comparison of architectures, and allows field-derived data to be recorded and communicated in a geometric or object-based format that is easily translated to computer-based models (e.g. Deutsch and Tran, 2002) for other applications such as groundwater and hydrocarbon reservoir characterization.

AEA facilitates the characterization of sedimentary heterogeneity at various scales (e.g. Heinz and Aigner, 2003; Slomka and Eyles, 2013) and has been applied to the analysis of sediments of deep-marine (e.g. Clark and Pickering, 1996; Drinkwater and Pickering, 2001; Hubbard et al., 2008), fluvial (e.g. Miall, 1988; Hornung and Aigner, 1999; Ghazi and Mountney, 2009), and glacial (e.g. Boyce and Eyles, 2000) origin. The foundation of AEA is the delineation of a bounding surface hierarchy, which is assigned based on the degree of environmental change represented at each facies contact (Miall, 2010), and therefore provides the framework for systematic delineation of heterogeneity at various scales of resolution (Miall, 1988). A six-tiered bounding surface hierarchy was developed in this study (Fig. 2.7). Lower order surfaces (first- to fourth-order) record autogenic controls on the depositional system (e.g. bedform migration, scour of the bed by subglacial fluvial erosion, shearing and incremental deposition of diamicts by lodgement and plastering) and higher order surfaces (fifth- to seventh-order) record larger-scale allogenic controls acting on the depositional environment (e.g., climate, paleotopography, geothermal regime; Beerbower, 1964; Miall, 1988, 2010). First- to third-order surfaces are conformable facies contacts that record deposition under stable environmental conditions, such as bedding or lamination in diamict facies, or slight changes in depositional conditions (e.g., surfaces of reactivation recorded by cross-cutting erosional surfaces between diamict beds or shear laminae; Boyce and Eyles, 2000). Packages of facies associations delineated by fourth-order surfaces record deposition of genetically-related sediments with a distinct geometry and form ‘architectural elements’; these are the basic building blocks of a sedimentary deposit (Figs. 2.7-2.9; Beerbower, 1964; Miall, 1985). Facies associations bounded by even higher-order surfaces represent major changes within a depositional system (‘element associations’; fifth-order), a major environmental change resulting in the evolution of new depositional environments (may be equivalent to a stratigraphic unit; sixth-order), and the initiation of an entirely new basin fill (seventh-order; Fig. 2.7). In this study, bounding surfaces and facies types were delineated on sedimentological logs and field sketches, and elements were superimposed on photomosaics of outcrop faces (Figs. 2.3, 2.10).

The grouping of genetically-related facies (facies associations) with a characteristic geometry, bounded by fourth-order surfaces, allowed the characterization of five architectural elements (AEs). Architectural elements are named by utilizing

Fig. 2.7 Bounding surface hierarchy utilized in this study, including a sketch and corresponding field photograph of each order of bounding surface (DS, MZ, diamict and mixed zone elements; EA1, EA2, element associations 1 and 2; modified from Boyce and Eyles, 2000).

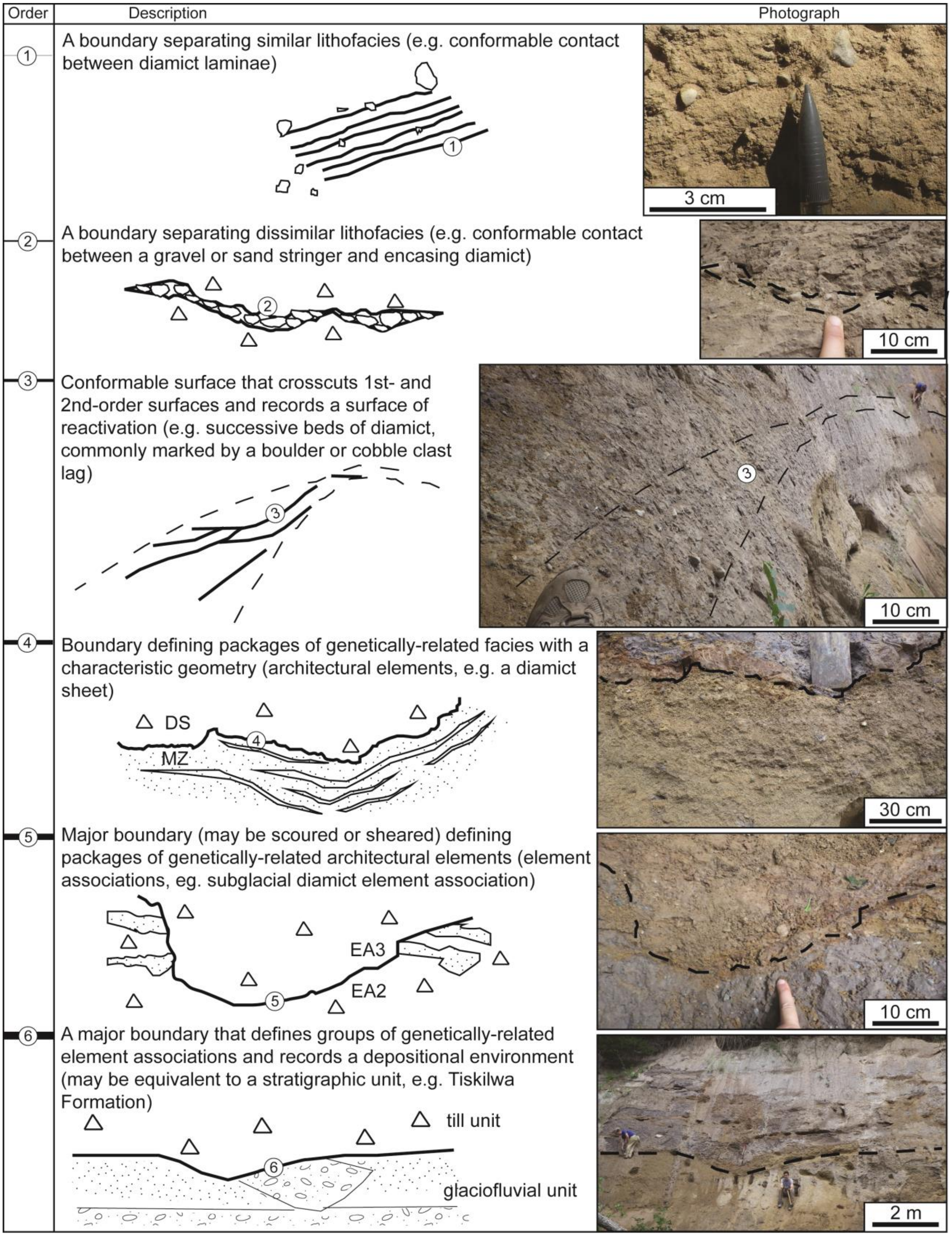
Order
Description
Photograph
1
A boundary separating similar lithofacies (e.g. conformable contact between diamict laminae)
3 cm
2
A boundary separating dissimilar lithofacies (e.g. conformable contact between a gravel or sand stringer and encasing diamict)
10 cm
3
Conformable surface that crosscuts 1st- and 2nd-order surfaces and records a surface of reactivation (e.g. successive beds of diamict, commonly marked by a boulder or cobble clast lag)
10 cm
4
Boundary defining packages of genetically-related facies with a characteristic geometry (architectural elements, e.g. a diamict sheet)
DS
MZ
30 cm
5
Major boundary (may be scoured or sheared) defining packages of genetically-related architectural elements (element associations, eg. subglacial diamict element association)
EA3
EA2
10 cm
6
A major boundary that defines groups of genetically-related element associations and records a depositional environment (may be equivalent to a stratigraphic unit, e.g. Tiskilwa Formation)
till unit
glaciofluvial unit
2 m

descriptive terminology including the predominant lithological characteristic (e.g. coarse-grained or mixed) and external geometry (e.g. lens or sheet; Bridge, 1993). Grouping of spatially- and genetically-related AEs and their relationship to fifth-order surfaces served as the basis for delineation of five larger-scale architectural units, termed element associations (EA1-5; Fig. 2.9). EAs are distinguished by their internal architecture and depositional history; hence, they are named using a variable combination of their characteristic architecture (e.g. multi-storey or complex), predominant facies or AE (e.g. diamict sheet or lens-dominated), and depositional processes (e.g. glaciotectonite).

2.3 ARCHITECTURAL ELEMENTS

The grouping of genetically-related facies bounded by fourth-order surfaces allowed the characterization of five architectural elements (AEs), including diamict sheet (DS), coarse-grained lens (CL), mixed zone (MZ), diamict lens (DL), and coarse-grained sheet (CS; Fig. 2.9). Genetically-related architectural elements are grouped to form five element associations (EA1-5; discussed in a later section).

2.3.1 Diamict sheet (DS) element

Description

The diamict sheet (DS) element is the most common element delineated in this study. DS elements have tabular, undulating geometries, and are predominately comprised of diamict facies (Dmm, Dmd, Dml; Fig. 2.4; see Table 2.1 for facies descriptions). DS elements recorded in this study are a few tens of centimetres to 1 meter thick and at least

20 metres wide. Upper and lower bounding surfaces are erosional to conformable in nature, and planar to irregular in geometry (Figs. 2.10, 2.11). Lower bounding surfaces are commonly erosional (e.g. Fig. 2.11I-M), and in places where erosion is not apparent, they are demarcated by a break in bedding and a change in facies. Lower bounding surfaces are commonly delineated across all or most of the outcrop section (at least 30 m wide). The location of the upper bounding surface of a DS element is most easily identified by delineating the lower bounding surface of an overlying deposit (e.g. diamict or coarse-grained sheet).

DS elements contain rare sand wisps (Sm facies; Fig. 2.11E, F) and gravel stringers (Gm facies; Figs. 2.7, 2.8) demarcated by second-order surfaces. Sand wisps (Fig. 2.11E just above the finger) and gravel stringers can be traced a few centimetres to tens of centimetres laterally across the outcrop section. They are irregular to elongate in shape. Gravel stringers are commonly a single clast in thickness to a few clasts thick (see Fig. 2.7). Sand stringers (annotated in Figs. 2.8C, 2.11F) are a few centimetres thick and have an elongate or ribbon-like geometry, and can be traced a few metres across the outcrop face. Stringers and wisps occur throughout the till. DS elements also contain discontinuous gravel lags (including faceted and striated boulders) overlying cross-cutting third-order surfaces (Figs. 2.8, 2.11F), and diamict lens (DL; Fig. 2.11J) and coarse-grained lens (CL; Figs. 2.8, 2.11H-M) elements bounded by fourth-order surfaces.

Interpretation

The DS element is interpreted to record deposition of a subglacial till bed by a combination of lodgement and deformation processes (Evans et al., 2006). The sand wisps and gravel stringers (second-order surfaces) are interpreted to record intensely sheared coarse-grained facies within the DS element, and gravel lags along cross-cutting third-order surfaces are interpreted to record clustering of clasts along local shear planes developed by deposition of till 'slices' during glacial overriding (Boulton and Paul, 1976; Benn and Evans, 1996; Boyce and Eyles, 2000). Gravel lags containing rare boulders may have been emplaced by lodgement onto the subglacial bed where frictional forces exceeded the applied force of flowing ice (Evans et al., 2006).

2.3.2 Coarse-grained Lens (CL) element

Description

Coarse-grained lens (CL) elements consist of massive (Sm) and deformed (Sd) medium- to coarse-grained sand facies (Fig. 2.5), massive (Gm), deformed (Gd) and crudely stratified (Gs) granule- to pebble-sized gravel facies (Fig. 2.6), and very rare fine-grained (Fmd) facies (Figs. 2.6, 2.8, 2.11H; Table 2.1). The bounding surface between CL elements and surrounding DS elements is sharp, irregular, and in some places shows evidence of shearing and ductile and brittle deformation (described below; Figs. 2.8, 2.11H, M).

Four sub-types of CL element geometries are recorded, including: pods, digitate pockets (with finger-like projections), irregular pockets, and spindles (Fig. 2.8). The two

Fig. 2.8 Subtypes of coarse-grained lens (CL) geometries photographed on outcrop exposures. (A) Pods (gravel facies). (B) Digitate pocket. (C) Irregular pocket (sand stringers directly overlie the pencil). (D) Spindle (sand-facies; CL in parentheses is an irregular pocket). (E) Irregular sand pocket with faults, including normal and reverse faults and horizontal surfaces of displacement (shear plane). (F) Irregular gravel pocket with a zone of horizontal displacement surfaces (shear planes). (G) Irregular-shaped CL elements interconnected by a sand bed (Stop 1-3).

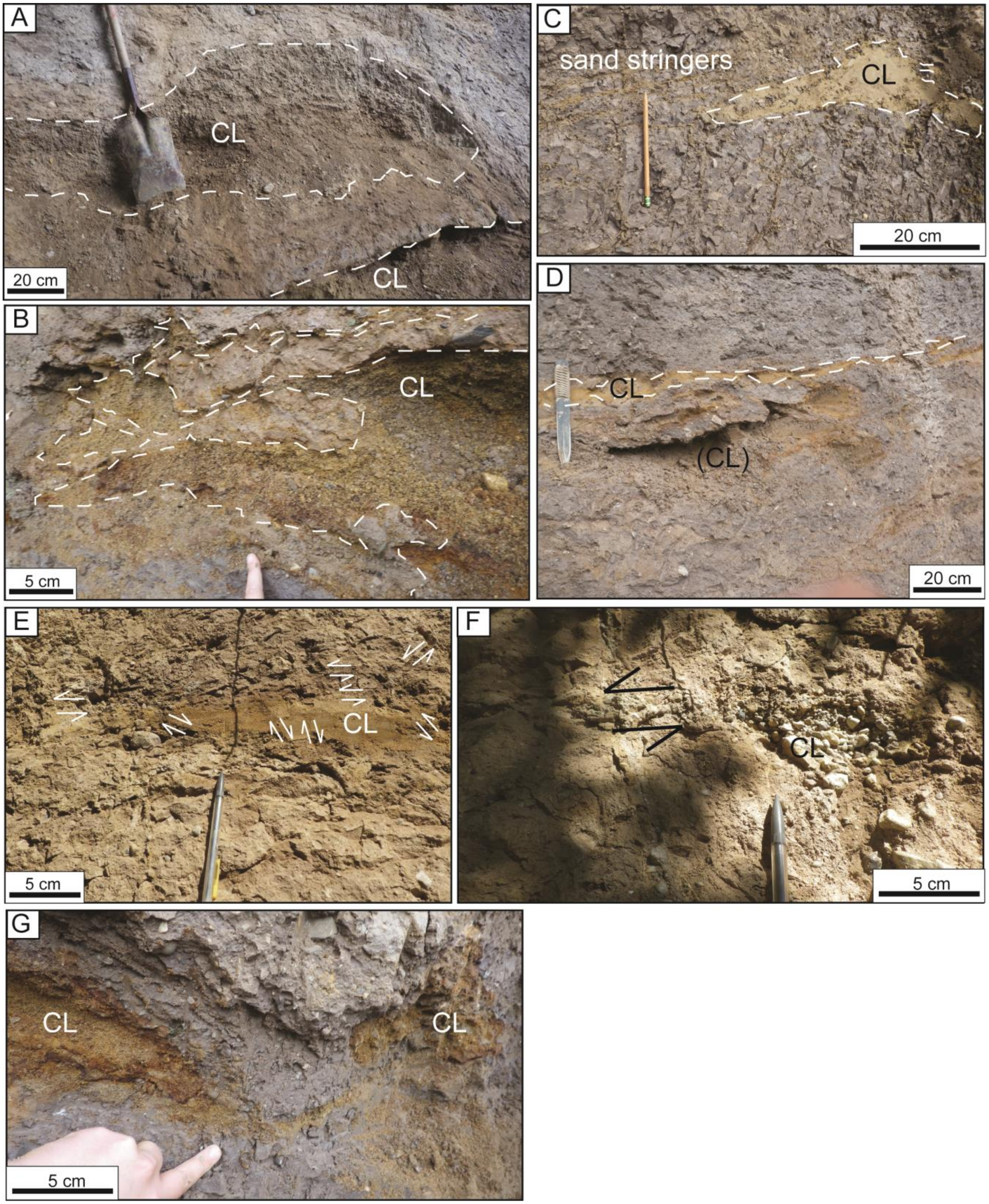
A
CL
CL
20 cm
B
CL
5 cm
C
sand stringers
CL
20 cm
D
CL
(CL)
20 cm
E
CL
5 cm
F
CL
5 cm
G
CL
CL
5 cm

most common geometries of CL elements are irregular pockets (Fig. 2.8C) and spindles (Fig. 2.8D), which can be either disconnected (fully encased in diamict facies) or interconnected (maintain topology or by thin sand stringers between CL elements; Fig. 2.8G). Irregular CL elements are 1-40 cm thick and 20 cm-1 m wide, and commonly form distinct horizons on the exposed outcrop face, separated in the vertical direction by DS elements (Figs. 2.10, 2.11H). Irregular CL elements are composed of massive and deformed sand and gravel facies with rare crudely cross-bedded sand facies and massive and deformed fine-grained facies (Table 2.1). Spindles form thin, elongated lenses (1-15 cm thick and 50 cm-2 m wide), and are composed of deformed and massive sand and gravel facies that do not contain any primary sedimentary structure. Spindles and irregular CL elements contain normal faults (and rare reverse faults) and their upper surface is commonly deformed and displaced by horizontal subparallel lineations that can be traced into the surrounding diamict element along which sand and gravel facies appear to be attenuated from the main body of the CL element (Fig. 2.8E,F). The upper surface commonly contains planar layers of sand and gravel facies, along which the long axes of gravel clasts (within the CL elements and overlying DS elements) appear to crudely align and form sand and gravel stringers on the lee side (down ice paleoflow direction) of CL elements.

Pods form isolated, lens-shaped elements that are 0.5-1m thick and 1-1.5m wide, and consist of gravel facies (Gm, Gs, Gd) that show evidence of brittle deformation in the form of reverse faults throughout the pods and which is most apparent on their upper surface (Figs. 2.8A; 2.11J). Digitate pockets are the least common CL element, and consist of highly deformed sand and gravel facies (and rare deformed and massive fine-grained facies and crudely cross-bedded sand facies) forming discontinuous, interconnected lenses that interfinger with diamict facies (Fig. 2.8B). CL elements contain piping features that form hollows in the outcrop face, and mineral precipitation (dark-coloured) and oxidation (orange-yellow) of sand and gravel facies, causing discoloration of CL elements.

Interpretation

CL elements are interpreted to have formed in a subglacial depositional environment, either in subglaciofluvial conduits or by subglacial entrainment and deformation of coarse-grained substrate material (Kessler et al., 2012). Deformed facies and the paucity of primary sedimentary structure within irregular, spindle, and digitate CL elements is interpreted to record soft-sediment deformation, which may have occurred concurrently or after deposition of these sediments in a subglacial setting or during entrainment of CL elements in a subglacial traction zone. Normal and reverse faults cross cut and offset deformed and massive facies within CL elements, and are interpreted to record post-depositional brittle deformation, likely as a result of glaciotectonization in a subglacial depositional setting. The Gs facies within pods (Figs. 2.6A, 2.8A) may reflect rigid-body conditions whereby they resisted intense shear deformation, which allowed for preservation of primary sedimentary structure (Boulton and Hindmarsh, 1987). The horizontal planes and zones of displacement on the upper surface of CL elements (Fig. 2.8E, F) are interpreted to record a shear plane or zone of multiple shear planes, which likely formed as a result of subglacial glaciotectonization by overriding ice (Hart and Boulton, 1991).

The irregular, spindle, and digitate CL elements are composed of deformed and massive sand, gravel, and rare fine-grained facies, and primary sedimentary structure (crudely cross-bedded sand facies) is rare. Hence, the geometry and spatial arrangement of these CL elements, and the nature of their bounding surfaces (e.g. sheared, deformed, erosional) are utilized to interpret their depositional history. Digitate and irregular pocket-shaped CL elements that are commonly interconnected and form distinct horizons at a similar stratigraphic position on the outcrop face (Fig. 2.10) are interpreted to have formed concurrently, and may have been deposited in subglacial canals (Walder and Fowler, 1994) likely during periods of ice-bed separation and high meltwater and sediment discharge (similar to coarse-grained lenses described by Boyce and Eyles, 2000; Meriano and Eyles, 2009). Isolated, disconnected CL elements within diamict sheet (DS) elements are interpreted to record entrainment of substratum sand facies in a subglacial deforming till bed. Spindle-shaped CL elements are interpreted to record subglacial shear and elongation or attenuation of previously deposited (irregular and digitate?) CL elements (Hart and Boulton, 1991; Kessler et al., 2012).

2.3.3 Mixed Zone (MZ) element

Description

The MZ element is located at the base of the till sheet (composing EA1) and comprises highly deformed, massive, and crudely stratified gravel, sand, and diamict facies (Fig.

2.11A-D; Table 2.1). MZ elements are >5 m wide, 5-50 cm thick, and can be traced laterally across the outcrop face. They form an irregular, undulating sheet-like geometry (Fig. 2.10). The lower bounding surface of MZ elements is highly irregular, sharp, and erosional, and rarely gradational in some places with underlying glaciofluvial sand and gravel facies (Fig. 2.11A). In the thickest parts of MZ elements, diamict facies (Dmd and Dms) form thin (0.5-3 cm thick), discontinuous beds with a 'pinch and swell' or boudinaged geometry that can be traced laterally for at least 1 m across the outcrop face (Fig. 2.11B). Sand, gravel, and diamict facies within the thickest part of the MZ elements form discontinuous, deformed and attenuated or elongated layers that have a stratified appearance (Fig. 2.11B). The thinnest parts of MZ elements are composed of massive sand-rich gravel facies. The upper bounding surface of MZ elements is sharp and planar to undulating, and rarely gradational where sand is incorporated into the lowermost 5 cm of overlying diamict facies (of EA2; Figs. 2.9; 2.11C, D).

Interpretation

The MZ elements are interpreted to have formed in a subglacial shear zone between the glacier sole and bed (Hart and Boulton, 1991; Piotrowski et al., 2006). Large-scale deformation structures are not apparent or recorded here; however, this element is interpreted as a subglacial shear zone based on its facies characteristics including an erosional lower surface, apparently elongated or stretched subparallel layers of sand, gravel (with very rare preservation of primary sedimentary structure), and diamict facies, the ‘pinch and swell’ geometry of diamict facies which suggests extension forming boudins (Fig. 2.11B,C), and its stratigraphic position (directly above the Henry Fm sands and gravels and at the base of the Tiskilwa till). It is similar in appearance to the shear zone of Phillips et al. (2002), the upper deformed sand of Larsen and Piotrowski (2003), and the lower part of Till Unit A of Piotrowski et al. (2006), and may be similar to the mixing zone of Hooyer and Iverson (2000).

MZ elements are interpreted to record intense subglacial glaciotectonism of the uppermost part of the underlying glaciofluvial sediment (Wickham et al., 1988; Benn and Evans, 1996) beneath the glacier sole, which likely involved intense shearing, ductile deformation, and complete reworking of the original primary sedimentary structure. Thin, discontinuous beds of diamict were likely entrained from the overlying glacier sole and subsequently sheared to form boudinaged geometries (Larsen and Piotrowski, 2003; Evans et al., 2006).

2.3.4 Diamict Lens (DL) element

Description

Diamict lens (DL) elements are most commonly recognized in the mid-section of the Stop 1-3 outcrop exposure (Fig. 2.10). DL elements consist of massive and deformed diamict facies which form irregular pod-like geometries that are commonly brecciated or fragmented, with the interstices infilled with laminated and massive diamict facies (originating from the surrounding DS element; Figs. 2.4, 2.11J; Table 2.1). DL elements are embedded in DS elements and readily distinguished by a change in matrix colour (due to differences in mineralogy or groundwater staining), grain size of matrix material and gravel clasts, and facies characteristics such as a massive, blocky appearance (Figs. 2.3A, 2.11J,K; Table 2.1). DL elements are composed of similar facies (Dmm) to the diamict sheet (DS) element of EA2 and, in places, appear to originate from diamict facies 'ripped up' from EA2 (Fig. 2.11K). The facies contact between DL and DS elements is sharp and conformable, and, in places, gradational with the surrounding laminated diamict facies of the DS element.

Interpretation

The facies characteristics and matrix colour of the DL elements is similar to that of the diamict sheet (DS) element of EA2 (Fig. 2.11D-G). Hence, DL elements are interpreted to record entrainment of rafts of previously deposited till into the subglacial traction zone through subglacial erosion and deformation, and rotation and brecciation of DL elements during subglacial transport (Evans et al., 2006).

2.3.5 Coarse-grained Sheet (CS) element

Description

The coarse-grained sheet (CS) element is observed in the Stop 1-5 outcrop exposure, where it forms a laterally continuous tabular bed (10-50cm thick) that can be continuously traced for at least 5 m across the outcrop face (Fig. 2.10B). The lower bounding surface of the CS element is sharp, erosional and irregular to planar, and directly overlies a DS element. The upper bounding surface is loaded with irregular bodies of massive and deformed diamict facies that protrude downwards into the CS element from the overlying DS element (Fig. 2.11G).

This element is comprised of deformed sand and gravel facies, stratified and deformed diamict facies, and rare discontinuous and deformed lenses of fine-grained facies (Fig. 2.11G). Internal facies are bounded by gently to steeply dipping (10 to 40 degrees) erosional facies contacts (commonly overlain by thin beds of diamict) and cross cut by normal faults. Brecciated diamict lenses within deformed sand and gravel facies are common near the upper part of the CS element. Evidence of soft-sediment deformation as a result of dewatering is common in sand facies (Sd), which do not contain any preserved primary sedimentary structures.

Interpretation

The CS element is interpreted to record deposition of sand and gravel facies by meltwater in a laterally shifting or unstable subglacial canal system, probably as a result of high porewater pressure on the bed and subsequent ice-bed separation (Walder and Fowler, 1994; Ng, 2000). This element is interpreted to have formed in a subglaciofluvial depositional setting on the basis of its stratigraphic position (located between two diamict sheet elements of EA2 and EA3), geometry (irregular and laterally continuous sheet), the nature of its bounding surfaces (planar to irregular and erosional lower surface and loaded to deformed upper surface), cross-cutting relationship of beds and thin interbeds of diamict stringers and lenses, crudely preserved bedding (layers and pockets of different grain sizes), and the absence of well-defined kinematic evidence commonly associated with glaciotectonization of coarse-grained sediment rafts such as folds, sand augens, boudins, attenuated layers, and thrust faults (e.g. Lee and Phillips, 2008).

Diamict beds and brecciated lenses within CS elements probably resulted from direct meltout or meltwater erosion of overlying till from the basal debris zone, and subsequent deposition within the subglacial conduit. Shearing and loading of facies within the upper part of the CS element probably occurred after the glacier sole reattached to its bed, and brittle and ductile deformation of the CS element in the form of faulting and dewatering is likely a post-depositional product as a result of ice-bed re-attachment or collapse of ice- or sediment-supported conduit walls (Boulton and Hindmarsh, 1987).

2.4 ELEMENT ASSOCIATIONS (EAs)

Grouping of genetically-related architectural elements within the Tiskilwa Fm. and their relationship to fifth-order bounding surfaces allowed the delineation of five element associations (EAs), which are the largest-scale architectural subunits that can be correlated and mapped across a local study area within a depositional environment (e.g. Slomka and Eyles, 2013; Figs. 2.9, 2.10, 2.12). EAs are identified on the basis of internal facies and their architecture (including facies geometry, spatial arrangement, and spatial relationship to internal bounding surfaces) and external form (geometry of packages of spatially- and genetically-related AEs and the nature of bounding surfaces delineating these packages; Figs. 2.10, 2.11). The architecture of individual EAs (i.e. spatial arrangement and relationship of elements and hierarchy of bounding surfaces) provide insight to major spatiotemporal changes in depositional conditions (controlled by allo- and autogenic processes) within a depositional environment (Beerbower, 1964; Miall, 2010; Slomka and Eyles, 2013).

Fig. 2.9 Architectural hierarchy of the Tiskilwa Fm. at various scales of resolution (depositional environment or stratigraphic unit, element association, architectural element, and facies), including descriptions of architectural elements as recorded in this study. Facies codes indicate diamict facies (laminated, Dml; massive Dmm; deformed, Dmd; and stratified, Dms), sand facies (stratified, Ss; deformed, Sd; massive, Sm), gravel facies (stratified, Gs; massive, Gm; deformed, Gs), and fine-grained facies (Fmd). See Table 2.1 for facies descriptions and Fig. 2.10 for element associations delineated on outcrop and correlated across the local study area.

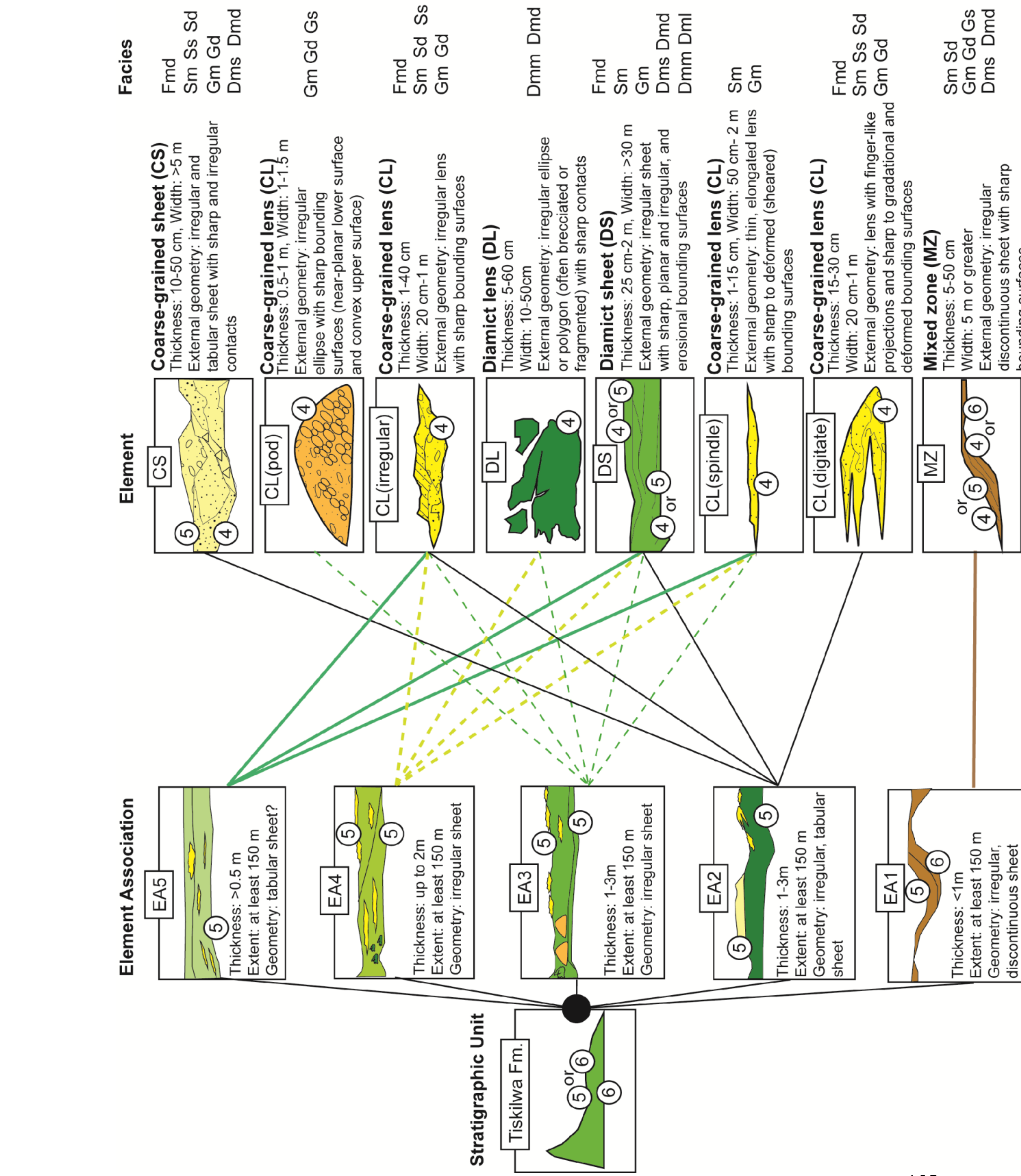
Stratigraphic Unit
Tiskilwa Fm.
5 or 6
6
Element Association
EA5
5
Thickness: >0.5 m
Extent: at least 150 m
Geometry: tabular sheet?
EA4
5
5
Thickness: up to 2m
Extent: at least 150 m
Geometry: irregular sheet
EA3
5
5
Thickness: 1-3m
Extent: at least 150 m
Geometry: irregular sheet
EA2
5
5
Thickness: 1-3m
Extent: at least 150 m
Geometry: irregular, tabular sheet
EA1
5
6
Thickness: <1m
Extent: at least 150 m
Geometry: irregular, discontinuous sheet
Element
CS
5
4
CL(pod)
4
CL(irregular)
4
DL
4
DS
4 or 5
4 or 5
CL(spindle)
4
CL(digitate)
4
MZ
4 or 5
4 or 6
Coarse-grained sheet (CS)
Thickness: 10-50 cm, Width: >5 m
External geometry: irregular and tabular sheet with sharp and irregular contacts
Coarse-grained lens (CL)
Thickness: 0.5-1 m, Width: 1-1.5 m
External geometry: irregular ellipse with sharp bounding surfaces (near-planar lower surface and convex upper surface)
Coarse-grained lens (CL)
Thickness: 1-40 cm
Width: 20 cm-1 m
External geometry: irregular lens with sharp bounding surfaces
Diamict lens (DL)
Thickness: 5-60 cm
Width: 10-50cm
External geometry: irregular ellipse or polygon (often brecciated or fragmented) with sharp contacts
Diamict sheet (DS)
Thickness: 25 cm-2 m, Width: >30 m
External geometry: irregular sheet with sharp, planar and irregular, and erosional bounding surfaces
Coarse-grained lens (CL)
Thickness: 1-15 cm, Width: 50 cm- 2 m
External geometry: thin, elongated lens with sharp to deformed (sheared) bounding surfaces
Coarse-grained lens (CL)
Thickness: 15-30 cm
Width: 20 cm-1 m
External geometry: lens with finger-like projections and sharp to gradational and deformed bounding surfaces
Mixed zone (MZ)
Thickness: 5-50 cm
Width: 5 m or greater
External geometry: irregular discontinuous sheet with sharp bounding surfaces
Facies
Fmd
Sm Ss Sd
Gm Gd
Dms Dmd
Gm Gd Gs
Fmd
Sm Sd Ss
Gm Gd
Dmm Dmd
Fmd
Sm
Gm
Dms Dmd
Dmm Dml
Sm
Gm
Fmd
Sm Ss Sd
Gm Gd
Sm Sd
Gm Gd Gs
Dms Dmd

Fig. 2.10 Bounding surfaces, architectural elements (AEs), and element associations (EAs) delineated on photomosaics of the two outcrop faces. (A) Stop 1-3, orientated northwest to southeast. (B) Stop 1-5, orientated northeast to southwest. The upper image is a photomosaic of the outcrop face, the middle image includes the outcrop face with bounding surfaces delineated by white lines (thickest lines indicate sixth-order surfaces, medium-width lines indicate fifth-order surfaces, and thin lines indicate fourth-order surfaces of DS, CS and MZ elements), and the bottom image is a sketch of the outcrop face with AEs and bounding surfaces (note fourth-order surfaces bound all AEs). Dashed lines indicate parts of a surface that are fully or partially covered by debris and the red line outlines the fully exposed part of the outcrop face. AEs include mixed zone (MZ), coarse-grained lens (CL), coarse-grained sheet (CS), diamict lens (DL), and diamict sheet (DS) elements. Refer to Fig. 2.1 for outcrop locations, Fig. 2.3 for logs (RH1-5), and Fig. 2.9 for the internal composition of elements and element associations.

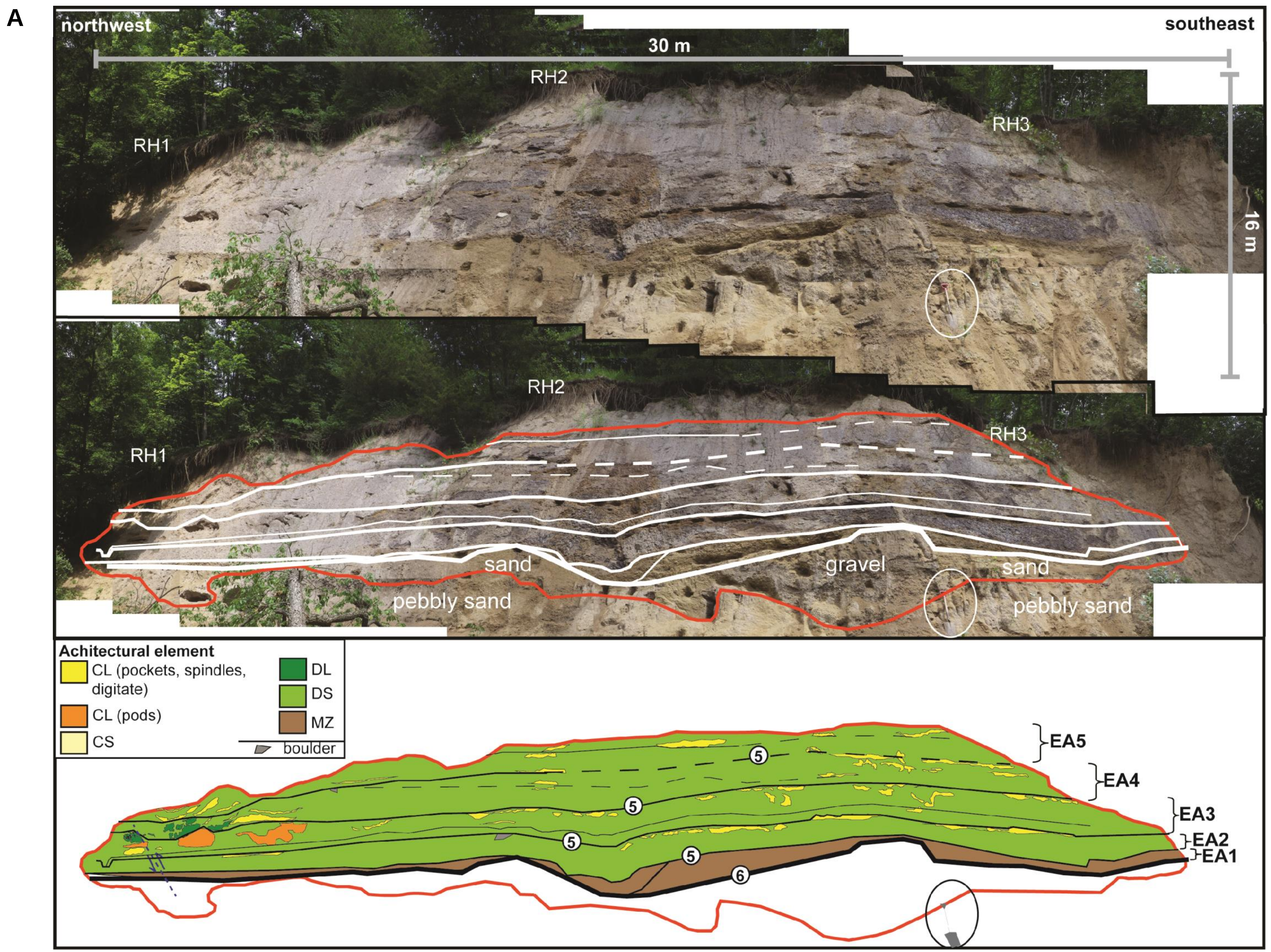
A
northwest
southeast
30 m
16 m
RH1
RH2
RH3
sand
gravel
sand
pebbly sand
pebbly sand
Achitectural element
CL (pockets, spindles, digitate)
CL (pods)
CS
DL
DS
MZ
boulder
EA5
EA4
EA3
EA2
EA1
5
6

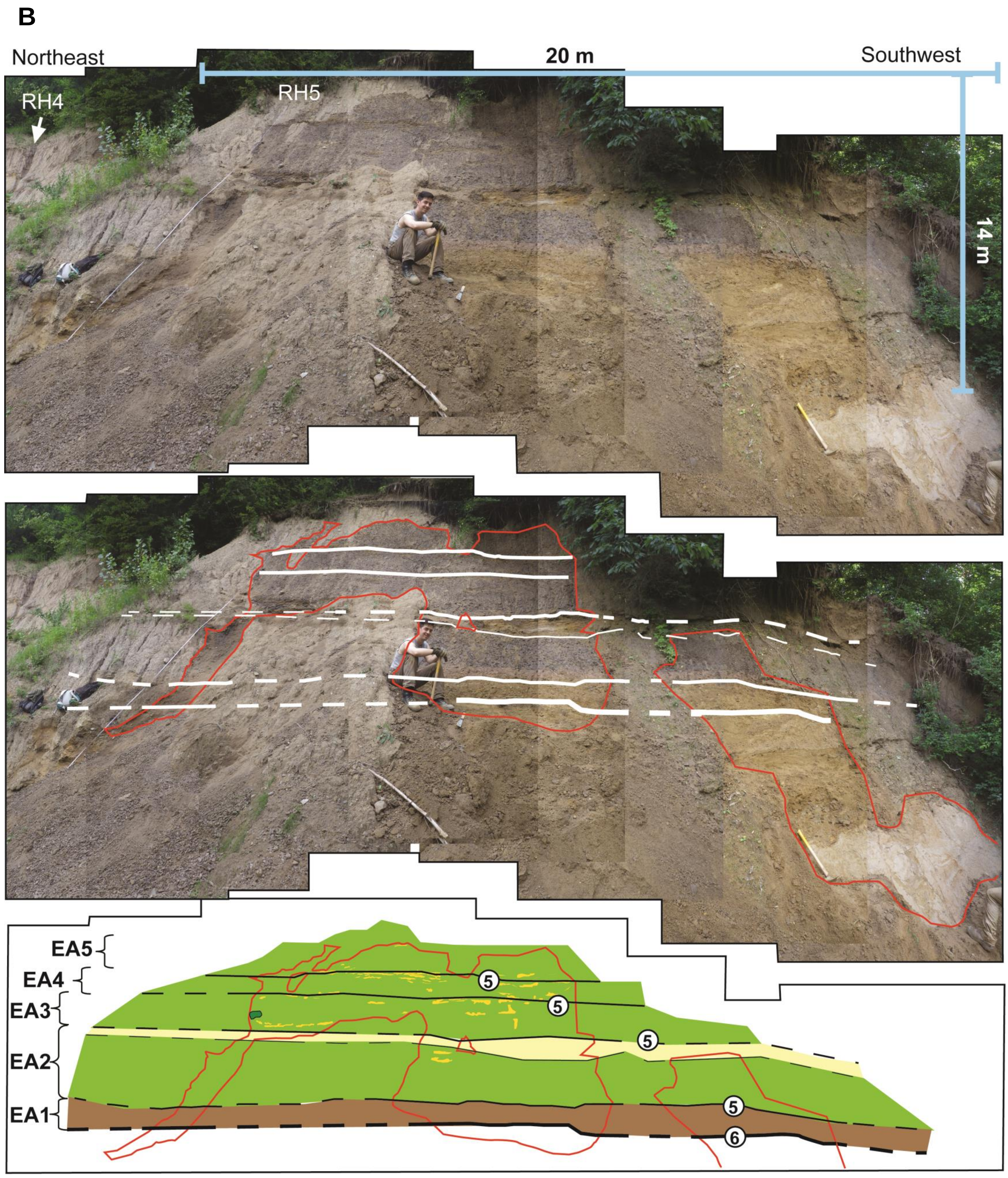
B
Northeast
20 m
Southwest
RH4
RH5
14 m
EA5
EA4
EA3
EA2
EA1
5
6

Fig. 2.11 Detailed view of sediments exposed in outcrop. (A) Boundary (dashed line) separating element association 1 (EA1; mixed zone element, MZ) and underlying glaciofluvial sand and gravel (RH1). (B) Internal facies composition of a MZ element (in EA1; RH2). (C) Facies contact between EA1 and EA2 (diamict sheet element, DS; RH2). (D) Red-coloured diamict facies at the base of EA1 (boundary separating a DS element of EA1 and MZ element of EA2). (E) Sand stringer in a DS element (EA2; RH3), F. boundary separating EA2 and EA3 (RH2). (G) Coarse-grained sheet (CS) element of EA2 overlain by EA3 (RH5). (H) Coarse-grained lens (CL) elements of EA2 (RH3). (I) Boundary separating EA2 and EA3 (RH1). (J) Diamict lens (DL), CL elements (including gravel pods; 'gp') and reverse faults within EA3, which is overlain by EA4 and EA5 (RH1). (K) Bounding surfaces separating EA1-5 (RH1). (L) Conformable bounding surface separating two DS elements of EA4 (RH2). (M) Conformable undulating bounding surface separating DS elements EA5 (RH2).

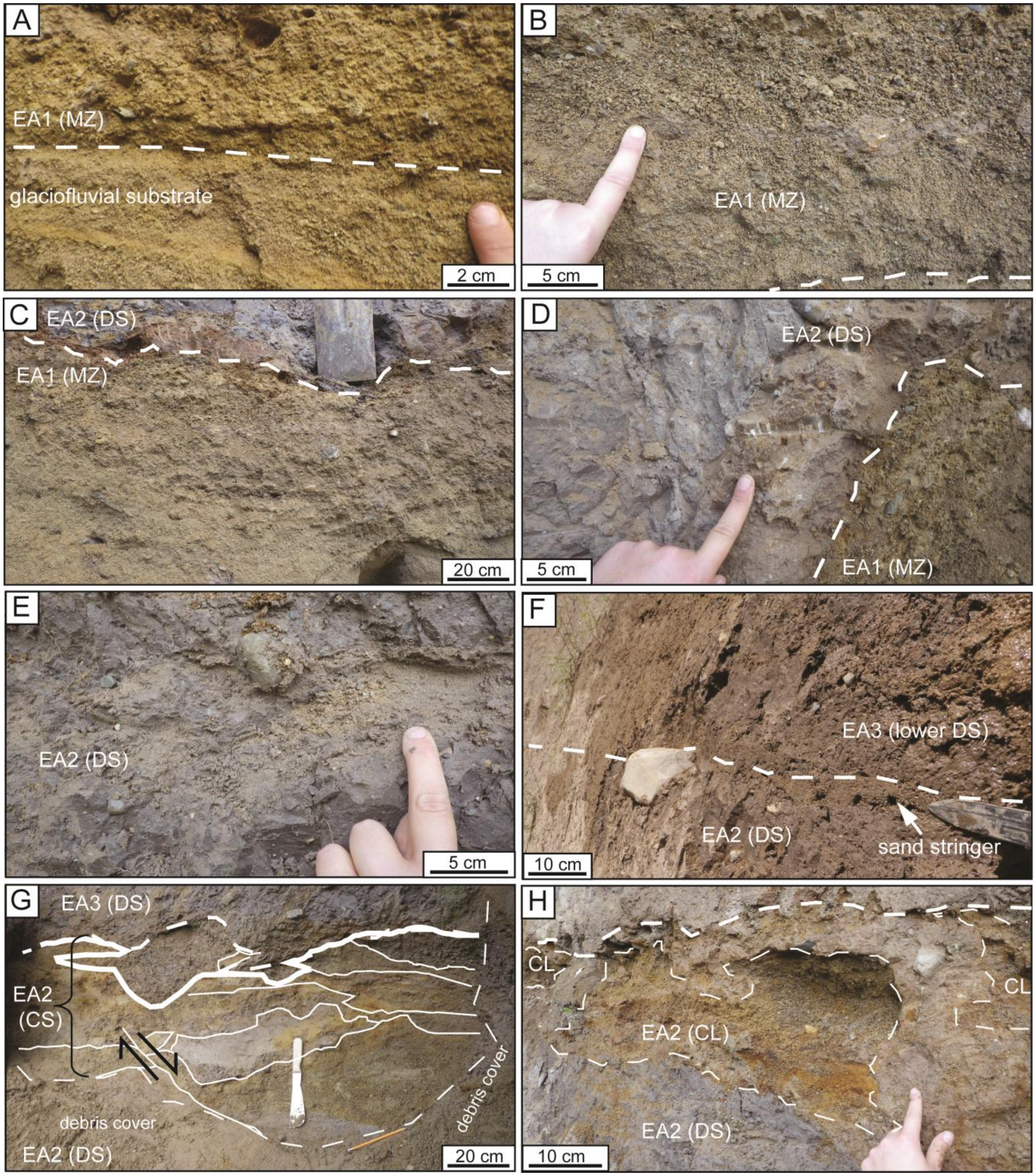
A
EA1 (MZ)
glaciofluvial substrate
2 cm
B
EA1 (MZ)
5 cm
C
EA2 (DS)
EA1 (MZ)
20 cm
D
EA2 (DS)
EA1 (MZ)
5 cm
E
EA2 (DS)
5 cm
F
EA3 (lower DS)
EA2 (DS)
sand stringer
10 cm
G
EA3 (DS)
EA2
(CS)
debris cover
debris cover
EA2 (DS)
20 cm
H
CL
CL
EA2 (CL)
EA2 (DS)
10 cm

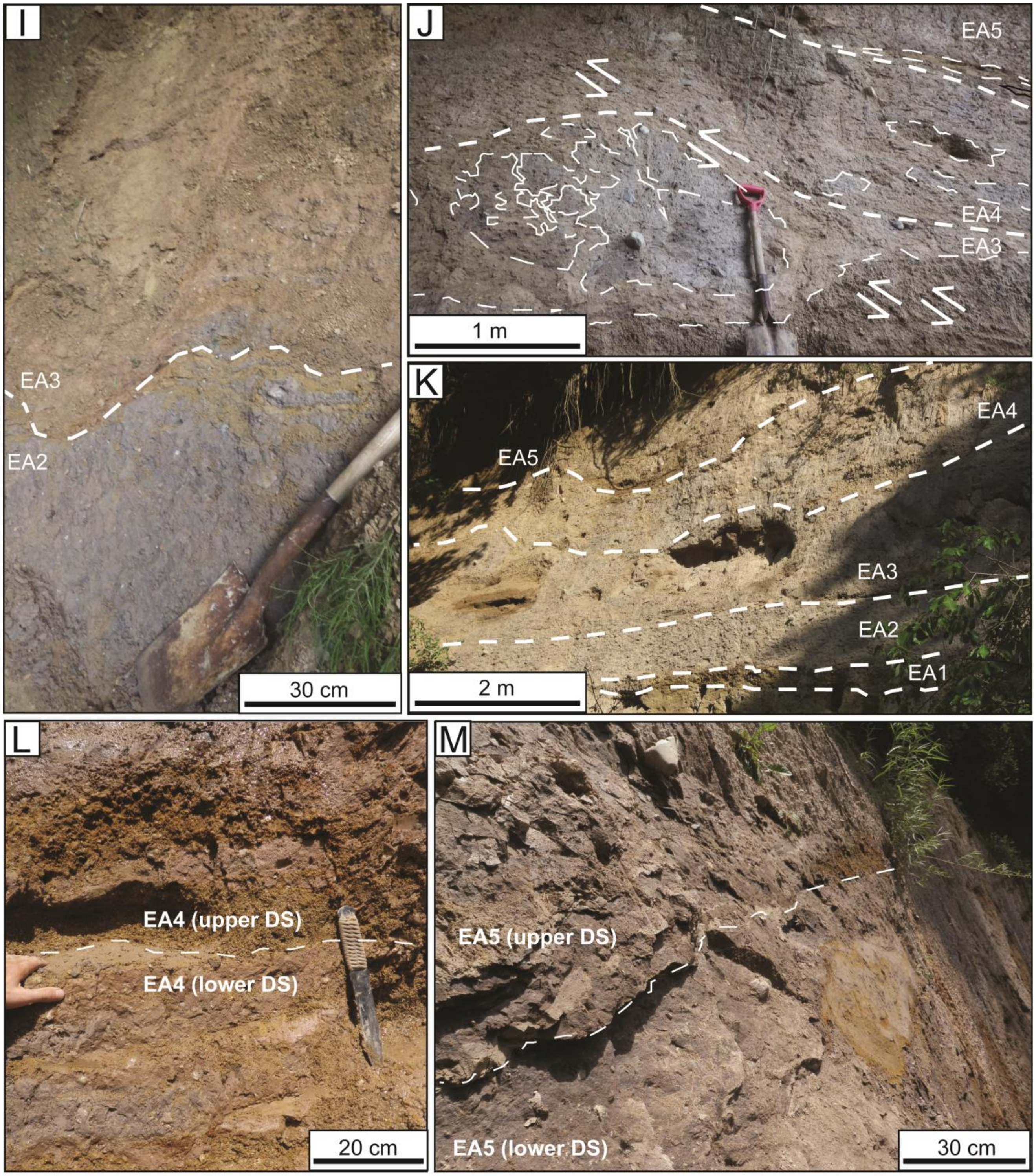
I
EA3
EA2
30 cm
J
EA5
EA4
EA3
1 m
K
EA4
EA5
EA3
EA2
EA1
2 m
L
EA4 (upper DS)
EA4 (lower DS)
20 cm
M
EA5 (upper DS)
EA5 (lower DS)
30 cm

EAs identified in the Tiskilwa Fm. include a glaciotectonite complex (EA1) and four subglacial diamict packages (EA2-5) differentiated by internal architecture and separated by coarse-grained meltwater deposits and an erosional, sheared bounding surface (Figs. 2.9, 2.10). Packages of subglacial diamict consist of simple (EA2), pod- and pocket-dominated (EA3), multi-storey (EA4), and multi-storey sand lens-dominated (EA5) architectures (Fig. 2.9).

2.4.1 Glaciotectonite complex (EA1)

Description

This unit is located in the lowermost stratigraphic position of the Tiskilwa Fm. on the outcrop exposures (Figs. 2.10, 2.12) and directly overlies glaciofluvial sand and gravel facies of the Henry Fm. This unit is characterized by mixed zone (MZ) architectural elements (Figs. 2.10-12A). EA1 is commonly thin (tens of cms) and planar in geometry; however two locations at Stop 1-3 (Fig. 2.10A) show local thickening associated with packages of gravel facies within the underlying glaciofluvial substrate material. EA1 is thickest where it overlies the lee-side of substratum gravel bodies and thinnest above the mid-point of gravel bodies and sheets of sand facies in the underlying glaciofluvial unit (Fig. 2.10A). The lower and upper bounding surfaces of EA1 are irregular to planar in geometry, and sharp and erosional in nature (Figs. 2.10, 2.11A-D).

Interpretation

EA1 is interpreted to have formed primarily by entrainment and attenuation of coarse-grained substrate material in a shear zone between the glacier sole and underlying glaciofluvial substrate material (Henry Fm.). The permeable nature of sand and gravel facies comprising the substratum likely allowed rapid subglacial drainage of meltwater and low pore water pressures at the ice-bed interface. These conditions probably resulted in strong coupling between the glacier sole and its bed, and substrate entrainment and deformation (Boulton and Hindmarsh, 1987; Hart and Boulton, 1991; Piotrowski and Kraus, 1997; Boulton et al., 2001; Evans and Twigg, 2002; Phillips et al., 2002). Frozen bed (permafrost) conditions are possible; however, evidence of permafrost such as sand wedges, upturned strata, involutions, and other cryoturbation features are not exposed or recorded here (e.g. Van Vliet-Lanoë et al., 2004).

Gravel-rich packages of sediment in the underlying glaciofluvial unit (Henry Fm.; Fig. 2.10A) are interpreted to record gravel bars that formed a positive relief paleotopography (McDonald and Banerjee, 1971; Miall, 1977) over which the ice advanced (Willman and Frye, 1970). The coarse-grained nature of substratum gravel facies probably facilitated rapid subglacial drainage of meltwater and allowed gravels to act as rigid bodies that resisted intense glaciotectonization, and may have formed subglacial cavities on their lee side (Boulton and Hindmarsh, 1987). The crudely stratified and coarse-grained facies component of EA1, which is similar in lithology and clast characteristics to the underlying glaciofluvial sediments, suggests incorporation and incomplete homogenization of coarse-grained substrate material in a subglacial traction zone. The sharp, erosional lower bounding surface of EA1 is interpreted to have formed as a décollement plane separating sand and gravel facies of the glaciofluvial substratum (belonging to the Henry Fm.) and glaciotectonized (sheared) material of EA1 (Benn and Evans, 1996; Hart, 1998).

The spatial relationship between the external geometry of EA1, its internal composition (facies types, bounding surfaces, and MZ elements), and underlying paleotopography, suggest EA1 formed by a multi-process, time-transgressive combination of: 1) strong coupling at the ice-bed interface facilitated by the highly permeable nature of the coarse-grained substrate material; 2) subglacial mobilization of coarse-grained substrate material in a shear zone, forming a décollement plane; 3) deposition of the MZ elements by frictional retardation and gravitational lowering of MZ elements into a subglacial cavity (Boulton, 1982; Benn and Evans, 2010); and 4) truncation, and in some places, complete removal, of MZ elements by subsequent glacier erosion (Boulton, 1987; Larsen and Piotrowski, 2003; Carlson et al., 2004; Piotrowski et al., 2006).

This unit is similar in composition, geometry, and stratigraphic position to the previously regionally-mapped discontinuous 'mixed-composition zone' in which older sediments are incorporated into the base of the Tiskilwa Fm. (Wickham et al., 1988), the sheared sand facies of the glaciofluvial substrate material (‘upper part of Facies B’) described by Johnson and Hansel (1990) from the base of the Tiskilwa Fm. exposed in the Wedron Quarry, and the transitional contact between the Delavan Till and underlying sand-rich unit described by Carlson et al. (2004) from outcrop sections near Henry in north-central Illinois (Fig. 2.1).

2.4.2 Subglacial diamict EA2 (simple architecture)

Description

EA2 is characterized by an architecture consisting of one diamict sheet (DS) element (containing a gravel lag at the top) overlain by a horizon of discontinuous and interconnected coarse-grained lens (CL) and sheet (CS) elements (Figs. 2.9, 2.10, 2.11). EA2 is located near the base of the till sheet and directly overlies EA1. It has a tabular geometry and a palimpsest relationship with the paleotopography of the underlying substrate (Henry Fm. and EA1; Fig. 2.10). The lower bounding surface of EA2 is uneven and undulating in geometry, and erosional where it truncates underlying mixed zone (MZ) elements of EA1 (Fig. 2.11C, D). The bottom 10-20 cm of the lower DS element of EA2 forms an irregular layer of sand-rich matrix-supported massive diamict (Dmm) that has a distinctive pinkish-red colour (Figs. 2.11C, D).

The DS element of EA2 is primarily composed of clay-rich massive diamict (Dmm) facies and rare, thin (<5 cm thick) discontinuous deformed beds of massive sand (Sm) facies (Fig. 2.11E). It has an undulating tabular geometry and is directly overlain by discontinuous and interconnected CL elements, gravel lag, and a thin sand and gravel stringer at Stop 1-3 (Figs. 2.10A, 2.11F, H) and a coarse-grained sheet (CS) element at Stop 1-5 (Figs. 2.10B, 2.11G). In some places on the outcrop exposure at Stop 1-3, the DS element of EA2 is directly overlain, and truncated, by EA3 (Figs. 2.10A, 2.11K). CL elements are composed of massive and deformed sand and gravel facies, and pocket- and spindle-shaped geometries (Figs. 2.8C, D, 2.11H). The upper surface of CL elements (Stop 1-3) contains subhorizontal lineations along which horizontal displacement of sand facies is apparent, and interfingers with diamict facies of the overlying EA3 (Fig. 2.11F-H).

The nature of the upper bounding surface of EA2 varies across the outcrop exposures (Fig. 2.10). In places, it is uneven and undulating, and truncated by EA3 (e.g. northwest part of Stop 1-3; Figs. 2.10A, 2.11I). In other places, it is near planar and difficult to distinguish (Fig. 2.11K), but a textural change in matrix grain size of the diamict (Fig. 2.3A), a colour change to a mixture of reddish brown and greyish-blue matrix material, and a gravel lag and horizon of CL and CS elements can be utilized to delineate the upper bounding surface of EA2 (Fig. 2.11F-I).

Interpretation

EA2 is interpreted to record deposition of a subglacial traction till-meltwater complex that formed by a multi-stage process, including 1) truncation and erosion of the upper surface of EA1 by subglacial shear and entrainment of coarse-grained facies (from EA1) into the base of the overriding subglacial traction till (DS element of EA2), 2) deposition of the DS element primarily by the synchronous processes of subglacial deformation and frictional retardation, which resulted in the lodging of clasts on the bed (DS element; Boulton et al., 2001; Evans and Hiemstra, 2005), and 3) accumulation of meltwater at the ice-bed interface, as a result of the impermeable nature of the clay-rich diamict facies composing the subglacial traction till (DS element), localized scour of canals, and deposition of coarse-grained facies within and on the margins of conduits, forming CL and CS elements and a sand and gravel stringer (Walder and Fowler, 1994; Piotrowski and Tulaczyk, 1999).

Sand facies from the underlying MZ elements of EA1 were ingested in the subglacial traction zone during ice advance and contribute to the formation of the basal reddish sand-rich diamict layer (similar to the mixing zone of Hooyer and Iverson, 2000; Fig. 2.11C, D). However, the predominantly fine-grained and massive diamict (Dmm) facies in the DS element of EA2 (Fig. 2.3) indicate that very little coarse-grained substrate material from EA1 was entrained in the body of the till bed, or alternatively, grain crushing and complete homogenization of coarse-grained substrate material occurred prior to final deposition of the till (Boulton et al., 1974).

The impermeable nature of clay-rich diamict facies (Dmm) comprising the main body of the DS element would inhibit effective drainage of meltwater, resulting in pore water pressures exceeding ice overburden pressure and decoupling at the ice-bed interface (Boulton and Hindmarsh, 1987). Local meltwater erosion (by scour into the bed and possibly by thermal erosion upwards into the ice) and decoupling of the glacier sole from its bed would allow the development of a subglacial canal network on the upper surface of the DS element (Walder and Fowler, 1994). The coarse-grained lenses and sheets (CL and CS elements) are interpreted to have formed by deposition in such subglacial meltwater canals (Piotrowski and Tulaczyk, 1999; Boyce and Eyles, 2000).

This element association (EA2) most closely resembles the fine-grained ‘lower zone' in which grey shale bedrock is incorporated into the base of the Tiskilwa Fm. (Wickham et al., 1988), the diamict and intercalated sorted sediment (‘Facies C’) recorded from exposures of the Tiskilwa Fm. in Wedron Quarry (Johnson and Hansel, 1990), and the Delevan Till Member (Oakland facies; Fig. 2.2) described by Hansel and Johnson (1996) and Carlson et al. (2004).

2.4.3 Subglacial diamict EA3 (pod- and pocket-dominated architecture)

Description

A distinctive characteristic of EA3 is the presence of large pod-shaped CL elements composed of crudely cross-bedded, massive, and deformed gravel facies that are aligned at approximately the same stratigraphic position (Figs. 2.8A, 2.10A, 2.11K). EA3 is also characterized by a complex internal architecture that is composed of at least two diamict sheet (DS) elements, different types of coarse-grained lenses (CL), and diamict lens (DL) elements (Figs. 2.8-2.11I-K).

EA3 directly overlies EA2 and is recorded at both outcrop sites (Fig. 2.10). At Stop 1-3, the architecture of EA3 transitions in a down-ice direction (from northeast to southwest) from stacked DS elements overlain by spindle- and lens-shaped CL elements aligned in a horizon across the outcrop face (similar to the architecture of EA3 at Stop 1-5; Fig. 2.10B) to DS elements containing DL elements and different types of CL elements including gravel pods (Fig. 2.10A). The matrix texture of diamict facies comprising DS elements coarsens-upwards from the base of EA3 (Fig. 2.3). The lower DS element is composed of diamict facies with multiple cross-cutting surfaces (third-order) demarcated by clast lags (consisting of cobble- to boulder- sized gravel; Fig. 2.7) and rare CL elements (Figs. 2.10, 2.11). The upper DS element has a more complex architecture than the lower DS element of EA3; it consists of a more silt-rich matrix diamict facies, an abundance of laminated diamict (Dml) facies, and contains diamict lens (DL) and different types of coarse-grained lens (CL) elements, including gravel pods (Figs. 2.9-2.11).

At Stop 1-3, the lower bounding surface of EA3 transitions, in a down-ice direction, from planar and erosional or irregular and deformed in places (directly overlying the upper surface of CL elements of EA2, which is apparently sheared; Figs. 2.10A, 2.11H), irregular and gradational (with diamict 'rip-ups' from EA2; Fig. 2.11K), to a highly irregular and erosional surface that scours the upper 30 cm of EA2 (Fig. 2.11I). At Stop 1-5, the lower bounding surface is planar to irregular, and erosional to deformed (Figs. 2.10B, 2.11G). The upper bounding surface of EA3 is planar to irregular, truncated by overlying EA4 (Fig. 2.11K), and demarcated by discontinuous and interconnected CL elements forming a horizon on the outcrop face (Fig. 2.10). Reverse faulting is common in EA3, which rarely can be traced downwards into EA2 and EA1 and upwards into the base of EA4 (Figs. 2.10A, 2.11J).

Interpretation

EA3 is interpreted to have formed primarily by subglacial deformation and records changing subglacial conditions following the deposition of EA2. The erosional lower bounding surface of EA3 is interpreted to record re-attachment of the ice to its bed (suggesting draining of subglacial meltwaters and lower porewater pressure following deposition of EA2) and increased shear stress at the ice-bed interface. The lower DS element (containing cross-cutting third-order surfaces) is interpreted to record closing of the canal network and resumed deposition of till in slices, likely as a result of a combination of lodgement and shearing. The absence of a 'mixed zone' (similar to the sand-rich lower part of EA2) suggests limited to no incorporation of sand facies from EA2 into the base of EA3 at this location. Diamict lens (DL) and gravel pod (CL) elements in the upper DS element do not show evidence of intense shear strain (e.g. lamination and attenuation), suggesting transport and deposition under high porewater pressures, possibly in a deformable bed (Boulton and Hindmarsh, 1987).

The matrix within diamict sheet (DS) elements (Dmm facies) in EA3 is slightly coarser-grained than in the diamict facies of EA2, which probably reflects entrainment and homogenization of coarse-grained substrate material from up-ice locations (possibly from CL and CS elements of EA2). The lower DS element of EA3 is interpreted to record a zone of intense shear, in which the cross-cutting third-order surfaces with gravel lags formed during minor phases of shearing of till, which was probably deposited in slices (similar to the B horizon of Evans et al., 2006). This deformation may have occurred at the same time as underlying CL elements of EA2 were deformed by shearing.

The upper DS element of EA3 is interpreted to have formed primarily by subglacial deformation as a subglacial traction till (similar to the A horizon of Evans et al., 2006). Diamict lens (DL) elements within the upper DS element of EA3 (Fig. 2.11J) are composed of similar facies (Dmm) to the diamict sheet of EA2, and are interpreted to record entrainment of rafts of diamict from EA2. Deposition of diamict rafts (DL elements) probably occurred soon after entrainment, with insufficient transport time and distance or shear strain for complete homogenization of the deforming bed. Gravel pods (subtype of CL elements; Fig. 2.8A) probably acted as rigid bodies that resisted intense plastic deformation during subglacial transport (Boulton and Hindmarsh, 1987). The apparently laminated diamict (Dml) facies (consisting of diamict layers that are 1 cm or less in thickness; Fig. 2.4A; Table 2.1) surrounding DL and CL elements (within the upper DS element) is interpreted to record the generation of small-scale shear planes between rotating DL and CL elements during subglacial deformation (similar in appearance to the micromorphologic observations of shear planes of Hiemstra and Rijsdijk, 2003).

The fine-grained diamict facies of DS elements of EA2 and EA3 likely impeded infiltration of meltwater into the groundwater system and facilitated high porewater pressure and local decoupling at the ice-bed interface. This would allow the formation of a subglacial meltwater canal network on the surface of the upper DS element of EA3 (similar to that on the surface of EA2; Walder and Fowler, 1994). The ultimate deposition of the upper and lower DS elements of EA3 (the A and B horizons respectively) is interpreted to be a result of reduced shear strain as a consequence of meltwater accumulation and ice-bed decoupling.

The EA3 element association most closely resembles ‘Facies D’ (homogeneous diamicton) recorded in Wedron Quarry, which consists of four beds of diamict facies with shear planes, boulder pavements, and channel-shaped lenses of sand and gravel facies (Johnson and Hansel, 1990). However, correlation to previously described subunits elsewhere in Illinois is difficult due to the lithostratigraphic framework utilized to classify the Tiskilwa Fm., of which EA3 most likely forms the lower part of the main undivided unit (Fig. 2.2; Hansel and Johnson, 1996).

2.4.4 Subglacial diamict EA4 (multi-storey architecture)

Description

EA4 is composed of a multi-storey architecture consisting of two stacked DS elements, spindle- and irregular-shaped CL elements (made of sand and gravel facies), and very rare DL elements (Figs. 2.10, 2.11). The DS elements consist of silt-rich diamict facies that coarsen upwards from the base of EA4 (Figs. 2.3, 2.10).

The lower bounding surface of EA4 is planar and conformable where it overlies CL elements of EA3 (southeast part of Stop 1-3; Fig. 2.10A) to erosional where it truncates the upper surface of EA3 (in the northwest part of the outcrop at Stop 1-3; Figs. 2.10A, 2.11K). The lower DS element of EA4 is composed of laminated diamict (Dml) facies at the base, and contains an increasing number of thin (few cms) stringers of sand and gravel facies toward the top (Fig. 2.11L). The lower DS element is truncated by the upper DS element (Figs. 2.10A, 2.11L), which contains rare CL elements (gravel facies) at the base and an abundance of spindle-shaped CL elements (sand facies) near the top. CL elements at the top of EA4 are aligned in a horizon across the outcrop exposure (southeast part of Stop 1-3 and at Stop 1-5; Fig. 2.10). The upper bounding surface of EA4 is demarcated by a gravel lag, and is truncated by overlying EA5 with evidence of shearing of CL elements (Fig. 2.10).

Interpretation

EA4 is interpreted to record stacking of at least two depositional slices of subglacial traction till, primarily by shearing and frictional retardation (Boyce and Eyles, 2000).

EA4 is interpreted to have formed by similar subglacial depositional processes to EA2 and EA3. The erosional lower bounding surface and overlying DS element (comprised of Dml facies) are interpreted to record scour and shear of the upper surface of EA3 as a result of coupled ice-bed conditions during ice overriding. The stacking of DS elements in EA4 probably records lateral changes in ice-bed conditions or subglacial thrusting of a depositional slice of till, which was subsequently truncated by overriding ice during deposition of EA5 (Boyce and Eyles, 2000).

EA4 is most similar to 'Facies D' described by Johnson and Hansel (1990) but, for reasons similar to EA3, it is difficult to determine which subunits in the Tiskilwa Fm. and other units in the Wedron Group, that have been previously described using a lithostratigraphic framework, are equivalent to EA4 .

2.4.5 Subglacial diamict EA5 (multi-storey sand lens-dominated architecture)

Description

EA5 occurs in the uppermost stratigraphic position on the outcrop face and is the youngest unit recorded in this study (Fig. 2.10), although the top of the Tiskilwa Fm. extends above the extent of the outcrop exposures (and is overlain by Peoria Silt and the Lemont Fm.; Fig. 2.1C). EA5 is separated from EA4 by a planar erosional lower bounding surface demarcated by a discontinuous gravel lag (upper surface of EA4), and is characterized by an increased abundance of spindle-shaped coarse-grained lens (CL) elements comprised of sand- and fine-grained facies and sand-stringers, and diamict facies with a blocky structure and cross-cutting subvertical joints (Fig. 2.11M).

EA5 consists of two stacked DS elements separated by an undulating conformable bounding surface (Fig. 2.11M). The lower DS element has a simple architecture dominated by clay-rich diamict facies (Dmm) and rare sheared to well-preserved CL elements and sand stringers near its base (Fig. 2.5A). The upper DS element contains highly stratified diamict facies interbedded with abundant CL elements comprised of sand- and fine-grained facies. The upper DS element contains crude undulating beds (bed thickness ranges from 5-30 cm) of diamict facies interbedded with fine-grained facies, with conformable bedding surfaces that are commonly overlain by thin (less than 5 cm thick) irregular and discontinuous beds of fine-grained facies (Fmd) and CL elements (Figs. 2.3, 2.5C, 2.11M). At Stop 1-5, only the lower DS element of EA5 is exposed.

The CL elements in EA5 are commonly located at the base of DS elements and stratification within CL elements is better developed (or preserved) than in stratigraphically-lower EAs (EA2-EA4). Facies contacts between individual beds within CL elements show flame and pillow structures and the external bounding surfaces of the larger-scale CL elements are loaded and show evidence of shearing (Fig. 2.5D). CL elements also contain normal faults that cross-cut soft-sediment deformation structures. A near-vertical jointing network near the top of EA5 gives a ‘blocky’ appearance to the unit, and joints are commonly infilled with medium-grained sand which may have been injected into the fractures concurrently or immediately following joint development. The upper bounding surface of EA5 is not exposed.

Interpretation

The increased abundance of coarse- and fine-grained facies, and the conformable and undulating bedding geometry in the upper part of EA5, suggest increased supply of meltwater, less intense subglacial deformation, and deposition from disintegrating or stagnating ice either in a subglacial or ice-marginal setting (Lawson, 1981; Johnson and Hansel, 1990; Wysota, 2007). Subsequent remoulding and shearing of saturated debris by subglacial deformation and water escape during intermittent ice advance is also suggested (Johnson and Hansel, 1990; Evans et al., 2006).

Loaded facies contacts between CL and diamict sheet (DS) elements are interpreted to record saturated conditions and water escape after their deposition, and normal faults that offset soft-sediment deformation features within CL elements are interpreted to record shifting or collapse of sediment. The matrix texture of DS elements in EA5 is finer-grained than diamict facies in EA4, which suggests a lesser amount of coarse-grained facies were homogenized into the subglacial traction till during subglacial transport. Instead, CL elements were likely formed in situ, as a result of increased meltwater production and sediment delivery during ice disintegration (Johnson and Hansel, 1990).

EA5 is similar to ‘Facies E’ (heterogeneous diamicton and sorted sediment) described from Wedron Quarry (Johnson and Hansel, 1990) because it contains abundant lenses and beds of sorted sediment (fine-grained, sand, and gravel facies), conformably overlies older deposits, and does not show evidence of extensive subglacial deformation (i.e. homogenization of material). However, unlike 'Facies E' (Johnson and Hansel, 1990), evidence of shear of CL elements suggests applied force by subglacial deformation contributed, in part, to the formation of EA5.

2.5 DISCUSSION

Sedimentary architecture is commonly delineated using two fundamental approaches, including sequence stratigraphy and allostratigaphy; however, these approaches as stand-alone methods are not straightforward for architectural analysis of glacial deposits, and the fundamental principles on which these methods are based may not directly apply in glaciated terrain. Sequence stratigraphy is based on the characterization of cyclic successions of sediments and delineation of bounding discontinuities and correlative conformities which are controlled by relative sea level changes (Catuneanu et al., 2009). Although sequence stratigraphic analysis has been conducted on glacial sediments deposited on marine continental shelves (e.g. El-ghali, 2005; Huuse et al., 2012; Lang et al., 2012), a sequence stratigraphic approach is not appropriate for the analysis of sedimentary architecture in non-marine continental glaciated settings because these systems are controlled by other external factors such as isostasy, climate and relative position of the ice margin, bed topography, the hydrologic system, and in some areas, the geothermal regime and volcanic activity (Evans, 2005; Benn and Evans, 2010). Secondly, glacial sedimentary packages are rarely cyclic due to the dynamic nature of glacial environments, and sediments are often removed or truncated by glaciofluvial processes or subsequent ice advance at relatively small spatiotemporal scales compared to sequence cycles ($1x10^5$ to $2x10^6$ years and 10's to

1000's of kilometres; Mitchum and Van Wagoner, 1991). Hence, the delineation of fundamental sequence boundaries, including a maximum flooding surface, and low-, high-, and transgressive systems tracts may not be possible (see Martini and Brookfield (1995) for a modified sequence stratigraphic approach applied to glaciolacustrine sediments exposed in outcrop sections in southern Ontario, Canada).

The chronostratigraphic framework of allostratigraphy is more appropriate than the base-level framework of sequence stratigraphy for the analysis of subsurface non-marine glacial successions (Räsänen et al., 2009; Hughes, 2010); however, it poses several difficulties including: 1) the dynamic erosional and aggradational processes of glacial systems makes identification of time-correlative sedimentary packages and surfaces between different depositional environments (and application of Walther's Law) difficult; 2) allostratigraphy lacks a systematic method for delineating and organizing sedimentary geometry (i.e. components of a system) and architecture (the spatial arrangement of these components) at different scales of resolution, making visualization, systematic organization, and communication of the detailed till architecture difficult; and 3) it does not facilitate understanding of the evolution of the subglacial mosaic at local scales.

AEA is based on observation of physical characteristics (nature of facies contacts and change in facies associations) which are visible on all or part of the outcrop face, delineation of sedimentary geometry (packaging facies associations), and understanding depositional processes at different scales of resolution (Miall, 1985; 2010). These foundational components makes AEA flexible and allows modification of the bounding surface hierarchy for analysis of sedimentary architecture in other depositional environments, including subglacial deposits (e.g. Boyce and Eyles, 2000; Fig. 2.7). AEA, as utilized in this study, facilitated the deconstruction of the Tiskilwa Fm. into its basic building blocks (facies associations) nested within a framework (bounding surfaces). Analysis of these basic components allowed the characterization of the detailed sedimentary geometry (architectural elements) of the Tiskilwa Fm. at a local scale (Fig. 2.9), and facilitated the organization of the sedimentary architecture into five mappable subunits (element associations), which provided insight to the spatiotemporal changes in subglacial processes that constructed the till architecture (Figs. 2.12, 2.13). The Tiskilwa Fm., as recorded here, has a complex architecture and heterogeneity at various scales of resolution (Fig. 2.13). The Tiskilwa Fm. exposed at the two sections in Rattlesnake Hollow records a system of laterally shifting subglacial conditions and processes at a local-scale. Architectural elements and element associations identified here within the Tiskilwa Fm. have a unique architecture and their internal facies association, spatial arrangement, and relationship to a hierarchy of facies contacts are utilized together to understand the environmental controls on its deposition, including local paleotopography, substratum permeability, subglacial meltwater activity, and supply of coarse-grained sediment (Fig. 2.12).

In comparison to models of alluvial plain geomorphology and architecture, the spatiotemporal organization of processes and geomorphic components of a subglacial bed are poorly understood, largely as a result of the inaccessibility of the subglacial depositional system; however studies of ancient and modern glacier beds and their deposits have inferred a mosaic of spatial and temporal processes (Boyce and Eyles, 1991; Alley et al., 1997; Clark and Meehan, 2001; Bjornsson, 2002; Ó Cofaigh et al., 2002; Shaw, 2002; Swift et al., 2002; Rippin et al. 2003). The dynamic and often erosional nature of subglacial environments makes application of Walther's Law (Middleton, 1973), and hence spatiotemporal paleoenvironmental reconstruction, difficult. Subglacial systems are thought to organize spatiotemporal processes in response to stress distribution operating on the subglacial bed (Ng, 2000), whereby a change in the system will result in stress redistribution to maintain 'dynamic equilibrium', similar to the response of the fluvial plain to changes in discharge or sediment supply (Ahnert, 1994; Thorn and Welford, 1994). The process of decoupling at the ice-bed interface is a subglacial process that results from dynamic disequilibrium in the subglacial system (e.g. an accumulation of meltwater; Boulton et al., 2009), and has been used to explain changes in the hydrological regime, the location and rate of basal sliding (surging), and the formation of deforming or 'sticky' spots on the glacier bed (Boulton, 1996; Piotrowski and Kraus, 1997; Fischer et al., 1999; Tulaczyk, 1999; Ng, 2000; Fischer and Clarke, 2001; van der Meer et al., 2003; Larsen et al., 2004; Kjaer et al., 2006; Meriano and Eyles, 2009).

Application of AEA to the analysis of the Tiskilwa Fm., as presented here, allows for detailed reconstruction of the depositional history of a subglacial complex (Figs. 2.12, 2.13). Analysis of the architectures recorded here, and comparison of these results to data and interpretations recorded from till in other studies of ancient and modern glaciated terrain (discussed above) is an iterative process. The sedimentological and architectural characteristics of the Tiskilwa Fm. recorded here is most convincingly explained by the 'ice-bed mosaic' model of Piotrowski et al. (2004) and subglacial continuum of processes such as lodgement and deformation of Evans et al. (2006). The Tiskilwa Fm. is interpreted to have formed by ice advance over highly transmissive glaciofluvial sediments and a pre-existing paleotopography (EA1), till aggradation and the formation of a localized meltwater canal network incised into the bed (EA2), aggradation of a deformable subglacial traction till and entrainment of coarse-grained material, with subsequent formation of a meltwater canal network on the bed (EA3), stacking of depositional slices of subglacial traction till (EA4), and increased supply of fine-grained facies (and meltwater?) which may record deposition during ice stagnation, possibly in a subglacial to ice-marginal setting (EA5). As a whole, the succession is composed of at least three stacked depositional successions (Figs. 2.12, 2.13), interpreted to be controlled by similar environmental conditions, and each succession records, from the base upwards:

(1) subglacial shearing of substrate material during ice-bed coupling and advance (Hart and Boulton, 1991; Benn and Evans, 1996);

(2) till aggradation primarily by deformation of a subglacial traction till (similar to the A horizon of Bolton and Hindmarsh, 1987; Benn and Evans, 1996);

(3) development of a local 'disequilibrium' on the subglacial bed as a result of accumulation of meltwater at the ice-bed interface, resulting in high porewater pressures, localized ice-bed decoupling, and formation and infill of subglacial canals (Walder and Fowler, 1994; Boulton, 1996; Boulton et al., 2009);

(4) stress redistribution in other areas on the bed, resulting in patches of a strongly coupled ice-bed interface, scour of the substrate, and bed deformation (Piotrowski and Kraus, 1997; Ng, 2000; Fischer and Clarke, 2001; Piotrowski et al., 2004); and
(5) drainage of meltwater through canals, resulting in ice-bed recoupling and a dynamic equilibrium state in the subglacial system (Boulton and Hindmarsh, 1987; Boulton et al., 2009).

The succession described above is interpreted to have formed by a negative feedback mechanism initiated by an accumulation of meltwater on the subglacial bed (Boulton and Hindmarsh, 1987; Ng, 2000; Boulton et al., 2009). A fine-grained substrate does not facilitate significant drainage of meltwater to the groundwater system; hence, increased porewater pressure and decreased shear strength ('disequilibrium') would likely result in localized decoupling at the ice-bed interface (Boulton and Hindmarsh, 1987; Boulton, 1996; Piotrowski and Kraus, 1997; Boulton et al., 2001; Fischer and Clarke, 2001). Local stress instabilities on the bed (e.g. localized accumulation of meltwater and basal sliding) are thought to be balanced by redistributing stress elsewhere, thereby resulting in 'sticky spots' and scour in other parts of the bed (Fig. 2.12; Fischer et al., 1999; Ng, 2000). The successions recorded in this study (EAs1-5) suggest that local meltwater activity was concentrated in irregular areas of the bed surface, commonly in, but not restricted to, topographic lows on the bed, which are ultimately controlled by the local paleotopography of the underlying glaciofluvial unit (Henry Fm; see Fig. 2.10A; Boyce and Eyles, 2000). In these areas of meltwater activity, coarse-grained lens (CL)

Fig. 2.12 Conceptual block diagram of the Tiskilwa Fm. illustrating the depositional history of EA1-3 by a ‘succession’ of stress redistribution on the subglacial bed (the succession is repeated for the remainder of EA3 and EA4). (A) Ice-bed coupling resulting in the deposition of sheared substrate in subglacial cavities (EA1) and fine-grained subglacial traction till (DS element of EA2). (B) Accumulation of meltwater over an irregular substrate surface, resulting in decoupling at the ice-bed interface and meltwater scour and infill of a subglacial canal network (CL and CS elements of EA2) accompanied by strong coupling and subglacial erosion elsewhere on the bed. (C) Ice-bed coupling resulting in entrainment and shear of the underlying substrate and deposition of a subglacial traction till (lower DS element of EA3), which records the initiation of another succession.

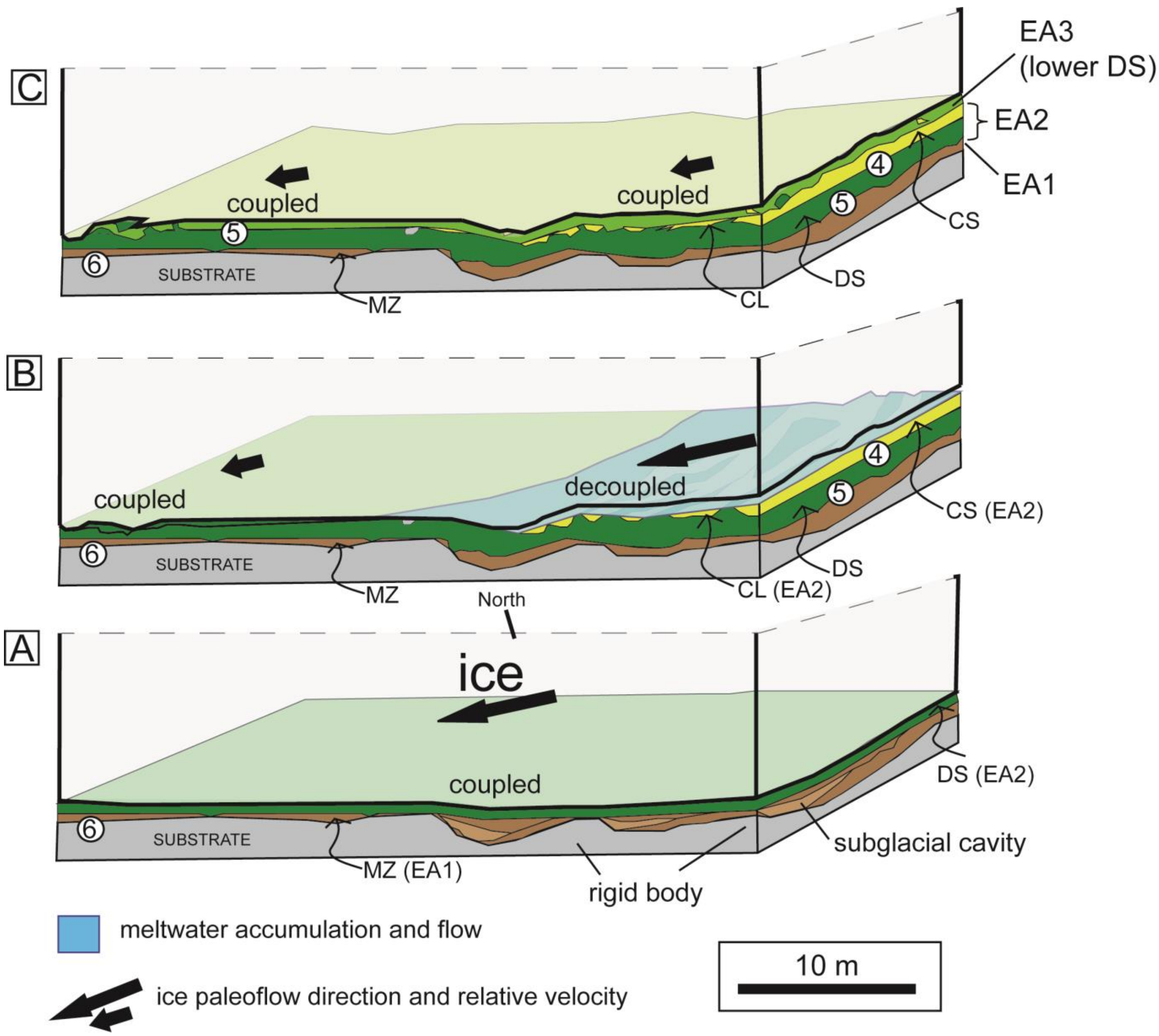
C
EA3
(lower DS)
EA2
EA1
coupled
coupled
4
5
5
6
SUBSTRATE
MZ
CL
DS
CS
B
coupled
decoupled
4
5
6
SUBSTRATE
MZ
CL (EA2)
DS
CS (EA2)
A
North
ice
coupled
6
SUBSTRATE
MZ (EA1)
rigid body
subglacial cavity
DS (EA2)
meltwater accumulation and flow
ice paleoflow direction and relative velocity
10 m

elements are preserved and there is little to no scour of the substrate, suggesting low shear strain within the bed during and closely following deposition; these areas probably facilitated ice movement by basal sliding. However, in areas of low relief paleotopography, evidence of scour and more intense shear is common (see Fig. 2.10) which suggests these areas underwent intense bed deformation and likely facilitated ice movement primarily by subglacial deformation processes (Evans et al., 2006; Benn and Evans, 2010).

At a local scale (as recorded in this study), sixth-order surfaces separating deposits of different depositional environments (e.g. subglacial till and glaciofluvial outwash) are equivalent to the boundary delineating lithostratigraphic Formations (Tiskilwa and Henry Fms.). Field data recorded from other sites in the study area and elsewhere in Illinois in future studies may provide insight to the significance of certain bounding surfaces or parts of surfaces, including surfaces that delineate formal lithostratigraphic Groups, Formations, and Members (e.g. diamict packages illustrated in Figs. 2.1D, 2.2). An understanding of the regional-scale relationship between bedrock topography, meltwater drainage, subglacial depositional conditions, and unit geometries in the study area requires examination of the Tiskilwa Fm. (and Wedron and Mason Groups) exposed at other locations, and is not discussed further here.

2.5.1 Hydrogeological implications

Delineation of the internal architecture of the Tiskilwa Fm. till sheet has significant implications for hydrogeological investigations, specifically in areas where till sheets are characterized as relatively impermeable hydrostratigraphic layers (aquitards; Anderson, 1989). Quantitative hydrogeologic and engineering data were not collected as part of this study; however, the hydrogeological significance of the sediment packages described here is based on hydrogeologic and physical properties of tills with similar facies associations and architecture (Keller et al., 1985; Gerber et al., 2001; Nilsson et al., 2001; Meriano and Eyles, 2009).

On the Rattlesnake Hollow exposures, piping features and mineral precipitation and oxidation causing discoloration of CL elements likely indicate flow of groundwater through these elements. The interconnectivity of coarse-grained lenses and sheets (CL and CS elements) and sub-vertical secondary structures (faults and joints) is most significant for understanding groundwater and contaminant flow through the body of the till sheet, both horizontally across the local study area (c. 5.6×10^3 m^2) and vertically from the surface to deeper subsurface units that may host productive aquifers (Anderson, 1989; Herzog et al. 1989; Gerber and Howard, 2000; Gerber et al., 2001). CL elements that form stratigraphic horizons on the outcrop exposure are commonly interconnected by thin beds of sand facies, and likely form laterally extensive sheets (CS elements) and interconnected canal systems in three-dimensional space (Fig. 2.12; Walder and Fowler, 1994).

EA1 has a complex internal architecture and external geometry, and can be mapped across the study area between Stop 1-3 and Stop 1-5 (c. 150 m; Figs. 2.11, 2.13). EA1 comprises poorly-sorted coarse-grained facies and likely forms a moderately high horizontal conductivity flow pathway beneath the till sheet (Fig. 2.12B). This could have significant hydrogeological implications, particularly if EA1 is hydraulically connected to permeable layers within the overlying till of EA2 and more deeply buried coarse-grained units (e.g. Henry Fm.). EA2 is composed of a fine-grained diamict sheet that can be mapped between the two outcrop faces (Figs. 2.10, 2.12), and likely forms a confining layer over the coarse-grained glaciofluvial sediments and EA1. However, thin sand beds and subvertical joints within the diamict sheet may facilitate fluid flow through the till, from overlying coarse-grained lenses to EA1 (Fig. 2.13; Keller et al., 1985; Nilsson et al., 2001). The most complex units recorded in this study are EA3 and EA4, and although diamict sheet (DS) elements within these units have a fine-grained texture, they are commonly dissected by CL elements, thin sand and gravel stringers, gravel lags and fractures (Figs. 2.10, 2.13). The spatial arrangement, topology, and facies characteristics of these features within DS elements (of EA3 and EA4) may form complex and perhaps highly conductive fluid flow pathways through the till (Gerber and Howard, 1996; Nilsson et al., 2001). EA5 contains a large concentration of interconnected CL elements, interbedded diamict, sand, and gravel facies, and subvertical joints infilled with sand, which would likely facilitate the flow of groundwater through EA5 and contribute to fluid flow through the full thickness of the till sheet into the glaciofluvial unit of the underlying Henry Fm. (and may form a ‘leaky’ aquitard; Gerber and Howard, 1996; Gerber et al., 2001; Meriano and Eyles, 2009). Future studies including field-derived sedimentological data on the spatial continuity of individual diamict sheet (DS) elements, the topology of coarse-grained lens (CL) and sheet (CS) elements, and the nature of the fracture system,

Fig. 2.13 Sedimentary heterogeneity of the Tiskilwa Fm. at various scales of resolution (based on data recorded from outcrop at Stop 1-3 and 1-5; Fig. 2.10), including the depositional environment (and stratigraphic unit; sixth-order surface), element association (fifth-order), architectural element (fourth-order), and facies types (first- to third-order). Please refer to Fig. 2.3 for facies colour codes and Fig. 2.7 for descriptions of bounding surfaces.

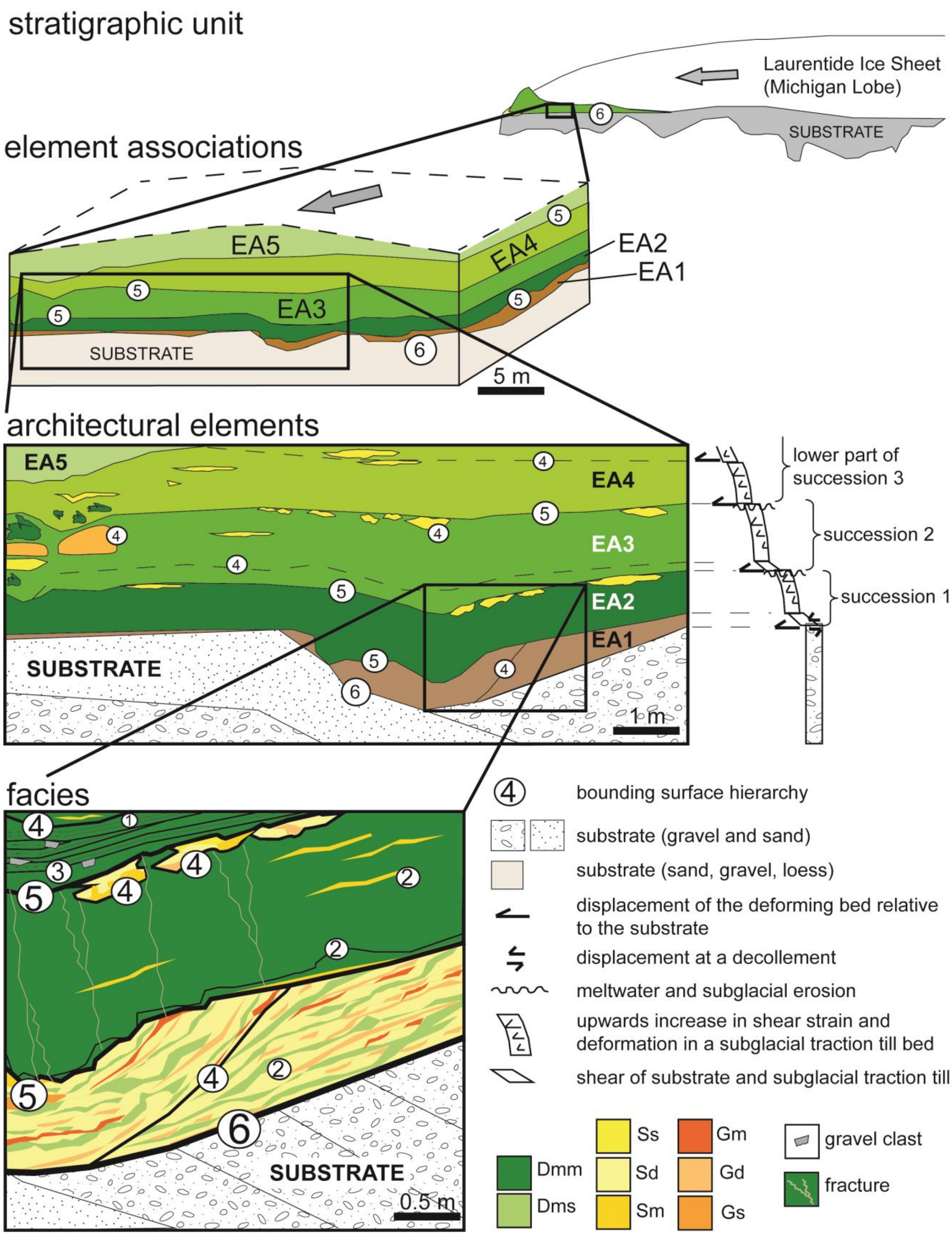
stratigraphic unit
Laurentide Ice Sheet (Michigan Lobe)
SUBSTRATE
element associations
EA5
EA4
EA3
EA2
EA1
SUBSTRATE
5 m
architectural elements
EA5
EA4
EA3
EA2
EA1
SUBSTRATE
1 m
lower part of succession 3
succession 2
succession 1
facies
SUBSTRATE
0.5 m
bounding surface hierarchy
substrate (gravel and sand)
substrate (sand, gravel, loess)
displacement of the deforming bed relative to the substrate
displacement at a decollement
meltwater and subglacial erosion
upwards increase in shear strain and deformation in a subglacial traction till bed
shear of substrate and subglacial traction till
Dmm
Dms
Ss
Sd
Sm
Gm
Gd
Gs
gravel clast
fracture

integrated with hydrogeological data, is crucial for understanding the hydrostratigraphic framework of the Tiskilwa Fm. and the vulnerability of aquifers hosted in more deeply buried coarse-grained sediment.

2.6 CONCLUSIONS

This study applies architectural element analysis (AEA) to the detailed delineation of the geometry and heterogeneity of the Tiskilwa Fm., which is composed of a stacked succession of subglacial diamict and meltwater deposits, and exposed in stream cuts in north-central Illinois. A bounding surface hierarchy (first- to sixth-order) was defined on the basis of the nature of facies, facies contacts, and the change in facies associations on either side of a contact. This hierarchy of surfaces delineates the basic architectural framework of the Tiskilwa Fm. and facilitates the analysis of sedimentary heterogeneity at various scales of resolution. AEA, as applied here, allows for the characterization of five architectural elements (delineated by fourth-order surfaces), which form the basic building blocks of the till, including coarse-grained lens (CL) and sheet (CS), diamict lens (DL) and sheet (DS), and mixed zone (MZ) elements. Analysis of the spatial arrangement and stratigraphic position of architectural elements and bounding surfaces on two outcrop faces allows for the characterization of five larger-scale architectural units (element associations; EA1-5).

The internal architecture of each EA and the change in the nature of fifth-order bounding surfaces across the outcrop faces suggest at least three depositional successions are recorded in the till deposits. Each succession consists of a ‘cycle’ of coupling-decoupling-recoupling processes operating at the ice-bed interface, initiated by stress disequilibrium (i.e. accumulation of meltwater) in the subglacial system. The results of this study provide sedimentological evidence for the occurrence of a spatiotemporal mosaic of subglacial processes, and the contemporaneous formation of ‘sticky’ deforming spots and areas of basal sliding on the subglacial bed. The spatial distribution of these areas is likely controlled by factors such as substratum paleotopography, facies composition, and meltwater availability. Detailed sedimentological analysis of deposits within the Tiskilwa Fm. in other areas of Illinois, and integration of other data types (e.g. geophysical and hydrogeological data) and techniques (e.g. tracer tests and modern analogues studies), will enhance delineation of the internal architecture and paleoenvironmental reconstruction of Late Quaternary events involved in the formation of the Wedron Group. The approach presented here can also be applied to the analysis of subglacial deposits in previously glaciated areas elsewhere to better understand the spatiotemporal arrangement of subglacial processes and the sedimentological record of these processes at a local scale as preserved in Quaternary glaciogenic successions.

Acknowledgements

The authors offer sincere thanks to Kevin Elmer and Olivier Caron for fieldwork assistance. Sedimentology Editors (Stephen Rice and Vern Manville) and reviewers (Emrys Phillips and an anonymous reviewer) provided insightful and constructive comments and suggestions. Funding was provided by the Illinois State Geological

Survey, an NSERC Discovery Grant award to C. Eyles, and an NSERC PGS-D grant to J. Slomka.

REFERENCES

Ahnert, F. (1994) Equilibrium, scale and inheritance in geomorphology. *Geomorphology*, **11**, 125-140.

Allen, J.R.L. (1963) The classification of cross-stratified units, with notes on their origin. *Sedimentology*, **2**, 93-114.

Allen, J.R.L. (1968) The nature and origin of bed-form hierarchies. *Sedimentology*, **10**, 161-182.

Allen, J.R.L. (1983) Studies in fluvialite sedimentation bars, bar-complexes and sandstone sheets (low-sinuosity braided streams) in the brownstones (L. Devonian), Welsh Borders. *Sed. Geol.*, **33**, 237-293.

Alley, R.B., Cuffey, K.M., Evenson, E.B., Strasser, J.C., Lawson, D.E. and **Larson, G.J.** (1997) How glaciers entrain and transport basal sediment: physical constraints. *Quatern. Sci. Rev.*, **16**, 1017-1038.

Anderson, M.P. (1989) Hydrogeologic facies models to delineate large-scale spatial trends in glacial and glaciofluvial sediments. *Geol. Soc. Am. Bull.*, **101**, 501-511.

Beerbower, J. R. (1964) Cyclothems and cyclic depositional mechanisms in alluvial Plain sedimentation. Symposium on cyclic sedimentation, *Kansas Geo. Sur. Bull.* **169**, 31- 42.

Benn, D. and **Evans, D.J.A.** (1996) The interpretation and classification of subglacially deformed materials. *Quatern. Sci. Rev.*, **15**, 23-52.

Benn, D. and **Evans, D.J.A.** (2010) Glaciers and Glaciation, 2nd edn. Hodder Education: London, UK. 802 pp.

Berg, R.C., Weibel, C.P., Stumpf, A.J. and **McKay, E.D.** (2009) Bedrock Topography of the Middle Illinois River Valley, Bureau, Marshall, Peoria, Putnam, and Woodford Counties, Illinois: Illinois State Geological Survey, Illinois Map 15, 1:62,500. (http://www.isgs.illinois.edu/sites/isgs/files/maps/regional/mid-il-valley-bt.pdf)

Björnsson, H. (2002) Subglacial lakes and jökulhlaups in Iceland. *Global Planet. Change*, **35**, 255-271.

Boulton, G.S., Dent, D.L. and **Morris, E.M.** (1974) Subglacial shearing and crushing, and the role of water pressures in tills from south-east Iceland. *Geogr. Ann., Series A, Phys. Geogr.*, **56**, 135-145.

Boulton, G.S. and **Paul, M.A.** (1976) The influence of genetic processes on some geotechnical properties of glacial tills. *Quat. J. Eng. Geol. Hydrog.*, **9**, 159-194.

Boulton, G.S. (1982) Subglacial processes and the development of glacial bedforms. In: *Research in Glacial, Glaciofluvial, and Glacio-lacustrine Systems* (Eds. R. Davidson Arnott, W. Nickling, and B.D. Fahey), pp.1-31. Geobooks, Norwich.

Boulton, G.S. 1987. A theory of drumlin Fm. by subglacial sediment deformation. In: *Drumlin Symposium* (Eds. J. Menzies and J. Rose), pp. 25-80. Balkema, Rotterdam.

Boulton, G.S. and **Hindmarsh, R.C.A.** (1987) Sediment deformation beneath glaciers: rheology and geological consequences. *J. Geophys. Res.*, **92**, 9059-9082.

Boulton, G.S. (1996) The origin of till sequences by subglacial sediment deformation beneath mid-latitude ice sheets. *Ann. Glaciol.*, **22**, 75-84.

Boulton, G.S., Dobbie, K.E. and **Zatsepin, S.** (2001) Sediment deformation beneath glaciers and its coupling to the subglacial hydraulic system. *Quatern. Int.*, **86**, 3-28.

Boulton, G.S., Hagdorn, M., Maillot, P.B. and **Zatsepin, S.** (2009) Drainage beneath ice sheets: groundwater-channel coupling, and the origin of esker systems from former ice sheets. *Quatern. Sci. Rev.*, **28**, 621-638.

Boyce, J.I. and **Eyles, N.** (1991) Drumlins carved by deforming till streams below the Laurentide ice sheet. *Geology,* **19**, 787-790.

Boyce, J.I. and **Eyles, N.** (2000) Architectural element analysis applied to glacial deposits: Internal geometry of a late Pleistocene till sheet, Ontario, Canada. Geol. *Soc. Am. Bull.*, **112**, 98-118.

Carlson, A.E., Jenson, J.W. and **Clark, P.U.** (2004) Sedimentological observations from the Tiskilwa Till, Illinois, and Sky Pilot Till, Manitoba. *Geographie physique et Quaternaire*, **58**, 4001-4011.

Catuneanu, O., Abreu, V., Bhattacharya, J.P., Blum M.D., Dalrymple, R.W., Eriksson P.G., Fielding, C.R., Fisher, W.L., Galloway, W.E., Gibling, M.R., Giles, K.A., Holbrook, J.M., Jordan, R., Kendall, C.G.St.C., Macurda, B., Martinsen, O.J., Miall, A.D., Neal, J.E., Nummedal, D., Pomar, L., Posamentier, H.W., Pratt, B.R., Sarg, J.F., Shanley, K.W., Steel, R.J., Strasser, A., Tucker, M.E., and **Winker, C.** (2009) Towards the standardization of sequence stratigraphy. *Earth-Sci. Rev.*, **92**, 1-33.

Clark, J.D. and **Pickering, K.T.** (1996) Architectural elements and growth patterns of submarine channels: Application to hydrocarbon exploration. *AAPG Bull.*, **80**, 194-221.

Clark, C.D. and **Meehan, R.T.** (2001) Subglacial bedform geomorphology of the Irish Ice Sheet reveals major configuration changes during growth and decay. *J. Quatern. Sci.*, **16**, 483-496.

Deutsch, C.V. and **Tran, T.T.** (2002) FLUVSIM: a program for object-based stochastic modeling of fluvial depositional systems. *Comput. Geosci.*, **28**, 525-535

Drinkwater, N.J. and **Pickering, K.T.** (2001) Architectural elements in a high-continuity sand-prone turbidite system, late Precambrian Kongsfjord Fm., northern Norway: Application to hydrocarbon reservoir characterization. *AAPG Bull.*, **85**, 1731-1757.

El-ghali, M.A.K. (2005) Depositional environments and sequence stratigraphy of paralic glacial, paraglacial and postglacial Upper Ordovician siliciclastic deposits in the Murzuq Basin, SW Libya. *Sed. Geol.*, **177**, 145-173.

Engelhardt, H. and **Kamb, B.** (1998) Basal sliding of Ice Stream B, West Antarctica. *J. Glaciol.*, **44**, 223-230.

Evans, D.J.A. and **Twigg, D.R.** (2002) The active temperate glacial landsystem: a model based on Breidamerkurjokull and Fjallsjokull, Iceland. *Quatern. Sci. Rev.*, **21**, 2143-2177.

Evans, D.J.A. (2005) Glacial Landsystems. (Ed. D.J.A. Evans). Hodder Arnold: London, UK. 532 pp.

Evans, D.J.A. and **Hiemstra, J.F.** (2005) Till deposition by glacier submarginal, incremental thickening. *Earth Surf. Proc. Land.*, **30**, 1633-1662.

Evans, D.J.A., Phillips, E.R., Hiemstra, J.F. and **Auton, C.A.** (2006) Subglacial till: Fm., sedimentary characteristics and classification. *Earth-Sci. Rev.*, **78**, 115-176.

Eyles, N., Eyles, C.H. and **Miall, A.D**. (1983) Lithofacies types and vertical profile models; an alternative approach to the description and environmental interpretation of glacial diamict and diamictite sequences. *Sedimentology*, **30**, 393-410.

Fischer, U., Clarke, G.K.C. and **Blatter, H.** (1999) Evidence for temporally varying "sticky spots" at the base of Trapridge Glacier, Yukon Territory, Canada. *J. Glaciol.*, **45**, 352-360.

Fischer, U. and **Clarke, G.K.C.** (2001) Review of subglacial hydro-mechanical coupling: Trapridge Glacier, Yukon Territory, Canada. *Quatern. Int.*, **86**, 29-43.

Ghazi, S. and **Mountney, N.P.** (2009) Facies and architectural element analysis of a meandering fluvial succession: The Permian Warchha Sandstone, Salt Range, Pakistan. *Sed. Geol.*, **221**, 99-126.

Gerber, R.E. and **Howard, K.W.F.** (1996) Evidence for recent groundwater flow through Late Wisconsinan till near Toronto, Ontario. *Can. Geotech. J.*, **33**, 538-555.

Gerber, R.E. and **Howard, K.** (2000) Recharge through a regional till aquitard: three-dimensional flow model water balance approach. *Groundwater*, **38**, 410-422.

Gerber, R.E., Boyce, J.I. and **Howard, K.W.F.** (2001) Evaluation of heterogeneity and field-scale groundwater flow regime in a leaky till aquitard. *Hydrogeology J.*, **9**, 60-78.

Hansel, A.K. and **Johnson, W.H.** (1996) Wedron and Mason Groups: Lithostratigraphic reclassification of deposits of the Wisconsin Episode, Lake Michigan area. *Illinois State Geol. Sur. Bull.*, pp. 104.

Hansel, A.K. and **McKay, E.D.** (2010) Chapter 12: Quaternary Period. In: *Geology of Illinois* (Eds. D.R. Kolata and C.K. Nimz), pp. 216-247. University of Illinois Board of Trustees, Illinois State Geological Survey, Champaign, IL, USA.

Hart, J.K. and **Boulton, G.S.** (1991) The interrelation of glaciotectonic and glaciodepositional processes within the glacial environment. *Quatern. Sci. Rev.*, **10**, 335-350.

Hart, J.K. (1998). The deforming bed/debris-rich basal ice continuum and its implcations for the formation of glacial landforms (flutes) and sediments (melt-out till). *Quatern. Sci. Rev.*, **17**, 737-754.

Heinz, J. and **Aigner, T.** (2003) Hierarchical dynamic stratigraphy in various Quaternary gravel deposits, Rhine glacier area (SW Germany): implications for hydrostratigraphy. *Int. J. Earth Sci.*, **92**, 923-938.

Herzog, B.L., Griffin, R.A., Stohr, C.J., Follmer, L.R., Morse, W.J., and **Su, W.J.** (1989) Investigation of failure mechanisms and migration of organic chemicals at Wilsonville, Illinois. Ground Water Monitor. Rev., **9**, 82-89.

Hiemstra, J.F. and **Rijsdijk, K.F.** (2003) Observing artificially induced strain: implications for subglacial deformation. *J. Quatern. Sci.*, **18**, 373–383.

Hooyer, T.S. and **Iverson, N.R.** (2000) Diffusive mixing between shearing granular layers: constraints on bed deformation from till contacts. *J. Glaciol*, **46**, 641-651.

Hornung, J. and **Aigner, T.** (1999) Reservoir and aquifer characterization of fluvial architectural elements: Stubensandstein, Upper Triassic, southwest Germany. *Sed. Geol.*, **129**, 215-280.

Hubbard, S.M., Romans, B.W. and **Graham, S.A.** (2008) Deep-water foreland basin deposits of the Cerro Toro Fm., Magallanes basin, Chile: architectural elements of a sinuous basin axial channel belt. *Sedimentology*, **55**, 1333-1359.

Hughes, P.D. (2010) Geomorphology and Quaternary stratigraphy: The roles of morpho-, litho-, and allostratigraphy. *Geomorphology*, **123**, 189-199.

Huuse, M., Le Heron, D.P., Dixon, R., Redfern, J., Moscariello, A., and **Craig, J.** (2012) Glaciogenic reservoirs and hydrocarbon systems: an introduction. *Geol. Soc. London*, **368**, 1-28.

Illinois State Geological Survey (ISGS), Illinois Height Modernization Program, and Illinois Department of Transportation (2011) LiDAR of Marshall County. Illinois LiDAR county database: Illinois State Geological Survey.

Johnson, W.H. and **Hansel, A.K.** (1990) Multiple Wisconsinan glacigenic sequences at Wedron, Illinois. *J. Sed. Petrol.*, **60**, 26-41.

Keller, C.K., van der Kamp, G and **Cherry, J.A.** (1985) Fracture permeability and groundwater flow in clayey till near Saskatoon, Saskatchewan. *Can. Geotech. J.*, **23**, 229-240.

Kempton, J. P., W J. Morse and **A. P. Visocky** (1982) Hydrogeologic Evaluation of Sand and Gravel Aquifers for Municipal Groundwater Supplies in East-Central Illinois: Illinois State Geological Survey and Illinois State Water Survey Cooperative Groundwater Report 8, pp. 59.

Kessler, T.C., Klint, K.E.S., Nilsson, B. and **Bjerg, P.L.** (2012) Characterization of sand lenses embedded in tills. *Quatern. Sci. Rev.*, **53**, 55-71.

Kjaer, K.H., Larsen, E., van der Meer, J., Ingolfsson, O., Kruger, J., Benediktsson, I.O., Knudsen, C.G. and **Schomacker, A.** (2006) Subglacial decoupling at the sediment/bedrock interface: a new mechanism for rapid flowing ice. *Quatern. Sci. Rev.*, **25**, 2704-2712.

Lang, J., Dixon, R. J., Le Heron, D. P., and **Winsemann, J.** (2012) Depositional architecture and sequence stratigraphic correlation of Upper Ordovician glaciogenic deposits, Illizi Basin, Algeria. *Geol. Soc. London*, **368**, 293-317.

Larsen, N.K. and **Piotrowski, J.A.** (2003) Fabric pattern in a basal till succession and its significance for reconstructing subglacial processes. *J. Sed. Res.*, **73**, 725-734.

Larsen, N.K., Piotrowski, J.A. and **Kronborg, C.** (2004) A multiproxy study of a basal till: a time-transgressive accretion and deformation hypothesis. *J. Quatern. Sci.*, **19**, 9-21.

Lawson, D.E. (1981) Distinguishing characteristics of diamictons at the margin of the Matanuska Glacier, Alaska. *Ann. Glaciol.*, **2**, 78-84.

Lee, J.R., and **Phillips, E.R.** (2008) Progressive soft sediment deformation within a subglacial shear zone- a hybrid mosaic- pervasive deformation model for Middle Pleistocene glaciotectonised sediments from eastern England. *Quatern. Sci. Rev.*, **27**, 1350-1362.

Martini, I.P. and **Brookfield, M.E.** (1995) Sequence analysis of Upper Pleistocene (Wisconsinan) glaciolacustrine deposits of the north-shore bluffs of Lake Ontario, Canada. *J. Sed. Res.*, **B65**, 388-400.

McDonald, B.C. and **Banerjee, I.** (1971) Sediments and bed forms on a braided outwash plain. *Can. J. Earth Sci.*, **8**, 1282-1301.

McKay, E.D., III, Berg, R.C., Stumpf, A.J. and **Weibel, C.P.** (2007) Surficial geology of Chillicothe Quadrangle, Peoria, Marshall, and Woodford Counties, Illinois: Illinois State Geological Survey, Illinois Preliminary Geologic Map, IPGM Chillicothe-SG, 1:24,000. (http://isgs.illinois.edu/?q=maps/isgs-quads/chillicothe-surficial-geology-2007)

McKay, E. D. III, Berg, R. C., Hansel, A.K., Kemmis, T.J. and **Stumpf, A.J.** (2008) Quaternary deposits and history of the Ancient Mississippi River Valley, northcentral Illinois. Fifty-first Midwest Friends of the Pleistocene Field Trip, an ISGS centennial field trip. Illinois State Geological Survey, Guidebook 35. Illinois Department of Natural Resources.

Meriano, M. and **Eyles, N.** (2009) Quantitative assessment of the hydraulic role of subglaciofluvial interbeds in promoting deposition of deformation till (Northern Till, Ontario). *Quatern. Sci. Rev.*, **28**, 608-620.

Miall, A.D. (1977) A review of the braided-river depositional environment. *Earth-Sci. Rev.*, **13**, 1-62.

Miall, A.D. (1985) Architectural-element analysis: A new method of facies analysis applied to fluvial deposits. *Earth-Sci. Rev.*, **22**, 261-308.

Miall, A.D. (1988) Architectural elements and bounding surfaces in fluvial deposits: anatomy of the Kayenta Fm. (Lower Jurassic), southwest Colorado. *Sed. Geol.*, **55**, 233-262.

Miall, A.D. (2010) Alluvial Deposits. In: *Facies Models 4* (Eds. N. P. James and R.W. Dalrymple). Geological Association of Canada, St. Johns, Newfoundland, 575 pp.

Middleton, G.V. (1973) Johannes Walther's Law of the correlation of facies. *Geol. Soc. Am. Bull.*, **84**, 979-988.

Mitchum, R.M., Jr. and **Van Wagoner, J.C.** (1991) High-frequency sequences and their stacking patterns: sequence-stratigraphic evidence of high-frequency eustatic cycles. *Sed. Geol.*, **70**, 131-160.

Ng, F.S.L. (2000) Coupled ice-till deformation near subglacial channels and cavities. *J. Glaciol.*, **46**, 580-598.

Nilsson, B., Sidle, R.C., Klint, K.E., Boggild, C.E. and **Broholm, K.** (2001) Mass transport and scale-dependent hydraulic tests in a heterogeneous glacial till-sandy aquifer system. *J. Hydrol.*, **243**, 162-179.

Ó Cofaigh, C., Pudsey, C.J., Dowdeswell, J.A. and **Morris, P.** (2002) Evolution of subglacial beforms along a paleo-ice stream, Antarctic Peninsula continental shelf. *Geophys. Res. Lett.*, **29**, pp.41.

Phillips, E.R., Evans D.J.A. and **Auton, C.A.** (2002) Polyphase deformation at an oscillating ice margin following the Loch Lomond Readvance, central Scotland, UK. *Sed. Geol.*, **149**, 157-182.

Piotrowski, J.A. and **Kraus, A.** (1997) Response of sediment to ice sheet loading in northwestern Germany: effective stresses and glacier bed stability. *J. Glaciol.*, **4**, 495-502.

Piotrowski, J.A. and **Tulaczyk, S.** (1999) Subglacial conditions under the last ice sheet in northwest Germany: ice-bed separation and enhanced basal sliding? *Quatern. Sci. Rev.*, **18**, 737-751.

Piotrowski, J.A., Larsen, N.K. and **Junge, F.W.** (2004) Reflections on soft subglacial beds as a mosaic of deforming and stable spots. *Quatern. Sci. Rev.*, **23**, 993-1000.

Piotrowski, J.A., Larsen, N.K., Menzies, J., and **Wysota, W.** (2006) Formation of subglacial till under transient bed conditions: deposition, deformation, and basal decoupling under a Weichselian ice sheet lobe, central Poland. *Sedimentology*, **53**, 83-106.

Räsänen, M.E., Auir, J.M., Huitti, J.V., Klap, A.K., and **Virtasalo, J.J.** (2009) A shift from lithostratigraphic to allostratigraphic classification of Quaternary glacial deposits. *GSA Today*, **19**, 4-11.

Rippin, D., Willis, I., Arnold, N., Hodson, A., Moore, J., Kohler, J. and **Björnsson, H.** (2003) Changes in geometry and subglacial drainage of Midre Lovenbreen, Svalbard, determined from digital elevation models. Earth Surf. Process. Landforms, **28**, 273-298.

Rodvang, S.J. and **Simpkins, W.W.** (2001) Agricultural contaminants in Quaternary aquitards: A review of occurrence and fate in North America. *Hydrogeology J.*, **9**, 44-59.

Shaw, J. (2002) The meltwater hypothesis for subglacial bedforms. *Quatern. Int.*, **90**, 5-22.

Slomka, J.M. and **Eyles C.H.** (2013) Characterizing heterogeneity of a glaciofluvial deposit using architectural elements, Limehouse, Ontario, Canada. *Can. J. Earth Sci.*, **50**, 911-929.

Swift, D.A., Nienow, P.W., Spedding, N. and **Hoey, T.B.** (2002) Geomorphic implications of subglacial drainage configuration: rates of basal sediment evacuation controlled by seasonal drainage system evolution. *Sed. Geol.*, **149**, 5-19.

Thorn, C.E. and **Welford, M.R.** (1994) The equilibrium concept in geomorphology. *Ann. Assoc. Am. Geog.*, **84**, 666-696.

Tulaczyk, S. (1999) Ice sliding over weak, fine-grained tills: dependence of ice-till interactions on till granulometry. In: *Glacial Processes: Past and Present* (Eds. D.M. Mickelson and J.W. Attig), *Geological Society of America, Special Paper*, 337, 159-177.

van der Meer, J.J.M., Menzies, J. and **Rose, J.** (2003) Subglacial till: the deforming glacier bed. *Quatern. Sci. Rev.*, **22**, 1659-1685.

van Vliet-Lanoë, B., Magyari, A., and Meilliez, F. (2004). Distinguishing between tectonic and periglacial deformations of Quaternary continental deposits in Europe. *Glob. Planet. Change.*, **43**, 103-127.

Walder , J.S. and **Fowler, A.** (1994) Channelized subglacial drainage over a deformable bed. *J. Glaciol.*, **40**, 134, 3-15.

Wickham, S.S. and **Johnson, W.H.** (1981) The Tiskilwa Till, a regional view of its origin and depositional processes. *Ann. Glaciol.*, **2**, 176-182.

Wickham, S.S., Johnson, W.H. and **Glass, H.D.** (1988) Regional geology of the Tiskilwa Till Member, Wedron Fm., Northeastern Illinois. *Illinois State Geological Survey Circular*, 43, pp. 35.

Willman, H.B. and **Frye, J.C.** (1970) Pleistocene Stratigraphy of Illinois. *Illinois State Geol. Sur. Bull.*, 94, pp. 204

Wysota, W. (2007) Successive subglacial depositional processes as intepreted from basal tills in the Lower Vistula valley (N Poland). *Sed. Geol.*, **193**, 21-31.

CHAPTER 3: ARCHITECTURAL-LANDSYSTEM ANALYSIS OF A MODERN GLACIAL LANDSCAPE, SÓLHEIMAJÖKULL, SOUTHERN ICELAND

Abstract

Glacial terrains are commonly recorded using a landsystems approach, which allows detailed documentation of the geomorphological evolution of the landscape. However, landsystem analysis of Quaternary subsurface stratigraphies in which landforms are not apparent or preserved is problematic, making delineation of the sedimentary architecture of a glaciated basin infill difficult. The purpose of this study is to delineate the sedimentary architecture of the Sólheimajökull (southern Iceland) glacial landsystem and to provide an architectural framework for allostratigraphy and modern analogue purposes. An integrated architectural-landsystem approach is applied here, which utilizes principles from both architectural element analysis (AEA; Miall, 1985) and landsystem analysis (Evans, 2005). A bounding surface hierarchy (fourth- to seventh-order surfaces) provides a framework within which the architecture is organized. Fieldwork was conducted at Sólheimajökull glacier in 2012 and 2013, and twenty-two different surface features (bounded by fourth-order surfaces) were mapped, which were grouped into four different landsystem tracts (glaciofluvial, ice contact, jökulhlaup, and colluvial slope; bounded by sixth-order surfaces). Landsystem tracts were deconstructed into smaller architectural units (components; bounded by fifth-order surfaces), which allowed the delineation of eight allostratigraphic units that record the evolution of the glacial landsystem from approximately 7000 years BP to 2013 AD. The results of this study can provide insight to interpretation and delineation of the sedimentary architecture of other modern glacial landsystems and subsurface Quaternary deposits in North America and other formerly glaciated areas.

3.1 INTRODUCTION

Studies at modern glacier margins allow first-hand documentation of the geomorphology, sedimentology, and sedimentation processes active in these environments, which can be utilized to understand the depositional and paleoenvironmental history of older Quaternary glacial successions (e.g. Boulton, 1972; Evans et al., 1999). Glacial landforms, and the sediments they contain, are commonly recorded using a landsystems approach (e.g. Evans and Rea, 1999; Evans et al., 1999; Andrzejewski, 2002; Delaney, 2002; Evans and Twigg, 2002; Spedding and Evans, 2002; Benn and Lukas, 2006; Golledge, 2007; Evans et al., 2008) which involves grouping genetically related sediment-landform assemblages into mappable units. The landsystems approach allows reconstruction of the geomorphological evolution of a glacial landscape, including its depositional and erosional history, based on the location, spatial relationship, and degree of preservation of sediment-landform associations (Evans, 2005). However, application of the landsystems approach for paleoenvironmental reconstruction of deeply buried subsurface deposits (in which the surface expression of landforms is not apparent or preserved) is problematic, making seamless delineation of the sedimentary architecture of a glaciated basin infill, from shallow to deep subsurface units, difficult.

Subsurface sedimentary geometries of glacial deposits are commonly delineated from exposed outcrop sections and by correlating units between boreholes, and may be analysed using stratigraphic methods such as lithostratigraphy (e.g. Meyer and Eyles, 2007), sequence stratigraphy (e.g. El-ghali, 2005), and allostratigraphy (e.g. Eyles et al., 1998). The dynamic, and inherently erosional, nature of glacial depositional environments makes application of Walther's Law (Middleton, 1973) difficult; hence, principles of lithostratigraphy and formal lithostratigaphic units (e.g. Willman and Frye, 1970) may not be the most appropriate methods for characterizing complex glacial successions (Räsänen et al., 2009; Hughes, 2010). Sequence stratigraphy has been utilized for the analysis of glacial successions deposited in marine-influenced (e.g. Powell and Cooper, 2002; El-ghali, 2005) and glaciolacustrine (e.g. Martini and Brookfield, 1995) depositional environments; however, sequence stratigraphy is based on identification of fluctuations in sea level, the delineation of highstand and lowstand systems tracts, and identification of key surfaces (discontinuities and their correlative conformities) including a maximum flooding surface, which may not be applicable in glaciated terrain where marine influence is negligible or absent. Allostratigraphic principles are suitable for the analysis of the architecture of non-marine glacial successions because delineation of discontinuities is not reliant on sea level change. However, as a stand-alone method, allostratigraphy does not facilitate the characterization of the architecture and geometry of glacial deposits at various scales of resolution (e.g. facies associations to mappable units), and allostratigraphic units (and their bounding discontinuities) are often difficult to delineate between different depositional environments that have complex spatial relationships.

Architectural element analysis (AEA) is an informal stratigraphic method (NACSN, 2005) for the delineation and characterization of sedimentary geometry at different scales of resolution (e.g. bedform to major basin fill), which is nested in a framework of hierarchical bounding surfaces. The bounding surfaces represent unconformities of different scales and serve as a framework within which the sedimentary architecture is structured (Miall, 1988). AEA was developed for the analysis of ancient fluvial sediments exposed in outcrop sections (Allen, 1983; Miall, 1985) and has since been modified and applied for the analysis of sediments deposited in fluvial (e.g. Miall, 1994; Ghazi and Mountney, 2009), deep marine (e.g. Hubbard et al., 2008), deltaic (e.g. Eriksson et al. 1995), subglacial (e.g. Boyce and Eyles 2000), and glaciofluvial (e.g. Slomka and Eyles, 2013) depositional environments.

The purpose of this study is to delineate the sedimentary architecture of the Sólheimajökull landsystem utilizing an integrated architectural-landsystems approach in order to: 1) test the applicability of AEA in a modern glacial depositional environment; 2) characterize the main architectural components of the landscape; 3) understand the allo- and autogenic controls on the sedimentary architecture; and 4) provide an architectural model of the Sólheimajökull landsystem for modern analogue and allostratigraphic purposes. This paper is the first of its kind to explore and utilize an integrated architectural-landsystem methodology to delineate the sedimentary architecture of a glaciated landscape. Translation of landsystem units into hybrid architectural-landsystem units has significant implications for delineation of the sedimentary architecture of other modern ice margins and subsurface glacial deposits within previously glaciated terrains, and facilitates the construction of architectural models at various scales of resolution that may be utilized for other applications such as groundwater investigations and source water protection programs in areas where coarse-grained glaciofluvial units host significant aquifers.

3.2 STUDY AREA AND GEOLOGIC HISTORY

Sólheimajökull is a non-surging, temperate outlet glacier of the Mýrdalsjökull ice cap located in southern Iceland (Fig. 3.1; Björnsson, 2002; Scharrer et al., 2008). The accumulation area (altitude of 1300 m a.s.l.) sits above the southwestern part of the Katla volcano caldera (Scharrer et al., 2008). Sólheimajökull is blanketed with supraglacial debris derived from the 1918 Katla eruption, the 1999 jökulhlaup event (a catastrophic release of glacial meltwater), and steep bedrock valley slopes (including Jökulhaus, a prominent bedrock outlier; Fig. 3.1). The Little Ice Age (c. 1750-1920 AD; Dugmore and Sugden, 1991) glacial position is demarcated by a series of prominent end moraines from which the ice margin underwent punctuated retreat until about 1970 AD (Fig. 3.1). After this period of recession, the ice margin advanced to the 1995 ice margin position (Fig. 3.1), followed by continuous retreat (average of 50 m per year) to its present-day position (Maizels, 1991; Friis, 2011; Schomacker et al., 2012). The glacier snout is presently retreating into a bedrock trough that has been subglacially scoured in some places to 50 m below sea level, and is presently occupied by an ice-contact lake (Mackintosh et al., 2002).

Meltwater from the ice margin is drained by the Jökulsá á Sólheimasandi, which also receives meltwater discharged from Jökulsárgil river (flowing from Jökulsárgilsjökull in the north; Sigurðsson and Williams, 1991), Hólsárgil river (flowing southeast of Jökulhaus), and several other smaller streams (Russell et al., 2010a; Fig. 3.1). Along much of its length, Jökulsá is contained within a steep-walled valley incised by glaciofluvial erosion and widened by jökulhlaups. Older glacial sediments are exposed in

Fig. 3.1 Study area at Sólheimajökull in southern Iceland. A. Major geomorphic features of the distal proglacial area, including the Jökulsá river valley, sandar (Sólheimasandur and Skogasandur), major terraces (Pumice and Palagonite Terraces), minor bluffs (marked by hatched lines), and fans (Skoga, Holsa, Husa, and Klifandi fans). Thirteen stratigraphic units (identified by Maizels, 1989, 1991) comprise the sandar, and approximate ages are provided (note that Units 2-4 are not exposed at the surface; after Maizels, 1989, 1991; Friis 2011, Schomacker et al. 2012; Mountney and Russell, 2006). The location of B is outlined in red, and allostratigraphic units (AUs) delineated in this study are provided in parentheses. B. Terminal and lateral moraines are represented by dashed lines and ages of ice marginal positions are indicated (satellite image from 27 August 2010; Google Earth, 2014). C. Net cumulative change in the position of the ice margin of Sólheimajökull since 1930 AD to 2010 AD (modified from Schomacker et al., 2012; original data from the Iceland Glaciological Society database).

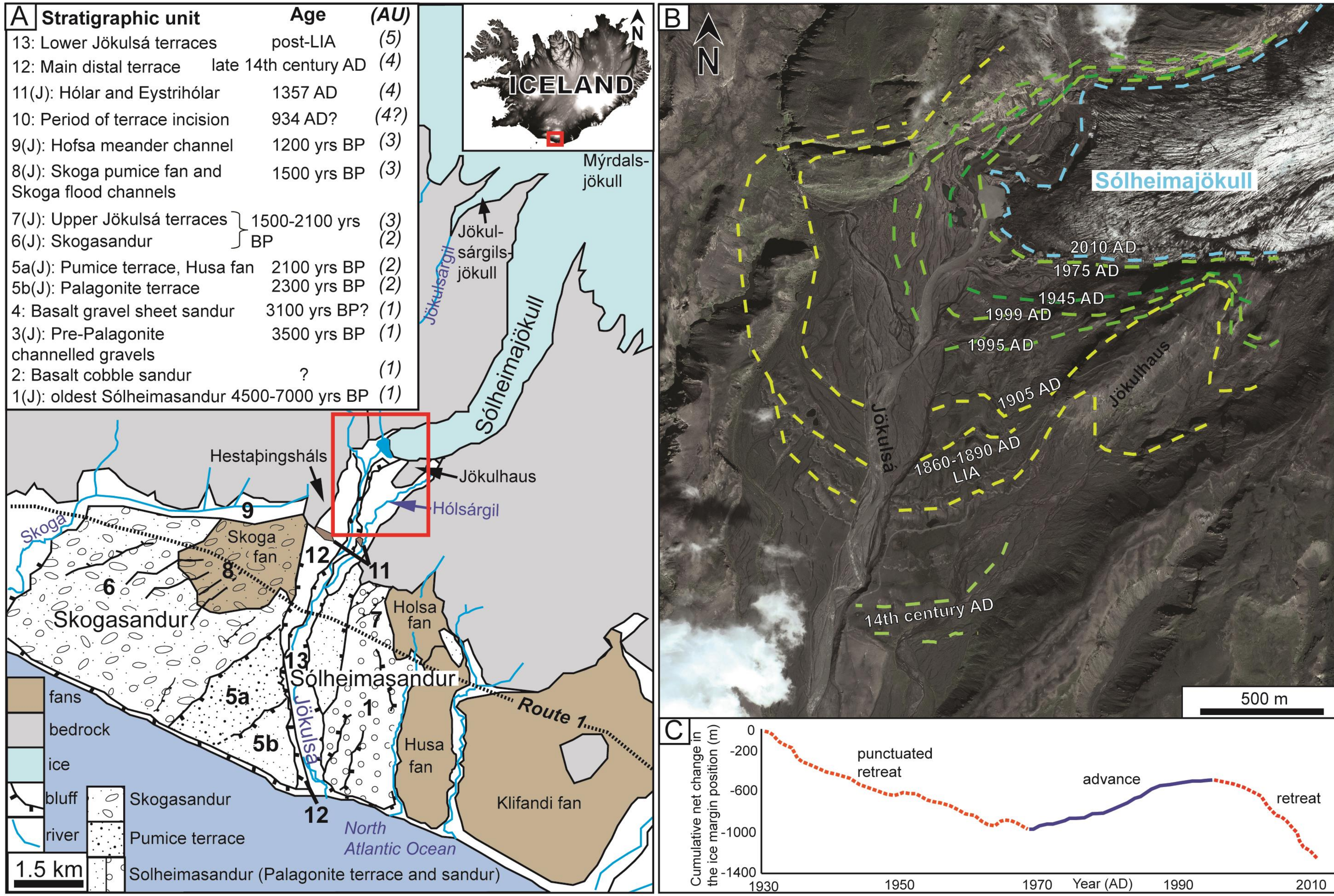

A
Stratigraphic unit
Age
(AU)
13: Lower Jökulsá terraces post-LIA (5)
12: Main distal terrace late 14th century AD (4)
11(J): Hólar and Eystrihólar 1357 AD (4)
10: Period of terrace incision 934 AD? (4?)
9(J): Hofsa meander channel 1200 yrs BP (3)
8(J): Skoga pumice fan and Skoga flood channels 1500 yrs BP (3)
7(J): Upper Jökulsá terraces 1500-2100 yrs BP (3)
6(J): Skogasandur (2)
5a(J): Pumice terrace, Husa fan 2100 yrs BP (2)
5b(J): Palagonite terrace 2300 yrs BP (2)
4: Basalt gravel sheet sandur 3100 yrs BP? (1)
3(J): Pre-Palagonite channelled gravels 3500 yrs BP (1)
2: Basalt cobble sandur ? (1)
1(J): oldest Sólheimasandur 4500-7000 yrs BP (1)
ICELAND
N
Mýrdals-jökull
Jökul-sárgils-jökull
Jökulsárgil
Sólheimajökull
Hestaþingsháls
Jökulhaus
Hólsárgil
Skoga
Skoga fan
Skogasandur
Sólheimasandur
Holsa fan
Husa fan
Klifandi fan
Route 1
Jökulsá
North Atlantic Ocean
fans
bedrock
ice
bluff
river
Skogasandur
Pumice terrace
Solheimasandur (Palagonite terrace and sandur)
1.5 km
B
N
Sólheimajökull
2010 AD
1975 AD
1945 AD
1999 AD
1995 AD
1905 AD
Jökulhaus
Jökulsá
1860-1890 AD LIA
14th century AD
500 m
C
Cumulative net change in the ice margin position (m)
0
-200
-600
-1000
-1400
punctuated retreat
advance
retreat
1930
1950
1970
1990
2010
Year (AD)

the valley walls and preserved in a series of terraces (Fig. 3.1; Friis, 2011). Beyond the road bridge along Route 1 (Fig. 3.1), Jökulsá flows towards the North Atlantic Ocean in a valley train between two outwash sandar, Skogasandur and Sólheimasandur (Fig. 3.1). Maizels (1989, 1991) identified thirteen stratigraphic units that make up the two sandar (Figs. 3.1A, 3.2) and dated the units using stratigraphic and geomorphic relationships, lichenometry, tephrachronology, and radiocarbon dating techniques (Maizels and Dugmore, 1985; Maizels, 1989, 1991). Both sandar are constructed from repeated jökulhlaups, glaciofluvial reworking, and alluvial fans (Figs. 3.1, 3.2A, D; Maizels, 1989).

Five jökulhlaups generated by volcanic activity of Katla (termed ‘kötluhlaups’; Maizels, 1989) have impacted Sólheimajökull in recorded history (Fig. 3.2B; Eliasson et al., 2006; Russell et al., 2010a,b), and at least eight major jökulhlaups have impacted Skogasandur and Sólheimasandur from 4500 BP to 1357 AD (Figs. 3.1A, 3.2A; Maizels, 1989, 1991). Minor jökulhlaups are also known to be generated from ice-dammed lakes in Jökulsárgil valley (Fig. 3.1), the most recent of which was recorded in 1936 (Thorarinsson, 1939; Maizels, 1991; Björnsson, 2002; Russell et al., 2010a). Active volcanic eruption sites on Katla are now most common and active in the Kötlujökull catchment (northeast of Sólheimajökull; Maizels, 1989; Eliasson et al., 2008; Scharrer et al., 2008); hence, most recent jökulhlaups at Mýrdalsjökull have impacted Kötlujökull and Mýrdalssandur (Russell et al., 2006). However, the most recent jökulhlaup to impact Sólheimajökull was on 18 July 1999 AD, and was generated by volcanic activity beneath the Mýrdalsjökull ice cap (Russell et al., 2010a,b). Meltwater was routed down the

Fig. 3.2 Jökulhlaup history at Sólheimajökull. A. Maximum paleodischarge and recurrence interval of floods at Sólheimajökull since 4500 years BP (see Fig. 3.1 for spatial extent of stratigraphic units; modified from Maizels, 1991). B. Five volcanic eruptions of Katla have resulted in a jökulhlaup (kötluhlaup) at Sólheimajökull in recorded history since the 8th Century (modified from Friis, 2011). C. Hydrograph of the 1999 AD jökulhlaup showing a rapid rise to peak discharge and waning flood to normal base flow on 18 July (modified from Russell et al., 2010). D. Subsurface units of Skogasandur and Sólheimasandur recorded by Maizels (1989, 1991) (i) along Route 1 and (ii) distal sediments recorded from bluffs along shoreline of the North Atlantic. Numbers correspond to allostratigraphic units in A (in parentheses) and Fig. 3.1 (modified from Maizels 1989).

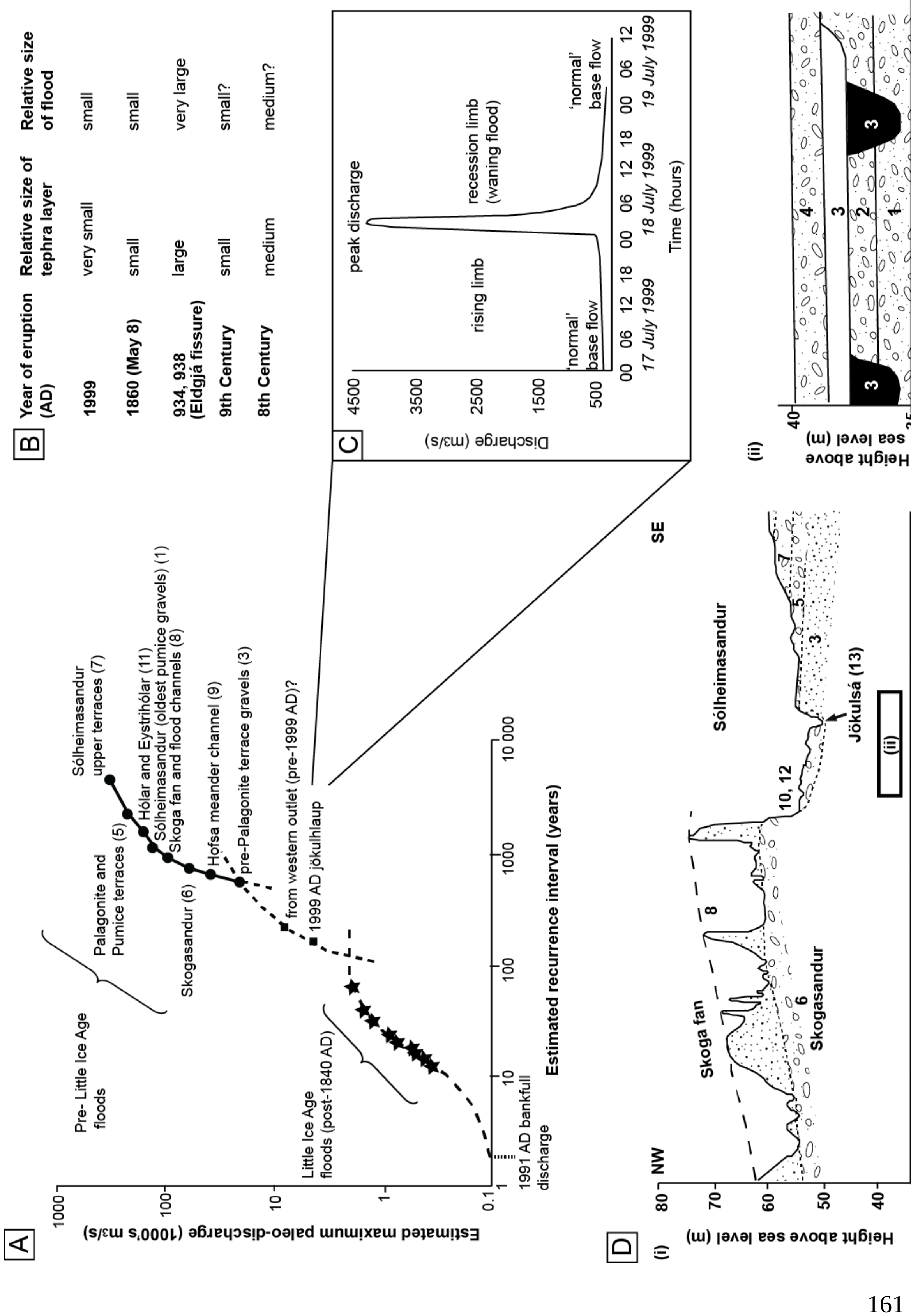
A
Estimated maximum paleo-discharge (1000's m3/s)
Estimated recurrence interval (years)
Pre- Little Ice Age floods
Little Ice Age floods (post-1840 AD)
1991 AD bankfull discharge
Palagonite and Pumice terraces (5)
Skogasandur (6)
Sólheimasandur upper terraces (7)
Hólar and Eystrihólar (11)
Sólheimasandur (oldest pumice gravels) (1)
Skoga fan and flood channels (8)
Hofsa meander channel (9)
pre-Palagonite terrace gravels (3)
from western outlet (pre-1999 AD)?
1999 AD jökulhlaup
B
Year of eruption (AD)
Relative size of tephra layer
Relative size of flood
1999 very small small
1860 (May 8) small small
934, 938 (Eldgjá fissure) large very large
9th Century small small?
8th Century medium medium?
C
Discharge (m3/s)
peak discharge
rising limb
recession limb (waning flood)
'normal' base flow
17 July 1999
18 July 1999
19 July 1999
Time (hours)
D
(i)
Height above sea level (m)
NW
SE
Skoga fan
Skogasandur
Sólheimasandur
10, 12
Jökulsá (13)
(ii)
Distance (m)
Height above sea level (m)

western margin of the glacier ('Main Western Outlet') and formed an ice-dammed lake in Jökulsárgil valley (Fig. 3.1). Smaller jökulhlaup routeways were located at the central and eastern areas of the ice margin, and most of the jökulhlaup flow was contained within the Jökulsá valley (Maizels, 1989; Lawler et al., 1996; Roberts et al., 2000; Russell et al., 2002; Roberts and Russell, 2002; Russell et al., 2010a). Draining of the ice-dammed lake resulted in the deposition of a boulder fan in the ice-marginal area, and retreat of the ice margin since 1999 AD has exposed a large esker which forms remnant ice-cored hummocks in the ice-contact lake (Schomacker et al., 2012).

3.3 METHODS

Fieldwork at Sólheimajökull was conducted over a total of four weeks during May (2012 and 2013) and August (2013) on the east (north of Route 1) and west (south of Route 1) sides of Jökulsá (Fig. 3.3). Twelve transects record surface features and sediment types which were documented in hand-drawn sketch maps and in ESRI ArcPad using a handheld Thales MobileMapper CE global positioning system (GPS; Fig. 3.3). Transects originate from exposed bedrock surfaces (where available) on the valley walls, and include data on relative change in surface topography (y-axis), distance (x-axis), surface features, sediment type, spatial relationships (e.g. over- and underlying, interfingering) and the nature of contacts (e.g. erosional, truncated, gradational, sharp, conformable) between surface features and associated sediments (Figs. 3.4-3.9).

GPS data of surface features were integrated with 2010 LiDAR data (2 m resolution; courtesy of the University of Iceland), detailed sketch maps, transect data, and

Fig. 3.3 Location of data utilized in this study, collected during fieldwork at Sólheimajökull in May 2012 and 2013 and August 2013. A. Landsystems tracts and components recorded in the field and identified by remote sensing of 2008 Google Earth and LiDAR imagery, overlain on 2m x 2 m LiDAR data from 2010 (LiDAR data courtesy of the University of Iceland). The locations of the ice-proximal and distal areas and transects 11 and 12, as referred to in this study, are indicated. B. Transects 1-10 overlain on LiDAR data of the ice-proximal area, including the modern Jökulsá river, Hólsárgil tributary stream, and Jökulhaus bedrock outlier.

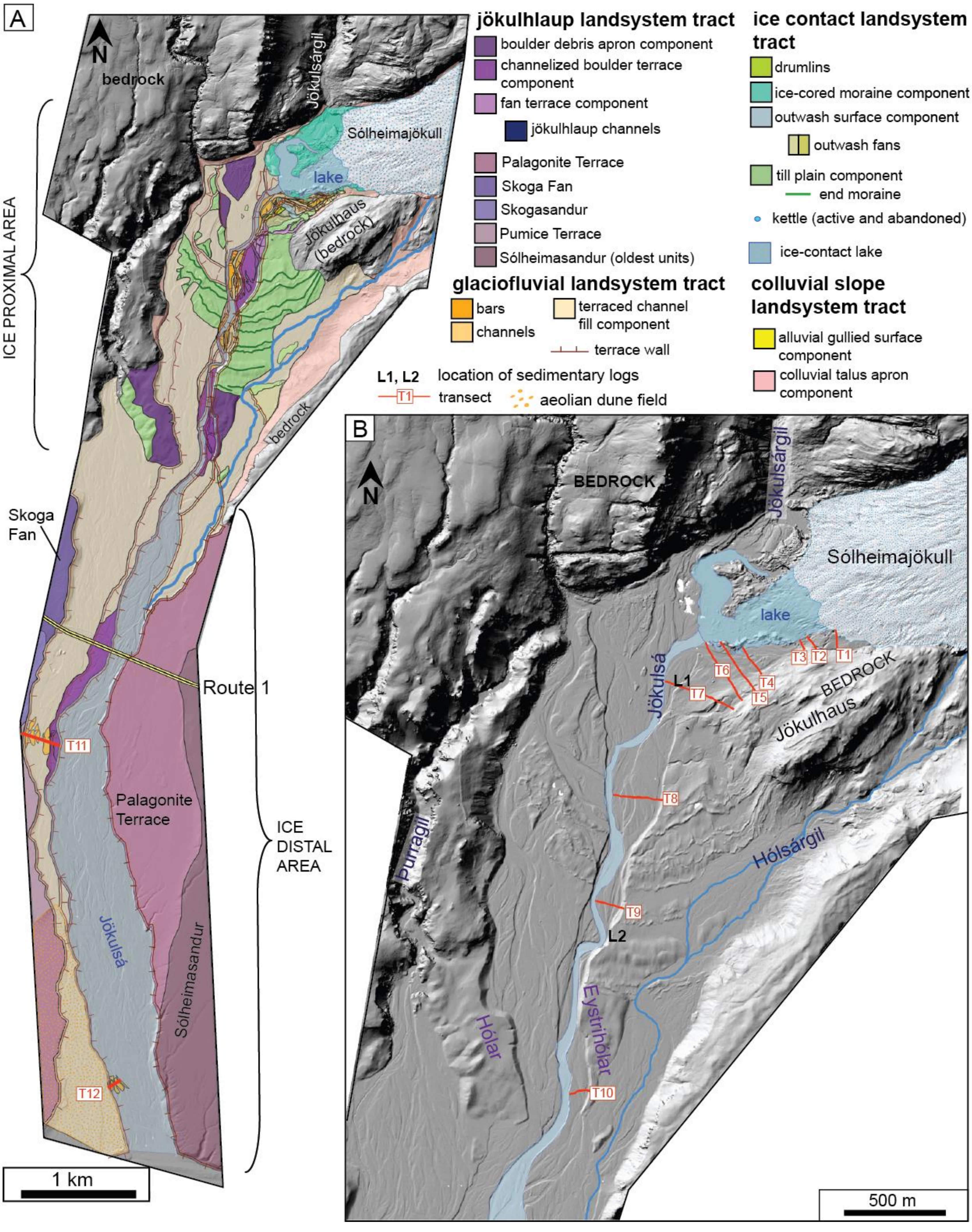
A
bedrock
Jökulsárgil
Sólheimajökull
lake
Jökulhaus (bedrock)
ICE PROXIMAL AREA
bedrock
Skoga Fan
Route 1
T11
Palagonite Terrace
ICE DISTAL AREA
Jökulsá
Sólheimasandur
T12
1 km
jökulhlaup landsystem tract
boulder debris apron component
channelized boulder terrace component
fan terrace component
jökulhlaup channels
Palagonite Terrace
Skoga Fan
Skogasandur
Pumice Terrace
Sólheimasandur (oldest units)
glaciofluvial landsystem tract
bars
channels
terraced channel fill component
terrace wall
ice contact landsystem tract
drumlins
ice-cored moraine component
outwash surface component
outwash fans
till plain component
end moraine
kettle (active and abandoned)
ice-contact lake
colluvial slope landsystem tract
alluvial gullied surface component
colluvial talus apron component
L1, L2 location of sedimentary logs
T1 transect
aeolian dune field
B
BEDROCK
Jökulsárgil
Sólheimajökull
lake
T1 T2 T3 T4 T5 T6 T7
L1
Jökulsá
BEDROCK
Jökulhaus
T8
Purragil
Hólsárgil
T9
L2
Eystrihólar
Hólar
T10
500 m

2010 satellite imagery (from Google Earth) in order to comprehensively reconstruct the Sólheimajökull landsystem (Fig. 3.10). Surface features and transects were input to a geographic information system (GIS; ESRI ArcMap) and overlain on a 2010 LiDAR image and a georeferenced 2010 satellite image (Google Earth) which encompass the ice-marginal area, bedrock valley slopes, and Jökulsá valley from the ice margin southward to the North Atlantic Ocean (Figs. 3.1, 3.3). Remote sensing of the LiDAR and satellite imagery was utilized to delineate surface features in areas where fieldwork was not conducted due to inaccessibility to the west (north of Route 1) and east (south of Route 1) of Jökulsá, as well as in the Hólsárgil valley (Figs. 3.1, 3.3). ‘Ice-proximal’ is defined here as terrain located north of the tenth century end moraine and ‘ice-distal’ refers to terrain located south of this moraine (Figs. 3.1, 3.3). ‘Ice-marginal’ is used here to refer to terrain that is in direct contact or in close proximity to the ice (i.e. subglacial or supraglacial positions, or abutting the ice in a proglacial setting).

Automated topographic profiles along transect lines were derived from the LiDAR data (using ‘interpolate line’ function in ArcMap 3D Analyst) and integrated with field-derived topographic profile data (Figs. 3.6-3.9). The LiDAR dataset collected in 2010 does not accurately (within 2 m) represent the surface elevation of ice-marginal features recorded during fieldwork in 2012 and 2013 because the glacier in 2010 still covered the 2012-2013 ice-marginal area; however, transect data recorded at the ice-margin during field work in 2012-2013 (Fig. 3.8B) provides an estimate of surface topography and relative changes in surface elevation.

Vector shapefiles (points, lines, and polygons) of surface features were converted to interpolated shapes (Functional Surface toolset of 3D Analyst Tools in ArcToolbox) based on surface elevations from the LiDAR data (using a Linear interpolation method), and imported to ArcScene for three-dimensional analysis of the composition and evolution of the landsystem architecture (Fig. 3.10). Previous studies at Sólheimajökull helped to constrain former ice margin positions, timing of geologic events, and the formation of sedimentary deposits in the proglacial area, and provide insight into the three-dimensional geometry and spatial relationship of sediments in the subsurface (Thorarinsson, 1943; Crittenden, 1975; Maizels, 1989, 1991; Dugmore and Sugden, 1991; Dugmore et al., 2000; Mackintosh et al., 2002; Russell et al., 2010a,b; Friis, 2011; Schomacker et al., 2012).

3.4 SEDIMENTARY ARCHITECTURE

An integrated architectural-landsystem approach is utilized here, whereby principles of landsystems analysis (Eyles, 1983; Evans, 2005) and architectural element analysis (AEA; Allen, 1983; Miall, 1985) are combined to characterize the sedimentary architecture of the Sólheimajökull landsystem. The basic framework of AEA is a hierarchical ranking of lithofacies contacts (Fig. 3.4) that record environmental changes at various spatial scales. Lithofacies contacts are assigned a numerical order in accord with the degree of environmental change recorded at each contact, and a single contact can transition between different orders of the surface hierarchy (Miall 1988, 2010). The degree of environmental change recorded by a bounding surface is controlled by internal

Fig. 3.4 Bounding surface hierarchy utilized in this study (modified from Miall, 2010; Slomka and Eyles, 2013).

Order	Description of bounding surfaces	Surface expression	Control
1	A conformable facies contact separating similar lithofacies	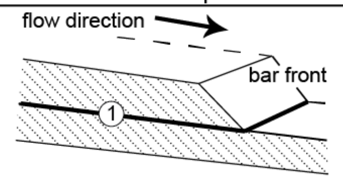	autogenic
2	A conformable facies contact separating dissimilar lithofacies	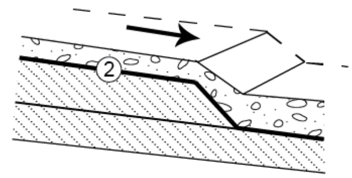	autogenic
3	Conformable (but can be erosional) facies contact which crosscuts 1st- and 2nd-order surfaces, separating similar and dissimilar lithofacies. It may be a surface of reactivation.	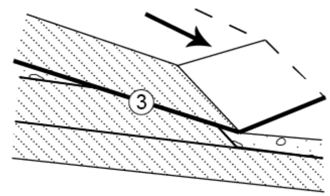	autogenic
4	Facies contact that delineates packages of genetically-related lithofacies associations with a characteristic geometry and lithofacies composition (delineates surface features, e.g. bars)	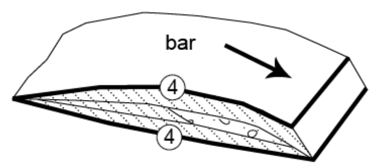	autogenic
5	Conformable boundary defining groups of similar and genetically related surface features (delineates landsystem tract components, e.g. glaciofluvial terraces)	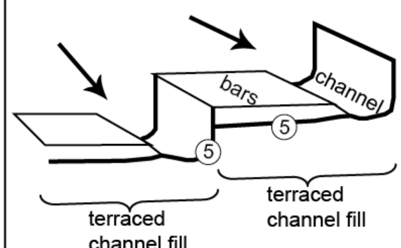	autogenic and allogenic
6	A major contact separating groups of genetically related landsystem tract components and delineates a landsystem tract, e.g. boundary between glaciofluvial and ice-contact landsystem tracts (defines a depositional environment and may be equivalent to a mappable lithostratigraphic unit)	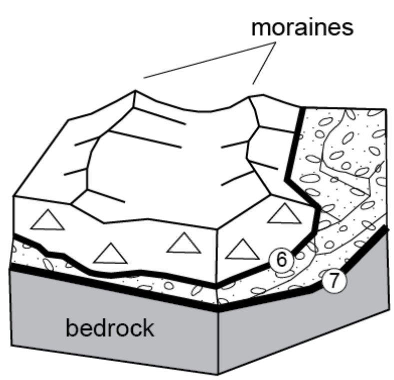	allogenic
7	A surface demarcating the base of a major depositional complex (delineates a landsystem, e.g. surface between volcanic bedrock and overlying unlithified sediments of glacial origin)		allogenic

(autogenic) and external (allogenic) controls on depositional, erosional, and transport processes within a depositional system (Miall, 2010).

Lithofacies contacts that separate similar lithofacies types are delineated by first- to third-order surfaces (e.g. set and co-set boundaries within a migrating bedform; Fig. 3.4) and record autogenic controls within a depositional system, such as a change in paleocurrent strength and direction (Beerbower, 1964; Miall, 2010). Lithofacies contacts that record larger-scale autogenic controls in a depositional system (e.g. downstream migration of a bar) are delineated by fourth-order lithofacies contacts, which delineate packages of genetically related strata (e.g. bars and channels in a fluvial depositional environment with a characteristic geometry, named ‘architectural elements’; Miall, 1985).

Major changes in a depositional system (as a result of auto- and/or allogenic controls) are delineated by fifth-order lithofacies contacts (e.g. channel avulsion or step-wise channel incision) and environmental changes operating on a basin-wide scale (e.g. retreat of an ice margin) are recorded by sixth-order contacts delineating depositional environments (these may be equivalent to lithostratigraphic unit boundaries in vertical succession; Fig. 3.4). Seventh-order surfaces record major allogenic changes, such as tectonic uplift and climatic variation (e.g. the boundary separating volcanogenic bedrock and overlying unlithified glaciogenic sediments).

By integrating the bounding surface hierarchy (of AEA) and the hierarchical classification of sediment-landform associations (of landsystems analysis; Evans, 2005), the Sólheimajökull landsystem is deconstructed here (Figs. 3.5, A1) into a hierarchy of genetically related sediment-landform packages that are delineated by lithofacies contacts at three different scales of resolution, including landsystem surface features (fourth-order), components (fifth-order), and tracts (sixth-order; Figs. 3.4, 3.5). The ‘surface feature’ is the smallest-scale package, which herein is defined as a positive (e.g. drumlin), negative (e.g. kettle), or negligible (e.g. ice-contact outwash fan) relief landform that has a characteristic external geometry, is composed of genetically related sediments, and delineated by a fourth-order bounding surface. A total of twenty-two different surface features are delineated in this study (Fig. 3.5). Analysis of the sedimentary composition, orientation, spatial relationship, and genetic origin of these surface features allowed the identification of four landsystem tracts (delineated by sixth-order surfaces) which are the largest-scale sediment-landform packages mapped within the Sólheimajökull landsystem (Figs. 3.5-3.9) and include jökulhlaup, glaciofluvial, ice-contact, and colluvial slope tracts. In order to understand landsystem tract development, the internal architecture of the landsystem tracts was deconstructed into a third group of smaller architectural packages made of genetically related surface features (herein named ‘landsystem tract components’ delineated by fifth-order surfaces; Fig. 3.5). The orientation, topographic position, spatial orientation and relationship, and nature of sedimentary contacts (e.g. erosional, truncated, gradational, and sharp) of surface features within each landsystem tract were analysed, and spatially and genetically related surface features were grouped into nine landsystem tract components delineated by fifth-order bounding surfaces (Figs. 3.4, 3.5). The components record different allo- and autogenic controls within a single depositional environment or landsystem tract, and are discussed in detail below.

Fig. 3.5 Sediment-landform hierarchy of the Sólheimajökull landsystem delineated in this study, including the glaciofluvial, jökulhlaup, ice contact, and colluvial slope landsystem tracts (bounded by sixth-order surfaces), landsystem tract components (bounded by fifth-order surfaces), and surface features (bounded by fourth-order surfaces).

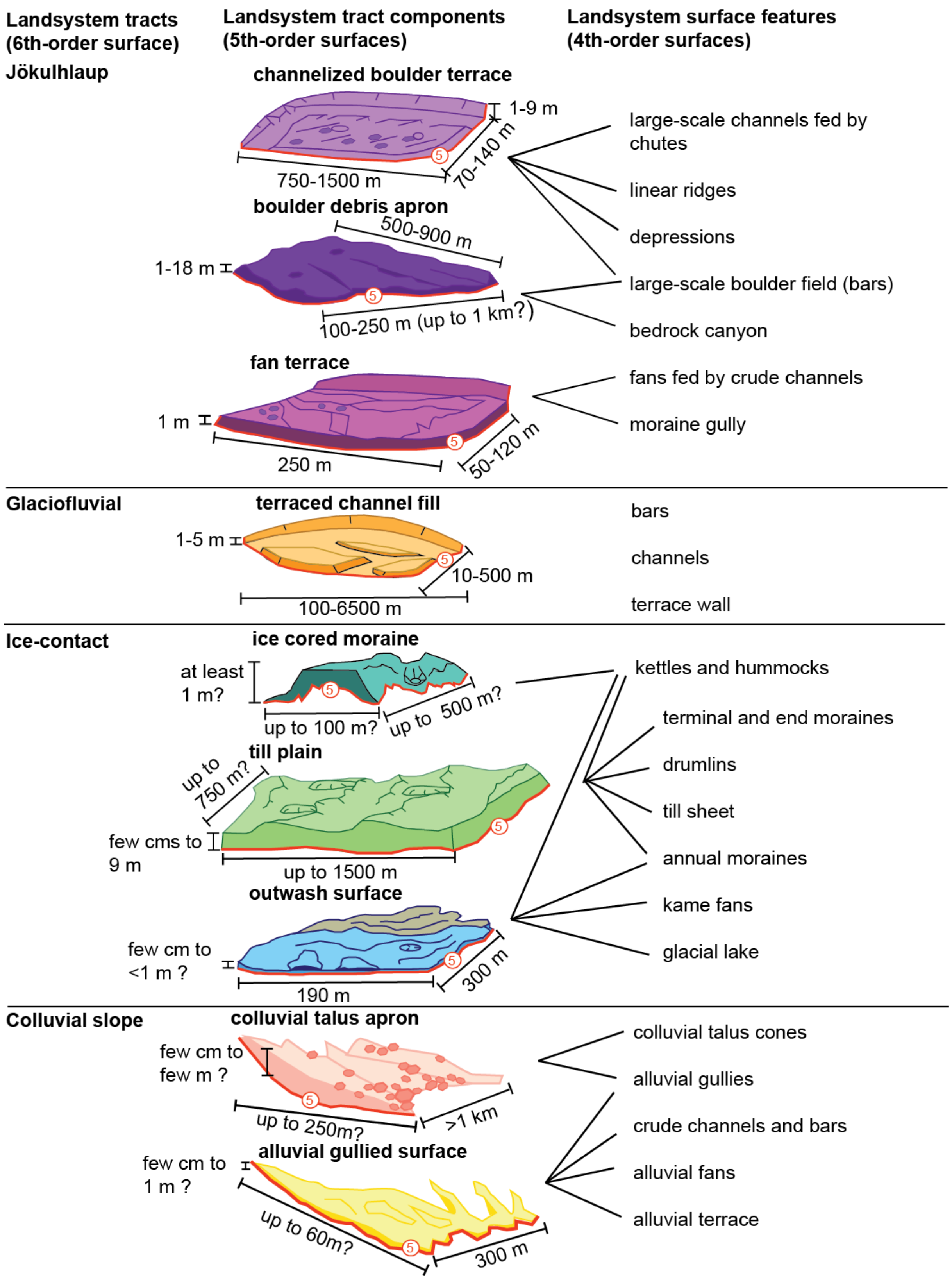

Landsystem tracts (6th-order surface)
Landsystem tract components (5th-order surfaces)
Landsystem surface features (4th-order surfaces)
Jökulhlaup
channelized boulder terrace
1-9 m
70-140 m
750-1500 m
large-scale channels fed by chutes
linear ridges
depressions
boulder debris apron
500-900 m
1-18 m
100-250 m (up to 1 km?)
large-scale boulder field (bars)
bedrock canyon
fan terrace
1 m
250 m
50-120 m
fans fed by crude channels
moraine gully
Glaciofluvial
terraced channel fill
1-5 m
10-500 m
100-6500 m
bars
channels
terrace wall
Ice-contact
ice cored moraine
at least 1 m?
up to 100 m?
up to 500 m?
kettles and hummocks
terminal and end moraines
till plain
up to 750 m?
few cms to 9 m
up to 1500 m
drumlins
till sheet
annual moraines
outwash surface
few cm to <1 m ?
190 m
300 m
kame fans
glacial lake
Colluvial slope
colluvial talus apron
few cm to few m ?
up to 250m?
>1 km
colluvial talus cones
alluvial gullies
alluvial gullied surface
few cm to 1 m ?
up to 60m?
300 m
crude channels and bars
alluvial fans
alluvial terrace
5

3.4.1 Jökulhlaup landsystem tract

The jökulhlaup landsystem tract is the most widespread tract in the Sólheimajökull landsystem; however, in the Jökulsá valley, it is most common in the ice-proximal area where it overlies older deposits of the glaciofluvial and ice-contact landsystem tracts (Fig. 3.6; Russell et al., 2010a). The surface features of historical jökulhlaups are difficult to identify in distal areas within the Jökulsá valley, probably as a result of rapid downstream attenuation of peak flow and sediment transport capacity (documented from the 1999 AD jökulhlaup) and sediment reworking (Russell et al., 2010a). Large-scale boulder fields are the most distinctive surface feature in the jökulhlaup landsystem tract; other surface features include large-scale channels with chutes, broad fans dissected by crude channels, a moraine gully, circular depressions, linear sediment ridges, and bedrock canyons (Figs. 3.5, 3.6). The jökulhlaup landsystem tract is patchy and irregular in geometry (Fig. 3.6), and mapped here as three different components including a channelized boulder terrace, fan terrace, and debris apron (Figs. 3.5, 3.6).

3.4.1.1 Channelized boulder terrace component

The channelized boulder terrace component is composed of a large-scale boulder field dissected by a large-scale channel fed by chutes (Fig 3.6A). The geometry of channelized boulder terrace components is elliptical in plan view, tabular and irregular in cross sectional view, and elongated parallel to the Jökulsá valley (Figs. 3.5, 3.6). This component is located along the margins of the Jökulsá river (Figs. 3.6D), and dissected by the glaciofluvial landsystem tract (Fig. 3.6B).

Fig. 3.6 Jökulhlaup landsystem tract architecture. A. Oblique ArcScene view of jökulhlaup landsystem tract components (and units of Maizels, 1989, 1991) overlain on a hillshade of 2010 LiDAR data (2m x 2m), including the location of transects (T) 8, 10, 11 (LiDAR courtesy of the University of Iceland; no vertical exaggeration). B. Transect 10 with surface features, components, and bounding surfaces (circled numbers) annotated. C. Transect 8 with surface features, components, and bounding surfaces (circled numbers) annotated. D. Plan view of the channelized boulder terrace and fan terrace components (fifth-order surfaces) and the jökulhlaup landsystem tract (sixth-order surface) at transect 8. Note other landsystem tracts are faded.

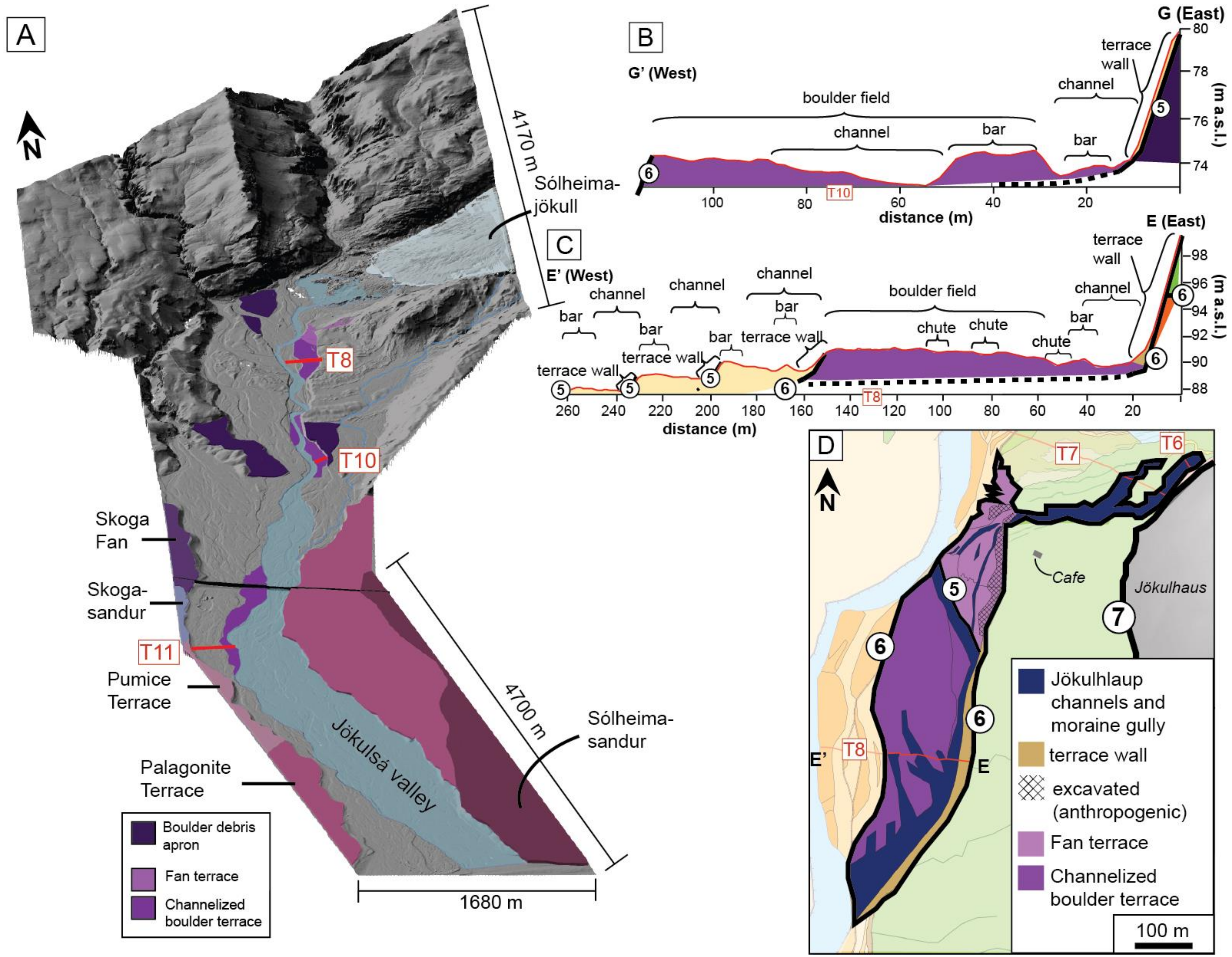
A
N
4170 m
Sólheima-
jökull
T8
T10
Skoga
Fan
Skoga-
sandur
T11
Pumice
Terrace
4700 m
Sólheima-
sandur
Jökulsá valley
Palagonite
Terrace
Boulder debris
apron
Fan terrace
Channelized
boulder terrace
1680 m
B
G' (West)
G (East)
boulder field
channel
bar
terrace
wall
elevation
(m a.s.l.)
distance (m)
C
E' (West)
E (East)
chute
D
T7
T6
Cafe
Jökulhaus
E'
E
Jökulhlaup
channels and
moraine gully
terrace wall
excavated
(anthropogenic)
Fan terrace
Channelized
boulder terrace
100 m

Boulder fields (surface feature; Fig. 3.5) are made of poorly sorted coarse-grained sediment with an abundance of boulders (up to at least 5 m in diameter) dispersed over a surface up to 1500 m in length (parallel to paleoflow direction) and 140 m wide (perpendicular to paleoflow direction; Figs. 3.5, 3.6). Boulder fields commonly contain linear gravel ridges that form streamlined positive relief features (< 1 m in height and several tens of metres long), which give the boulder field an undulating surface topography (Fig. 3.6B,C). Rare circular depressions in the boulder field are infilled with sand-sized sediment and encircled with cobbles and boulders (Fig. A1). Boulder fields are dissected by a trunk channel (up to 20 m wide and 600 m long) that is commonly confluent with large chutes (10 m wide and 300 m long) and secondary channels that are orientated transverse to the axis of the main trunk channel (Fig. 3.6A). The large-scale trunk channel is infilled with finer-grained sediment (sand to cobble-sized grains), and is bounded on one side by a terrace wall that is 1 to 9 m high in the ice-proximal area (Figs. 3.6B, C) and 3 m high in the ice-distal area (Fig. 3.7F, A1).

The channelized boulder terrace components recorded here were formed during the 1999 AD jökulhlaup event in areas of flow expansion under peak flow discharges of about 4500 m^3s^{-1} (Fig. 3.2C) in the ice-proximal area (transect 8) to 1700 m^3s^{-1} in the ice-distal area (transect 11; Figs. 3.3, 3.6; Russell et al., 2000, 2010a). The linear sediment ridges are interpreted to record streamlining and reworking of coarse-grained sediment during waning jökulhlaup flood flow (Fig. 3.2C), which also likely contributed to the formation of chutes draining floodwater into the main trunk channel (Fig. 3.3.6A; Maizels, 1997; Russell et al., 2000). Circular depressions in the boulder terrace are interpreted to be rimmed kettles (Maizels, 1997), formed by meltout of ice blocks transported during the jökulhlaup flood (Russell et al., 2010a).

3.4.1.2 Fan terrace component

The fan terrace component (up to 250 m in length and 120 m wide) consists of superimposed fan surface features dissected by crude channels. Fan apices are located at the mouth of a large (5 m deep and 20 m wide; Fig. 3.8C) moraine gully incised into an end moraine (Fig. 3.6A), which contains sand- and granule-sized sediment and rare boulders at its base. Two confluent hanging valleys form the head of the gully, which widens at the confluence and narrows at the gully mouth (Fig. 3.6A). Fans are composed of poorly sorted coarse-grained sediment (1 m thick deposit) of cobble- to boulder- sized grains closest to the apices that become finer-grained (sand and pebbles) and thinner (a few centimeters thick) toward the distal fan margins. Superimposed fans form a raised terrace surface (1 to 2 m thick), which is incised by the trunk channel of the channelized boulder terrace component (demarcating a fifth-order bounding surface; Fig. 3.6). Crude channels (up to 1 m deep and infilled with boulders) dissect the fan surface, which at their mouths form small-scale chutes to the main trunk channel of the channelized boulder terrace component (Fig. 3.6A).

The moraine gully was formed during the 1999 jökulhlaup event in an ice-marginal position, and the superimposed fans are interpreted to have formed as a result of flow expansion as floodwater flowing at peak discharge (Fig. 3.2D) exited the confined moraine gully (minor eastern outlet; Fig. 3.6A; Russell et al. 2000). The spatial relationship between the fan terrace component and the trunk channel of the channelized boulder terrace component suggests the fans formed concurrently or slightly prior to trunk channel incision (Fig. 3.2D). Small-scale chutes and channels that dissect the fan terrace surface (Fig. A1) were probably formed during waning stage flow (Fig. 3.2D) as floodwaters drained from the fan terrace.

3.4.1.3 Boulder debris apron component

The boulder debris apron component has an irregular geometry (up to 900 m in length and 250 m to 1 km wide; Figs. 3.5, 3.6) and is composed of poorly sorted, coarse-grained jökulhlaup debris with clusters of large boulders (up to 10 m in diameter; Fig. 3.6D). Boulder debris aprons are composed of boulder fields and may be dissected by crude gullies and kettle scours (Maizels, 1991; Russell et al., 2010a). The spatial relationship between boulder debris aprons and former ice margin positions (Figs. 3.1, 3.6) suggests they likely formed at or near the ice margin under peak jökulhlaup flows, as was recorded during the 1999 AD jökulhlaup event (forming the 'boulder bar' of Russell et al., 2010).

3.4.2 Glaciofluvial landsystem tract

The glaciofluvial landsystem tract is the most widespread tract within the Jökulsá valley (Fig. 3.7G); however active glaciofluvial transport and depositional processes are presently operating only in relatively narrow ribbons of terrain occupied by the Jökulsá and Hólsárgil rivers (Fig. 3.1). Deposits of the glaciofluvial landsystem tract are at least 10 m thick, 1200 m wide (perpendicular to the Jökulsá river), and 8 km long (measured from the ice-margin to the shore of the North Atlantic; Figs. 3.1, 3.7H). In the ice-

Fig. 3.7 Glaciofluvial landsystem tract architecture. Surface features, components, and bounding surfaces (circled numbers) annotated on: A. transect 4, B. transect 5, C. transect 9, D. transect 11, and E. transect 12. Plan view of surface features (channels and bars), components (fifth-order) and landsystem tract (sixth-order) delineated in: F. the ice-proximal area at transects 4-7 and G. the ice-distal area at transects 11 and 12 (and jökulhlaup units). H. Oblique ArcScene view of terraced channel fill components overlain on a hillshade of 2010 LiDAR data (2m x 2m), including the location of F. and G. (LiDAR courtesy of the University of Iceland; no vertical exaggeration). Note other landsystem tracts are faded.

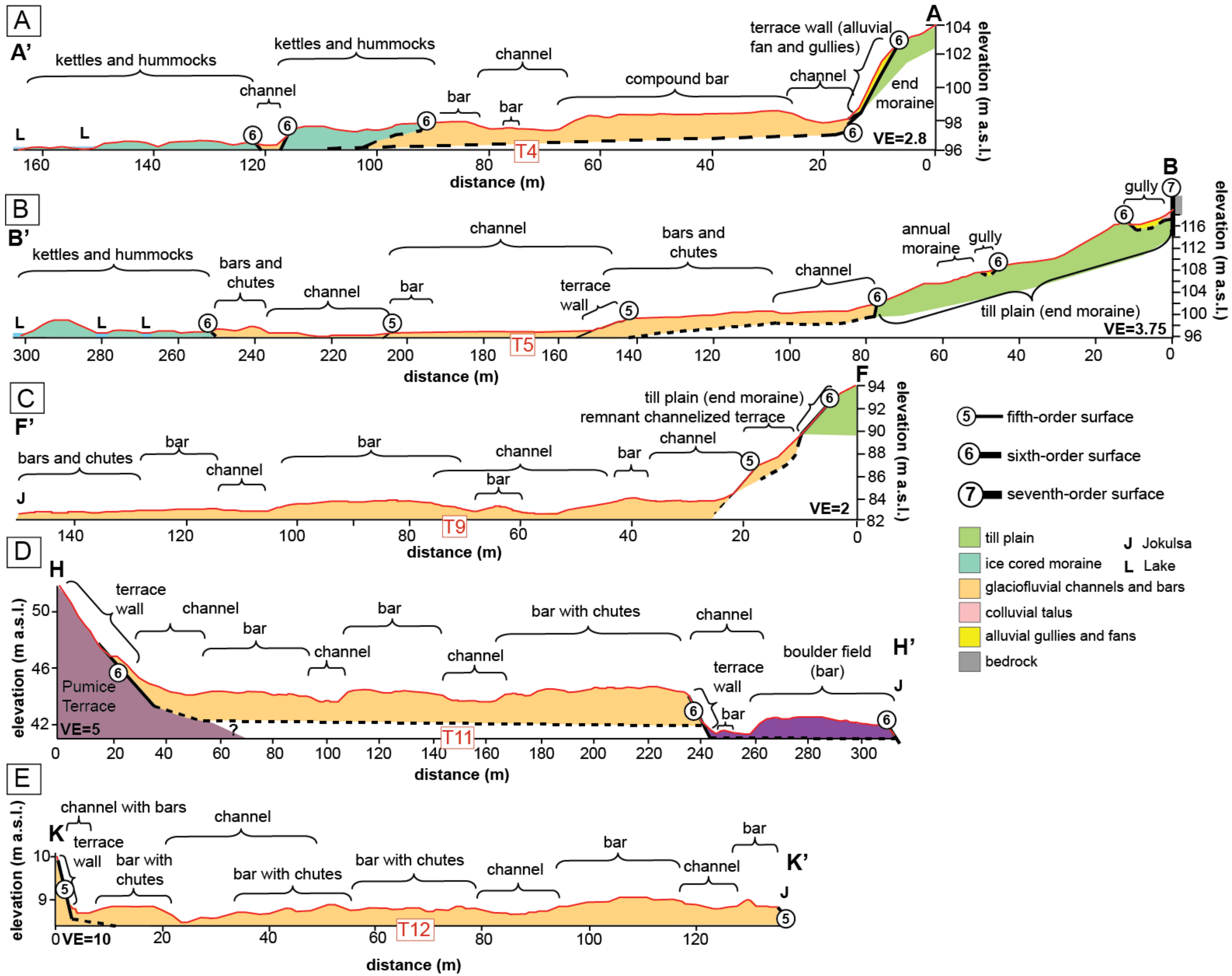

A
A'
A
kettles and hummocks
channel
kettles and hummocks
bar
channel
bar
compound bar
channel
terrace wall (alluvial fan and gullies)
end moraine
VE=2.8
T4
distance (m)
elevation (m a.s.l.)
B
B'
B
kettles and hummocks
bars and chutes
channel
channel
bar
terrace wall
bars and chutes
channel
annual moraine
gully
gully
till plain (end moraine)
VE=3.75
T5
distance (m)
elevation (m a.s.l.)
C
F'
F
bars and chutes
bar
channel
bar
channel
bar
bar
channel
remnant channelized terrace
till plain (end moraine)
VE=2
T9
distance (m)
elevation (m a.s.l.)
fifth-order surface
sixth-order surface
seventh-order surface
till plain
ice cored moraine
glaciofluvial channels and bars
colluvial talus
alluvial gullies and fans
bedrock
J Jokulsa
L Lake
D
H
H'
terrace wall
channel
bar
channel
bar
channel
bar with chutes
channel
terrace wall
bar
boulder field (bar)
Pumice Terrace
VE=5
T11
distance (m)
elevation (m a.s.l.)
E
K
K'
channel with bars
terrace wall
bar with chutes
channel
bar with chutes
bar with chutes
channel
bar
channel
bar
VE=10
T12
distance (m)
elevation (m a.s.l.)

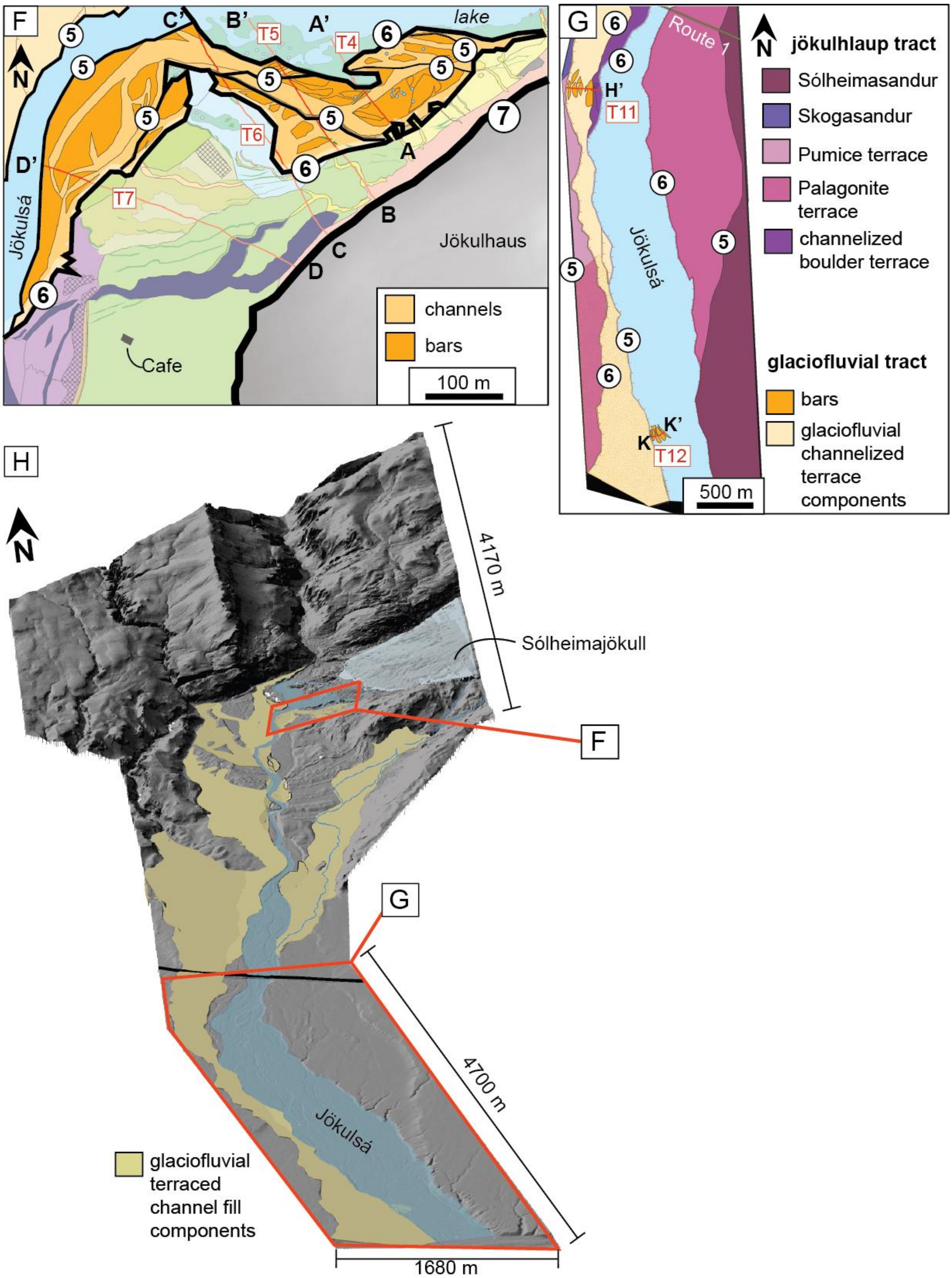
F
lake
C'
B'
A'
T5
T4
T6
T7
D'
A
B
C
D
Jökulsá
Jökulhaus
Cafe
channels
bars
100 m
G
Route 1
H'
T11
Jökulsá
K
K'
T12
500 m
jökulhlaup tract
Sólheimasandur
Skogasandur
Pumice terrace
Palagonite terrace
channelized boulder terrace
glaciofluvial tract
bars
glaciofluvial channelized terrace components
H
4170 m
Sólheimajökull
F
G
4700 m
Jökulsá
glaciofluvial terraced channel fill components
1680 m

proximal zone, the glaciofluvial landsystem tract commonly truncates and is overlain by the ice-contact and jökulhlaup landsystem tracts (separated by a sixth-order surface; Figs. 3.6B-C, 3.8C-D); whereas in the ice-distal area, it commonly incises the jökulhlaup landsystem tract (Fig. 3.7D, G). The internal architecture of the glaciofluvial landsystem tract is composed of well-defined gravel bars, channels, and terrace wall surface features, which are grouped into larger-scale architectural units called ‘terraced channel fill components’ (Figs. 3.5, 3.7).

3.4.2.1 Terraced channel fill component

Terraced channel fill components commonly contain a main channel positioned between a terrace wall (forming one margin of the channel) and a swarm of bars dissected by smaller channels on the other margin of the main channel (Fig. 3.7). The channels, bars, and terrace walls within an individual component are commonly orientated in approximately the same longitudinal direction (Fig. 3.7F) and individual components are located at different topographic positions (Fig. 3.7A-E). Terraced channel fill components are up to 500 m wide and 6500 m long (Figs. 3.5, 3.7). The three-dimensional internal architecture of the glaciofluvial landsystem tract is complex due to the intricate spatial relationship of components, making delineation and correlation of stacked, incised, and truncated components difficult.

Gravel bars are the most common surface feature recorded in the glaciofluvial landsystem tract. Bars are composed of sand- to cobble-sized sediment and are commonly dissected by bar top chutes. Bars are generally lentoid to spindle shaped in plan view and tabular to low relief semi-ellipsoid in cross-section. Bars are a few centimeters to 2 m thick, up to at least 20 m wide (perpendicular to paleoflow direction), and a few metres to at least 200 m long (parallel to paleoflow direction) in the ice-proximal area, and <2 m thick, up to 80 m wide, and up to 250 m long in the ice-distal area adjacent to the active Jökulsá (Fig. 3.7). Larger-scale bars commonly have well-defined, steep margins that are truncated by or gradational with channel surface features, whereas the margins of smaller-scale bars are gradational with channel bases.

Channels form a complex, interconnected network of ribbon-like geometries (Figs. 3.3, 3.7), and are delineated by their topographic position relative to bar surfaces, the finer-grained nature of sediments that infill channels (compared to the coarse-grained sediment composition of bars), cross-cutting relationships between two or more confluent channels and location and position of channel margins. Channel surface features are located between bars and in areas that are topographically lower than bar surfaces (Fig. 3.7). Channels may contain small-scale low relief bars along their margin or in the centre of the channel. The channel base commonly has a planar longitudinal geometry and concave-up cross-sectional geometry (Fig. 3.7), however channels that contain small-scale bars have convex-up and undulating longitudinal geometries. Channels are a few tens of metres wide and at least 100 m long and are commonly interconnected with other channels along their length (Fig. 3.7, A1). The active Jökulsá occupies a single steep-walled channel in the ice-marginal area but widens and occupies several interconnected (braided) channels in the ice-distal area (Fig. 3.7).

Terrace walls are 1-5 m high and closely associated with channels because they commonly demarcate a channel margin (Fig. A1). Terrace walls are readily delineated in the field and remotely sensed from LiDAR and satellite imagery because of a sharp break in slope and change in the orientation of bar and channel surface features (Figs. 3.1, 3.3, 3.7). Terrace walls are commonly orientated obliquely to the active Jökulsá river (except for those delineating the active Jökulsá valley train).

The terraced channel fill components are interpreted as remnant segments of the Jökulsá valley train formed by adjustment of the glaciofluvial system and step-wise incision of older glaciofluvial and jökulhlaup deposits (Williams and Rust, 1969; Marren and Toomath, 2013). Channels are interpreted to record main conduits through which the Jökulsá river flowed during normal base flow conditions, and which may become reactivated during high stage flow (e.g. as a result of peak melt and intense rainfall events; Williams and Rust, 1969) or jökulhlaups (Russell et al., 2010a). Bars are interpreted to be ‘storage sites’ for coarse-grained bedload recording transport of coarse-grained sediment during non-jökulhlaup floods, and deposition during normal base flow conditions or channel abandonment (Miall, 1977). Bars may become reactivated, reworked, or completely removed during successive flood events or jökulhlaups. Terrace walls (those not associated with the 1999 AD jökulhlaup) are interpreted to record the geomorphic response of the glaciofluvial landsystem tract to rapid glacier retreat (50 m per year) and non-jökulhlaup floods, whereby the Jökulsá has down cut through older deposits (Thompson and Jones, 1986; Maizels, 1991; Marren and Toomath, 2013).

3.4.3 Ice-contact landsystem tract

The ice-contact landsystem tract is the predominant tract in the ice-marginal area of the Sólheimajökull landsystem (Fig. 3.8A) and it does not extend beyond the southern extent of the exposed bedrock valley (Fig. 3.1, 3.3). It is most evident directly at the ice margin where ice cored moraine is formed from englacial esker sediments and supraglacial debris that blanket stagnant or ‘dead’ ice, and where low-relief kame fans are deposited in the Jökulsá ice-contact lake (transect 1, Fig. 3.8). It has the most complex internal architecture of the landsystem tracts, and is composed of surface features including kettles, hummocks, moraines (annual, end, and terminal), drumlins, till sheets, kame fans, eskers, and low relief surfaces of ephemeral ice-contact glacial lakes and ponds (Figs. 3.5, 3.8). The ice-contact landsystem tract consists of three components (delineated by fifth-order bounding surfaces) formed in subglacial and ice-marginal (till plain component), supraglacial (ice cored moraine component), and ice-marginal to proglacial (outwash surface component) depositional settings (Figs. 3.5, 3.8).

3.4.3.1 Till plain component

The most spatially extensive component in this tract is the till plain (Fig. 3.8A), which consists of end and terminal moraines, drumlins, annual moraines, and rare kettle ponds and hummocks (Fig. 3.5). It is best preserved on an upper terrace surface, where end moraines form positive relief features with a saw tooth plan form and asymmetrical cross sectional geometry, and are interspersed with kettle ponds and low relief drumlinoid features (Figs. 3.3, 3.8; Schomacker et al. 2012). The internal composition of the till plain component is exposed in vertical outcrop sections along terrace walls and the moraine

Fig. 3.8 Ice contact landsystem tract architecture. A. Oblique ArcScene view of till plain, outwash surface (including the fan surface), and ice cored moraine components overlain on a hillshade of 2010 LiDAR data (2m x 2m; LiDAR courtesy of the University of Iceland; no vertical exaggeration). Surface features, components, and bounding surfaces (circled numbers) annotated on B. Transect 1; C. Transect 6; and D. Transect 7. E. Plan view of the ice contact landsystem tract (sixth-order surfaces) at transects 1-7, including the outwash surface component (including the outwash kame fan surface), till plain, and ice cored moraine components (fifth-order surfaces). Note other landsystem tracts are faded.

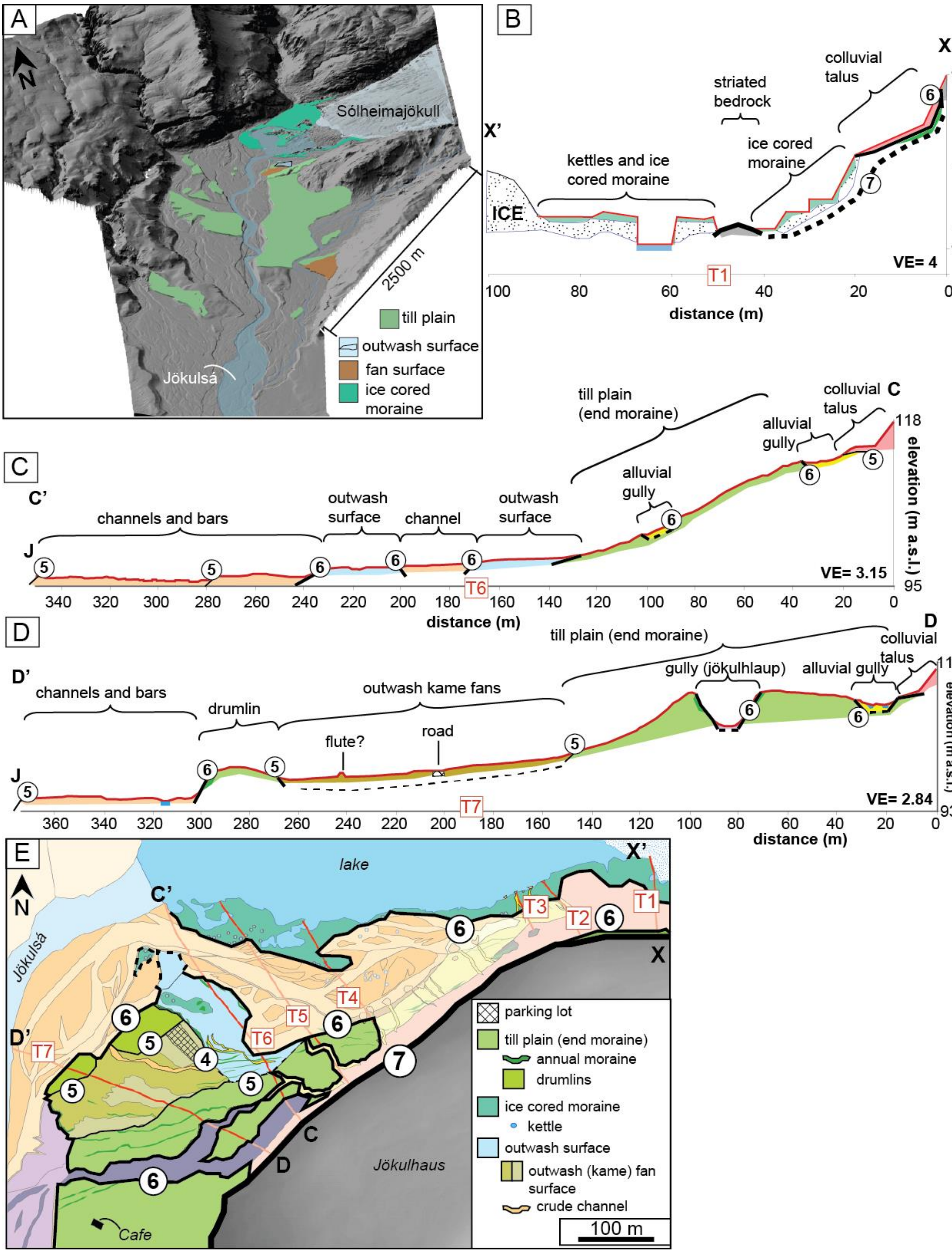

A
N
Sólheimajökull
2500 m
Jökulsá
till plain
outwash surface
fan surface
ice cored moraine
B
X'
X
ICE
kettles and ice cored moraine
striated bedrock
ice cored moraine
colluvial talus
T1
VE= 4
distance (m)
elevation (m a.s.l.)
C
C'
C
J
channels and bars
outwash surface
channel
outwash surface
till plain (end moraine)
alluvial gully
alluvial gully
colluvial talus
T6
VE= 3.15
distance (m)
elevation (m a.s.l.)
D
D'
D
J
channels and bars
drumlin
outwash kame fans
flute?
road
till plain (end moraine)
gully (jökulhlaup)
alluvial gully
colluvial talus
T7
VE= 2.84
distance (m)
elevation (m a.s.l.)
E
N
lake
Jökulsá
Jökulhaus
Cafe
T1
T2
T3
T4
T5
T6
T7
parking lot
till plain (end moraine)
annual moraine
drumlins
ice cored moraine
kettle
outwash surface
outwash (kame) fan surface
crude channel
100 m

gully (e.g. transects 7, 8; Figs. 3.6, 3.8). The internal sedimentary composition of the till plain consists of till interbedded with coarse-grained lenses, and moraines commonly overlie older (pre-LIA) deposits of the glaciofluvial landsystem tract (Schomacker et al., 2012). Annual push moraines form discontinuous, linear, sharp-crested and flat-topped positive relief features up to 1 m high, a few metres wide, and hundreds of metres long (Fig. 3.8E). They are composed of coarse-grained sand to cobble-sized sediment. Preservation of annual moraines is low due to their susceptibility to reworking by alluvial and glaciofluvial processes (Schomacker et al., 2012). The till plain component is commonly incised, and in some places completely removed, by the jökulhlaup, colluvial, and glaciofluvial landsystem tracts (delineated by a sixth-order surface; Fig. 3.8D, E).

3.4.3.2 Ice cored moraine component

The ice cored moraine component consists of poorly sorted debris (silt- to boulder-sized sediment) that forms discontinuous, irregular-shaped positive relief features. The ice cored moraine component is located at the ice margin (in the Jökulsá ice-contact lake) and along the margins of the lake (Fig. 3.8), and forms broad zones that are up to 500 m long (parallel to ice margin), 100 m wide (measured perpendicular to ice margin), and up to 1 m thick (Fig. 3.8). The ice cored moraine component contains former englacial esker sediments and supraglacial debris now resting on stagnant ice; downwasting of the 'dead' ice has resulted in the formation of kettles and hummocks on the surface of the ice cored moraine (Fig. 3.8). Kettles form circular depressions that are commonly ice- or sediment-walled and water-filled, and contain a slurry of saturated unconsolidated diamict. The ice cored moraine component commonly interfingers with the ice contact outwash surface component (which includes the Jökulsá ice contact lake; Figs. 3.5, 3.8E), and the colluvial landsystem tract. Isolated blocks of buried glacial ice are partially exposed along the bedrock valley walls underneath colluvial debris which suggests the ice-cored moraine component is likely more extensive than shown here (Fig. 3.8). Along the margins of the ice-contact lake, the ice cored moraine component forms hummocky ridges orientated parallel to the shoreline. Hummocks are positive-relief features that commonly consist of an ice core blanketed by stratified supraglacial debris. Hummocks contain concentrations of cobble to boulder sized clasts around their base which are actively transported by backwasting under the influence of gravity (Eyles, 1979).

The ice cored moraine component is interpreted to record the former location of the ice margin, where sediments deposited in englacial and supraglacial positions are exposed. With continued glacial retreat, the ice-cored moraine component may be completely reworked by glaciofluvial and glaciolacustrine processes and is not likely to be preserved in the stratigraphic record (Schomacker and Kjær, 2007). However, ice-cored hummocks are a common feature in the Jökulsá ice-contact glacial lake, and complete downwasting of ice may result in hummocks preserved as boulder concentrations in the ice-contact outwash surface component (Figs. 3.5, 3.8E).

3.4.3.3 Outwash surface component

The outwash surface conformably overlies the till plain component (fifth-order surface; Fig. 3.8C, D) and is composed of a fan surface (interpreted as kame fans) where fan apices originate from a ‘low-relief’ surface (fourth-order contact) and are overlain by annual moraines (Fig. 3.8E). The ‘low relief’ surface forms a flat to gently undulating topography with a paucity of well-defined surface features, and is overlain by moderately well sorted granule- to pebble-sized (and rare cobble- to boulder-sized) sediment. The margins of the outwash surface component contain annual push moraines, except on the northwest margin where the surface is truncated by the glaciofluvial landsystem tract (Fig. 3.8E). Lobe-shaped deposits of cobbles and boulders form poorly-defined 'bars' with gradational margins that are dissected by crude chutes along the eastern margin of the outwash surface (Fig. 3.8E).

The presence of kettles, hummocks, kame fans and annual push moraines indicate that this component was formed, at least in part, in an ice-contact depositional setting. The low relief topography, poorly developed lobate gravel bars, and fan surface are suggestive of sorting by meltwater, probably in an ephemeral ponded lake environment, similar to the depositional setting of the present-day ice margin in the shallow parts of the Jökulsá ice-contact lake.

3.4.4 Colluvial slope landsystem tract

The colluvial slope landsystem tract is spatially and genetically associated with bedrock valley walls, and is characterized by two main components that are commonly superimposed, including a colluvial talus apron (dominated by gravitational processes) and an alluvial gullied surface (dominated by processes due to the action of surface water draining from higher elevations; Fig. 3.5). The colluvial slope landsystem tract is composed of debris cones and aprons, alluvial gullies and fans, crude channels and bars, and alluvial terraces (formed by surface water draining from higher elevations and

Fig. 3.9 Colluvial slope landsystem tract architecture. A. Plan view of the colluvial slope landsystem tract (bounded by the sixth- and seventh-order surfaces) at transects 2-6, including the colluvial talus apron and alluvial gullied surface (including alluvial terrace and fan features) components (fifth-order surfaces). Note other landsystem tracts are faded. Surface features, components, and bounding surfaces (circled numbers) annotated on B. Transect 2; and C. Transect 3. D. Oblique ArcScene view of the colluvial talus apron and alluvial surface components overlain on a hillshade of 2010 LiDAR data (2 m x 2 m; LiDAR courtesy of the University of Iceland; no vertical exaggeration).

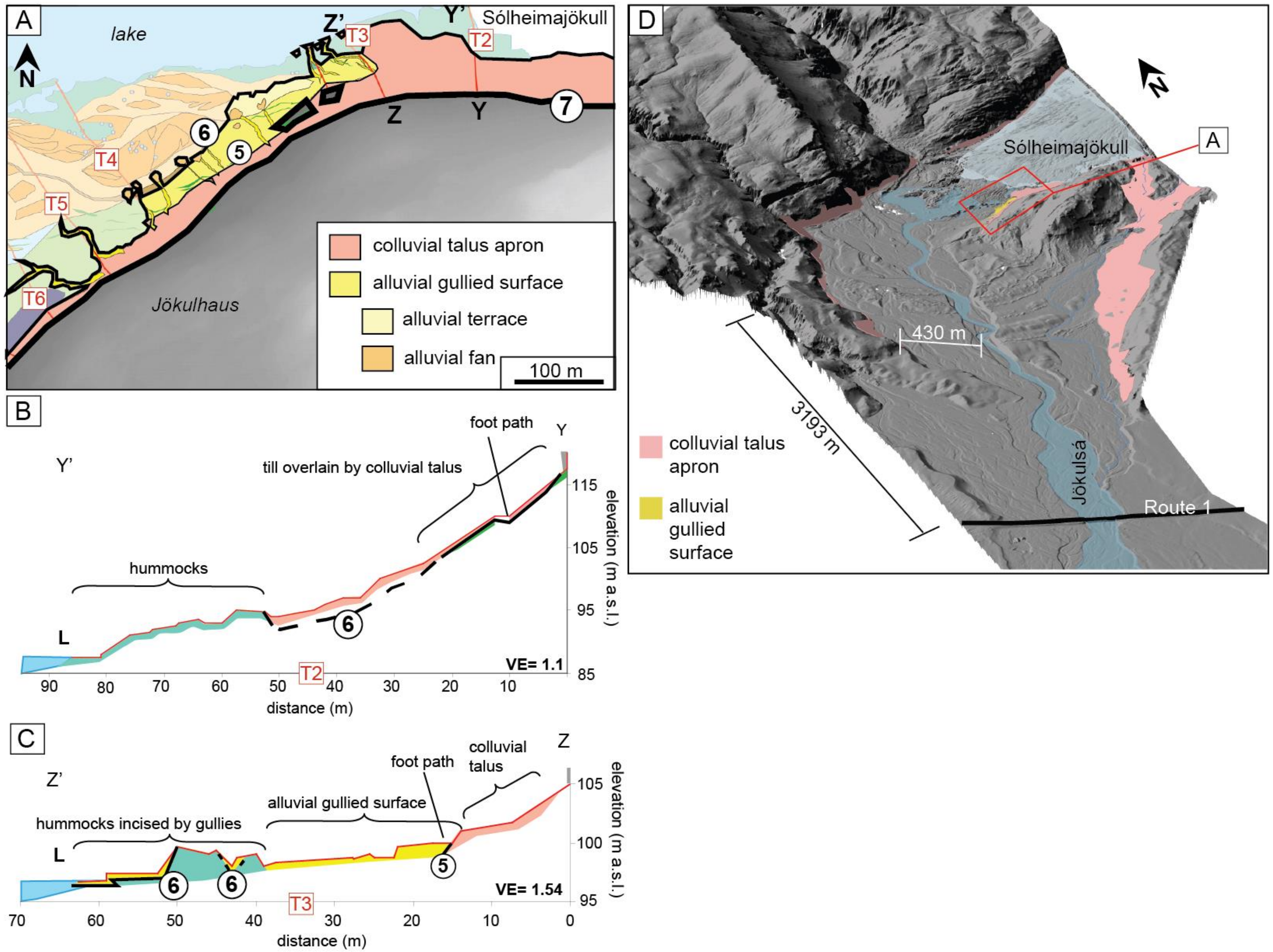
A
lake
N
Z'
T3
Y'
Sólheimajökull
T2
Z
Y
7
6
5
T4
T5
T6
Jökulhaus
colluvial talus apron
alluvial gullied surface
alluvial terrace
alluvial fan
100 m
B
foot path
Y
Y'
till overlain by colluvial talus
hummocks
L
6
VE= 1.1
T2
distance (m)
elevation (m a.s.l.)
C
Z
Z'
foot path
colluvial talus
alluvial gullied surface
hummocks incised by gullies
L
6
5
VE= 1.54
T3
distance (m)
elevation (m a.s.l.)
D
N
Sólheimajökull
A
430 m
3193 m
colluvial talus apron
alluvial gullied surface
Jökulsá
Route 1

depositing sediment onto the valley floor below; Figs. 3.5, 3.9). In the ice-marginal area, the colluvial slope landsystem tract directly overlies the lateral margins of Sólheimajökull and interfingers with the ice-contact landsystem tract (transect 1; Fig. 3.8). In the ice-proximal area, it overlies and truncates the ice-contact landsystem tract and overlies the glaciofluvial landsystem tract (transects 2-3; Figs. 3.8C, D, 3.9).

3.4.4.1 Colluvial talus apron component

The colluvial talus apron component forms a sheet of poorly sorted colluvium derived from rockfall debris and lateral moraines deposited at higher elevations on Jökulhaus, and from supraglacial debris transported by Sólheimajökull adjacent to the bedrock valley walls. Sand- to boulder-sized sediment (up to at least 5 m in diameter) forms cone-shaped deposits that rest directly on high angle exposures of bedrock, and coalesce downslope to form sheet- or apron-like geometries (Figs. 3.8, 3.9). It forms steep talus aprons where it directly overlies the lateral margins of Sólheimajökull; slide scars that expose vertical bedrock walls are common features at the head of the colluvial talus apron. At the ice margin, this component is underlain by isolated blocks of stagnant ice and till deposited on the Jökulhaus bedrock valley walls (Figs. 3.8, 3.9) and interfingers with the ice contact landsystem tract (separated by a sixth-order bounding surface with a complex geometry). In the ice-proximal area further from the ice margin, the colluvial talus apron is commonly reworked and truncated by the alluvial gullied surface component (Figs. 3.8, 3.9) and overlies the ice contact landsystem tract.

The colluvial talus apron forms a minor component of the Sólheimajökull landsystem, and its spatial location and preservation is dependent on the location of exposed bedrock slopes and active colluvial processes. This component is interpreted to form by rockfall of unstable materials perched at higher elevations (likely originating from lateral moraines) and resedimentation of supraglacial debris by downwasting of the lateral margins of Sólheimajökull (Eyles, 1979; Blikra and Nemec, 1998). Rockslides were not observed at the ice margin, however slide scars and oversteepened colluvial talus aprons overlying the lateral margins of Sólheimajökull suggest rockslides initiate resedimentation of lateral moraine material during downwasting of glacial ice, and may be triggered by the oversteepening of talus apron slopes and intense rainfall events (Sigurdsson and Williams, 1991).

3.4.4.2 Alluvial gullied surface component

This component is characterized by an irregular gullied surface on the colluvial slope covered with crudely sorted clusters of cobbles and boulders. It conformably overlies and truncates the colluvial talus apron component (separated by a fifth-order bounding surface), and both incises and is overlain by the ice-contact landsystem tract (sixth-order surface; Figs. 3.8, 3.9). Gullies form linear, meandering negative-relief surface features that are orientated roughly parallel to the colluvial slope direction; however poorly-developed gullies near the ice margin (transects 2 and 3; Figs. 3.9B, C) are orientated obliquely to the colluvial slope direction (Fig. 3.9A). Gullies are at least a few tens of centimetres deep, contain cobbles and boulders, and commonly terminate in small-scale fans of sand-sized sediment in the Jökulsá ice contact lake or in channels at the base of the colluvial slope (Fig. 3.9). Between gullies, cobbles and boulders are crudely sorted and form crude positive relief bar-like features. In one location, several small-scale (approx. 2 metres wide) alluvial fans coalesce to form an 'alluvial terrace' that overlies the surface of the glaciofluvial landsystem tract (Fig. 3.9).

This component is interpreted to form by reworking of the colluvial talus apron by surface runoff generated during heavy rainfall, during which surface runoff drains through gullies, transporting sand and finer-grained sediment and destabilizing cobbles and boulders on the gully slopes (this process was observed during fieldwork in 2013). The orientation and spatial relationship of some gullies to the colluvial slope direction and annual moraines suggest these gullies formed from meltwater draining the ice margin prior to ice-marginal retreat to its present day location.

3.5. LANDSYSTEM ALLOSTRATIGRAPHIC FRAMEWORK

A landsystem tract records the time-transgressive development of a single depositional environment; hence, fragments of different landsystem tracts formed contemporaneously at different stages of glacier margin advance and retreat (Evans, 2005). Landsystem tract components (and fifth-order bounding surfaces) are utilized here to define allostratigraphic packages (Hughes, 2010) that facilitate paleoenvironmental reconstruction of the evolution of the Sólheimajökull landsystem (Fig. 3.10). Eight allostratigraphic units (AU1-8) compose the landsystem, and are described below.

3.5.1 Allostratigraphic Unit 1: Sandur sheets and fans assemblage (c. 3100-7000 yrs BP)

AU1 comprises the oldest deposits of Sólheimasandur and is composed of interbedded units of glaciofluvial (units 2 and 4; Figs. 1, 2) and jökulhlaup (units 1(J) and 3(J); Figs. 3.1, 3.2) outwash deposits that were deposited on a broad sandur plain that is at least 7 km wide (Figs. 1A, 2D, 11C; Maizels, 1989). Coarse-grained gravels and sands form broad, sheet fans extending from the Þurragil bedrock gorge and other nearby bedrock channels (Fig. 3.10A; Maizels, 1989, 1991; Russell et al., 2010). The fans aggraded to a thickness of at least 12 m and are located at a stratigraphic position about 35-50 m a.s.l. (Fig. 3.2D; Maizels, 1989). The outermost lateral moraines at Sólheimajökull have been dated by Dugmore and Sugden (1991) and are only preserved on bedrock slopes. This assemblage is interpreted to have formed in an ice-proximal depositional setting 7000-3100 BP, during which the ice margin underwent two major periods of ice advance onto the sandur plain at 7000 BP (Drangagil stage; maximum southern extent shown in Fig. 3.10A) and 3100 BP (Hólsárgil stage; Dugmore and Sugden, 1991). The extent of the glacier snout is estimated based on ice margin reconstructions by Dugmore and Sugden (1991; Fig. 3.10A).

3.5.2 Allostratigraphic Unit 2: Sandur terraces assemblage (c. 2100-<3100 yrs BP)

Retreat of the Sólheimajökull ice margin from its position in 3100 BP resulted in it occupying an area closer to the bedrock valley mouth (Fig. 3.10B). Several jökulhlaup flood events resulted in the deposition of terraced fans that are more spatially-restricted (up to 3250 m wide) but thicker (at least 13 m thick; Maizels 1989) than those in AU1, forming the Palagonite and Pumice Terraces and Husa Fan (Figs. 3.1, 3.2, 3.10B). Glaciofluvial processes reworked the jökulhlaup surfaces and deposited relatively thin deposits of sand and gravel on Sólheimasandur and Skogasandur (Maizels, 1991). The position of the ice margin at this time is estimated on the basis of the extent of the Palagonite Terrace and estimated equilibrium line altitude (900 m, similar to the 1200 BP equilibrium line altitude; Mackintosh et al., 2002). The jökulhlaup deposits are laterally extensive across the sandur, which suggests they flowed in an unconfined depositional setting on the sandur plain. Jökulhlaup flows likely occupied and eroded bedrock canyons and truncated older sandur deposits (Russell et al., 2010a).

3.5.3 Allostratigraphic Unit 3: Skoga jökulhlaup assemblage (c. 1200-<2100 yrs BP)

This unit records one of the largest jökulhlaup events recorded at Sólheimajökull (Fig. 3.2), which resulted in the formation of the Skoga Pumice Fan (up to 2300 m wide and 15 m thick; Maizels 1989). A smaller-scale jökulhlaup (1200 BP) generated floodwaters that incised the north and west margins of the Skoga Fan and formed the Hófsá (Skoga) meander channel and Holsa Fan (Figs. 3.1, 3.2, 3.10C; Maizels, 1989). Post-flood glaciofluvial processes reworked the margins of Skoga Fan and the surface of Skogasandur, and truncated older Sólheimasandur deposits (Fig. 3.10C; Maizels 1989; 1991). The most distal end moraine preserved in the Jökulsá valley is located at the mouth of the bedrock valley (Figs. 3.8, 3.10D). The moraine forms remnant ridges that have been dated to the sixth to seventh centuries by Dugmore and Sugden (1991; Ytzagil stage;

1200-1400 yrs BP), and is interpreted to record a period of ice stagnation during the later stages of the formation of AU3.

3.5.4 Allostratigraphic Unit 4: Fourteenth-century component assemblage

Thick jökulhlaup deposits (Hólar and Eystrihólar; unit 11(J); Fig. 3.1) abut the AU3 end moraine and were deposited from a large-scale jökulhlaup in 1357 AD (Figs. 3.2, 3.10D; Einarsson et al., 1980; Maizels 1989). Hólar and Eystrihólar are at least 10 m thick and 1 km wide, and form two distinct debris-apron components (Figs. 3.5, 3.6) that are now dissected by Jökulsá (Figs. 3.1; 3.10H). A large terraced outwash (kame?) fan surface is located on the east side of the ice margin adjacent to a (late fourteenth-century?) end moraine remnant (Figs. 3.8A; 3.10D, E).

Hólar and Eystrihólar were likely more extensive than at present, and are interpreted to have formed as a continuous large-scale debris apron in an ice-marginal depositional setting (reconstructed in Fig. 3.10D; Russell et al. 2010a) by jökulhlaup flows, which probably truncated and removed most of the AU3 moraine and early-fourteenth century moraine (Fig. 3.10D). Subsequent ice-marginal retreat into the bedrock valley (at a topographically higher elevation than the sandur plain; Fig. 3.6A) likely resulted in downcutting of the glaciofluvial outwash system (Figs. 3.7D, 3.10D), forming the uppermost glaciofluvial terrace (unit 12; Figs. 3.1A, 3.2D).

Reconstruction of the upper glaciofluvial terrace (Fig. 3.10D) suggests the main outwash drainage outlets were located at the lateral margins of Sólheimajökull. The orientation of channels and bars on the upper glaciofluvial terrace (see lower left corner of Fig. 3.3B) suggest meltwater flowed from the bedrock canyon on the west margin of Sólheimajökull and incised the early fourteenth-century moraine on the eastern margin (Fig. 3.10D). The terraced fan surface located at the eastern ice margin is interpreted to have developed as an ice-contact outwash fan (outwash surface component; Fig. 3.5) formed under non-flood conditions (possibly during an extended period of ice stagnation?) and is preserved between a moraine ridge and the colluvial slope (Fig. 3.10E). Younger glaciofluvial systems likely truncated and removed part of this allostratigraphic component assemblage (Fig. 3.10E).

3.5.5 Allostratigraphic Unit 5: Little Ice Age component assemblage

An extensive till plain was deposited during the LIA (c. 1535 to 1920 AD; Fig. 3.10E; Mackintosh et al., 2002; Schomacker et al., 2012) and several prominent end moraines were formed during extended periods of ice-marginal stagnation (Fig. 3.1; Russell et al., 2010a; Schomacker et al., 2012). The outer margins of the till plain end moraine closest to the western bedrock valley wall (Fig. 3.10E) are truncated by several channel features. The orientation of channels, bars, and terrace walls (Fig. 3.3B) are interpreted to record an outwash system that exited the ice margin from several outlets close to the western bedrock valley wall, and through the Hólsárgil valley on the east side of Jökulhaus from a smaller ice tongue (Fig. 3.10E; Crittenden, 1975). Historical eyewitness accounts suggest the deep bedrock gorge on the western bedrock slope actively drained meltwaters until at least 1930 AD (Friis, 2011), and the reconstructed position of the ice margin (in Fig. 3.10E) allowed diversion of meltwater into the bedrock canyon and onto

Fig. 3.10 Evolution and allostratigraphy of the Sólheimajökull landsystem. Landsystem tract components are overlain on a hillshade of 2010 LiDAR data (2m x 2m; LiDAR courtesy of the University of Iceland). Timing and ages of allostratigraphic units and ice-marginal extents are approximated based on data available from other studies. Faded colours indicate features located beyond the mapping boundaries of this study and interpreted extents of components prior to erosion (no vertical exaggeration; refer to Fig. 3.3 for legend).

A. Allostratigraphic Unit 1: Sandur sheets and fans assemblage composed of fan-shaped interbedded jökulhlaup and glaciofluvial sediments deposited 3100-7000 years BP during maximum extent of ice-margin. Meltwater and sediment are supplied to the sandur by the ice margin and bedrock canyons (e.g. Þurragil; after Maizels, 1989, 1991; Dugmore and Sugden, 1991; Dugmore et al., 2000). Data and illustration overlain on a 30 m resolution ASTER GDEM (ASTER GDEM is a product of METI and NASA; NASA 2013**). B. Allostratigraphic Unit 2: Sandur terraces assemblage formed 2100-2300 years BP**, composed of the Pumice and Palagonite Terraces (forming fans in the subsurface) and Husa fan deposited by jökulhlaups and minor glaciofluvial units that reworked terrace surfaces. Meltwater and sediment are delivered to the sandur by the ice margin and bedrock canyons (e.g. Þurragil; after Maizels, 1989; Dugmore et al., 2000). Data and illustration overlain on a 30 m resolution ASTER GDEM (ASTER GDEM is a product of METI and NASA; NASA 2013). **C. Allostratigraphic Unit 3: Skoga jökulhlaup assemblage formed 1200-1550 years BP** and composed of the Skoga pumice fan and gullies, Hófsá meander channel, Holsa fan, and washed Skogasandur surface. Jökulhlaups are mainly hosted in bedrock canyons (e.g. Þurragil and Holsa) and 'normal' meltwater flows are sourced from the ice margin (after Maizels, 1989, 1991; Dugmore et al., 2000). Note change of scale. **D. Allostratigraphic unit 4: Fourteenth-century component assemblage formed 1300-1400 AD** (approximately 1357 AD or 593 years BP). This unit is composed of an early fourteenth-century terminal moraine, Hólar and Eystrihólar jökulhlaup deposits, the uppermost glaciofluvial terrace (that incises older sandar deposits), and an ice-proximal outwash fan. Outwash point sources include the bedrock canyons and the eastern ice margin (based on Crittenden, 1975; Einarsson et al., 1980; Maizels 1989; Friis, 2011; Schomacker et al., 2012). **E. Allostratigraphic Unit 5: Little Ice Age component assemblage**, formed 1750-1920 AD (ice marginal position at 1860-1890 AD shown here). This unit is composed of an extensive till plain and a glaciofluvial terrace that incises older deposits. Meltwater flowed from the western ice margin through a deeply cut bedrock canyon onto the upper glaciofluvial terrace, from the eastern ice margin through conduits incised through the till plain end moraine, and from the eastern ice margin through the Hólsárgil valley. Ice-dammed lakes in Jökulsárgil valley likely resulted in periodic flood events (after Maizels, 1989, 1991; Friis, 2011; Schomacker et al., 2012). **F. Allostratigraphic unit 6: 1920-1999 AD component assemblage.** This unit includes post-LIA glaciofluvial terraces and till plain end moraines, and the jökulhlaup deposits formed during the 1999 AD jökulhlaup on 18 July. During the 1999 AD jökulhlaup, meltwater was dammed in the Jökulsárgil valley and catastrophically drained through a subglacial conduit, which eroded and steepened the terrace walls of the Jökulsá valley. Jökulhlaup meltwater also drained from the central part of the ice margin, and minor outlets were located on the eastern margin (including a moraine gully and channel that incised through the till plain into the Jökulsá valley (Russell et al., 2010a). Following the 1999 AD jökulhlaup, glaciofluvial systems reworked the margins of jökulhlaup deposits (after Russell et al., 2010a; Friis, 2011; Schomacker et al., 2012). **G. Allostratigraphic unit 7: 2000-2007 AD component assemblage.** Ice retreat from the 1999 AD end moraine resulted in downcutting of the Jökulsá system through the 1999 AD jökulhlaup deposits and older glaciofluvial terraces. At the eastern ice margin, kame fans were deposited, and an ephemeral ice contact lake developed (Friis, 2011; Schomacker et al., 2012). **H. Allostratigraphic unit 8: 2008- 2013 AD.** This unit represents the most recent landsystem components delineated in this study. Retreat of the ice margin into an overdeepened basin resulted in the formation of an ice contact lake encircled with an extensive cover of ice-cored moraine. Ice retreat resulted in unblocking of the Jökulsárgil valley (which delivers meltwater and sediment to the lake) and further incision of Jökulsá (which occupies a singly main channel in the ice-proximal area; data collected during fieldwork in May 2012, 2013 and August 2013).

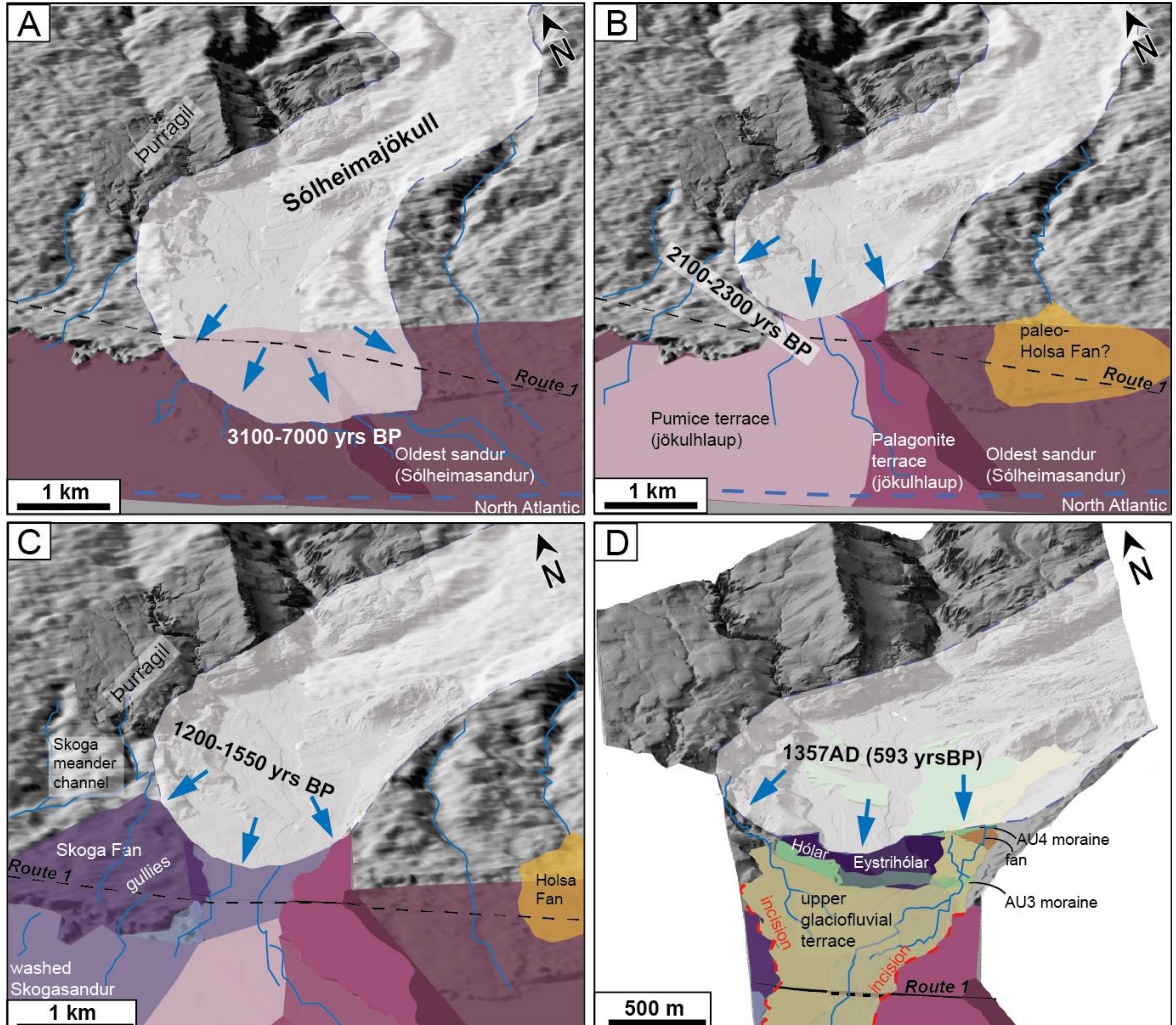
A
N
Þurragil
Sólheimajökull
Route 1
3100-7000 yrs BP
Oldest sandur
(Sólheimasandur)
1 km
North Atlantic
B
N
2100-2300 yrs BP
paleo-
Holsa Fan?
Route 1
Pumice terrace
(jökulhlaup)
Palagonite
terrace
(jökulhlaup)
Oldest sandur
(Sólheimasandur)
1 km
North Atlantic
C
N
Þurragil
Skoga
meander
channel
1200-1550 yrs BP
Skoga Fan
gullies
Route 1
Holsa
Fan
washed
Skogasandur
1 km
D
N
1357AD (593 yrsBP)
Hólar
Eystrihólar
AU4 moraine
fan
AU3 moraine
upper
glaciofluvial
terrace
incision
incision
Route 1
500 m

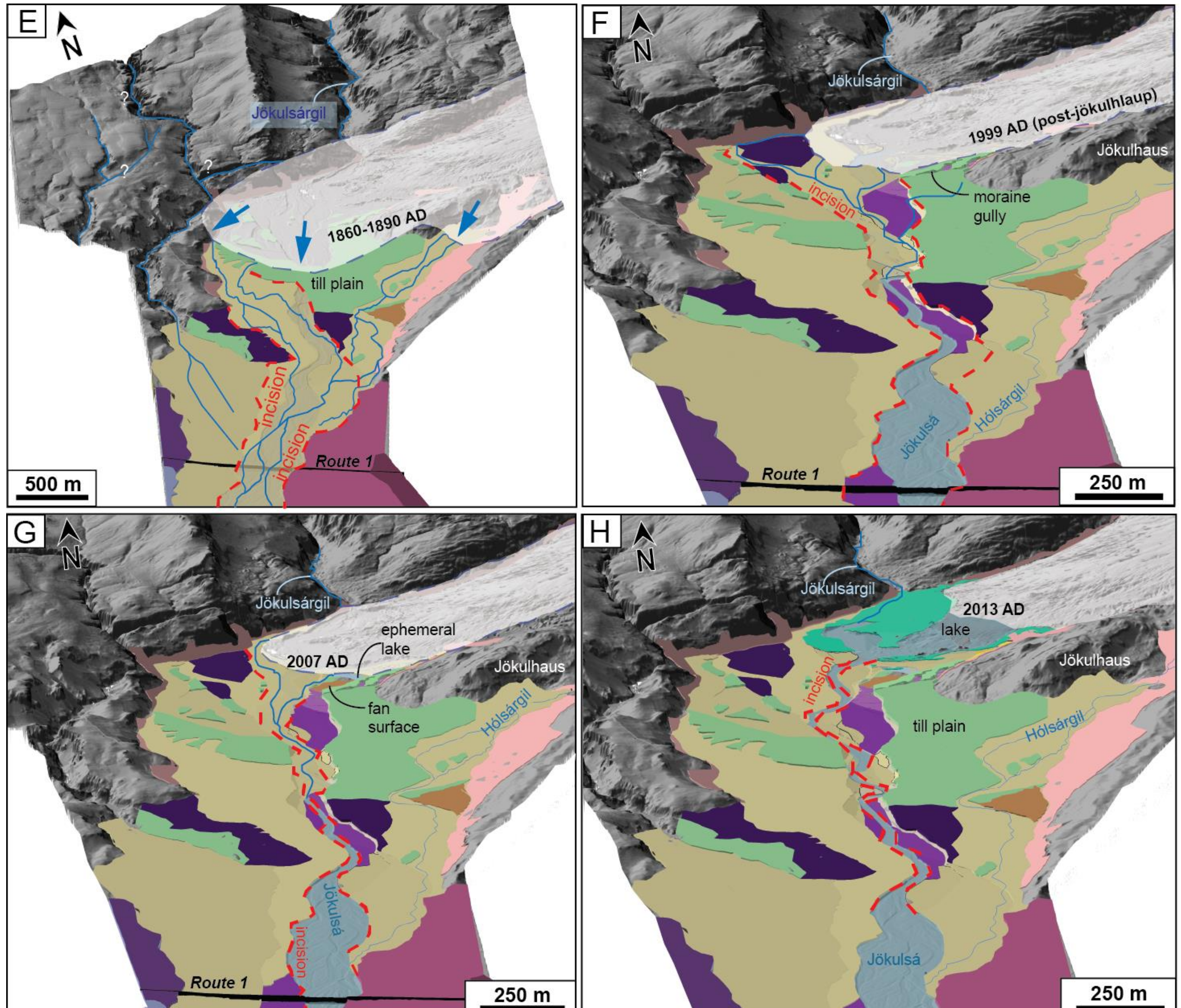
E
N
Jökulsárgil
?
?
?
1860-1890 AD
till plain
incision
incision
Route 1
500 m
F
N
Jökulsárgil
1999 AD (post-jökulhlaup)
Jökulhaus
incision
moraine
gully
Hólsárgil
Jökulsá
Route 1
250 m
G
N
Jökulsárgil
ephemeral
lake
2007 AD
Jökulhaus
fan
surface
Hólsárgil
Jökulsá
incision
Route 1
250 m
H
N
Jökulsárgil
2013 AD
lake
Jökulhaus
incision
till plain
Hólsárgil
Jökulsá
250 m

the upper glaciofluvial terrace. Ice-marginal retreat and smaller-scale jökulhlaups and flood events (Fig. 3.2; Maizels, 1989) likely resulted in the incision of the upper glaciofluvial terrace (Fig. 3.10E; Marren and Toomath, 2013).

3.5.6 Allostratigraphic Unit 6: 1920-1999 AD component assemblage

Sólheimajökull underwent punctuated retreat following the LIA (Fig. 3.1; Schomacker et al., 2012) which resulted in downcutting of the glaciofluvial system through the till plain on the west side of Jökulsá, and the formation of several glaciofluvial terraces behind the LIA moraines (Figs. 3.1, 3.3, 3.7, 3.10F). During the 1999 AD jökulhlaup, an ice-dammed lake formed in the Jökulsárgil valley and catastrophically drained into the Jökulsá valley. As a result, a large boulder fan (debris apron component; Figs. 3.5, 3.6) was deposited on an old vegetated glaciofluvial surface at the ice margin (Fig. 3.10F), and peak flows eroded and widened the Jökulsá valley in the ice-proximal area (Russell et al., 2010a). A narrow gully was incised into the moraine, which diverted flow into the Jökulsá valley and formed a fan terrace component (Figs. 3.5, 3.6; 10F). Jökulhlaup flow was generally restricted to the pre-existing Jökulsá valley, although a minor flood route on the east side of Jökulsá incised a broad channel between the 1905 AD and 1995 AD end moraines (Fig. 3.1), which funneled floodwaters into Jökulsá (Russell et al., 2010; Schomacker et al. 2012). Large channelized boulder terraces (Figs. 3.5, 3.6) formed in the Jökulsá valley in areas of flow expansion and coarse sediment deposition (Fig. 3.10F; Russell et al., 2010a). Post-jökulhlaup reworking by glaciofluvial processes resulted in erosion of the ice-marginal debris apron and downcutting of main outwash channels.

Only minor geomorphic changes are recorded in the ice-distal areas (Russell et al., 2010a).

3.5.7 Allostratigraphic Unit 7: 2000-2007 AD component assemblage

The Sólheimajökull ice margin rapidly retreated following the 1999 AD jökulhlaup event (Fig. 3.1) resulting in the incision of AU6 and the formation of several small glaciofluvial terraces in the ice-proximal area (Fig. 3.10G). An ice-proximal outwash fan surface and ephemeral lake (‘ice contact outwash surface’ component; Fig. 3.5) were formed on the eastern ice margin (Fig. 3.10G), which overlie drumlins and the 1945 AD ice margin position (Figs. 3.1, 3.8). Annual push moraines are located on the outwash surface, although their long-term preservation is low (Fig. 3.8). Narrowing of the active Jökulsá valley since AU4 is evident in the ice-proximal area (Fig. 3.10G), but major geomorphic changes are not recorded in the ice-distal area.

3.5.8 Allostratigraphic Unit 8: 2008-2013 AD component assemblage

The ice-marginal area of the present-day (current as of 2013 AD) landsystem has changed significantly since AU7 (Fig. 3.10H). The most striking difference is the formation of a large ice-contact lake into which Jökulsárgil flows and from which Jökulsá receives meltwater (Fig. 3.10H). The glacier snout of Sólheimajökull is retreating into an overdeepened bedrock low at least 2.5 km long (up-valley) and nearly 100 m deep (Mackintosh et al., 1999), which allows accumulation of meltwater in the basin. The lake is encircled with, and contains, ice-cored moraine and small remnants of the 1999 AD jökulhlaup esker (Figs. 3.8, 3.10H). Several small step-wise glaciofluvial terraces were formed at the ice margin as ice retreated from the 2007 AD position (Fig 3.7A). The Jökulsá has incised the AU7 ice-marginal glaciofluvial terraces (Fig. 3.10G) and flow is confined to a single main channel that receives meltwater from smaller streams in the ice-distal area (Fig. 3.10H). Colluvial debris covers the lateral ice margins of Sólheimajökull and contains alluvial gullies that funnel meltwater and stormwater towards the ice margin and into the lake (Fig. 3.9). Annual push moraines are common on colluvial slopes but they have a low preservation potential and are easily reworked by alluvial and glaciofluvial processes.

3.6. DISCUSSION

3.6.1 Architectural-landsystem models

The integrated architectural-landsystem approach utilized in this study helped to deconstruct the Sólheimajökull glacial landsystem into its basic architectural components, which facilitated paleoenvironmental reconstruction and provided insight into the allostratigraphic packages formed during the evolution of the landsystem (Fig. 3.10). The results of this study serve as the basis for three conceptual architectural-landsystem models for the ice-marginal, ice-proximal, and ice-distal areas (Fig. 3.11) of a temperate, non-surging, bedrock valley glacial landsystem in which jökulhlaups significantly contribute to its development (Fig. 3.10).

3.6.1.1 Ice-marginal architecture

The architecture of ice-marginal environments shows the greatest heterogeneity of surface features and landsystem tract components in the glacial landsystem (Figs. 3.5, 3.11A). Landsystem tracts have complex spatial relationships, and commonly crosscut and interfinger (Fig. 3.11A). The glaciofluvial landsystem tract incises, truncates, and removes other tracts; however, incision by the glaciofluvial landsystem tract is not as pronounced in ice-marginal environments as in other areas of the landsystem (Fig. 3.11B,C). Glaciofluvial terrace walls are commonly orientated parallel to the ice margin and converge in a bottleneck-type geometry away from the ice margin into a single main channel (Figs. 3.7H, 3.10, 3.11A). Bounding surfaces delineating a single surface feature or component commonly transition between fourth- and sixth-order (Fig. 3.11Aiii). Several bounding surfaces are orientated parallel to the ice margin (Fig. 3.11Aiii), indicating a strong ice-marginal influence on the overall architecture of the system. Preservation of ice-contact deposits is highest on topographically elevated areas near the bedrock valley walls and lowest closer to the central valley where glaciofluvial erosion is most active (Fig. 3.11Ai).

3.6.1.2 Ice-proximal architecture

The architecture of ice-proximal environments is less heterogeneous than in ice-marginal environments, but glaciofluvial incision is more pronounced (Fig. 3.11B). In this setting, the glaciofluvial system incises and removes the previously deposited till plain and truncates older glaciofluvial deposits. Jökulhlaup deposits also truncate glaciofluvial and ice contact deposits and are preserved on upper terraces (associated with valley erosion

Fig. 3.11 Conceptual architectural models of the A. ice-marginal, B. ice-proximal, and D. ice-distal areas of the landsystem based on data in this study, showing idealized (i) landsystem components, (ii) bounding surfaces, and (iii) a bounding surface model. The general location of each model is indicated by corresponding letters in the block diagram (D).

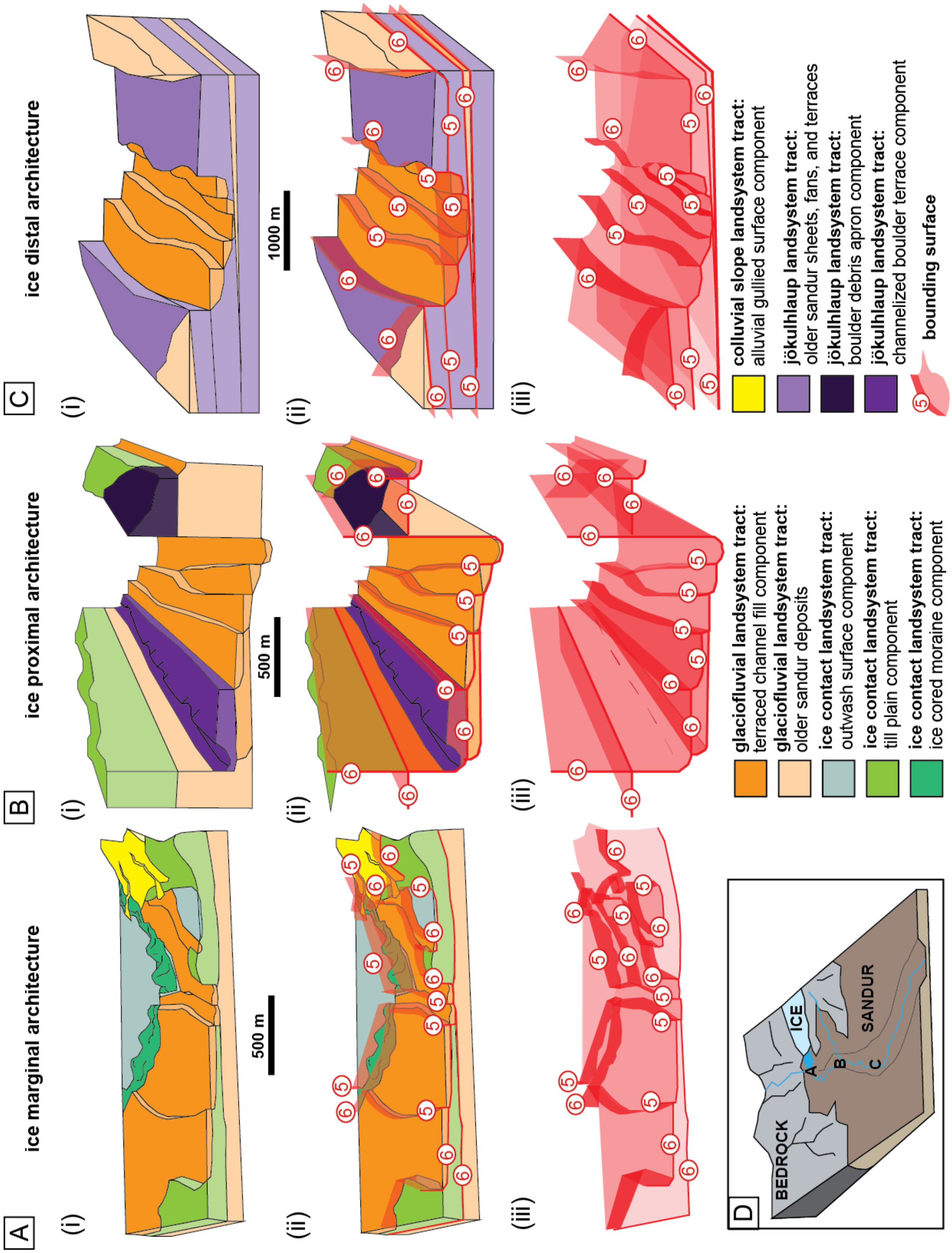
A
ice marginal architecture
(i)
(ii)
(iii)
500 m
B
ice proximal architecture
500 m
C
ice distal architecture
1000 m
D
BEDROCK
ICE
SANDUR
glaciofluvial landsystem tract:
terraced channel fill component
glaciofluvial landsystem tract:
older sandur deposits
ice contact landsystem tract:
outwash surface component
ice contact landsystem tract:
till plain component
ice contact landsystem tract:
ice cored moraine component
colluvial slope landsystem tract:
alluvial gullied surface component
jökulhlaup landsystem tract:
older sandur sheets, fans, and terraces
jökulhlaup landsystem tract:
boulder debris apron component
jökulhlaup landsystem tract:
channelized boulder terrace component
bounding surface

and widening). Fewer incisions may be recorded in this depositional setting than in the ice-marginal area, but glaciofluvial terraces will likely be larger (in thickness and spatial extent) and have a higher preservation potential with continued ice-marginal retreat, glaciofluvial downcutting, and confinement of the active outwash stream to a single main channel. Bounding surfaces delineating the glaciofluvial landsystem tract components are commonly orientated parallel (or quasi-parallel) to the Jökulsá valley walls and perpendicular to the orientation of the ice margin (Fig. 3.11Biii).

3.6.1.3 Ice-distal architecture

The architecture of ice-distal environments is the least heterogeneous of all, composed primarily of jökulhlaup landsystem tract deposits characterized by sheet- and fan-geometries and including minor deposits of the glaciofluvial landsystem tract (Fig. 3.11C). The most recent jökulhlaup deposits form terrace features that reflect the geometry of fan lobes deposited by unconfined flows on the sandur plain, and reworked by glaciofluvial erosion. Ice-marginal retreat results in downcutting of the active glaciofluvial system (at least 30 m of relief at Sólheimajökull), confining younger glaciofluvial (and flood) deposits to a steep-walled valley train. Bounding surfaces of older jökulhlaup deposits form stacked sheets; surfaces delineating younger glaciofluvial deposits are orientated perpendicular to these older jökulhlaup surfaces (Fig. 3.11Ciii).

3.6.2 Modern analogue applications

The architectural models described above (Fig. 3.11) provide a framework that can be applied to the analysis of Quaternary subsurface deposits in previously glaciated terrains in North America and Europe using sedimentary data from outcrop exposures, fully cored boreholes, and geophysical methods. Sixth-order bounding surfaces (Fig. 3.4) delineate landsystem tracts (depositional environments), which can be deconstructed into their basic building blocks (landsystem tract components) delineated by fifth-order bounding surfaces (Figs. 3.4-3.9). Landsystem tract components provide insight into the evolution of a landsystem and are useful for delineating the landsystem architecture on scales of hundreds of metres to kilometres (Figs. 3.10, 3.11). The position and spatial arrangement of landsystem tract components (fifth-order surfaces) changes over time in response to allogenic controls (such as the position of the ice margin, change in meltwater discharge, and volcanism). Understanding the nature (e.g. magnitude, source location, and recurrence interval) of these external controls can provide insight into the evolution of the system architecture and can aid in predictive mapping of landsystem components in areas with a paucity or absence of subsurface data. The component-scale unit characterized in this study (Fig. 3.5) is similar to the ‘element association’ delineated from vertical outcrop exposures by Slomka and Eyles (2013), the larger-scale till packages identified by Boyce and Eyles (2000), and the jökulhlaup packages delineated by Duller et al. (2008) and Marren et al. (2009). Surface features (or ‘architectural elements’ in outcrop; Miall, 1985) delineated by fourth-order surfaces (Figs. 3.4, 3.5) are mapped within components and allow detailed characterization of the internal architecture and heterogeneity of a unit at site-specific, high-resolution scales of study (metres to tens of metres).

In the Quaternary sedimentary record of North America, evidence of jökulhlaups from the Laurentide Ice Sheet may not be present, due to the absence of volcanic zones and strong geothermal centres associated with the generation of high magnitude hlaups and extensive sandur plains (Maizels, 1997; Marren et al., 2009; Björnsson, 2002). However, floods generated from rapid drainage of ice-dammed lakes may have occurred and could be recorded as irregularly-shaped, spatially-limited fans or aprons of oversized clasts (usually boulders) and kettle scours (‘debris apron components’; Fig. 3.5; Roberts et al., 2003; Russell et al., 2010a,b). Many such events may not have been discriminated in the Quaternary record to date due to a lack of definitive identification criteria.

The ice-contact landsystem tract has low preservation potential in the Jökulsá valley (Fig. 3.8), probably as a result of the fine-grained nature of tills and the erosive power of glaciofluvial and jökulhlaup systems. The oldest moraines (4500-7000 BP) of the Sólheimajökull landsystem are preserved as lateral moraines at high elevations on bedrock slopes and the maximum extent of the glacier snout can only be estimated from the shape of the lateral moraines (Dugmore and Sugden, 1991). The low preservation potential of the ice contact landsystem tract may result in underestimation of maximum ice extent and hinder delineation of former ice margin positions. In comparison, the Quaternary record of ice-contact deposits from the Laurentide Ice Sheet in North America is rich (Colgan et al., 2005) and contains thick successions of tills (e.g. Karrow, 1974; Richmond and Fullerton, 1986); however, in many places, these till units are truncated and completely removed by glaciofluvial systems, making reconstruction of the depositional history, correlation of units, and characterization of aquifers and aquitards difficult (Shaver and Pusc, 1992; Gates et al., 2013).

The results of this study demonstrate that the location of the meltwater outlet into the glaciofluvial landsystem tract is a significant allogenic control on the proglacial landsystem architecture (Figs. 3.7H, 3.11). The point source location of water input to the proglacial area may be bedrock canyons, alluvial gullies, glacier margins, subglacial conduits, supraglacial streams, or an ice-contact lake (Fig. 3.10). The location and type of point source has a strong control on the orientation of glaciofluvial surface features (channels and bars) and larger-scale terraces (landsystem tract components; Fig. 3.7). Understanding the location and evolution of meltwater point sources may facilitate reconstruction of the geometry of glaciofluvial units, provide insight to former ice margin positions, and aid in prediction of the preservation of components of the ice contact landsystem tract (e.g. till units).

3.7. CONCLUSIONS

Architectural-landsystem analysis is utilized here to characterize and delineate the sedimentary architecture of the Sólheimajökull (southern Iceland) landsystem at various scales of resolution. A bounding surface framework organizes the multi-scale architecture, whereby the landsystem is deconstructed into landsystem tracts (delineated by sixth-order surfaces) that record depositional environments, landsystem tract components (delineated by fifth-order surfaces), and surface features (delineated by fourth-order bounding surfaces). Landsystem tract components facilitate paleoenvironmental reconstruction and the characterization of eight allostratigraphic units, which record the evolution of the Sólheimajökull landsystem. However, the results presented in this study are not a complete record of the geomorphology of the landsystem, and further investigation of sediments and landforms (e.g. lateral moraines on bedrock slopes, aeolian dunes, Jökulsá estuary, and tephra layers) would greatly help to refine the detailed architecture and depositional history of the Sólheimajökull landsystem. Integration of subsurface data (e.g. from outcrop, boreholes, and geophyscial data; Hansen et al., 2009), dating of surface and subsurface deposits (e.g. using tephrachronology or lichenometry; Dugmore and Sugden, 1991), and computer-based modeling of units and surfaces may also help to refine the complex spatial relationships and geometries of landsystem tracts and components, and provide further insight to the subsurface correlation of fifth-order bounding surfaces (delineating allostratigraphic units) and 3-dimensional subsurface architecture of the Sólheimajökull landsystem. Future work documenting the sedimentary architecture at the ice margin would provide insight to the preservation of surface features and landsystem tracts, and landsystem evolution, as a result of ice marginal retreat.

The approach utilized in this study can significantly enhance the development of an allostratigraphy and landsystem-based reconstruction of depositional histories in Quaternary-age and older subsurface glacial successions. This will enhance understanding of the connectivity, incision, lateral extent, and heterogeneity of glacial deposits at various scales of resolution, and may facilitate three-dimensional mapping and prediction of these units in the subsurface. The results of this study validate the applicability of architectural element analysis (AEA) for the delineation of stratigraphic architecture at a modern ice margin, and can be utilized as a guide for integrated architectural-landsystems analysis of glacial landscapes at modern ice margins elsewhere and in formerly glaciated areas in North America and Europe.

Acknowledgements

The authors would like to thank Dr. Helgi Bjornsson for helpful discussion and readings, and the University of Iceland for providing LiDAR data of the Solheimajökull area. The authors are grateful for the field assistance and thoughtful discussion provided by Riley Mulligan and Andrew Slomka. Funding was provided by a Travel and Field Research Grant from Graduate Studies (McMaster University), Ontario Graduate ScHólarship, and NSERC grant awarded to J. Slomka, and an NSERC Discovery Grant awarded to C.H. Eyles. The ASTER GDEM data was obtained through the NASA Land Processes Distributed Active Archive Center (LP DAAC), USGS/Earth Resources Observation and Science (EROS) Center, Sioux Falls, South Dakota (available at https://lpdaac.usgs.gov/data_access).

REFERENCES

Allen, J.R.L. 1983. Studies in fluviatile sedimentation: bars, bar-complexes and sandstone sheets (low-sinuosity braided streams) in the Brownstones (L. Devonian), Welsh Borders. Sed. Geol., 33, 237-293.

Andrzejewski, L. 2002. The impact of surges on the ice-marginal landsystem of Tungnaárjökull, Iceland. Sed. Geol., 149, 59-72.

Beerbower, J. R. 1964. Cyclothems and cyclic depositional mechanisms in alluvial plain sedimentation. Kansas Geol. Surv. Bull., 169, 31- 42.

Benn, D.I., Lukas, S. 2006. Younger Dryas glacial landsystems in North West Scotland: an assessment of modern analogues and palaeoclimatic implications. Quatern. Sci. Rev., 25, 2390-2408.

Björnsson, H. 2002. Subglacial lakes and jokulhlaups in Iceland. Global Planet. Change, 35, 255-271.

Blikra, L. H. and Nemec, W. 1998. Postglacial colluvium in western Norway: depositional processes, facies and palaeoclimatic record. Sedimentology, 45, 909-959.

Boulton, G.S. 1972. Modern Arctic glaciers as depositional models for former ice sheets. J. Geol. Soc. London, 128, 361-393.

Boyce, J.I., Eyles, N. 2000. Architectural element analysis applied to glacial deposits: Internal geometry of a late Pleistocene till sheet, Ontario, Canada. Geol. Soc. Am. Bull., 112, 98-118.

Colgan, P.M., Mickelson, D.M., Cutler, P.M. 2005. Ice-marginal terrestrial landsystems: southern Laurentide Ice Sheet margin (Chapter 16). In: Glacial Landsystems (Ed. D.J.A. Evans). Hodder Arnold, London. pp.111-142.

Crittenden, P.D. 1975. Nitrogen fixation by lichens on glacial drift in Iceland. New Phytol., 74(1), 41-49.

Delaney, C. 2002. Sedimentology of a glaciofluvial landsystem, Lough Rea area, Central Ireland: implications for ice margin characteristics during Devensian deglaciation. Sed. Geol., 149, 111-126.

Dugmore, A.J., Sugden, D.E. 1991. Do the anomalous fluctuations at Solheimajokull reflect ice-divide migration? Boreas, 20, 105-113.

Dugmore, A.J., Newton, A.J., Larsen, G., Cook, G.T. 2000. Tephrochronology, environmental change and the Norse settlement of Iceland. Envir. Archaeology, 5, 21-34.

Duller, R.A., Mountney, N.P., Russell, A.J., Cassidy, N.C. 2008. Architectural analysis of a volcaniclastic jökulhlaup deposit, southern Iceland: sedimentary evidence for supercritical flow. Sedimentology, 55, 939-964.

El-ghali, M.A.K. 2005. Depositional environments and sequence stratigraphy of paralic glacial, paraglacial and postglacial Upper Ordovician siliciclastic deposits in the Murzuq Basin, SW Libya. Sedimentary Geology, 177, 145-173.

Eliasson, J., Larsen, G., Gudmundsson, M.T., and Sigmundsson, F. 2006. Probabilistic model for eruptions and associated flood events in the Katla caldera, Iceland. Comp. Geosci., 10, 179-200.

Eriksson, P.G., Reczko, B.F.F., Boshoff, A.J., Schreiber, U.M., Van der Neut, M., Snyman, C.P. 1995. Architectural elements from Lower Proterozoic braid-delta and high-energy tidal flat deposits in the Magaliesberg Formation, Transvaal Superground, South Africa. Sed. Geol., 97, 99- 117.

Evans, D.J.A., Rea, B.R. 1999. Geomorphology and sedimentology of surging glaciers: a land-systems approach. Ann. Glaciol., 28, 75-82.

Evans, D.J.A., Lemmen, D.S., Rea, B.R. 1999. Glacial landsystems of the southwest Laurentide Ice Sheet: modern Icelandic analogues. J. Quatern. Sci., 14(7), 673-691.

Evans, D.J.A., Twigg, D. R. 2002. The active temperate glacial landsystem: a model based on Breiðamerkurjökull and Fjallsjökull, Iceland. Quatern. Sci. Rev., 21, 2143-2177.

Evans, D.J.A. 2005. Glacial landsystems. (Ed. D.J.A. Evans). Hodder Arnold, London, 532 pp.

Evans, D.J.A., Clark, C.D., Brice, R.R. 2008. Landform and sediment imprints of fast glacier flow in the southwest Laurentide Ice Sheet. J. Quatern. Sci., 23(3), 249-272.

Eyles, N. 1979. Facies of supraglacial sedimentation on Icelandic and Alpine temperate glaciers. Can. J. Earth Sci., 16, 1341-1361.

Eyles, N. 1983. Glacial geology: a landsystems approach. In: Glacial Geology. (Ed. N. Eyles). pp. 1-18. Pergamon Press, Oxford.

Eyles, C. H., Eyles, N., Gostin, V.A. 1998. Facies and allostratigraphy of high-latitude, glacially influenced marine strata of the Early Permian southern Sydney Basin, Australia. Sedimentology, 45, 121-161.

Friis, B. 2011. Late Holocene glacial history of Sólheimajökull, southern Iceland. (M.Sc. thesis) pp. 90. Faculty of Earth Sciences, University of Iceland.

Gates, J.B., Steele, G.V., Nasta, P., Szilagyi, J. 2013. Lithologic influences on groundwater recharge through incised glacial till from profile to regional scales: Evidence from glaciated Eastern Nebraska. Water Resour. Res., 50, 466-481.

Ghazi, S., Mountney, N.P. 2009. Facies and architectural element analysis of a meandering fluvial succession: the Permian Warchha Sandstone, Salt Range, Pakison. Sed. Geol., 221, 99- 126.

Golledge, N.R. 2007. An ice cap landsystem for palaeoglaciological reconstructions: characterizing the Younger Dryas in western Scotland. Quatern. Sci. Revs., 26, 213-229.

Hubbard, S.M., Romans, B.W., Graham, S.A. 2008. Deep-water foreland basin deposits of the Cerro Toro Formation, Magallanes basin, Chile: architectural elements of a sinuous basin axial channel belt. Sedimentology, 55, 1333-1359.

Hansen, L., Beylich, A., Burki, V., Eilertsen, R.S., Fredin, O., Larsen, E., Lyså, A., Nesje, A., Stalsberg, K., and Tonnesen, J.D. 2009. Stratigraphic architecture and infill history of a deglaciated bedrock valley based on georadar, seismic profiling and drilling. Sedimentology, 56, 1751-1773.

Hughes, P.D. 2010. Geomorphology and Quaternary stratigraphy: The roles of morpho-, litho-, and allostratigraphy. Geomorphology, 123, 189-199.

Karrow, P.F. 1974. Till stratigraphy in parts of southwestern Ontario. Geol. Soc. Am. Bull., 85, 761-768.

Knight, P.G., Tweed, F.S. 1991. Periodic drainage of ice-dammed lakes as a result of variations in glacier velocity. Hydrol. Process., 5, 175-184.

Lawler, D.M., Björnsson, H., Dolan, M. 1996. Impact of subglacial geothermal activity on meltwater quality in the Jökulsá a Sólheimasandi system, southern Iceland. Hydrol. Process., 10, 557-578.

Mackintosh, A. N., Dugmore, A. J., Jacobsen, F. M. 1999. Ice-thickness measurements on Sólheimajökull, southern Iceland and their relevance to its recent behaviour. Jökull, 48, 9-15.

Mackintosh, A. N., Dugmore, A. J., Hubbard, A.L. 2002. Holocene climatic changes in Iceland: evidence from modelling glacier length fluctuations at Sólheimajökull. Quatern. Int., 91, 39-52.

Maizels, J.K., Dugmore, A. J. 1985. Lichenometric dating and tephrochonology of sandur deposits, Solheimajokull, southern Iceland. Jökull, 35, 69-78.

Maizels, J. 1989. Sedimentology, paleoflow dynamics and flood history of jökulhlaup deposits: Paleohydrology of Holocene sediment sequences in southern Iceland sandur deposits. J. Sed. Pet., 59(2), 204-223.

Maizels, J.K. 1991. Origin and evolution of Holocene sandurs in areas of jökulhlaup drainage, south Iceland. In: Environmental Change in Iceland: Past and Present. (Eds. J.K. Maizels and C. Caseldine). pp. 267- 302. Kluwer Academic Publishers, Norwell, Massachusetts.

Maizels, J. 1997. Jökulhlaup deposits in proglacial areas. Quatern. Sci. Rev., 16, 793-819.

Marren, P. M., Russell, A. J., Rushmer, E.L. 2009. Sedimentology of a sandur formed by multiple jökulhlaup, Kverkfjöll, Iceland. Sed. Geol., 213, 77-88.

Marren, P. M., Toomath, S.C. 2013. Fluvial adjustments in response to glacier retreat: Skaftafellsjökull, Iceland. Boreas, 42, 57-70.

Meyer, P.A, Eyles, C.H. 2007. Nature and origin of sediments infilling poorly defined bedrock valleys adjacent to the Niagara Escarpment, southern Ontario, Canada. Can. J. Earth Sci., 44, 89-105.

Miall, A.D. 1977. A review of the braided-river depositional environment. Earth-Sci. Rev., 13, 1-62.

Miall, A.D. 1985. Architectural-element analysis: A new method of facies analysis applied to fluvial deposits. Earth-Sci. Rev., 22, 261-308.

Miall, A.D. 1988. Architectural elements and bounding surfaces in fluvial deposits: Anatomy of the Kayenta Formation (Lower Jurassic), southwest Colorado. Sed. Geol., 55, 233-262.

Miall, A.D. 1994. Reconstructing fluvial macroform architecture from two-dimensional outcrops: Examples from the Castlegate Sandstone, Book Cliffs, Utah. J. Sed. Res., B64(2), 146-158.

Miall, A.D. 2010. Alluvial Deposits. In: Facies Models 4. (Ed. N. P. James and R.W. Dalrymple). Geological Association of Canada, St. John’s, Newfoundland. pp. 105-137.

Middleton, G.V. 1973. Johannes Wather's Law of the Correlation of Facies. Geol. Soc. Am. Bull., 84, 979-988.

Mountney, N.P., Russell, A.J. 2006. Coastal aeolian dune development, Sólheimasandur, southern Iceland. Sed. Geol., 192, 167-181.

NASA Land Processes Distributed Active Archive Center (LP DAAC) 2013. ASTER GDEM V2. USGS/Earth Resources Observation and Science (EROS) Center, Sioux Falls, South Dakota., 2011.

North American Commission on Stratigraphic Nomenclature (NACSN) 2005. North American Stratigraphic Code. AAPG Bull., 89(11), 1547-1591.

Räsänen, M.E., Auri, J.M., Huitti, J.V., Virtasalo, J.J. 2009. A shift from lithostratigraphic to allostratigraphic classification of Quaternary glacial deposits. GSA Today, 19(2), 4-11.

Richmond, G.M., Fullerton, D.S. 1986. Summation of Quaternary glaciations in the United States of America. Quatern. Sci. Rev., 5, 183-196.

Powell, R. D., Cooper, J. M. 2002. A glacial sequence stratigraphic model for temperate, glaciated continental shelves. Geological Society, London, Special Publications, 203(1), 215-244.

Roberts, M.J., Russell, A.J., Tweed, F.S., Knudsen, Ó. 2000. Ice fracturing during jökulhlaups: Implications for englacial floodwater routing and outlet development. Earth Surf. Proc. Land., 25, 1429-1446.

Roberts, M.J. Russell, A.J. 2002. Controls on the development of supraglacial floodwater outlets during jökulhlaups: Implications for englacial floodwater routing and outlet development. In: The Extremes of the Extremes: Extraordinary Floods, Symposium Proceedings. IAHS, 271, 71-76.

Roberts, M.J., Tweed, F.S., Russell, A.J., Knudsen, Ó, Harris, T.D. 2003. Hydrologic and geomorphic effects of temporary ice-dammed lake formation during jökulhlaup. Earth Surf. Proc. Land., 28, 723-737.

Russell, A.J., Tweed, F.S., Knudsen, Ó. 2000. Flash flood at Sólheimajökull heralds the reawakening of an Icelandic subglacial volcano. Geology Today, May-June 2000: 102-106.

Russell, A.J., Tweed, F.S., Knudsen, Ó., Roberts, M.J., Harris, T.D., Marren, P.M. 2002. Impact of the July 1999 jökulhlaup on the proximal River Jökulsá á Sólheimasandi, Mýrdalsjökull Glacier, southern Iceland. In: The Extremes of the Extremes: Extraordinary Floods, Symposium Proceedings. IAHS, 271, 249-254.

Russell, A.J., Tweed, F.S., Roberts, M.J., Harris, T.D., Gudmundsson, M.T., Knudsen, Ó., Marren, P.M. 2010a. An unusual jökulhlaup resulting from subglacial volcanism, Sólheimajökull, Iceland. Quatern. Sci. Revs., 29, 1363-1381.

Russell, A. J., Duller, R., Mountney, N. P. 2010b. Volcanogenic Jökulhlaups (Glacier Outburst Floods) from Mýrdalsjökull: Impacts on Proglacial Environments. In: The Mýrdalsjökull Ice Cap, Iceland, glacial processes, sediments and landforms on an active volcano. (Eds. A. Schomacker, J. Kruger, K.H. Kjaer, Series Ed J.J.M. van der Meer). Dev. Quat. Sci., 13, 181–207.

Scharerr, K., Spieler, O., Mayer, Ch., Münzer, U. 2008. Imprints of sub-glacial volcanic activity on a glacier surface-SAR study of Katla volcano, Iceland. Bull. Volcanol., 70, 495-506.

Schomacker, A., Kjær, K.H. 2007. Origin and de-icing of multiple generations of ice-cored moraines at Brúarjökull, Iceland. Boreas, 36, 411-425.

Schomacker, A., Benediktsson, Í.Ö., Ingólfsson, Ó, Friis, B., Korsgaard, N.J., Kjær, K.H., Keiding J.K. 2012. Late Holocene and modern glacier changes in the marginal zone of Sólheimajökull, South Iceland. Jökull, 62, 111-130.

Shaver, R.B., Pusc, S.W. 1992. Hydraulic barriers in Pleistocene buried-valley aquifers. Ground Water, 30(1), 21-28.

Sigurdsson, O., Williams, R.S. Jr. 1991. Rockslides on the terminus of "Jökulsárgilsjökull", southern Iceland. Geogr. Ann., 73(3/4), 129-140.

Slomka, J.M., Eyles, C.H. 2013. Characterizing heterogeneity in a glaciofluvial deposit using architectural elements, Limehouse, Ontario, Canada. Can. J. Earth. Sci., 50, 911-929.

Spedding, N., Evans, D.J.A. 2002. Sediments and landforms at Kvíárjökull, southeast Iceland: a reappraisal of the glaciated valley landsystem. Sed. Geol., 149, 21-42.

Thompson, A., Jones, A. 1986. Rates and causes of proglacial river terrace formation in southeast Iceland: an application of lichenometric dating techniques. Boreas, 15: 231-246.

Thorarinsson, S. 1939. Hoffellsjökull, its movements and drainage. In: Vatnajokull. Scientific Results of the Swedish-Icelandic Investigations 1936-37-38, Chapter VIII-IX. Geogr. Ann., 21, 171-242.

Thorarinsson, S. 1943. Oscillations of the Iceland Glacioers in the last 250 years. In: Vatnajokull. Scientific Results of the Swedish-Icelandic Investigations 1936-37-38, Chapter XI. Geogr. Ann., 25, 1-54.

Williams, P.F., Rust, B.R. 1969. The sedimentology of a braided river. J. Sed. Petrol., 39(2), 649-679.

Willman, H.B., Frye, J.C. 1970. Pleistocene Stratigraphy of Illinois. Illinois State Geol. Sur. Bull., 94, pp. 204.

CHAPTER 4: DECONSTRUCTING THE SEDIMENTARY ARCHITECTURE OF QUATERNARY GLACIAL SEDIMENTS RECOVERED FROM FULLY-CORED BOREHOLES, GEORGETOWN, ONTARIO USING ARCHITECTURAL ELEMENT ANALYSIS

Abstract

The late Quaternary depositional history of southern Ontario is preserved in subsurface glacial units with complex stratigraphic relationships. Coarse-grained outwash units commonly host prospective aquifers, and their internal heterogeneity, geometry, and spatial relationship to fine-grained units (e.g. tills) which form confining layers, are important to understand for aquifer characterization and source water protection. In order to better characterize these relationships, this study applies concepts of architectural element analysis (a framework of bounding surface and unit hierarchies) to the delineation of subsurface sedimentary architecture from twenty-four fully cored boreholes drilled in the Georgetown area of southern Ontario. Thirteen facies types are characterized, including sand, gravel, diamict, and fine-grained (silt, clay, and very fine-grained sand) facies, separated by four orders of facies contacts (fourth- to seventh-order bounding surfaces). The grouping of facies associations (fourth-order) with characteristic vertical facies successions allowed the identification of 'architectural components' (fifth-order) which compose the internal architecture of larger-scale mappable units (architectural units; AUs; sixth-order). Eleven AUs were delineated in this study, and include: weathered bedrock and regolith (AU1), sandy glaciofluvial (AU2), till complexes (AU3, AU6), gravelly glaciofluvial (AU4, AU8), glaciolacustrine, glaciofluvial, and deltaic units (AU5, AU7), shale-rich diamict and gravels (AU9), colluvial-alluvial (AU10), and fluvial to slackwater deposits (AU11). Coarse-grained AUs (e.g. AU2, AU4, AU8) are prospective aquifers and laterally persistent fine-grained (glaciolacustrine) units may form significant barriers to groundwater flow. The spatial relationship of AUs

allowed the identification of at least six glaciofluvial/fluvial incision events within the complex stratigraphy, which in places, completely removed older till units and form geologic and hydraulic connections between otherwise disconnected units. The methods utilized in this study can be applied to architectural analysis of subsurface glacial stratigraphies in other regions of southern Ontario and elsewhere.

4.1 INTRODUCTION

The Quaternary geologic record of southern Ontario contains sedimentological evidence of significant changes in climate, including two glacial periods (Illinoian and Wisconsin Stages; 190 and 115 ka cal yrs BP; Barnett, 1992) during which the Laurentide Ice Sheet (LIS) deposited a thick succession of glacial sediments across much of northern North America (Barnet, 1992), an interglacial period (Sangamonian Stage; c. 115-135 ka cal. yrs BP; Barnett, 1992) recorded by fossils and organic-rich sediment indicating a climate warmer than present (Mott and Matthews, 1990), and the Holocene (c. 10 ka cal. yrs BP to present; Barnett, 1992) which experienced deglaciation and climatic warming, recorded by pollen assemblages (Terasmae, 1980). Paleoenvironmental changes as a result of climatic fluctuations are recorded in a complex assemblage of glacial (till and outwash) and non-glacial (mainly lacustrine and paleosol) deposits (Barnett, 1992). The most complete record of Quaternary glaciation in southern Ontario was deposited during the Wisconsin (c. 10-115 ka cal. yrs BP; Willman and Frye, 1970; Barnett, 1992), during which time the ice margin of the LIS experienced several periods of advance and retreat, resulting in complex glacial stratigraphies (Fig. 4.1; Karrow, 1974; Sharpe et al., 2004; Meyer and Eyles, 2007).

Within these complex Quaternary stratigraphies, coarse-grained outwash deposits commonly host significant regional aquifers, which serve as potable water sources for many communities across southern Ontario (e.g. sediments of the Oak Ridges Moraine; Sharpe et al., 2003, 2004). Source water protection and groundwater supply investigations in Ontario and North America require mapping of the geometry of such coarse-grained sedimentary units, in order to understand the interconnectivity of aquifers and associated aquitards, delineate contaminant migration pathways within these units, and to help determine the long term sustainability of aquifers for municipal water supplies (Gerber et al., 2001; Sharpe et al., 1996, 2002). The internal lithological heterogeneity of coarse-grained outwash sediment commonly varies over small lateral (typically 10s to 100s of metres) and vertical (sub-metre) scales (e.g. Miall, 1977; Maizels, 1993; Aitken, 1998; Heinz et al., 2003; Slomka and Eyles, 2013). This spatial complexity makes subsurface mapping of the detailed geometry and internal heterogeneity of glacial outwash stratigraphies difficult, particularly in areas that lack exposed outcrop sections or closely spaced (within 10s of m) fully-cored boreholes (Miall, 2014). Previous studies of regional aquifers and aquitards in southern Ontario have relied on the Ontario Water Well Information System (WWIS) database for spatially extensive subsurface data coverage (e.g. Logan et al., 2001; Sharpe et al., 2003; Russell et al., 2004). However, well records in the WWIS are often insufficient for detailed delineation of the subsurface sedimentary architecture, paleoenvironmental analysis, and reconstruction of the depositional history of thick Quaternary stratigraphies. This is because WWIS record descriptors are intended for hydrogeological purposes and commonly lack detailed sedimentological data such as sedimentary structure and the nature of contacts (bounding discontinuities) between sedimentary packages (Russell et al., 1998).

This study investigates the subsurface glacial sedimentary architecture of the Georgetown area (Halton Hills, Ontario; Fig. 4.1) through detailed analysis of fully cored boreholes, drilled in an area with a paucity of exposed outcrop and where three-dimensional geophysical data, such as seismic, are not available. Georgetown is dependent on groundwater as a potable water source, and ongoing groundwater investigations and source water protection projects are conducted in the Georgetown area under Ontario's Places to Grow and Clean Water Acts (Government of Ontario, 2005, 2006; Halton Region, 2013). Georgetown contains three main well fields (Lindsay Court, Princess Anne, and Cedarvale; Fig. 4.2) located within environmentally significant areas, and which extract groundwater hosted in coarse-grained units in buried bedrock valleys (Credit Valley Conservation, 2001, 2009; Halton Region, 2013); however, the detailed heterogeneity and interconnectivity of the sediments composing the aquifers, and their connectivity to shallow subsurface sediments is poorly understood. The local-scale connectivity of subsurface units is important to determine for land-use planning, aquifer sustainability, and source water protection issues, specifically in areas identified for future development (Town of Halton Hills, 2013).

The purpose of this study is to understand the detailed sedimentary heterogeneity and (geological) interconnectivity of subsurface sedimentary units in the Georgetown area by applying the basic concepts of architectural element analysis (Miall, 1985). The main objectives of this study are to: 1) characterize genetically-related facies types and delineate architectural units within the Quaternary subsurface stratigraphy; 2) deconstruct architectural units into their component building blocks, which constitute the sedimentary architecture; and 3) utilize the detailed sedimentary architecture as a basis for paleoenvironmental analysis and reconstruction of the depositional history of the study area. This study provides a new approach for the analysis of core data and subsurface mapping of glacial units based on a nested architectural framework and hierarchies of architectural element analysis. The results of this study provide an architectural framework for the subsurface glacial units in the study area, and offer insight into their local-scale heterogeneity and interconnectivity, which may be applied to future hydrogeological investigations in the Georgetown area. The methods utilized in this study can be applied to the delineation of subsurface sedimentary architectures of glaciated regions in other parts of southern Ontario and North America, and elsewhere.

4.1.1 Architectural Element Analysis

This study utilizes basic principles of architectural element analysis (AEA; Miall 1985), including the bounding surface hierarchy and scalar relationship of nested packages of genetically-related facies, to facilitate delineation of the Quaternary subsurface sedimentary architecture of the Georgetown area. AEA is a methodology introduced by Allen (1983) and Miall (1985, 1988) for the analysis of fluvial architecture recorded from exposed outcrop sediments. AEA enhances the facies model by including a geometric component to the description of facies associations (Walker, 1992), and facilitates systematic characterization of the heterogeneity of a sedimentary succession from local (facies) to regional (basin-fill) scales (Miall, 2010). The vertical succession and spatial arrangement of genetically-related facies and the nature of facies contacts are fundamental to the delineation of the bounding surface hierarchy of AEA (Miall, 1988). The bounding surface hierarchy is not reliant on determination of relative base level change (e.g. sequence stratigraphy; Vail et al., 1977; Brookfield and Martini, 1999; Catuneanu et al., 2009; Miall, 2014) and does not require identification of chronostratigraphic units (e.g. allostratigraphy; Bhattacharya and Posamentier, 1994; NACSN, 2005; SEPM, 2014); making AEA suitable for the analysis of complex glacial successions in non-marine depositional settings. Furthermore, the geometric component of AEA facilitates translation of geologic data to a format useful for hydrogeologic investigations (e.g. Davis et al., 1993; Klingbeil et al., 1999). AEA has been applied to the study of sediments exposed in outcrop (e.g. Miall, 1994; Eriksson et al., 1995; Hjellbakk et al., 1997; Hornung and Aigner, 1999; Ghazi and Mountney, 2009; Marren et al., 2009; Yuvaraj, 2011; Slomka and Eyles, 2013) and only recently has AEA been applied to subsurface core data (supported by outcrop sections and geophysical data; e.g. Boyce and Eyles, 2000).

4.2 GEOLOGICAL SETTING AND HISTORY

The study area is located in Georgetown, in the town of Halton Hills (Regional Municipality of Halton), which is 40 km west of Toronto (Fig. 4.1A). Paleozoic bedrock underlies much of southern Ontario and is well exposed along the Niagara Escarpment

(Fig. 4.1C). The Escarpment is composed of Silurian sandstone and dolostone (Whirpool and Manitoulin Formations) overlain by caprock carbonates (Amabel Formation) that dip to the southwest (Johnson et al., 1992), and forms a partly buried slope that runs north-south through the study area (Fig. 4.1B). Georgetown is located at the base of the Escarpment and is underlain by Ordovician shale (Queenston Formation; Brogly et al., 1998; Johnson et al., 1992), the surface of which is dissected by several bedrock valleys carved by Tertiary and Quaternary fluvial and glacial processes (Straw, 1968; Karrow, 2005; Gao, 2006; 2011; Figs. 1B, D); however the interconnectedness and continuity of bedrock valleys are not well understood (Figs. 1B, D; Eyles et al., 1993; Karrow, 2005; Meyer and Eyles, 2007). At least three main bedrock valleys underlie Georgetown, including: 1) the Georgetown-Acton bedrock valley, which trends west-east from the top of the Niagara Escarpment, through the Acton re-entrant, and toward the Princess Anne area; 2) the Georgetown-Huttonville bedrock valley that trends east-west through the Cedarvale area towards the confluence of Silver Creek and the Credit River; and a third valley that appears to trend north-south along the base of the Niagara Escarpment from north of the study area (Fig. 4.1D). The Georgetown-Acton and Georgetown-Huttonville valleys have previously been interpreted to form a continuous bedrock valley that trends toward Lake Ontario (Fig. 4.1C; Gao, 2011); however, the three main bedrock valleys (described above) appear to have irregular valley bases, poorly defined thalwegs and margins (possibly ‘terraced’ valley margins in places, e.g. the north part of the Credit River), and several crude tributary bedrock valleys (Fig. 4.1D), making delineation of bedrock valley continuity in the study area uncertain.

Fig. 4.1 Study area (Georgetown) in southern Ontario. A. Quaternary surficial geology map of southern Ontario, including the Halton, Wentworth, and Newmarket Tills, and major geomorphic surface features, including the Oak Ridges Moraine and Paris-Galt Moraines (PGM; data from OGS, 2010). Georgetown study area marked with red box. B. Quaternary surficial geology of the study area and bedrock-related surface features including the Terra Cotta outlier, Acton re-entrant, and Niagara Escarpment (green hatched line; data from OGS, 2010). Refer to A for surficial geology legend, and Fig. 4.2 for names of boreholes utilized in this study (red circles). Locations of boreholes of Meyer and Eyles (2007) are represented by yellow squares. C. Digital elevation model (DEM) showing major bedrock features of southern Ontario, including the Niagara Escarpment and Laurentian Channel, and the location of bedrock valleys (1: Erigan valley; 2: Dundas Valley; 3: minor re-entrant; 4: Campbelville re-entrant; 5: Georgetown valley; 6: Caledon East valley; 7: minor valley; 8: minor valley in Toronto; 9: valley near Orangeville; 10-12: re-entrant valleys; 13: Beaver valley; 14: Meaford valley; 15: Mount Forest valley; 16: Milverton valley; modified from Gao et al., 2006; Gao, 2011). Study area marked with red box. D. Bedrock DEM of the study area with major bedrock valleys, including the Georgetown-Acton valley and Georgetown-Huttonville valley. Borehole locations utilized in this study are indicated with red circles, and boreholes of Meyer and Eyles (2007) are represented by yellow squares. Refer to Fig. 4.2 for borehole names (data from Gao et al., 2006).

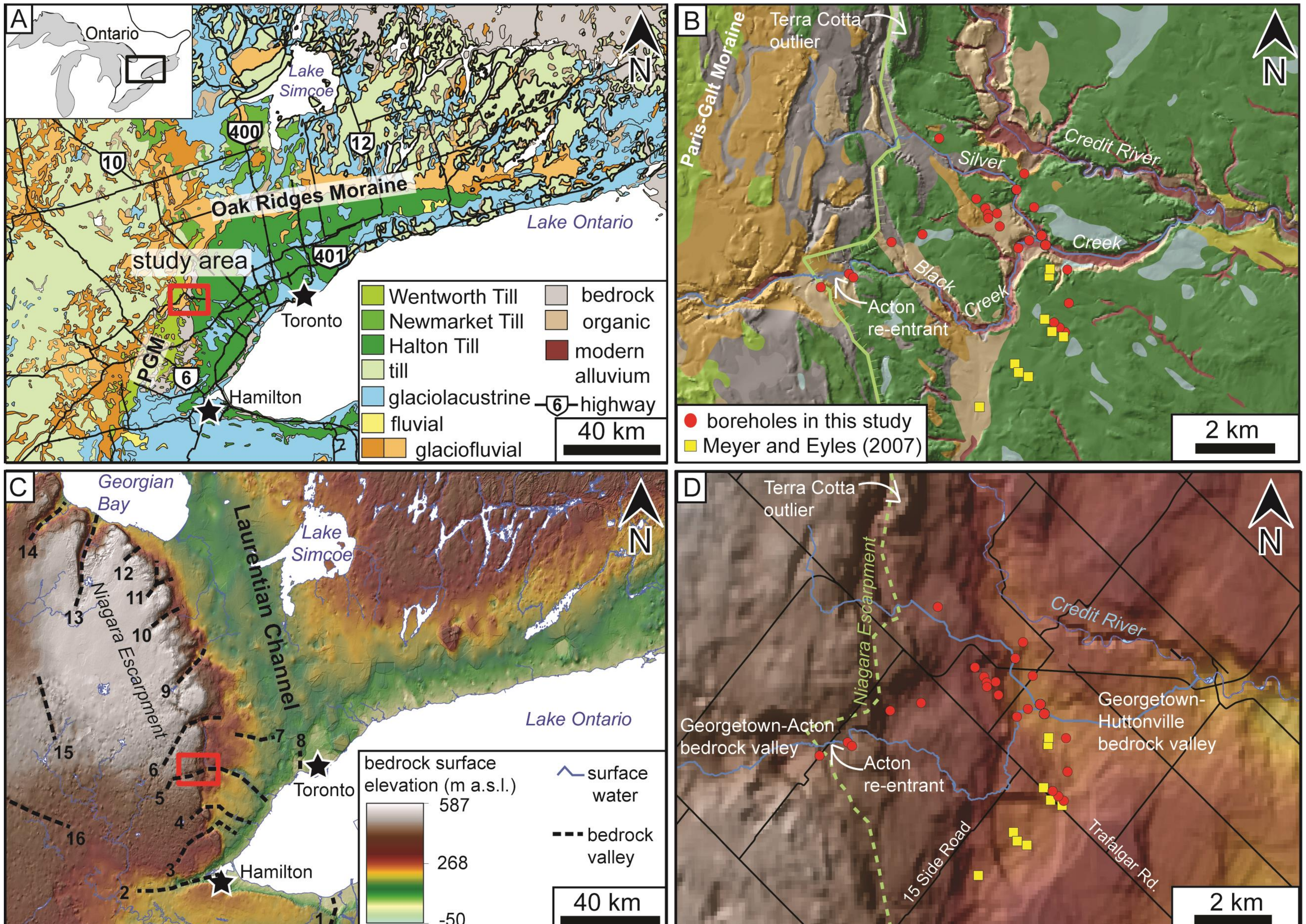
A
Ontario
Lake Simcoe
400
12
10
Oak Ridges Moraine
Lake Ontario
401
study area
Toronto
PGM
6
Hamilton
Wentworth Till
Newmarket Till
Halton Till
till
glaciolacustrine
fluvial
glaciofluvial
bedrock
organic
modern alluvium
highway
40 km
N
B
Terra Cotta outlier
Paris-Galt Moraine
Credit River
Silver
Creek
Black
Creek
Acton re-entrant
boreholes in this study
Meyer and Eyles (2007)
2 km
C
Georgian Bay
Lake Simcoe
Laurentian Channel
Niagara Escarpment
Lake Ontario
Toronto
Hamilton
bedrock surface elevation (m a.s.l.)
587
268
-50
surface water
bedrock valley
40 km
1
2
3
4
5
6
7
8
9
10
11
12
13
14
15
16
D
Terra Cotta outlier
Niagara Escarpment
Credit River
Georgetown-Huttonville bedrock valley
Georgetown-Acton bedrock valley
Acton re-entrant
15 Side Road
Trafalgar Rd.
2 km

The study area is located on the western margin of the Ontario basin below the Niagara Escarpment, which essentially separates the Erie and Ontario basins (Figs. 4.1, 4.3), and facilitated drainage of meltwater through outwash channels from the Ontario to Erie basins (Fig. 4.3; Barnett, 1992; Gao, 2011). Hence, understanding of the Quaternary geologic history of both the Erie and Ontario basins is important for reconstruction of the depositional history and paleoenvironmental evolution of the Georgetown area. The early- to mid-Wisconsin stratigraphy of the region is composed of fluvial, glaciolacustrine, and glaciodeltaic sediments equivalent to the Sunnybrook Formation and Thorncliffe Formation (a regional aquifer) exposed along the Scarborough Bluffs in Toronto (Fig. 4.3; Eyles and Eyles, 1983; Karrow et al., 2001). At the beginning of the Late Wisconsin (c. 20C ka yrs BP; Barnett, 1992), the LIS advanced into southern Ontario from the north and deposited the Catfish Creek Drift, which is well exposed along the north shoreline of Lake Erie (Fig. 4.2; Dreimanis and Gibbard, 2005). During a major southward ice advance (c. 14.8C ka yrs BP; Port Bruce Stadial), the LIS deposited the Port Stanley Drift in the Erie Basin and the Newmarket (or Northern) till in the Ontario basin (Figs. 4.3A, B; Barnett, 1992). The Newmarket Till forms a regional leaky aquitard in southern Ontario (Gerber et al., 2001). Subsequent retreat of the LIS resulted in the formation of lobate ice masses that were strongly controlled by the orientation of the lake basins and exposed an area of land called ‘Ontario Island’ (Fig. 4.3B; Barnett, 1992).

During the early Mackinaw Interstadial (c. 13.4C ka yrs BP), the Wentworth Till was deposited above (to the west of) the Escarpment, and the Paris and Galt Moraines formed at the ice margin (Figs. 4.3A, C; Barnett, 1992). Further retreat of the ice margin is recorded by glaciolacustrine sediment (paleo- or early Peel Ponds?; Barnett, 1992) and coarse-grained sediment, deposited in an interlobate zone as the Oak Ridges Moraine (ORM) began to form between the separating Ontario and Simcoe lobes (Fig. 4.3; Chapman and Putnam, 1984; Paterson and Cheel, 1997). During ice retreat into the Ontario basin, outwash channels flowed from the ORM and drained through re-entrant valleys cut into the Escarpment, and supplied meltwater and sediment to glacial Lake Whittlesey in the Erie basin (Fig. 4.3C; Barnett, 1992). The ORM provides a major aquifer recharge zone in southern Ontario (Figs. 4.1, 4.3; Sharpe et al., 2003).

During the Port Huron Stadial (c. 12-13C ka yrs BP; Barnett, 1992), the southern margin of the LIS underwent a short-lived re-advance as lobate ice masses which preferentially flowed along the Great Lakes basins, resulting in the formation of ephemeral proglacial lakes (e.g. glacial Lake Schomberg and late Peel Ponds; Barnett, 1992) ponded between the ice margin, the Niagara Escarpment, and the margins of the ORM (Fig. 4.3D; Costello and Walker, 1972; Sharpe et al. 2004). The lobate ice masses of the LIS also deposited localized till sheets and overrode the margins of the ORM, depositing the Halton Till (Figs. 1A,B, 3; Sharpe et al., 2004). The Halton Till extends from the northern shore of Lake Ontario to the southern flank of the ORM, and to the base of the Niagara Escarpment (Fig. 4.1A; Karrow, 2005; Barnett, 1992). The final stages of ice retreat from southern Ontario were accompanied by fluctuating lake levels in the Great Lakes basins (Fig. 4.3A), deposition of fine- and coarse-grained outwash sediment, and incision of older glacial stratigraphies by meltwater channels (Barnett,

Fig. 4.2 A. Location of boreholes utilized in this study represented by red circles and labeled with the abbreviated borehole name (see B for full borehole names and location coordinates). Boreholes of Meyer and Eyles (2007) are indicated by yellow squares. Transects at each study site are labeled (A-A’, B-B’, C-C’, D-D’) with a dashed line, and the location of municipal wells are indicated by stars. B. Borehole names and location coordinates, including borehole abbreviations used in A.

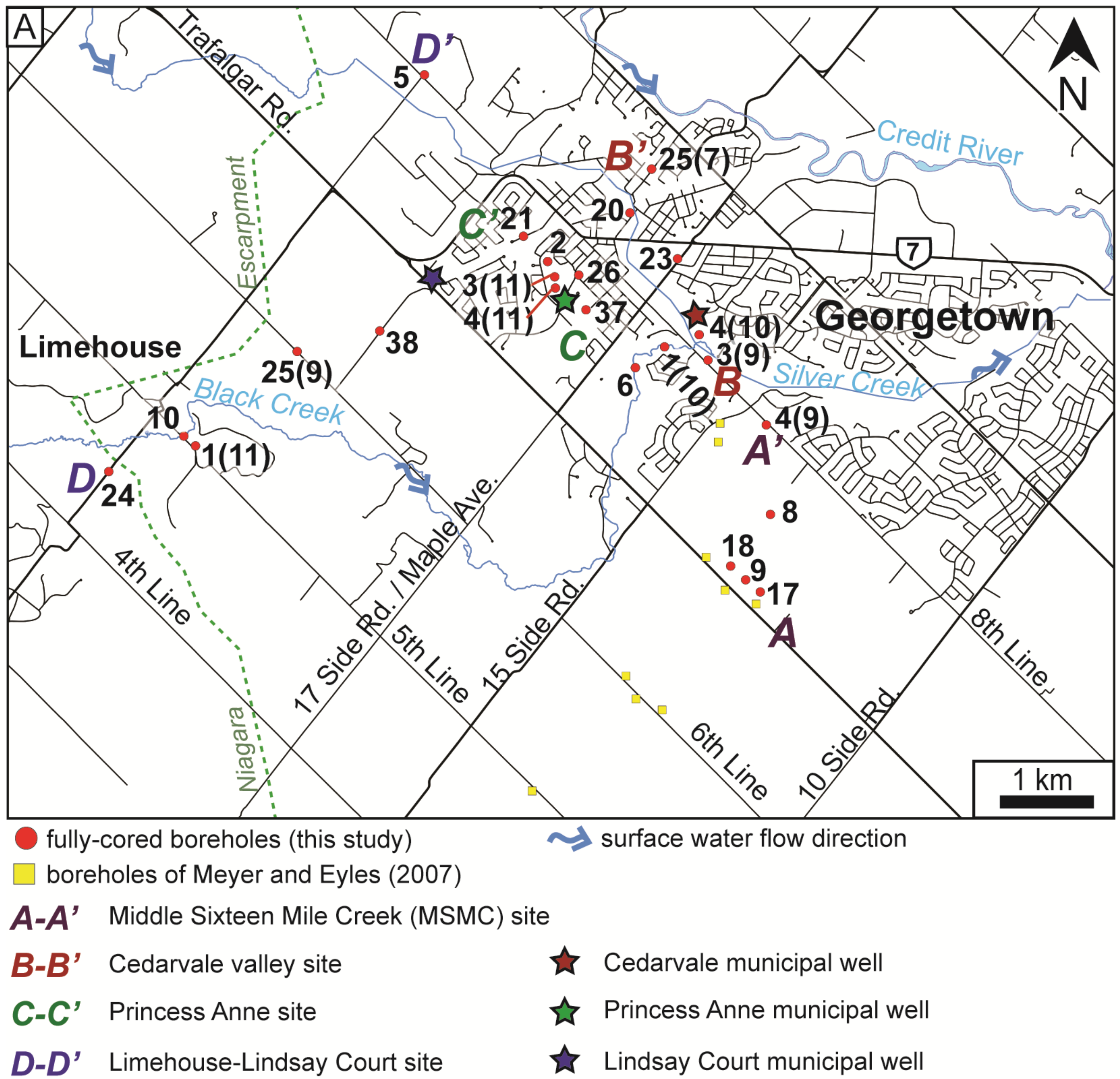

B

Borehole	Code (MW)	*NAD 1983, UTM 17T* Easting	Northing
MW20_06	20	586845	4833968
MW21_06	21	585811	4833741
MW23_07	23	587307	4833522
MW25_07	25(7)	587055	4834393
MW3_09	3(9)	587594	4832535
MW4_09	4(9)	588166	4831912
MW8_09	8	588208	4831039
MW9_09	9	587967	4830404
MW17_09	17	588109	4830286
MW18_09	18	587821	4830538
MW24_09	24	582007	4831704
MW25_09	25(9)	583628	4832646
MW26_09	26	586346	4833367
MW37_09	37	586417	4833026
MW38_09	38	584416	4832821
MW1_10	1(10)	587180	4832666
MW4_10	4(10)	587517	4832784
MW6_10	6	586897	4832463
MW10_10	10	582515	4831799
MW1_11	1(11)	582627	4831702
MW2_11	2	586046	4833495
MW3_11	3(11)	586114	4833347
MW4_11	4(11)	586121	4839238
MW5_11	5	584850	4835308

Fig. 4.3 Late Quaternary history of the study area. A. Time-distance diagram showing the relative position of the ice margin in the Erie and Ontario basins, including glacial lakes, moraines, and stratigraphic units that formed during the Middle and Late Wisconsin. B. Conceptual diagram illustrating the position of ice lobes of the Laurentide Ice Sheet (LIS; and an ice-free land mass called the 'Ontario Island') in southern Ontario during the Port Bruce Stadial. Star indicates location of Georgetown study area. Black arrows indicate margins of the ice sheet. C. Conceptual diagram of the southern margin of the LIS in southern Ontario during the Mackinaw Interstadial, including the Paris-Galt Moraines, Oak Ridges Moraine, and Peel Ponds in the Erie basin, glacial Lake Whittlesey in the Erie basin, and major meltwater outlets (wavy arrows). D. The southern margin of the LIS during ice margin advance in the Port Huron Stadial, which deposited Halton Till and ponded water between the ice margin and Niagara Escarpment (Peel Ponds; modified from Barnett, 1992; Meyer and Eyles, 2007; Slomka and Eyles, 2013).

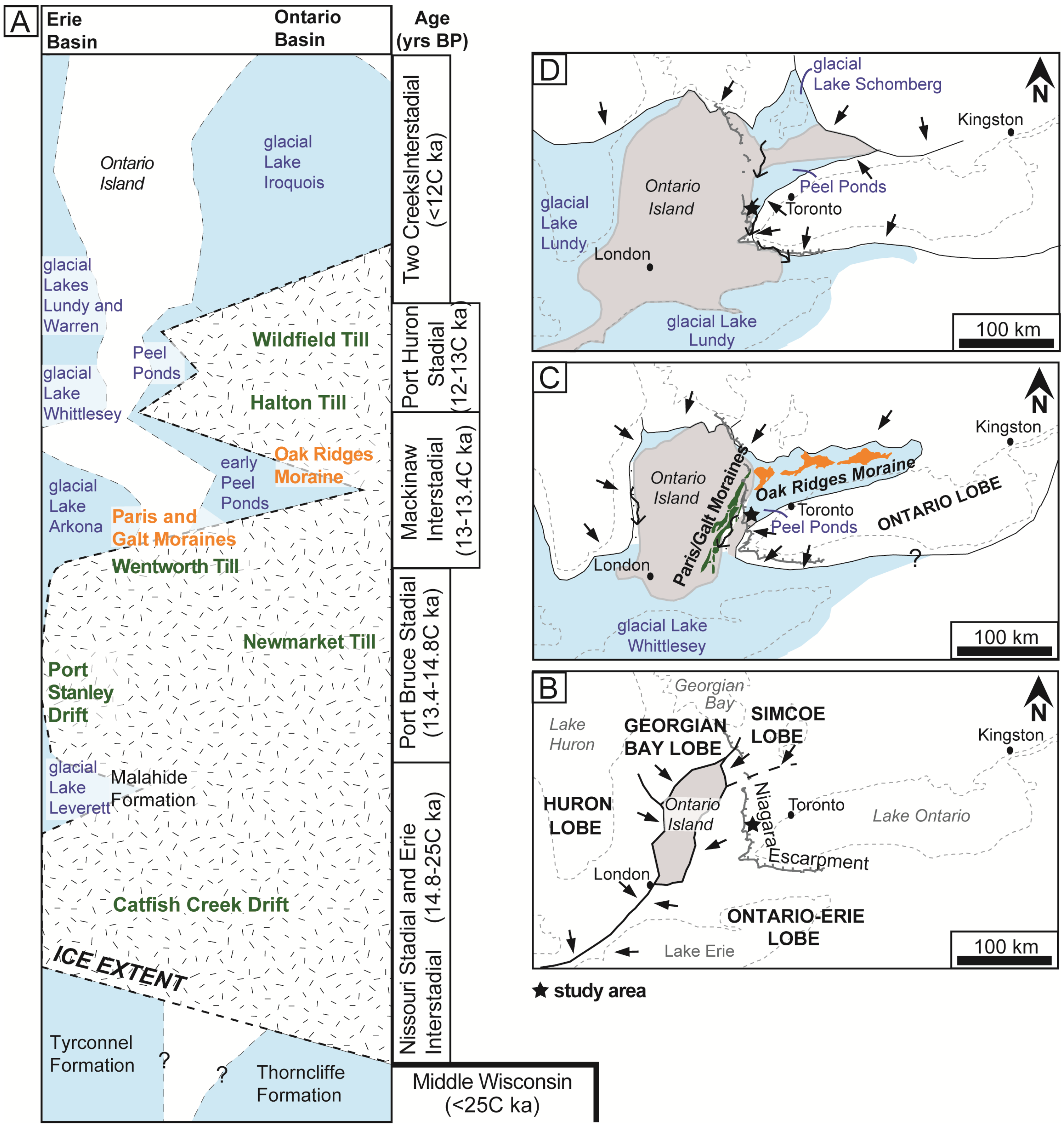
A
Erie Basin
Ontario Basin
Age (yrs BP)
Ontario Island
glacial Lake Iroquois
glacial Lakes Lundy and Warren
Peel Ponds
glacial Lake Whittlesey
Wildfield Till
Halton Till
early Peel Ponds
Oak Ridges Moraine
glacial Lake Arkona
Paris and Galt Moraines
Wentworth Till
Newmarket Till
Port Stanley Drift
glacial Lake Leverett
Malahide Formation
Catfish Creek Drift
ICE EXTENT
Tyrconnel Formation
Thorncliffe Formation
Two Creeks Interstadial (<12C ka)
Port Huron Stadial (12-13C ka)
Mackinaw Interstadial (13-13.4C ka)
Port Bruce Stadial (13.4-14.8C ka)
Nissouri Stadial and Erie Interstadial (14.8-25C ka)
Middle Wisconsin (<25C ka)
D
glacial Lake Schomberg
Kingston
Peel Ponds
Toronto
glacial Lake Lundy
London
glacial Lake Lundy
100 km
C
Kingston
Ontario Island
Paris/Galt Moraines
Oak Ridges Moraine
Toronto
Peel Ponds
ONTARIO LOBE
London
glacial Lake Whittlesey
100 km
B
Georgian Bay
Lake Huron
GEORGIAN BAY LOBE
SIMCOE LOBE
Kingston
HURON LOBE
Ontario Island
Niagara Escarpment
Toronto
Lake Ontario
London
ONTARIO-ERIE LOBE
Lake Erie
100 km
N
★ study area

1992). The subsurface stratigraphy preserved in the study area contains a sedimentary record of many of these Late Wisconsin events (Karrow, 2005; Meyer and Eyles, 2007).

4.3 METHODOLOGY

The Georgetown area is divided into four sub-sites utilized in this study, including Middle Sixteen Mile Creek (MSMC; A-A'), Cedarvale Valley (B'B'), Princess Anne (C-C'), and Limehouse-Lindsay Court (D-D'); the latter three sub-sites host producing municipal well fields (Fig. 4.2; Regional Municipality of Halton, 2011). These sub-sites were selected for study based on the availability of 24 fully-cored boreholes, which were drilled as part of an ongoing groundwater exploration program conducted by the Regional Municipality of Halton and allowed detailed analysis of subsurface sediments (Fig. 4.2). The boreholes were continuously cored in 1.5 m run intervals using the PQ coring technique (9 cm diameter core samples) and one borehole (MW25_09) was cored using a sonic drilling method. The core was logged in detail, recording grain size, sedimentary structure, clast characteristics (e.g. rounding, maximum diameter and lithology), facies types, and the nature of facies contacts (e.g. erosional, irregular, conformable; Figs. 4.4-4.10).

Thirteen facies types are identified in this study (Figs. 4.4, 4.5) and include: fine-grained facies (laminated, Fl; massive, Fm; deformed, Fd), sand facies (horizontally bedded and laminated, Sh, Sl; rippled, Sr; cross-bedded, Sc, including trough-cross bedded, St, and planar cross-bedded, Sp; deformed, Sd; and massive, Sm), gravel facies (massive, Gm; and bedded, including planar cross-bedded, Gp, horizontally bedded, Gh, and trough cross-bedded, Gt), and diamict facies (clast-supported and massive, Dcm; and matrix-supported and massive Dmm). Facies codes are followed by a lowercase letter in parantheses to indicate sand-rich (-s), clay-and silt-rich (-c), gravelly (-g), open-work (-o), or deformed (-d) sediments (Fig. 4.4, 4.7- 4.10). These facies codes will be referred to throughout this paper.

Analysis of the vertical succession of facies types and the nature of facies contacts in the core (Figs. 4.3- 4.6) allowed the delineation of a hierarchy of facies contacts (bounding surfaces) that are numerically ordered from fifth- to seventh-order (Fig. 4.6; Miall, 1988) based on the degree of change in facies on either side of the bounding surface, the nature of the bounding surface (e.g. erosional, conformable, U-shaped, planar), and the scale of the bounding surface (i.e. the lateral extent of correlation of the bounding surface between boreholes; Figs. 4.7- 4.10). Fourth-order surfaces delineate facies associations with a characteristic geometry (architectural elements) and reflect autogenic processes within a depositional system (Fig. 4.6; Miall, 2010). Fifth-order surfaces record major changes within a depositional environment (such as channel and fan lobe avulsion or periods of ice stagnation and increased meltwater production) as a result of allogenic and major autogenic controls. A sixth-order surface records allogenic controls on a depositional system and demarcates the base of a depositional environment. Seventh-order surfaces record major environmental changes within a basin complex, such as the unconformity separating the Paleozoic bedrock and unlithified Quaternary glacial sediments in Ontario (Fig. 4.6; Boyce and Eyles, 2000; Miall, 2010).

Fig. 4.4 Description and interpretation of facies types identified in this study. Refer to Fig. 4.5 for photos of each facies type.

Facies	Grain size and thickness	Sedimentary structure	Other	Interpretation
Fl	Silt (commonly red or white) and clay (commonly brown), rare very fine-grained sand (red, white) 1 cm-4 m	Laminations. May have symmetrical ripples, fine-upwards, and rare concretions at the base of silt layers overlying coarse-sand. Clay may have dessication cracks.	Erosional upper contacts, rare deformed clay clasts and cobble or pebbles (clasts commonly rest above silt laminations). May have rare thin (<1cm) beds of granule, loaded and angular contacts, convolute laminations, and pillows, and flame structures that disturb bedding (Fld)	Formed by fallout from suspension and debris flows (turbidity currents) in a (glacio)lacustrine environment, and subsequent soft-sediment deformation by water escape, sediment loading, and mass movement.
Fm	Silt, minor clay, very fine-grained sand 2 cm-6.2 m	Massive. May have diffuse grading, rare pebbles and boulders, and fine upwards.	Rare concretions at the base of silt layers, angular contacts with other facies, may contain rare pebbles to boulders and deformed sand rafts. May be interbedded with Gm(s), Fl, and Fd	Deposited in a (glacio)lacustrine environment. Clasts record the rainout of debris released from floating ice or runout clasts from debris flows.
Fd	Clay, silt, very fine- to fine-grained sand 2 cm-4 m	Flames, vertical water escape structures, breccia, loaded contacts, deformed layers, 'massive' or with crude diffuse changes in grain size, may fine upwards. No apparent primary structure preserved.	May contain rare cobbles and pebbles (Fd(g)), thin (<1 cm) stringers and deformed beds of coarse-grained sand and pebbles, deformed fine-grained sand and clay clasts. May have a planar to angular lower contact and scoured upper surface	Formed by soft-sediment deformation (water escape, sediment loading, and slumping) in a (glacio)la-custrine, fluvial, and deltaic environment, or by defor-mation at the base of an ice sheet. Clasts may record rainout of iceberg debris or runout clasts.
Sh, Sl	Very fine- to very coarse grained sand 2 cm-1 m	Horizontal lamination (beds <1 cm thick; Sl), well-de-fined or diffuse horizontal bedding (beds 1 cm thick or greater; Sh), may fine upwards. A sharp lower contact is common in Sh.	Sh may contain rare clasts of dolostone and shale (0.5-2 cm diameter), subangular to subrounded. Sl may contain convolute laminations (Sld)	Records fallout of sand from suspension (Sl) under low energy conditions and transport of sand grains as a sheet on the bed (Sh) under high energy conditions in a fluvial or deltaic environment
Sr	Fine- to medium-grained sand 30-93 cm	Well sorted, ripple cross lamination (high and low angle climbing, trough, and sinusoidal)	May have an erosional lower surface, land loaded or conformable upper surface. Ripples may be deformed (flame structures through ripples are common)	Ripple bedforms formed by saltation of sand grains by traction currents and deposition by separation eddies in a fluvial or deltaic depositional environment
Sc, St, Sp	Very fine- to coarse-grained sand 10 cm-1.5 m	Well sorted. Cross bedded (Sc), including trough (St) and planar (Sp) cross bedding. Sharp and conformable to erosional lower contacts are common	Commonly fine upwards, or may fine then coarsen upwards. May contain flame structures that cross-cut bedding. Commonly interbedded with Sr	Bedload transport of sand by migration of bedforms (bars and dunes), probably in (glacio)fluvial and deltaic depositional environments

Dmm	diamict, matrix-supported, massive	**-d**	deformed	**-(s)**	sand-rich	**-(g)**	gravel-rich
Dcm	diamict, clast-supported, massive	**(facies)**	minor facies	**-(c)**	clay and silt-rich	**-(o)**	open-work

Facies	Grain size and thickness	Sedimentary structure	Other	Interpretation
Sd	Very coarse- to fine-grained sand 7 cm-3.4 m	Convolute laminations and beds, loaded and deformed contacts, vertical water escape structures and recumbent folds, gradational to sharp and loaded to planar lower surface	Commonly interbedded with Fd and may contain concretions of silt and deformed clay clasts	Soft-sediment deformation of sand facies by water escape, sediment loading, and subglacial deformation
Sm	Fine- to very coarse-grained sand 16 cm-1.1.m	Massive, may fine or coarsen upwards. A conformable to sharp and planar to angular lower contact, and sharp upper contact are common	Rare cobble and pebble clasts	May record rapid deposition of sand in a subaqueous depositional environment, or deformation and overprinting of sedimentary structure
Gm(s)	Granule to cobble, medium-grained sand to granule matrix (which may fine upwards to medium- to fine-grained sand with trace mud) 2 cm-2.3 m	Clast supported, massive. Poorly to very poorly sorted. May fine or coarsen upwards. Erosional angular upper contact and sharp planar to angular or scoured lower contact are common (may have loaded or deformed contacts)	Shale, dolostone, quartzite, granite, gneiss, diorite, limestone (sub cm-3 cm in diameter), angular to rounded. Associated with Gp, Gt and Gh, may be interbedded with Gm(g). Rarely cemented with calcrete in sections 5-25 cm thick	Deposition of bedload by accumulation of gravel clasts on the bed under medium- to high-energy discharge, and subsequent (or concurrent) deposition of sand in interstices, probably in a glaciofluvial depositional environment
Gm(o)	Pebble to boulder Single clast thick, to 6 cm-10.5 m	Structureless, may be imbricated, may have a sharp lower contact	Shale, gneiss, granite, basalt?, sandstone, quartzite, dolostone (sub cm to 15 cm in diameter), angular-rounded	Deposition of bedload by rolling and accumulation of gravel clasts on the bed under high-energy discharge, probably in a glaciofluvial depositional environment
Gp, Gh, Gt	Pebble boulder, may contain coarse- to very coarse-grained sand matrix 60 cm-1 m	Poorly to well sorted. Openwork and sandy gravel. Crudely horizontally bedded (Gh), cross bedded (Gp), or trough cross bedded (Gt)	Subangular to well rounded dolostone, shale, granite gneiss, quartzite (0.5-10 cm in diameter)	Deposition of bedload by rolling and aggradation of gravel (Gh), and avalanching of gravel clasts down the lee-side of bar foresets (Gp,Gt), or as minor channel fill (Gt) by high-energy flows
Dcm	Silty clay to silty sand matrix, clast rich 3.5-8.5 m	Clast supported (granule to cobble), very poorly sorted, massive, consolidated to unconsolidated, matrix texture may coarsen-upwards	Rounded to angular shale clasts (1 mm->9 cm in diameter), undeformed and deformed blue silt clasts, may directly overlie fractured bedrock	In-situ weathering of fractured shale bedrock, or weathering of shale-rich sediment previously deposited by subglacial, colluvial, and alluvial processes
Dmm(s)	Silty sandy matrix with pebble, cobble, boulder 10 cm-7.2 m	Structureless, Very poorly sorted, matrix-supported, sand-rich, overconsolidated to poorly consolidated, reddish and greyish matrix colour	Angular to subrounded dolostone shale, feldspar, gneiss, granite clasts (0.5->9 cm) may be crudely stratified and contain deformed clay clasts and pockets of Gm(s)	Mixing and reworking of sediment with little to no sorting, probably by subglacial, mass flow, or alluvial processes
Dmm(c)	Silt to silty clay matrix with pebble to boulder clasts throughout 4 cm-5 m	Structureless, Very poorly sorted, matrix-supported, clay-and silt-rich, consolidated to overconsolidated, may be laminated in some places	Angular to subrounded shale and dolostone, granite, quartzite. May have a sharp lower contact overlain by a boulder	Mixing and compaction of sediment with little to no sorting, probably by subglacial depositional processes

Fig. 4.5 Photos of facies recovered in fully-cored boreholes. Facies codes refer to fine-grained facies (laminated, Fl; massive, Fm; deformed, Fd; gravelly, -g), sand facies (horizontally bedded and laminated, Sh, Sl; rippled, Sr; cross bedded, Sc, including trough cross-bedded, St; deformed, Sd; and massive, Sm), gravel facies made of granule- to boulder-sized sediment (massive and sandy, Gm(s); massive and open-work, Gm(o); cross-bedded including planar, Gp, and trough, Gt; and horizontally bedded and stratified, Gh), and diamict facies, including clast-supported massive diamicts (Dcm) and matrix-supported massive diamicts (Dmm; including sand-rich (-s) and clay-rich (-c)). Refer to Fig. 4.4 for facies descriptions and interpretations.


Diamict facies
Dmm(s)
Dmm(c)
Dcm
Dcm
Dcm
Bedrock (shale)
Gravel facies
Gm(s)
Gm(o)
Gt
Gh
Gp
cemeneted
Sand facies
Sl
Sh
Sd, Sm
Sd
Sc (St)
Sr
Fine-grained facies
Fl
Fm
Fm(g)
Fd
Fd

Fig. 4.6 Bounding surface and unit hierarchies utilized in this study, including the lateral and vertical scales of units and surfaces delineated in this study and their environmental controls.

Bounding surfaces		Packages of genetically-related facies			
Order	Description	Unit	Unit scale (lateral extent)	Unit scale (vertical extent)	Control
1	Set boundary separating similar facies	facies	not delineated	not delineated	autogenic
2	Coset boundary separating dissimilar facies	facies	not delineated	not delineated	autogenic
3	Surface which crosscuts first and second-order surfaces (may be erosional and a surface of reactivation)	facies	not delineated	not delineated	autogenic
4	Boundary separating facies associations (with a characteristic geometry)	architectural element (facies association)	<100s of metres	<1 m to few metres	autogenic
5	Boundary (may be erosional) defining groups of genetically related architectural elements (within a depositional environment)	architectural component	100s of metres	metres to <20 m	allogenic and autogenic
6	Major boundary delineating a depositional environment (may define a lithostratigraphic unit)	architectural unit	100s of metres to kilometres	10s of metres	allogenic
7	A major surface which marks the base of a depositional complex	basin fill, depositional complex	100s of kilometres	not delineated	allogenic

4.4 SUBSURFACE SEDIMENTARY ARCHITECTURE

Grouping of genetically-related facies types that occur in vertical succession in the cored boreholes allowed the delineation of eleven architectural units (AU1-11) which are bounded by sixth-order surfaces (Figs. 4.6, 4.11). Architectural units characterized and interpreted in this study include: weathered bedrock and regolith (AU1); sandy glaciofluvial (AU2); a multi-storey till complex (AU3), gravelly glaciofluvial (AU4), glaciolacustrine and deltaic (delta front and prodelta?; AU5), a tripartite till complex (AU6), sandy glaciofluvial and deltaic (delta front and delta plain?; AU7), coarsening-upward gravelly glaciofluvial (AU8), shale-rich gravel and diamict (AU9), colluvial-alluvial complex (Escarpment slope; AU10), and fluvial to slackwater (standing water; AU11; Figs. 4.11, 4.12). The term 'lithostratigraphic unit' is not used here because units in this study are not delineated on the basis of individual facies characteristics alone but according to their internal facies associations, the vertical lithofacies succession (e.g. fining-upward, no grading, chaotic), external geometry, stratigraphic position and elevation, and the spatial arrangement of bounding surfaces (Walker, 1992). AUs were correlated between boreholes (Figs. 4.7- 4.10) based on their facies composition, internal and external geometry, the nature of bounding surfaces, and by applying relative dating based on their stratigraphic position and by utilizing till sheets as regionally-extensive 'marker beds'. A mappable till unit that is regionally extensive (e.g. Newmarket Till) but is not present in a borehole is interpreted to have been truncated and removed by erosion. The geometry of depositional environments in modern glacial landsystems (e.g. Evans,

2005) is utilized to inform the correlation and predicted geometry of subsurface units (Fig. 4.6) between boreholes.

Analysis of the vertical stacking of facies within each AU (in a single borehole and between boreholes) allowed the grouping of packages of genetically-related facies that make up the large-scale architecture of units; these are herein named ‘architectural components’ and delineated by fifth-order bounding surfaces (Fig. 4.6). Architectural components are similar in scale to large channels and delta lobes of Miall (1992) and ‘element associations’ of Slomka and Eyles (2013). Components are characterized based on their characteristic vertical succession of facies types (e.g. fining- or coarsening-upward, interbedded and non-graded, heterogeneous or chaotic, tripartite complex, multi-storey), external geometry (e.g. channelized or concave-up, tabular sheet, wedge, irregular), and the nature of facies contacts (fifth-order surfaces are commonly erosional and can be correlated between boreholes; Figs. 4.7- 4.10)

Within each component, small-scale packages of genetically-related facies (recorded in vertical succession) are delineated by fourth-order surfaces and interpreted to record sedimentary packages at the scale of the architectural element (e.g. bars and small-scale channels in a fluvial system; Fig. 4.6; Miall, 1985; Walker, 1992); however, fourth-order surfaces are difficult to correlate laterally between boreholes, which is likely because the scale of the elements is smaller than the lateral distance between boreholes. As a result, the geometry of the elements is inferred based on their genetic interpretation and utilization of facies models, and illustrated in Fig. 4.12. This results in anisotropic spatial resolution of sedimentary heterogeneity, whereby delineation of the vertical sedimentary heterogeneity is higher-resolution than the lateral spatial heterogeneity of subsurface units; which is an inherent limitation of one-dimensional data, such as that from boreholes, for three-dimensional geologic investigations (Bridge and Tye, 2000; Miall, 2014). Lower order surfaces (first- to third-order; Fig. 4.9) are difficult to identify, characterize, and correlate laterally between boreholes; therefore these lower order surfaces are not included in this study.

Architectural units are described below in order of their stratigraphic position, from oldest to youngest; however, architectural components within different AUs may be time-equivalent. The stratigraphic order of AUs is largely inferred from relative dating in the absence of absolute dating control.

4.4.1 Architectural Unit 1 (AU1): weathered bedrock and regolith

AU1 is composed of diamict facies with a breccia-like appearance, and forms an undulating, sheet-like geometry (commonly 0.5 to 9 m thick; and 17 m thick on the Escarpment slope at MW25_09; Fig. 4.10) that generally parallels the bedrock topography. AU1 is bounded by a seventh-order lower bounding surface (resting directly on fractured shale bedrock, which contains evidence of permineralization in fractures), and a sharp and undulating sixth-order upper bounding surface (Figs. 4.7- 4.10). AU1 consists of a single architectural component that is composed of three architectural elements (separated by fourth-order surfaces) made of clast-supported (Dcm), matrix-supported (Dmm), and sand-rich diamict facies (Figs. 4.4, 4.5, 4.12). The diamict has a distinct reddish colour and gravel clasts are commonly very angular and of similar lithology to the bedrock (Queenston Formation shale; Fig. 4.5).

Fig. 4.7 Sedimentary logs recorded at the MSMC site (A-A’) including facies types and major bounding surfaces. Colours represent architectural units (AUs), which include weathered bedrock and regolith (AU1), sandy glaciofluvial (AU2), till complexes (AU3, AU6), gravelly glaciofluvial (AU4, AU8), glaciolacustrine, glaciofluvial, and deltaic units (AU5, AU7), shale-rich diamict and gravels (AU9), colluvial-alluvial (AU10), and fluvial to slackwater (AU11). Refer to Fig. 4.2 for transect and borehole locations and Fig. 4.4 for facies codes, descriptions, and interpretations.

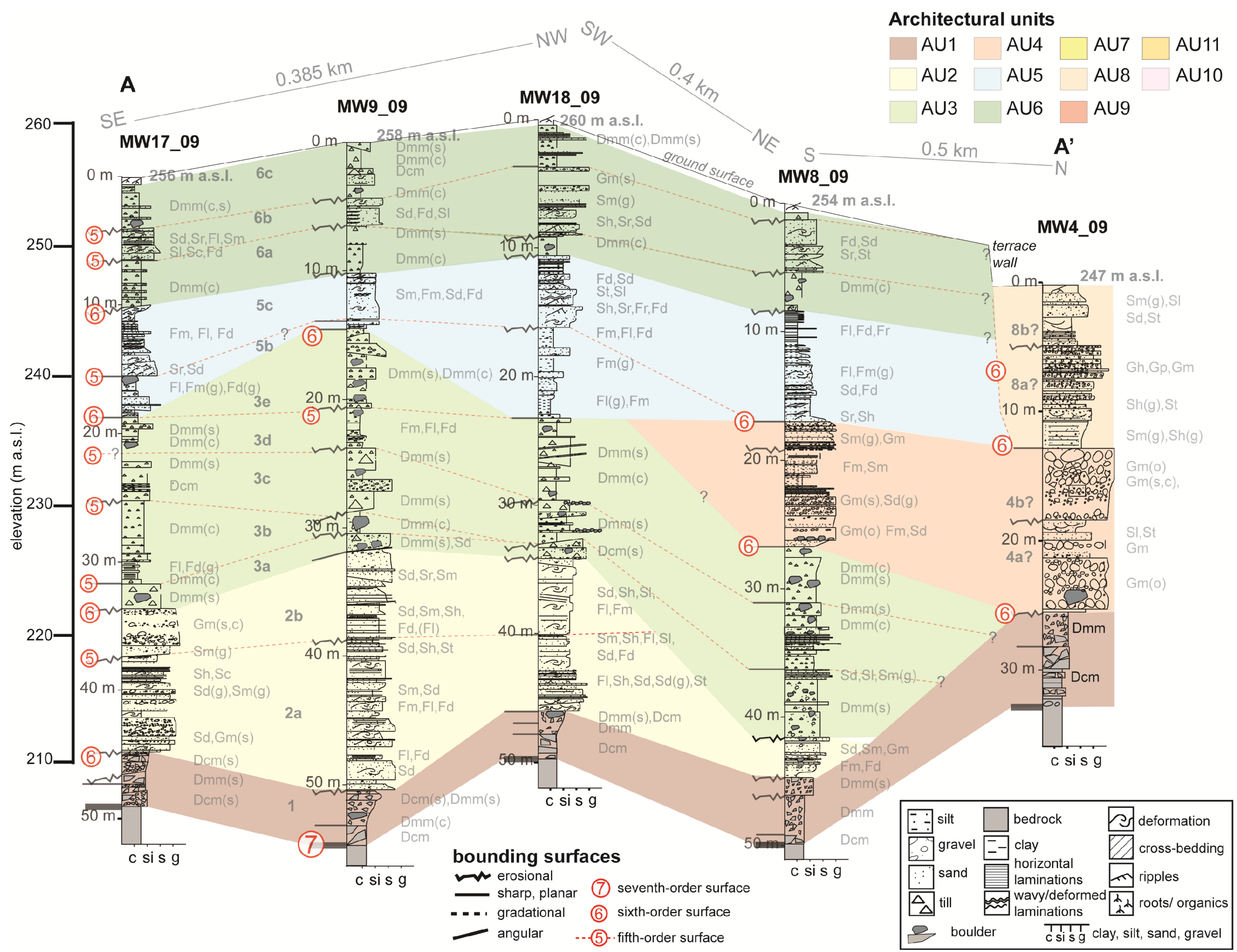

Architectural units
AU1 AU4 AU7 AU11
AU2 AU5 AU8 AU10
AU3 AU6 AU9
A
A'
SE
NW
SW
NE
S
N
0.385 km
0.4 km
0.5 km
MW17_09
MW9_09
MW18_09
MW8_09
MW4_09
256 m a.s.l.
258 m a.s.l.
260 m a.s.l.
254 m a.s.l.
247 m a.s.l.
elevation (m a.s.l.)
ground surface
terrace wall
bounding surfaces
erosional
sharp, planar
gradational
angular
seventh-order surface
sixth-order surface
fifth-order surface
silt
gravel
sand
till
boulder
bedrock
clay
horizontal laminations
wavy/deformed laminations
deformation
cross-bedding
ripples
roots/ organics
c si s g clay, silt, sand, gravel

Fig. 4.8 Sedimentary logs recorded in the Cedarvale valley (B-B') including facies types and major bounding surfaces. Refer to Fig. 4.2 for transect and borehole locations, Fig. 4.4 for facies codes, descriptions, and interpretations, and Fig. 4.7 for colour codes.

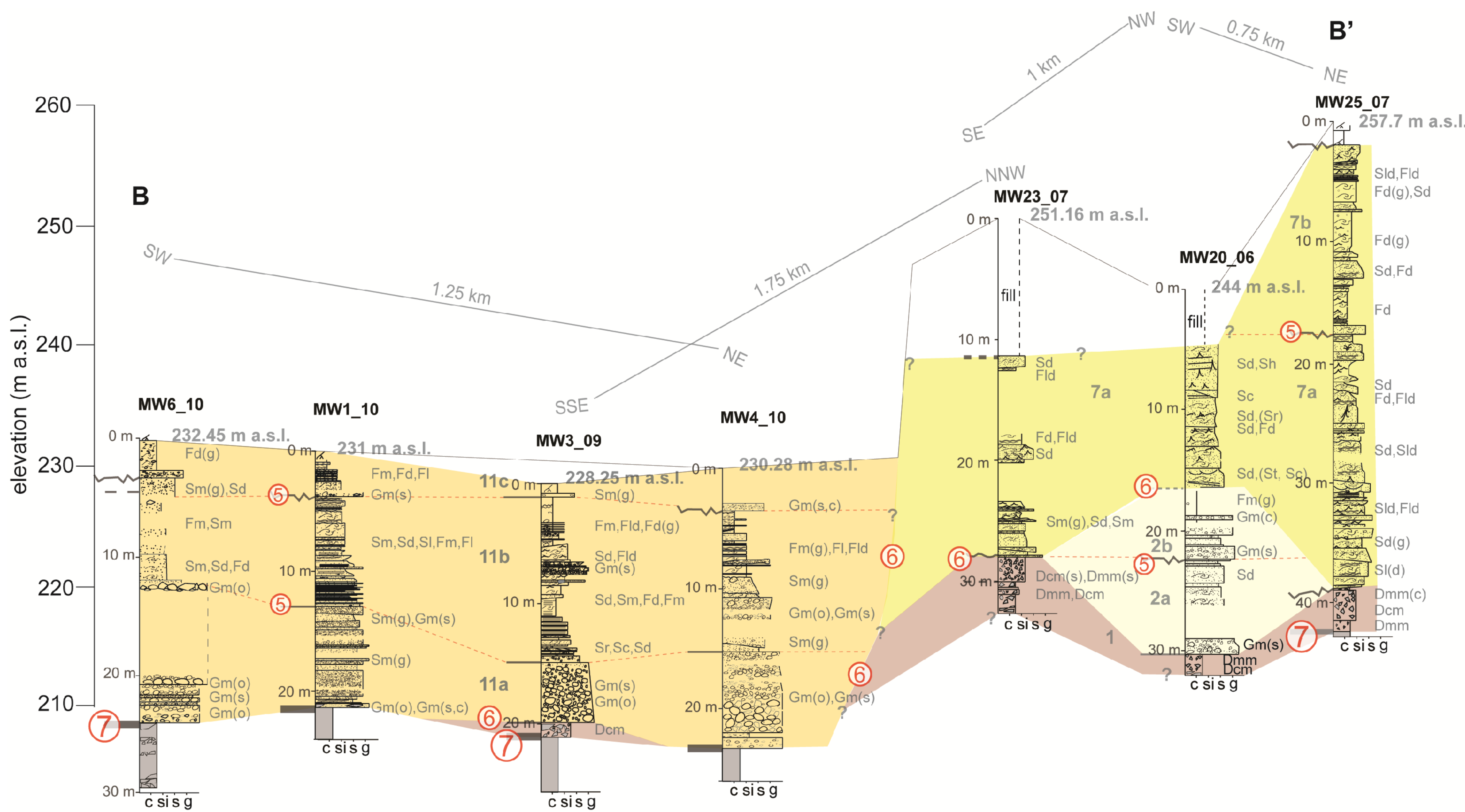
B
B'
elevation (m a.s.l.)
260
250
240
230
220
210
SW
1.25 km
NE
SSE
1.75 km
NNW
SE
1 km
NW
SW
0.75 km
NE
MW6_10
232.45 m a.s.l.
MW1_10
231 m a.s.l.
MW3_09
228.25 m a.s.l.
MW4_10
230.28 m a.s.l.
MW23_07
251.16 m a.s.l.
MW20_06
244 m a.s.l.
MW25_07
257.7 m a.s.l.
11a
11b
11c
7a
7b
2a
2b
1
fill
c si s g
Fd(g)
Sm(g),Sd
Fm,Sm
Sm,Sd,Fd
Gm(o)
Gm(s)
Fm,Fd,Fl
Sm,Sd,Sl,Fm,Fl
Sm(g),Gm(s)
Sm(g)
Gm(o),Gm(s,c)
Fm,Fld,Fd(g)
Sd,Fld
Sd,Sm,Fd,Fm
Sr,Sc,Sd
Dcm
Gm(s,c)
Fm(g),Fl,Fld
Gm(o),Gm(s)
Sd
Fld
Fd,Fld
Sm(g),Sd,Sm
Dcm(s),Dmm(s)
Dmm,Dcm
Sd,Sh
Sc
Sd,(Sr)
Sd,Fd
Sd,(St, Sc)
Fm(g)
Gm(c)
Dmm
Sld,Fld
Fd(g),Sd
Sd,Fd
Fd
Sd,Sld
Sd(g)
Sl(d)
Dmm(c)
0 m
10 m
20 m
30 m
40 m

Fig. 4.9 Sedimentary logs recorded in the Princess Anne site (C-C') including facies types and major bounding surfaces. Refer to Fig. 4.2 for borehole locations, Fig. 4.4 for facies codes, descriptions, and interpretations, and Fig. 4.7 for colour codes.

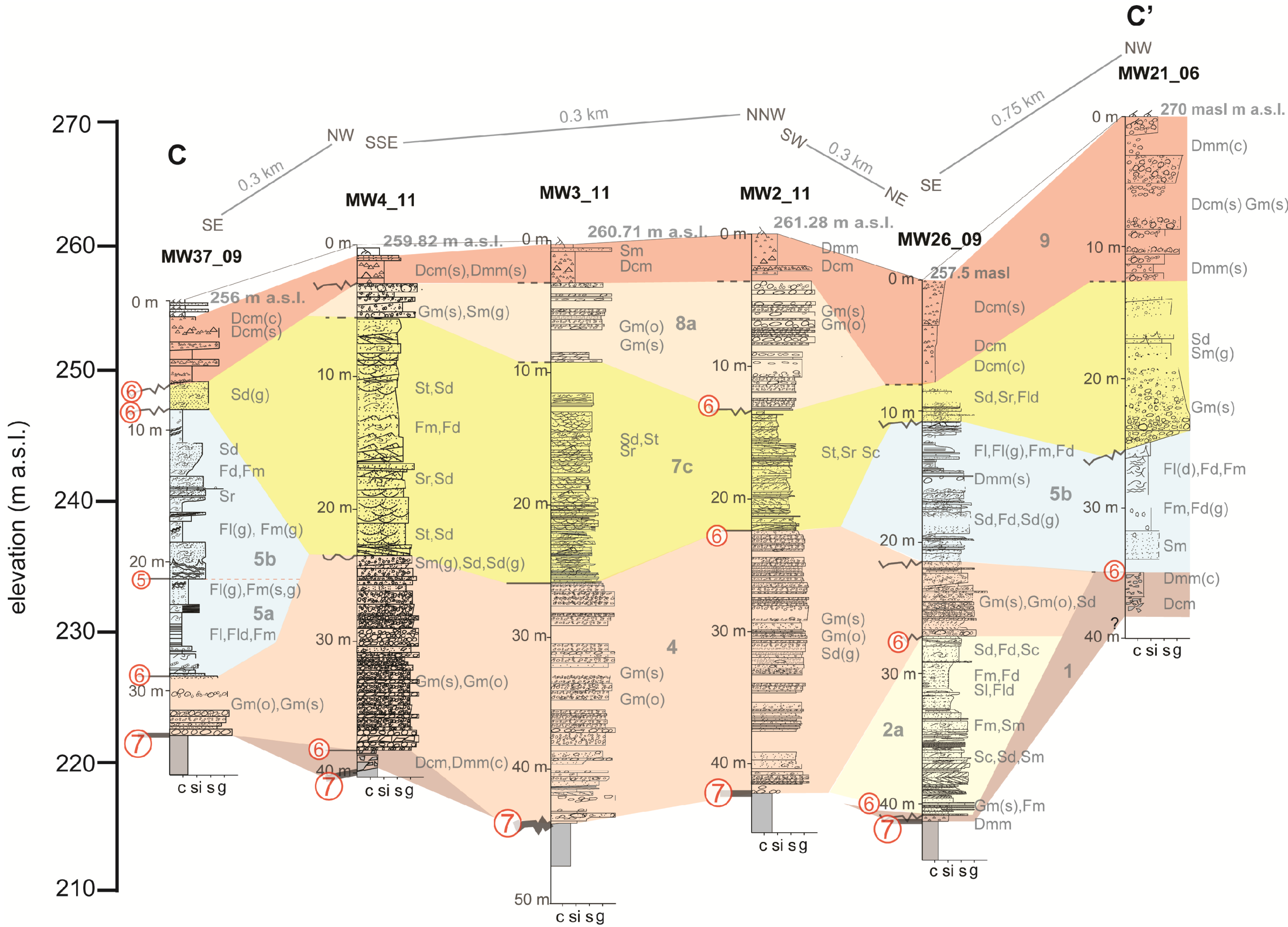

C
C'
elevation (m a.s.l.)
270
260
250
240
230
220
210
SE
0.3 km
NW
SSE
0.3 km
NNW
SW
0.3 km
NE
SE
0.75 km
NW
MW37_09
MW4_11
MW3_11
MW2_11
MW26_09
MW21_06
256 m a.s.l.
259.82 m a.s.l.
260.71 m a.s.l.
261.28 m a.s.l.
257.5 masl
270 masl m a.s.l.
Dcm(c)
Dcm(s)
Sd(g)
Sd
Fd,Fm
Sr
Fl(g), Fm(g)
5b
Fl(g),Fm(s,g)
5a
Fl,Fld,Fm
Gm(o),Gm(s)
Dcm(s),Dmm(s)
Gm(s),Sm(g)
St,Sd
Fm,Fd
Sr,Sd
St,Sd
Sm(g),Sd,Sd(g)
Gm(s),Gm(o)
Dcm,Dmm(c)
Sm
Dcm
Gm(o)
Gm(s)
8a
Sd,St
Sr
7c
4
Gm(s)
Gm(o)
Dmm
Dcm
Gm(s)
Gm(o)
St,Sr Sc
Gm(s)
Gm(o)
Sd(g)
9
Dcm(s)
Dcm
Dcm(c)
Sd,Sr,Fld
Fl,Fl(g),Fm,Fd
Dmm(s)
5b
Sd,Fd,Sd(g)
Gm(s),Gm(o),Sd
Sd,Fd,Sc
Fm,Fd
Sl,Fld
1
2a
Fm,Sm
Sc,Sd,Sm
Gm(s),Fm
Dmm
Dmm(c)
Dcm(s) Gm(s)
Dmm(s)
Sd
Sm(g)
Gm(s)
Fl(d),Fd,Fm
Fm,Fd(g)
Sm
Dmm(c)
Dcm
c si s g

Fig. 4.10 Sedimentary logs recorded in the Limehouse-Lindsay Court site (D-D') including facies types and major bounding surfaces. Refer to Fig. 4.2 for borehole locations, Fig. 4.4 for facies codes, descriptions, and interpretations, and Fig. 4.7 for colour codes.

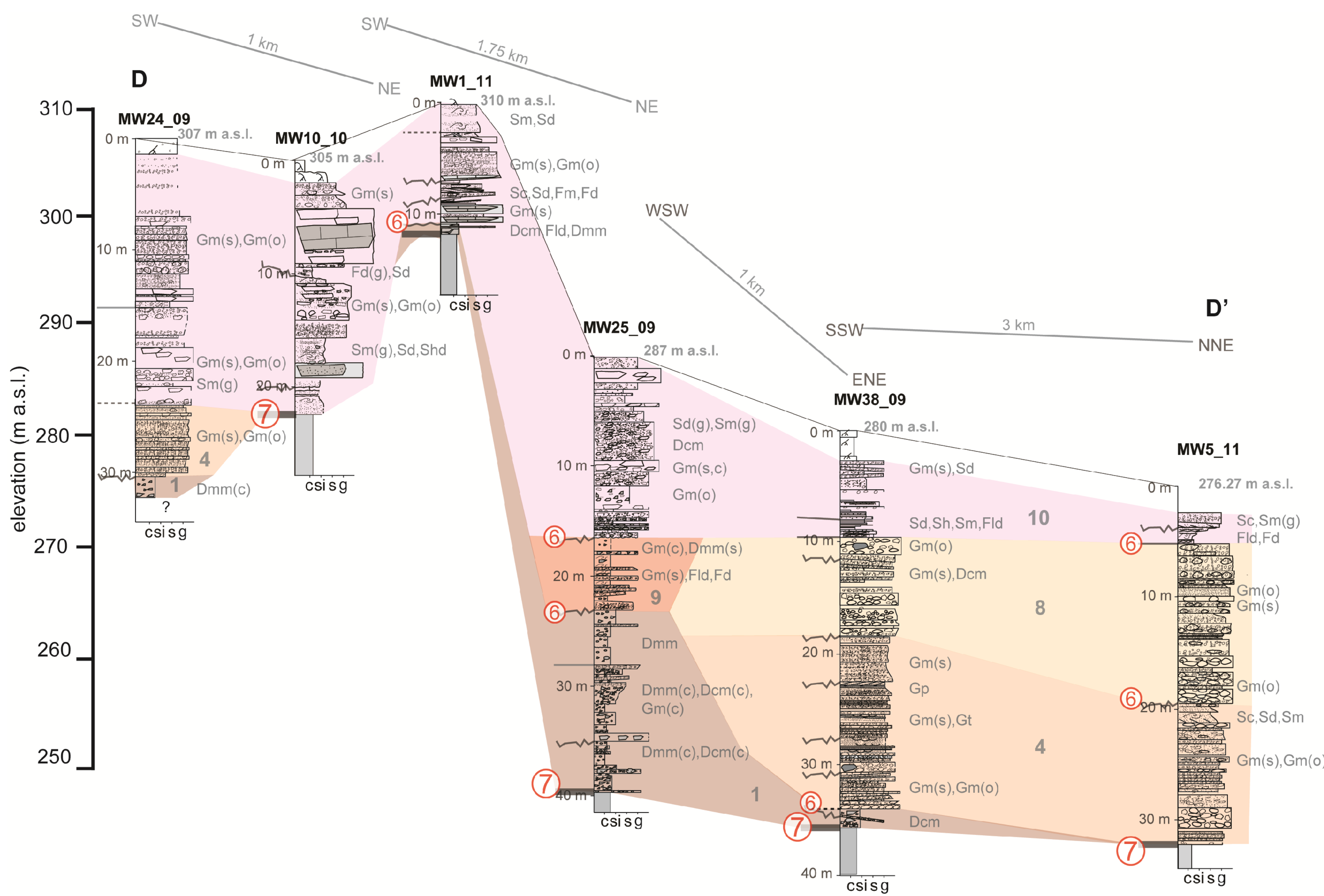
D
D'
SW
1 km
NE
SW
1.75 km
NE
WSW
1 km
ENE
SSW
3 km
NNE
elevation (m a.s.l.)
310
300
290
280
270
260
250
MW24_09
307 m a.s.l.
MW10_10
305 m a.s.l.
MW1_11
310 m a.s.l.
MW25_09
287 m a.s.l.
MW38_09
280 m a.s.l.
MW5_11
276.27 m a.s.l.
Sm,Sd
Gm(s),Gm(o)
Sc,Sd,Fm,Fd
Gm(s)
Dcm,Fld,Dmm
Gm(s)
Fd(g),Sd
Gm(s),Gm(o)
Sm(g),Sd,Shd
Gm(s),Gm(o)
Gm(s),Gm(o)
Sm(g)
Gm(s),Gm(o)
Dmm(c)
Sd(g),Sm(g)
Dcm
Gm(s,c)
Gm(o)
Gm(c),Dmm(s)
Gm(s),Fld,Fd
Dmm
Dmm(c),Dcm(c),
Gm(c)
Dmm(c),Dcm(c)
Gm(s),Sd
Sd,Sh,Sm,Fld
Gm(o)
Gm(s),Dcm
Gm(s)
Gp
Gm(s),Gt
Gm(s),Gm(o)
Dcm
Sc,Sm(g)
Fld,Fd
Gm(o)
Gm(s)
Gm(o)
Sc,Sd,Sm
Gm(s),Gm(o)
10
9
8
4
1
6
7
csi s g

Fig. 4.11 Summary and interpretation of architectural units (AUs) identified in this study. AUs include weathered bedrock and regolith (AU1), sandy glaciofluvial (AU2), till complexes (AU3, AU6), gravelly glaciofluvial (AU4, AU8), glaciolacustrine, glaciofluvial, and deltaic units (AU5, AU7), shale-rich diamict and gravels (AU9), colluvial-alluvial (AU10), and fluvial to slackwater (AU11). Refer to Fig. 4.4 for facies codes, descriptions, and interpretations and Figs. 7-10 for AUs delineated in sedimentary logs.

Unit	Facies types	Bounding surfaces	Interpretation	Units of Meyer & Eyles (2007)
AU11	Gm(s), Gm(o), Gm(c) Sm, Sm(g), Sd, Sd(g), Sl, Sh, Fm, Fm(g), Fl, Fld, Fd, Fd(g); rare Sr, Sc, Dcm(c)	Upper: planar to concave-up? (ground surface); Lower: sharp (probably erosional), concave-up	Incision and deposition in a fluvial system which transitions to a slackwater or lacustrine depositional environment, and recent alluvial fill	(not recorded)
AU10	Dmm(c), Dmm(s), Dcm(s), Gm(s), Gm(o), Gm(c), Sd, Sd(g), Sm(g), Sc, Sh, Sh(d), Sm(g,c), Fd, Fd(g), Fld (boulders are common)	Upper: ground surface; Lower: sharp, angular to irregular	Deposition of interbedded colluvial, fluvial, and 'slackwater' sediments in a bedrock valley re-entrant and slope depositional setting	(not recorded)
AU9	Dcm, Dcm(c), Dcm(s), Dmm, Dmm(s); rare Sm, Sd	Upper: ground surface; Lower: sharp, may be erosional, irregular	May record a coarse-grained till facies of FA6, or outwash gravels that are poorly sorted as a result of weathered shale clasts	(not recorded)
AU8	Gm, Gm(s), Gm(o), Gp, Gh,Sm, Sm(g), Sd, Sd(g), Sl, Sr, Sh, Sh(g), St; rare Fl, Fm, Gm(c), Dcm, Dcm(s), Dmm(s), Sc	Upper: sharp, may be erosional, planar to convex-up (rarely ground surface); Lower: sharp, may be erosional, concave-up	Incision and deposition in a gravelly glaciofluvial system	(not recorded)
AU7	St, Sr, Sd, Sc, Sm(g) Fd, Fd(g), Fm, Fld; rare Gm(s), Sh, Sld	Upper: planar to undulating, erosional (rarely ground surface); Lower: sharp, wavy to planar, may be erosional	Deposition within a sandy glaciofluvial and deltaic (delta plain or front?) depositional environment	(not recorded)
AU6	Dmm(c), Dmm(s), Sd, Sr, Sm, Sm(g), Sc, Sh, Sl, Fm, Fd, Fl, Fld(g), Gm(s); rare St, Dcm	Upper: planar to undulating (ground surface); Lower: erosional, sharp, planar to angular	A till complex formed by a continuum of subglacial and ice marginal depositional and erosional processes	SUVI (upper)
AU5	Sr, Sd, Sc, Sl, Sm, Sh, Fl, Fm, Fm(g), Fd, Fd(g); rare Dmm(c), Dmm(s), Sd(g), Sm(g), St, Fh, Fl(s), Fl(d), Fl(g), Fm(s)	Upper: erosional, convex-up; Lower: sharp, convex-up	Deposition in a glaciolacustrine and deltaic (delta front to pro-delta?) environment	SUVI (lower)
AU4	Gm, Gm(s), Gm(o), Sm, Sm(g), Sd, Sc, Fm, Fd, Fd(g); rare Gm(c),Sl, St, Dcm(s), Dcm(g), Fld	Upper: planar, sharp; Lower: sharp, erosional, concave-up	Incision and deposition in a gravelly glaciofluvial environment	SUV
AU3	Dmm, Dmm(s), Dmm(c), Dcm, Gm, Gm(s), Gm(c), Sd, Sm, Fm, Fl, Fd, Fd(g); rare Sl, Sm(g)	Upper: sharp, convex-up, conformable?; Lower: erosional to gradational, planar to angular and undulating	A till complex formed by a continuum of subglacial and ice-marginal depositional and erosional processes	SUIV
AU2	Sr, Sh, Sd, Sd(g), Sm, Sm(g), Sh, Sc, Gm(s), Gm(c), Gm(o), Fd, Fl, Fm, Fr; rare St, Sl	Upper: sharp, erosional, irregular?; Lower: erosional, undulating, concave-up?	Deposition within a sandy glaciofluvial depositional environment	SUII and SUIII
AU1	Dcm, Dcm(s), Dcm(c), Dmm, Dmm(s), Dmm(c); rare Gm(s)	Upper: sharp, erosional, undulating; Lower: sharp, planar to angular, undulating	Weathering of the bedrock surface, and reworking and deposition by colluvial and alluvial processes	SUI

The lowermost architectural element of AU1 is composed of clast-supported diamict facies (Dcm) containing boulders (>9 cm diameter) separated by thin beds of red and blue silty clay; Dcm facies are thickest on topographically higher locations on the bedrock surface (Fig. 4.7). The middle architectural element is mainly composed of Dmm facies (Figs. 4.4, 4.12), and directly overlies the lower architectural element (Dcm; commonly separated by a sharp facies contact). Dmm facies also occur in thin layers in bedrock fractures at depth (e.g. MW4_09; Figs. 4.2, 4.7). The upper architectural element is made of sand-rich diamict that is weakly consolidated and contains pebble to boulder sized clasts; Figs. 4.7- 4.10). Blue-coloured silt clasts and yellow sand clasts are common in the diamict matrix material of the upper element, and clasts are more rounded than the other elements. This element is thickest in topographically lower areas on the surface of the underlying elements (Fig. 4.7). Commonly, an oversized boulder (>9 cm diameter) is located at the top of AU1 (MW18_09, 17_09, 8_09; Fig. 4.7) and rare rounded to subrounded gravel clasts of dolomitic, quartzite and serpentine-rich lithologies are present in the upper element of AU1 (MW9_09; Fig. 4.7).

Interpretation

AU1 is interpreted to record accumulation of poorly sorted materials on the fractured and weathered bedrock surface, characteristic of a modern day ‘badland-type’ landscape. It is unlikely that sediments of AU1 have a direct glacial origin due to the paucity of far-travelled lithologies (e.g. granite and gneiss), the absence of bullet-shaped and striated clasts and a strong clast fabric, and the absence of evidence of secondary structures related to glaciotectonic deformation (Evans et al., 2006).

The diamicts of AU1 contain abundant angular and breccia-like shale clasts derived from the Queenston Formation and blanket the underlying bedrock, suggesting that they were primarily derived from the bedrock and probably formed in-situ, with limited reworking on low gradient slopes (Mottershead, 1971; Nadal-Romaro et al., 2007). The carbonaceous clay-rich composition of the Queenston Formation shale (Brogly et al., 1998) makes it highly susceptible to erosion by freeze-thaw, desiccation and swelling, surface runoff, fluvial reworking, and chemical erosion by dissolution (Nadal-Romaro et al., 2007).

Modern badlands contain a cover of weathered rock called regolith that undergoes spatiotemporal evolution as a result of bedrock lithology and various external climatic and slope processes (Nadal-Romaro et al., 2007). The diamict facies of AU1 are interpreted to record different stages of regolith development due to in-situ mechanical and chemical weathering of the bedrock (Nadal-Romaro et al., 2007). The lower diamict architectural element (Dcm facies) is interpreted to record early-stage development of regolith, whereby freeze-thaw processes opened fractures, making the exposed shale susceptible to chemical weathering. The middle architectural element (Dmm facies; Fig. 4.12) is interpreted to record a 'mature' regolith formed by mechanical and chemical weathering of shale clasts. The sand-rich and clast-supported diamict of the uppermost architectural element of AU1 (with rounded and far-travelled gravel clasts) is interpreted to record fluvial reworking of the regolith and incorporation of sand facies and other lithologies by ephemeral gully streams, similar to depositional processes operating in modern badland areas such as on the surface of the Queenston Formation exposed at

Cheltenham, Ontario (15 km north of the study area; Kasanin-Grubin, 2013), the Red Deer badlands (Alberta; Bryan and Campbell, 1980), and badlands in southeast Spain (e.g. Calvo-Cases and Harvey, 1996).

4.4.2 Architectural Unit 2 (AU2): sandy glaciofluvial

AU2 directly overlies AU1 and is separated from it by a sharp, erosional sixth-order bounding surface (Figs. 4.7- 4.9, 4.13). AU2 has an undulating and patchy sheet-like geometry (3 to 18 m thick), and is dominated by sand facies, but also contains fine-grained (silty sand and clay) and rare gravel facies (Fig. 4.7- 4.9). AU2 is absent where it is truncated by AU3 (interpreted here as till; Fig. 4.11) and stratigraphically younger glaciofluvial units in the northern part of the study area (Cedarvale and Limehouse-Lindsay Court; B-B' and D'D'; Fig. 4.2), and is commonly preserved as isolated remnants in bedrock valleys and topographically low areas on the bedrock surface (Figs. 4.7- 4.9).

The internal architecture of AU2 consists of two architectural components (fifth-order surfaces; Fig. 4.12) including a lowermost fining-upwards unit (AU2a) overlain by a coarsening-upwards unit (AU2b; Fig. 4.12). AU2a and AU2b consist of architectural elements (fourth-order surfaces) that have fining-upwards (and rare coarsening-upwards) facies successions superimposed on the component-scale facies succession (the average grain size within individual elements generally becomes finer-grained upwards in AU2a and coarser-grained upwards in AU2b; Figs. 4.7- 4.9, 4.12); however correlation of architectural elements between boreholes, and their lateral continuity and geometry, is uncertain.

AU2a has a sheet-like geometry with an undulating, sharp, and erosional lower bounding surface and a planar upper surface (Figs. 4.7- 4.9). It commonly contains Sd and Sc (very coarse- to medium-grained sands) at the base and fines-upwards to Fl and Fd (silt- to very fine-grained sand) and Sd, Sm, Sr, Sh, Sl (fine- to medium-grained sand; Figs. 4.4, 4.7- 4.9). AU2a is thickest in topographic lows on the surface of AU1 (e.g. MW9_09, 20_06, 26_09; Figs. 4.7- 4.9) and thinnest where it is truncated by the overlying unit AU3 (e.g. MW8_09; Fig. 4.7). AU2a is directly overlain by AU2b (except in MW8_09 and 26_09), which are separated by a planar to angular, sharp or erosional bounding surface (Figs. 4.7, 4.8). Facies composing AU2b coarsen upwards from fine-grained Fl, Sr, Fm, and Fd facies (silty very fine- to fine-grained sand) to Sl, Sh, and Sd (medium- to coarse-grained sands; MW18_09; Fig. 4.7); and from Sd and Sr (medium- to coarse-grained sand) and Sm(g) to Gm(s) facies (medium- to coarse-grained sand, and pebble-sized and rounded gravels; MW17_09, 9_09; Figs. 4.4, 4.7).

Interpretation

AU2 is interpreted to record deposition in a sandy glaciofluvial environment, similar to the modern South Saskatchewan River (Miall, 1977; Cant and Walker, 1978), that likely formed a braid plain occupying topographically low areas on the surface of AU1 and on bedrock (Meyer and Eyles, 2007). Fining- and coarsening-upwards architectural elements within AU2 (Fig. 4.12) are interpreted to record scour and fill of small-scale braid channels, with migrating bars and slackwater (standing water or water in which current flow is negligible) deposits (Cant, 1977; Skelly et al., 2003). The deformed nature of sand and fine-grained facies in AU2 may record saturated conditions and water escape, which likely formed as a result of sediment loading or subaqueous failure of channel margins (Martin and Turner, 1998).

The base of AU2a is interpreted to record scouring and reworking of the upper surface of AU1 by an early channel system that occupied bedrock valleys, and subsequently deposited coarse-grained sand and gravel facies. The fining-upward facies succession of AU2a is interpreted to record a decreased supply of coarse-grained sediment (and lower discharge rates?), likely as a result of a more distal sediment and water source (e.g. retreating ice margin) or lateral migration and abandonment of parts of the fluvial system (Costello and Walker, 1972; Cant, 1977). The planar erosional lower bounding surface of AU2b suggests widespread reworking and reactivation of the upper surface of AU2a. The coarsening-upwards succession of AU2b suggests increasing supply of coarse-grained sand and gravel and higher discharge rates (related to an advancing ice margin?; Costello and Walker, 1972; Miall, 1977).

4.4.3 Architectural Unit 3 (AU3): multi-storey till complex

Architectural unit 3 directly overlies AU2 in the MSMC site (A-A'; Fig. 4.2), and is not recorded at the other sites (Figs. 4.2, 4.7- 4.10). AU3 consists of an assemblage of matrix-supported diamicts interbedded with sand, gravel, and fine-grained facies (Fig. 4.7). AU3 is 10-18 m thick and is demarcated by sixth-order lower and upper bounding surfaces which have irregular and undulating geometries (Figs. 4.7, 4.12). The internal architecture of AU3 is composed of five different architectural components (AU3a-e; Figs. 4.7, 4.12).

AU3a is located at the base of AU3 and contains poorly consolidated Dmm(s) and rare Gm(s) and Sd facies, and outsized boulders (>9 cm diameter) are common at or near the base of the unit (Figs. 4.4, 4.5, 4.7). It has an irregular sheet-like geometry (0.5-5 m thick), and erosional, sharp to irregular upper (fifth-order) and lower (sixth-order) bounding surfaces (Fig. 4.7). This component directly overlies sand and gravel facies of AU2, and is overlain by diamict facies of AU3b and AU3c (Fig. 4.7).

AU3b directly overlies AU3a, separated by a sharp, erosional and planar fifth-order bounding surface. AU3b consists primarily of consolidated Dmm(c) interbedded with sands and a thick (2 m) unit of fine-grained facies (composed of a fining-upward succession of Fl and Fd of silt to silty clay; Figs. 4.4, 4.7) at the base of MW17_09 (in a topographically low area on the surface of AU3a; Fig. 4.7). AU3b has a wedge-shaped 2-dimensional geometry that pinches out toward the northwest (e.g toward MW18_09; Fig. 4.7).

AU3c overlies both AU3a and AU3b, and consists of a complex assemblage of consolidated Dmm(s) interbedded with Dcm, thick (approx. 1 m) gravels, and rare thin beds of fine- to medium-grained sands and silty sands (Fl, Fd, Sd, Sm; Figs. 4.4, 4.5, 4.7). Facies contacts within AU3c are commonly angular (apparently tilted in core) and erosional. AU3c is bounded by fifth-order surfaces that generally parallel the undulating topography of underlying AU3a,b (Fig. 4.7).

AU3d directly overlies AU3c and is composed of consolidated Dmm(c) with interbeds of Fl, Fm, and Fd (silt and clay) and rare Dmm(s) facies (Figs. 4.4, 4.5, 4.7). Outsized boulders (>9 cm diameter) are commonly recorded throughout the body of the unit (Fig. 4.7). AU3d has a tabular 2-dimensional geometry and maintains an approximate thickness of 4 m (except in MW18_09 where it is approx. 7 m; Fig. 4.7).

AU3e is delineated in a single borehole (MW9_09; Fig. 4.7) and consists of poorly consolidated (loose and not compacted) Dmm(s) interbedded with clay-rich diamict and sandy gravel facies. AU3e has a lensoid 2-dimensional geometry with a concave-down upper surface and planar lower surface (Fig. 4.7). Facies contacts within AU3e are commonly erosional and angular (dipping in a similar direction in core; although accurate dip azimuths cannot be determined). Outsized boulders (>9 cm diameter) are common throughout this unit (Fig. 4.7).

Interpretation

AU3 is interpreted to record deposition of a till sheet when ice covered the study area (Meyer and Eyles, 2007). The sand-rich diamict of AU3a is interpreted to record incorporation and mixing of underlying pre-existing sandy sediment into the basal debris zone of an overriding glacier, and may record a glaciotectonized zone (Boulton, 1996; Boyce and Eyles, 2000; Evans et al., 2006; Meriano and Eyles, 2009). AU3b-e are interpreted to record deposition of a subglacial traction till complex that was likely deposited by a continuum of subglacial processes such as deformation and lodgement, settling of fine-grained sediment from suspension (Fl, Fd, Fm) under subglacial lacustrine conditions, and deposition of bedload (sands and gravels) in subglacial fluvial environments and rafting of coarse-grained substrate material (Evans et al., 2006; Meriano and Eyles, 2009; Kessler et al., 2012). The interbedded poorly consolidated (loose) Dmm(s) and Gm(s) facies, and consolidated (compacted) diamict facies and large boulders (Figs. 4.4, 4.7) within AU3e may record ice stagnation and disintegration, which would allow deposition of supraglacial and englacial debris released from the glacier snout (possibly by backwasting or meltout?; Eyles, 1979, Krüger and Kjær, 2000; Kjær and Krüger, 2001), and minor ice margin fluctuations over these sediments would likely deposit interbeds of subglacial traction till (Evans et al., 2006).

4.4.4 Architectural Unit 4 (AU4): gravelly glaciofluvial

AU4 is delineated in the MSMC (A-A'), Princess Anne (C-C'), and Limehouse-Lindsay Court (D-D') sites, where it commonly overlies topographic lows on the bedrock surface (Figs. 4.1D, 4.2, 4.7, 4.8). AU4 is primarily composed of gravels (Gm) with minor sands (Sm, Sl, St, Sc) and fine-grained facies (silt and clay; Fm, Fd; Figs. 4.4, 4.7, 4.8, 4.10). It is 10-15 m thick, and is delineated by a concave-up sixth-order lower bounding surface and a planar upper bounding surface (Figs. 4.7, 4.8, 4.10). In places, the internal architecture of AU4 consists of fining-upward facies packages (architectural elements) including boulders and cobbles at the base to sand and sand-rich gravel facies, and coarsening-upwards packages comprising sand with cobbles and pebbles at the base to cobble and boulder-rich gravels at the top (Figs. 4.7, 4.8, 4.10). AU4 contains relatively thin beds (commonly <1 m thick) of clast-supported gravels that appear to have regular bedding intervals (see the lower part of MW 38_09 and MW4_11, Figs. 4.8, 4.10), rare sandy interbeds, and rare outsized boulders. Gravels located at approximately 232 m a.s.l. (MW4_09, 26_09, 4_11; Figs. 4.7, 4.9) are commonly cemented with calcrete. The coarse-grained nature of AU4 and poor recovery of core in places make delineation of components and fifth-order surfaces difficult; however, it is likely that the fining-upwards and coarsening-upwards packages within AU4 may be separated by a fifth-order surface. This unit almost always rests directly on bedrock or AU1 and has a broad, concave-up geometry (Fig. 4.13).

Interpretation

AU4 is interpreted to record glaciofluvial processes that incised, and in places completely removed, AU1-3 and deposited coarse-grained sand and gravel facies. The stratigraphic position of AU4 directly above (and apparently truncating) till of AU3 (Figs. 4.7, 4.13) suggests sands and gravels of AU4 were deposited during ice retreat from the study area, likely in an outwash valley train. The thickness of AU4, its external geometry, and paucity of major internal erosional surfaces (that can be readily identified in core and correlated between boreholes) suggest gravels were deposited in an outwash system that probably experienced net aggradation (Maizels, 1979). However, degradation may be recorded in MW4_09 and 37_09 where gravels appear to be truncated (Figs. 4.7, 4.9). The internal architecture of AU4 (i.e. components made of coarsening- and fining-upward sand and gravels) is interpreted to record deposition of bars and bedforms at the base of channels (Fig. 4.12; Miall, 1977). The relatively thin beds (commonly <1 m thick) of clast-supported gravel facies, sandy interbeds, and rare outsized boulders suggests flows were commonly of low magnitude (i.e. not dominated by jökulhlaups; Marren et al.,

2009) and gravel beds were deposited as bedload pulses by migrating bedforms (Ashmore, 1991). Floods were likely of relatively low magnitude and probably occurred frequently (depositing boulder beds) during ice marginal retreat; the highest magnitude floods likely deposited beds containing outsized boulders (MW4_09, 38_09; Figs. 4.7, 4.10; Maizels, 1997; Marren, 2005).

4.4.5 Architectural Unit 5 (AU5): glaciolacustrine and deltaic

This unit is recorded in the MSMC (A-A'; Fig. 4.7) and Princess Anne (C-C'; Fig. 4.9) sites, and directly overlies diamict of AU1, till of AU3, and gravel facies of AU4 (Figs. 4.7, 4.9). AU5 consists primarily of packages of fine-grained (clay, silt and very-fine grained sand), sand, and pebbly silty clay facies (Figs. 4.5, 4.7, 4.9), and has a laterally extensive sheet-like geometry (5-30 m thick) that appears to drape and infill topographic lows on the underlying substrate (Figs. 4.3, 4.5, 4.11- 4.12). AU5 has an irregular lower bounding surface that conformably overlies AU3 and AU4, and a gently sloping upper bounding surface (Figs. 4.7, 4.9). The internal architecture of AU5 consists of at least three architectural components (fifth-order surfaces) including two fining-upward facies packages (AU5a, AU5c) and an interbedded fine-grained sheet (AU5b; Figs. 4.7, 4.9, 4.12), which are discussed below.

AU5a consists of a fining-upward succession of Fl and Fd (silty clay and very fine-grained sand with rare gravel clasts) to Fl, Fm, and Fd (silt and clay; Fig. 4.9). This component has sharp and planar bounding surfaces (fifth- and sixth-order) and is recorded in one borehole (MW37_09) where it directly overlies an apparent topographic low on the surface of AU4 (Fig. 4.9). AU5b is composed of interbedded packages of Sr, Sd, and Sm facies, Fm and Fl (silt and clays with rare gravel clasts), and rare Dmm(s) facies (Figs. 4.4, 4.7, 4.9, 4.12). Sand beds in AU5b commonly have loaded contacts with each other, and sharp and erosional bases where they overlie fine-grained facies (silts and clays; Figs. 4.7, 4.9). AU5b thickens from approximately <1-5 m in the southwest (A-A'; Figs. 4.2, 4.7) to 30 m in the northeast (C-C'; Figs. 4.2, 4.9). AU5c is composed of a fining-upward succession of Sr and Sd (fine- to medium- grained sand) at the base to Fm, Fd, and Fl (made of silts, clays, and very-grained grained sand; Figs. 4.4, 4.7). The lower bounding surface of AU5c is erosional, and truncates and completely removes AU5b at MW8_09 (Fig. 4.7).

Interpretation

AU5 is interpreted to record deposition within a glaciolacustrine and deltaic depositional environment (Eyles and Eyles, 1983; Eyles and Clark, 1988). The lowermost component (AU5a) is interpreted to record deposition of silts and clays at the bottom of a glacial lake, and rare gravel clasts within deformed fine-grained facies are interpreted to record rainout of debris from floating ice or run out clasts deposited by mass flows on the lake margins (Eyles and Eyles, 1992). AU5b (interbedded sand and fine-grained facies) is interpreted to record a delta front facies succession (Eyles and Clark, 1988), and its stratigraphic position (above AU5a) suggests progradation of the delta over deeper-water deposits of AU5b. The fining-upward succession of AU5c is interpreted to record a decrease in sandy bedload and deposition of muds (silt and clay) by settling from suspension under 'quiescent' depositional conditions. The erosional lower bounding surface and fining-upward facies succession of AU5c may record (relatively short-lived?) fluctuating water levels (i.e. truncation of the underlying delta front facies of AU5b during a period of lowered water levels, and subsequent ponding or backfilling of the delta plain during higher lake levels). Short-term fluctuations in water levels are common in glaciolacustrine settings, and result from the opening and closing of meltwater outlets, seasonal meltwater fluctuations, and the position of the ice margin (Gustavson and Boothroyd, 1987; Matthews et al, 2000; Blass et al., 2003).

4.4.6 Architectural Unit 6 (AU6): tripartite till complex

AU6 directly overlies AU5 and is demarcated by a planar erosional sixth-order lower bounding surface. The upper surface of AU6 is the ground surface, and is not therefore designated with a hierarchical order. AU6 is delineated only in the south part of the study area (MSMC; A-A'; Figs. 4.2, 4.7) and has a sheet-like geometry. It consists of three components that are made of diamict facies (AU6a), sand and gravel facies (AU6b), and interbedded diamict and sand facies (AU6c; Figs. 4.7, 4.12). Although markedly different facies associations make up AU6b (compared to AU6a,c), it is always delineated in a stratigraphic position between AU6a,c, and which together form a distinct architecture that can be mapped across part of the study area (MSMC; Meyer and Eyles, 2007).

AU6a forms a sheet of consolidated Dmm(c) facies and has an erosional lower bounding surface that is commonly overlain by Fd facies (silty clays; Fig. 4.7). AU6a contains rare, thin (<1 m) interbeds of Dmm(s) facies (MW17_09) and rare boulders in the body of the unit (Fig. 4.7). This component is 4 m thick, except where it is truncated by AU6b and a fifth-order bounding surface (MW18_09; Fig. 4.7). AU6b is 3-4 m thick and consists primarily of sand facies (including Sr, Sd, Sm, Sl, Sh, St; Figs. 4.4, 4.7) and minor amounts of Fl and Fd (silt, clay and very fine-grained sand), and Gm(s) facies (Figs. 4.4, 4.7). AU6c is the uppermost component of AU6 and directly overlies AU6b, separated from it by an erosional planar surface (Figs. 4.7, 4.12). AU6c contains interbedded diamicts and sands (Sd, Sl), and minor fine-grained facies (made of silty clays). Sand and fine-grained facies commonly contain erosional and sharp bases where they overlie diamict facies (Fig. 4.7). Diamict facies in AU6c are consolidated to weakly consolidated ('loose'), and in places contain outsized boulders (>9 cm diameter; Fig. 4.7).

Interpretation

AU6 is interpreted as a till-outwash complex that records ice marginal fluctuations in the study area (Meyer and Eyles, 2007). AU6a is interpreted to record the initial phase of ice advance, which resulted in truncation and incorporation of fine-grained facies of AU5 and deposition of clay-rich subglacial traction till (Dmm(c); Figs. 4.4, 4.7). The till likely formed through a continuum of subglacial processes; however, lodgement appears to be the main subglacial process that deposited AU6a based on its consolidated nature, the presence of boulders, and paucity of deformed coarse-grained interbeds, although subglacial deformation certainly contributed to the formation of the diamict (Evans et al., 2006). AU6b forms a sand sheet that contains well preserved sedimentary structures indicative of traction currents (dunes and ripples) and deposition of suspended load, and is interpreted to have formed in a glaciofluvial depositional environment (Miall, 1977), likely during a minor period of ice marginal retreat from the MSMC area (based on its stratigraphic position between AU6a,c). It is unlikely that this component was deposited in a subglacial depositional setting due to the paucity of diamict facies, absence of outsized clasts, well-sorted nature of sand and fine-grained facies and preserved primary sedimentary structures, and the overall geometry of the unit (which is relatively thick and laterally extensive; Figs. 4.7; 4.12; Meyer and Eyles, 2007). AU6c contains a mélange of clay- and sand-rich diamict, sands, and fine-grained facies (Figs. 4.4, 4.7), and is interpreted to record a minor readvance of the ice margin. The consolidated diamict facies containing boulders at the base of AU6c, and its lower erosional surface (Fig. 4.7), may record advance of the ice margin and truncation of AU6b, and the mélange of diamicts, sands, and muds at the top of AU6c may record deposition in ice marginal channels or debris flows and backwasting of hummocky moraine debris during ice disintegration (Kjær and Krüger, 2001).

4.4.7 Architectural Unit 7 (AU7): sandy (glacio)fluvial to deltaic

AU7 is delineated in the northern part of the study area (B-B’ and C-C’; Figs. 4.2, 4.8, 4.9) and consists of a thick (14-40 m) succession of sands (fine- to coarse-grained sand which is commonly trough cross-bedded), fine-grained facies (made of silty sand to very fine-grained sand), and very rare gravel facies (Figs. 4.8, 4.9). The lower bounding surface of AU7 is highly undulating and may be erosional or conformable with underlying units (Figs. 4.8, 4.9, 4.12); AU7 is truncated by overlying units (AUs 8, 9) and modern streams (Silver Creek; Figs. 4.2, 4.13). AU7 consists of three components composed primarily of Sd and Sr facies (AU7a), Fd facies (made of clayey silt and very fine-grained sand; AU7b), and St and Sr facies (AU7c; Figs. 4.8, 4.9, 4.12).

AU7a is delineated in the Cedarvale area (B-B'; Figs. 4.2, 4.8), and consists of a fining-upwards succession of Sd, Sl, and rare St (fine-grained sands) and rare Fd (silty sands) that commonly form normally-graded beds (Fig. 4.8). Facies contacts are loaded, irregular, and erosional. AU7b is delineated in one borehole (MW25_07; Fig. 4.8) and consists primarily of a crude coarsening-upward succession of interbedded Fd and Sd (made of silty clays and very fine-grained sand with rare pebbles) and Sd facies with loaded or erosional facies contacts (Fig. 4.8). Flame structures, contorted bedding, and convolute lamination are common deformation structures in AU7a and AU7b.

AU7c is the coarsest-grained component of AU7 and is delineated in the Princess Anne area (C-C'; Figs. 4.2, 4.9). It consists of different architectural elements that have coarsening and fining-upward facies successions of Sc, Sd, and Sr and rare Fm and Fd (made of silt and clay) and sand-rich gravel facies (Figs. 4.4, 4.9). Climbing ripples (often orientated in alternating directions; e.g. MW2_11; Fig. 4.9) and trough cross-bedding are common primary sedimentary structures in AU7c (Fig. 4.9). Facies contacts in AU7c are erosional, irregular or loaded, and gradational (indistinct). AU7c has a concave-up lower bounding surface and rests directly on gravels of AU4 and fine-grained facies of AU5 (separated by a fifth-order surface); however, its lateral spatial relationship with sediments of AU5 and AU7a,b, is uncertain. AU7c is inferred to either overlie or grade into AU7a,b based on the nature of facies contacts and their stratigraphic position (elevation; Fig. 4.13).

Interpretation

AU7 is interpreted to record deposition in a sandy braided river to deltaic depositional environment (Miall, 1977; Bhattacharya and Walker, 1992). AU7a and AU7b components are interpreted to record subaqueous deposition of sand and fine-grained facies in a delta plain to delta front depositional setting (Eyles and Clark, 1988; Olariu and Bhattacharya, 2006). Secondary sedimentary structures (e.g. flames, convolute lamination, contorted bedding), loaded facies contacts, and unit thickness recorded in AU7a and AU7b suggest a large sediment supply (and high sedimentation rate?) which allowed a thick accumulation of sand and fine-grained facies. Erosional facies contacts at the base of sand beds suggest reactivation or incision of distributary channels during a pulse of bedload transport (Olariu and Bhattacharya, 2006). AU7c is interpreted to record transport and deposition of sands by traction currents in the form of migrating and superimposed bedforms (dunes and ripples; Reesink and Bridge, 2007), likely in a braided river depositional environment (delta plain?; Miall, 1977; McPherson et al., 1987; Hjellbakk et al., 1999). Alternating ripple foreset direction is interpreted to record changing paleocurrent direction, likely as a result of autogenic processes involved in channel and bedform migration (Miall, 1994). The paucity of till immediately above or below AU7 in the northern part of the study area makes relative dating of this unit difficult.

4.4.8 Architectural Unit 8 (AU8): gravelly glaciofluvial (coarsening-upward)

AU8 is delineated at the MSMC (A-A'), Princess Anne (C-C'), and Limehouse-Lindsay Court (D-D') sites (Figs. 4.2, 4.7, 4.9, 4.10) and comprises the 'upper gravels' of the study area (AU4 composes the 'lower gravels'). AU8 is 3-12 m thick and consists of a coarsening-upward succession of open-work and sand-rich gravel facies and minor Sc, Sr, Sm, and Sd facies (made of very fine-grained to pebbly coarse-gained sand; Figs. 4.7, 4.8, 4.10). The average grain size of AU8 appears to fine from the west (Limehouse-Lindsay Court; D-D') to the east of the study area (MSMC; A-A'; Figs. 4.7, 4.9, 4.10). The lower bounding surface of AU8 is planar and apparently concave-up where it incises underlying (older) units (AUs 4-7; Figs. 4.7, 4.9, 4.10). Its upper bounding surface is planar and AU8 is truncated in places by AU9 and AU10 (Figs. 4.9, 4.10). Gravels of AU8 are commonly cemented with calcrete at 270 m a.s.l. (MW5_11; Fig. 4.10) and 242 m a.s.l. (MW4_09; Fig. 4.7).

Delineation of architectural components within AU8 is difficult due to the coarse-grained nature of the sediments; however, it appears to be composed of fining-upward facies associations (architectural elements; Fig. 4.6) made of open-work pebbles and boulders with sand at the base to sands and sandy gravels at the top (Figs. 4.7, 4.9, 4.10) and a larger-scale (architectural component and unit-scale; Fig. 4.6) coarsening-upward succession. The large-scale coarsening-upward succession is utilized to differentiate gravels of AU8 from gravels of AU4.

Interpretation

AU8 is interpreted to record incision of older AUs and deposition of sands and gravels in a high-energy glaciofluvial outwash system. Downcutting and truncation of underlying AUs likely resulted from lowered base level (probably during retreat of the ice margin; AU6). The small-scale fining-upward facies associations are interpreted to record the migration of gravelly bedforms, and the large-scale coarsening-upward succession of AU8 is interpreted to record increased supply of cobbles and boulders and meltwater discharge to the outwash system (and may record aggradation of sediment during a minor re-advance of the ice margin; Maizels, 1979).

4.4.9. Architectural Unit 9 (AU9): shale-rich gravel and diamict

AU9 forms the uppermost subsurface unit at the Princess Anne site (C-C'; Figs. 4.2, 4.9) and overlies AU1 in Limehouse-Lindsay Court (MW25_09; D-D'; Figs. 2, 10). AU9 consists of clast-supported diamicts (sand- and clay-rich) interbedded with massive gravels, sands, and rare laminated and deformed silts and clays and matrix-supported massive diamicts (Figs. 4.4, 4.9, 4.10). Gravel beds commonly have erosional contacts with underlying diamicts. Facies in AU9 have a distinct reddish colour as a result of the abundant angular shale clasts of the Queenston Formation that commonly weather to clay. The reddish coloured diamict and gravels of AU9 are exposed in stream valleys in the Georgetown area (Karrow, 2005) and cross-bedded gravel facies and imbricated cobbles can be observed in streamcut sections along the northern part of Silver Creek (approximately 1 km north of MW21_06; Fig. 4.2). AU9 also contains abundant subrounded to well rounded gravel clasts of far-travelled lithologies typical of the

Canadian Shield (e.g. granite and gneiss). The lower bounding surface (sixth-order) of AU9 directly overlies AU7 and AU8, and is planar to undulating and erosional (Fig. 4.9). The upper bounding surface is irregular and demarcates the modern ground surface. AU9 has a sheet-like geometry that is 3-13 m thick, and the lateral spatial relationship of AU9 with AU1 and AU8 (D-D') suggest that AU9 has a concave-up geometry (Fig. 4.10).

Interpretation

Facies contacts and small-scale changes in facies types are not easy to identify in AU9 due to the abundance of highly weathered shale clasts, making paleoenvironmental reconstruction difficult. Interbedding of diamict and gravel facies (which can be clearly seen in MW21_06 and MW25_09; Figs. 4.9, 4.10) may record deposition in a fluvial or glaciofluvial outwash system that was supplied with an abundance of Queenston Formation shale (similar to the red gravels of Costello and Walker, 1972). The distinct reddish colour of AU9, the abundance of shale clasts of the Queenston Formation, and its coarse-grained nature suggest that AU9 was supplied with sediment from a source area adjacent to an exposed outcrop of Queenston Formation shale or from previously deposited sediment rich in Queenston shale (older tills?; Karrow, 2005).

4.4.10 Architectural Unit 10 (AU10): colluvial-alluvial complex

AU10 is delineated on the Escarpment slope in the Limehouse-Lindsay Court subsite (D-D'; Figs. 4.1D, 4.2, 4.10). AU10 is identified in boreholes that penetrate the top of the Escarpment (MW24_09, 10_10), the margin of a topographically high point (Limehouse outlier) on the bedrock surface in the Acton re-entrant (MW1_11; the uppermost lithology of the bedrock outlier is dolostone of the Amabel Formation; Karrow, 2005), and the base of the Escarpment slope (MW25_09, 38_09, 5_11; Figs. 4.1D, 4.2). The lower bounding surface of AU10 is highly undulating on the upper Escarpment slope (MW24_09 to 1_11), planar near the base of the Escarpment (MW25_09 to 5_11), and erosional where gravels overlie finer-grained sediments (of AU1 and AU9; MW1_11 and MW25_09; Fig. 4.10).

AU10 contains a diverse assemblage of facies types, including gravels (sand-rich and open-work gravels, and outsized boulders), diamicts (clay- and sand-rich matrix supported diamict and clast-supported diamict facies), sands (including Sc, Sh, Sd and Sm), and muds (Fm and Fd with rare gravel clasts and convolute laminations; Figs. 4.4, 4.10, 4.12). Facies contacts in AU10 are commonly conformable (non-erosional); however the coarse-grained texture of gravels makes delineation of the nature of facies contacts in core uncertain. Gravel clasts contained within AU10 are commonly subangular to very angular (rarely subrounded), of local and far-travelled lithologies, and contain large boulders of dolostone and sandstone. Clast-supported diamict facies are common in MW25_09 (at the base of the Escarpment) and rare matrix-supported massive diamict is recorded in MW1_11 (on the margin of the Limehouse bedrock outlier). Fine-grained facies in AU10 are very rare, and comprise deformed (contorted beds) of silt and clay that contain dipping beds of cobbles (with erosional bases; MW10_10; Fig. 4.10) and convolute lamination.

Facies in AU10 have complex spatial relationships, which makes characterization of the internal sedimentary architecture difficult. The facies succession in AU10 appears to become finer-grained with distance from the Escarpment (MW24_09 to MW5_11), and large boulders (> 1 m in diameter) are recorded only on the Escarpment and in close proximity to the Limehouse bedrock outlier (MW1_11; Fig. 4.6). The coarsest-grained deposits of AU10 are located adjacent to the bedrock outlier (MW10_10) and at the base of the Escarpment (MW25_09). AU10 shows a crude coarsening-upward facies succession at lower elevations on the Escarpment slope (MW25_09 to 5_11; Figs. 4.2, 4.10) passing from sands, silt and clay (and rare gravels) at the base to boulders and sandy gravels at the top of the unit (Fig. 4.10). Near the top of the Escarpment (MW24_09 to 1_11), AU10 contains interbedded sands, silty clays, sandy and open-work gravels and large, outsized boulders (Fig. 4.10).

Interpretation

AU10 is interpreted to record deposition by colluvial and alluvial processes operating on and adjacent to the Niagara Escarpment, and localized deposition of fine-grained facies in a ponded (slackwater) environment, possibly in a similar depositional setting to a colluvial or alluvial fan (Blair and McPherson, 1994; Blikra and Nemec, 1998; Nemec and Kazanci, 1999). The high degree of heterogeneity within AU10 suggests dynamic depositional conditions, and facies changes along D-D' suggest rapid downslope spatiotemporal changes in the magnitude of energy levels of depositional processes. Large outsized boulders (MW10_10, 1_11, 24_09; Fig. 4.10) are interpreted to record transport and deposition by rockfall; clast-supported diamict facies containing angular and subrounded clasts are interpreted to record mass wasting and remobilization of previously deposited sediments (possibly till and glaciofluvial sediments? Fig. 4.1) from locations higher upslope or on valley walls (Blair and McPherson, 1994). Thick successions of gravel facies (Gm) containing angular to subrounded clasts of local and far-travelled lithologies (MW24_09, 25_09; Fig. 4.10) are interpreted to record deposition in a high-energy alluvial (glaciofluvial?) system that likely reworked colluvial debris, and transported far-travelled lithologies from source areas elsewhere on the Escarpment (Fig. 4.1). Units with a similar architecture to AU3 and AU6 (interpreted as till) are not apparent here (Figs. 4.7, 4.10, 4.12).

4.4.11 Architectural Unit 11 (AU11): fluvial to slackwater (fining-upward channel fill)

AU11 is delineated in boreholes that are located in an underfit valley in the Cedarvale area (B-B'; Figs. 4.2 4.-8), which is occupied by Black Creek (flowing from the west, in the Acton Re-entrant) and Silver Creek (flowing from the north, in the area of MW5_11; Figs. 4.1, 4.2). The stream valley in the Cedarvale area has a well-defined U-shaped surface topography and its margins are terraced in places (CVC, 2001). AU11 comprises a fining-upward succession of architectural components (AU11a-c) including gravel (boulder and cobble) at the base (AU11a), sands and gravels, and fine-grained facies (AU11b), and predominantly silts, clays, and sands (AU11c) at the top (Figs. 4.8, 4.12). The three components of AU11 each have an internal fining-upward facies succession and are separated from each other by sharp to erosional fifth-order bounding surfaces (Figs. 4.8, 4.12). The average grain size of facies within AU11 becomes finer towards the southeast (MW3_09; Fig. 4.8). The lower bounding surface of AU11 is irregular, and the upper bounding surface is at the present day ground surface and dissected by modern stream systems (Black Creek and Silver Creek; Figs. 4.1, 4.2). AU11 is located in the Georgetown-Huttonville bedrock valley (Fig. 4.1D).

AU11a is the coarsest-grained component of AU11, and consists of open-work and sandy gravels (cobbles and boulders), and deformed and massive gravelly sands that rest directly on bedrock or lenses of AU1 (Fig. 4.8). Gravel clasts within AU11a are subangular to well-rounded and of local and far-travelled lithologies. Primary sedimentary structure is not recorded in this component, and lateral correlation of gravel beds is uncertain (a thick section of MW6_10 was not recovered in core; Fig. 4.8). AU11b has a concave-up lower bounding surface which is overlain by Sm, Sr, Sc, and Sd facies and massive sandy gravel facies, and fines-upwards to Fl, Fd, and Fm(g) (composed mostly of silts and clays) and minor Sd and Sm facies (Figs. 4.4, 4.8). AU11b also contains thin interbeds of massive sandy gravels (MW3_09) that commonly have erosional bases (Fig. 4.8). AU11c is the uppermost (youngest) component of AU11, and consists of an erosional lower bounding surface overlain by thin beds (<1 m) of Sm(g) and Gm(s), which either fine-upwards or abruptly change to muds and very-fine grained sand (Fd, Fl, and Fm; Fig. 4.8).

Interpretation

AU11 is interpreted to record incision of older units and deposition of channel fill deposits in a fluvial depositional environment (Miall, 1977; Germanoski and Schumm, 1993). The gravel facies within AU11 are similar to those recorded in AU4 and AU8, and the processes responsible for their deposition may have been very similar. However, the architecture (components and pattern of the vertical succession of facies) of the older AUs is not apparent in AU11 (Fig. 4.12). AU11a is located at a much lower topographic elevation than either AU4 or AU8 (Fig. 4.11) and its lateral spatial relationship with older AUs suggests that the fluvial system responsible for the deposition of AU11 downcut and removed these older units (Fig. 4.7- 4.10, 4.13).

The coarse-grained texture of gravel facies in AU11a suggest deposition in a high energy, competent fluvial system that was supplied with abundant cobbles and boulders. Gravels were likely transported as rolling bedload sheets or low relief bars during flood events, and sand probably infiltrated the interstices of gravels during periods of low energy discharge (Miall, 1977; Maizels, 1993). AU11b is interpreted to record decreased discharge and winnowing of the upper surface of AU11a, and deposition of fine-grained facies in slackwater areas of abandoned channels (Miall, 1992). Interbeds of massive sandy gravel facies in AU11b may record lateral migration of channels and reactivation of the fluvial plain (Miall, 1977). The fining-upward facies succession of AU11b (Figs. 4.8, 4.12) suggests abandonment of the fluvial system and deposition of fine-grained facies from suspension in a ponded or slackwater depositional environment (Miall, 1977, 1992). Diamict interbeds, rare pebbles and cobbles, and laminated fine-grained facies with erosional facies contacts are interpreted to record debris flow deposits (Eyles et al., 1983; Miall, 1992), which likely originated from mass wasting of sediments from the river valley slopes. AU11c is interpreted to record truncation of the upper surface of AU11b and reactivation of the fluvial systemm, probably as a result of lateral migration

Fig. 4.12. Sedimentary architecture of architectural units (AUs) delineated in this study. AUs include weathered bedrock and regolith (AU1), sandy glaciofluvial (AU2), till complexes (AU3, AU6), gravelly glaciofluvial (AU4, AU8), glaciolacustrine, glaciofluvial, and deltaic units (AU5, AU7), shale-rich diamict and gravels (AU9), colluvial-alluvial (AU10), and fluvial to slackwater (AU11). Refer to Fig. 4.4 for facies codes, descriptions, and interpretations, Figs. 4.7-4.10 for AUs delineated in boreholes, and Fig. 4.11 for a summary and interpretation of AUs.

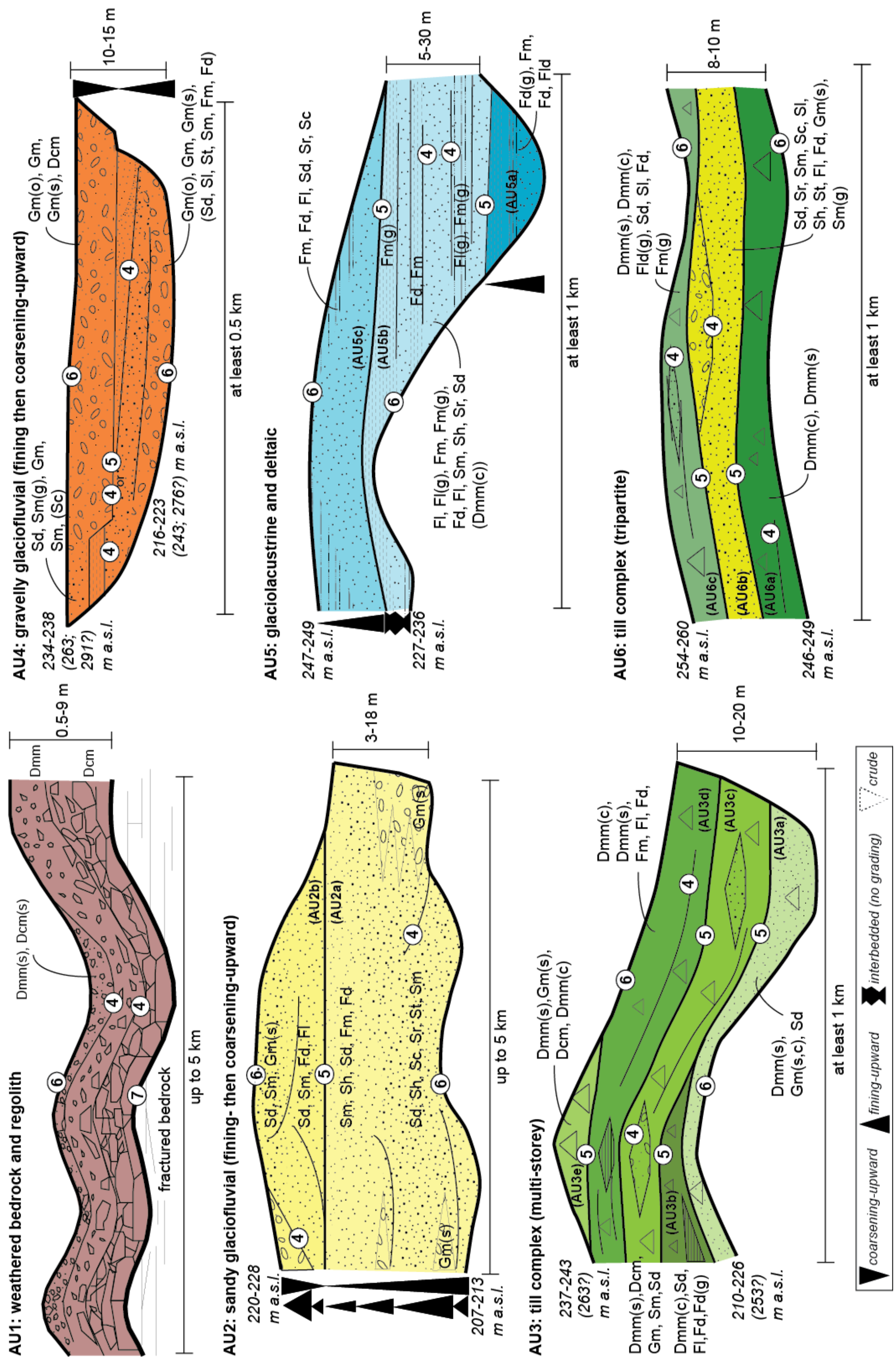
AU1: weathered bedrock and regolith
Dmm(s), Dcm(s)
fractured bedrock
up to 5 km
0.5-9 m
AU2: sandy glaciofluvial (fining- then coarsening-upward)
220-228 m a.s.l.
207-213 m a.s.l.
up to 5 km
3-18 m
AU3: till complex (multi-storey)
237-243 (263?) m a.s.l.
210-226 (253?) m a.s.l.
at least 1 km
10-20 m
AU4: gravelly glaciofluvial (fining then coarsening-upward)
234-238 (263; 291?) m a.s.l.
216-223 (243; 276?) m a.s.l.
at least 0.5 km
10-15 m
AU5: glaciolacustrine and deltaic
247-249 m a.s.l.
227-236 m a.s.l.
at least 1 km
5-30 m
AU6: till complex (tripartite)
254-260 m a.s.l.
246-249 m a.s.l.
at least 1 km
8-10 m
coarsening-upward
fining-upward
interbedded (no grading)
crude

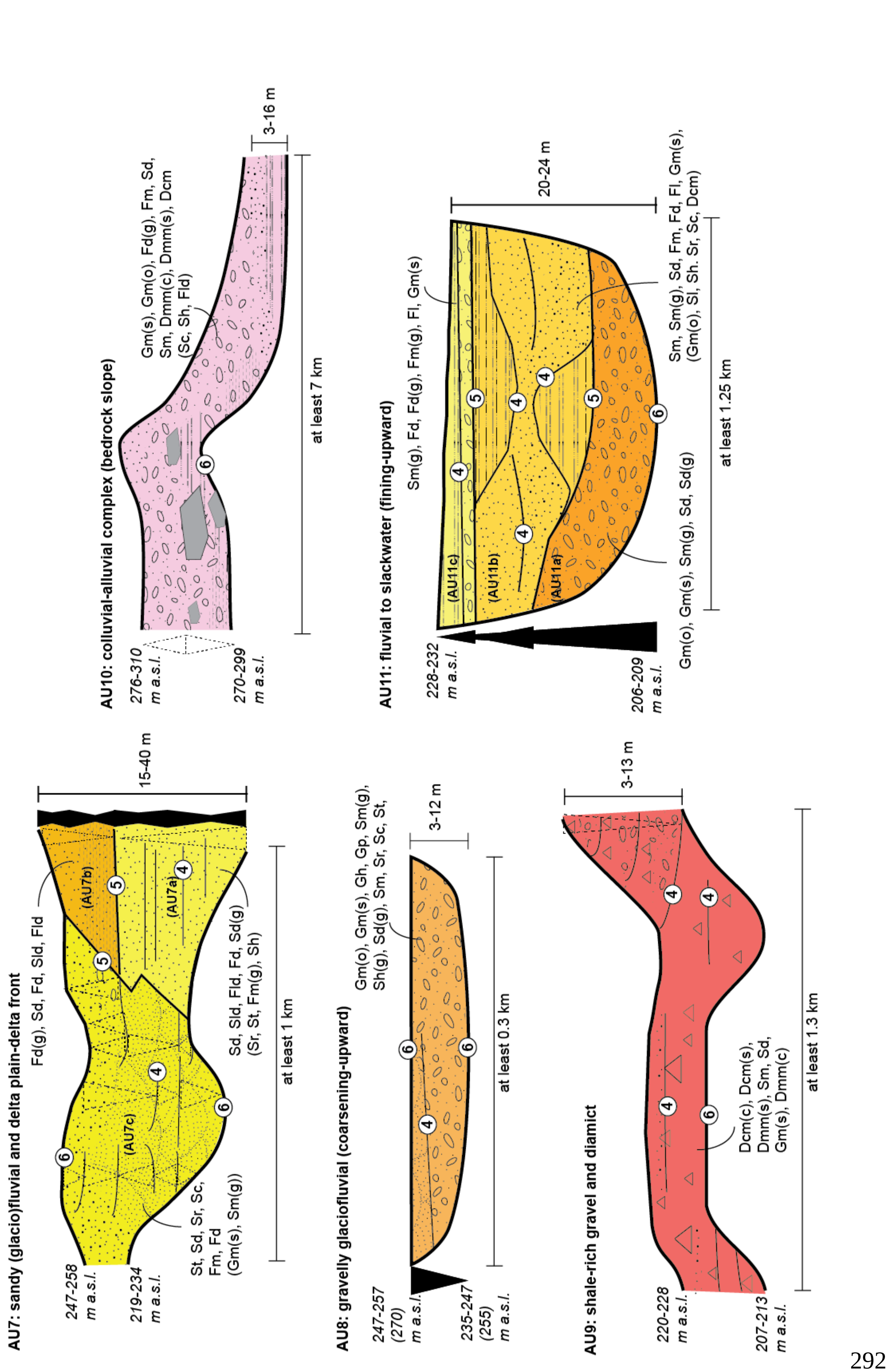
AU7: sandy (glacio)fluvial and delta plain-delta front
247-258 m a.s.l.
219-234 m a.s.l.
15-40 m
at least 1 km
Fd(g), Sd, Fd, Sld, Fld
Sd, Sld, Fld, Fd, Sd(g) (Sr, St, Fm(g), Sh)
St, Sd, Sr, Sc, Fm, Fd (Gm(s), Sm(g))
(AU7a)
(AU7b)
(AU7c)
AU8: gravelly glaciofluvial (coarsening-upward)
247-257 (270) m a.s.l.
235-247 (255) m a.s.l.
3-12 m
at least 0.3 km
Gm(o), Gm(s), Gh, Gp, Sm(g), Sh(g), Sd(g), Sm, Sr, Sc, St,
AU9: shale-rich gravel and diamict
220-228 m a.s.l.
207-213 m a.s.l.
3-13 m
at least 1.3 km
Dcm(c), Dcm(s), Dmm(s), Sm, Sd, Gm(s), Dmm(c)
AU10: colluvial-alluvial complex (bedrock slope)
276-310 m a.s.l.
270-299 m a.s.l.
3-16 m
at least 7 km
Gm(s), Gm(o), Fd(g), Fm, Sd, Sm, Dmm(c), Dmm(s), Dcm (Sc, Sh, Fld)
AU11: fluvial to slackwater (fining-upward)
228-232 m a.s.l.
206-209 m a.s.l.
20-24 m
at least 1.25 km
Sm(g), Fd, Fd(g), Fm(g), Fl, Gm(s)
Sm, Sm(g), Sd, Fm, Fd, Fl, Gm(s), (Gm(o), Sl, Sh, Sr, Sc, Dcm)
Gm(o), Gm(s), Sm(g), Sd, Sd(g)
(AU11a)
(AU11b)
(AU11c)

of the channel (and may be related to the modern Black and Silver Creeks?; Figs. 4.1, 4.2).

4.5 DISCUSSION

The dynamic nature of glacial depositional environments results in complex spatial relationships between sedimentary units. Understanding of the sedimentary heterogeneity and geometry of coarse-grained glacial units is imperative for determining past depositional histories of outwash systems, and for reservoir characterization, source water protection, and groundwater sustainability applications. AEA was developed for the analysis of sediments exposed in outcrop, and only recently has been applied to the analysis of buried subsurface sediments (assisted by outcrop, geophysical, and hydrogeological data; e.g. Boyce and Eyles, 2000; Gerber et al., 2001; Skelly et al., 2003). This study demonstrates the applicability of AEA to the analysis of sediments recovered from fully cored boreholes (in the absence of other data types) for the delineation of glacial sedimentary architecture at local (architectural elements) to regional (architectural units) scales (Davis et al., 1993). The main limitation of applying AEA to core data is the inability to visually delineate the sedimentary geometry of units based on physical observation of sediments in 2- and 3-dimensional space, which is readily apparent on outcrop sections (e.g. Slomka and Eyles, 2013). This introduces uncertainty to the correlation of units between boreholes (and their 2- and 3-dimensional geometry; Miall, 2014). Deconstructing the architecture of subsurface sediments from core is inherently tainted with uncertainty (Miall, 2014) and several plausible architectural models of the Georgetown area, based on the data available for this study (Figs. 4.7-4.10), may be constructed. Undoubtedly, integration of additional data (e.g. fully-cored boreholes and wireline logs, landform analysis, surface geophysics, and hydrogeological data; Davis et al., 1993; Boyce and Eyles, 2000; Gerber et al., 2001; Skelly et al., 2003; Hansen et al., 2009) and computer-based modeling (e.g. simulations of facies geometries; Bridge and Tye, 2000; Deutsch and Tran, 2002) in future studies would likely refine and enhance this subsurface architectural model.

The methods applied in this study, including the detailed recording of facies characteristics, the vertical succession of facies types, and nature of facies contacts (Figs. 4.7- 4.10), 'pattern recognition' of vertical facies successions (Walker, 1992), and the utilization of bounding surface and unit hierarchies (Fig. 4.6), facilitated characterization of the sedimentary architecture of the Georgetown area from large-scale units (architectural units) to small-scale facies associations (architectural elements; Figs. 4.6, 4.12). The sedimentary architecture (including facies, the vertical succession of facies, and bounding surfaces) of these unit hierarchies served as the basis for correlation between boreholes and provided a tool for detailed paleoenvironmental reconstruction and interpretation of depositional histories. The architectural model presented here demonstrates the complex spatial relationships that exist within subsurface glacial stratigraphies, particularly in areas affected by multiple incision events caused by downcutting glaciofluvial channel systems. These incision events add to the uncertainties of unit correlation as they often remove older deposits including till sheets that may be utilized as 'marker beds' for relative dating purposes (e.g. Fig. 4.13)

4.5.1 Depositional history

Georgetown is located at the base of the Niagara Escarpment and is underlain by at least three bedrock valleys buried by variable thicknesses of Quaternary sediment (Fig. 4.1D). The complex topography of the bedrock surface suggests the timing of bedrock valley formation was likely punctuated and time-transgressive (Straw, 1968). The architectural units characterized here, which overlie the irregular bedrock surface (a regional unconformity), are interpreted to record several Late Quaternary events (Fig. 4.3, 4.11).

The stratigraphic position of AU1 suggests it likely formed prior to the Late Wisconsin (>25C ka yrs BP; Fig. 4.3). The architecture of AU1, and its spatial relationship to the Escarpment, suggest AU1 may record deposition in an alluvial or colluvial fan depositional environment emanating from the Niagara Escarpment (Nemec and Kazanci, 1999). The cool moist climate during the Middle Wisconsin (Barnett, 1992) would have provided abundant moisture to facilitate the development of ground ice and conditions suitable for weathering of the bedrock surface and badland development; ephemeral stream systems likely drained surface water down the Escarpment slope and eroded far-travelled clasts from previously deposited sediment (Fig. 4.3). AU1 is equivalent to SUI of Meyer and Eyles (2007), and may be similar to the red gravels of Costello and Walker (1972).

AU2 appears to occupy a north-south trending bedrock valley (currently occupied by a section of Silver Creek; Figs. 4.1D, 4.2, 4.13) and is delineated in a relatively narrow zone extending from the MSMC area (A-A') to the boundary between the east Princess

Anne (C-C') and northwest Cedarvale (B-B') areas (MW26_09, 20_06; Fig. 4.13). AU2 is most continuous in the southern part of the study area (A-A'; Figs. 4.2, 4.13) and has previously been mapped as far south as Milton (approximately 15 km south of Georgetown; SUII and SUIII of Meyer and Eyles, 2007). The fluvial system of AU2 probably records advance of the Laurentide Ice Sheet (LIS) during the Middle Wisconsin (Fig. 4.3; Maizels, 1979; Dredge and Thorleifson, 1987; Barnett, 1992). The LIS would have provided a considerable amount of meltwater and coarse-grained debris at this time, which was likely transported in bedrock-hosted spillway systems along the top and base of the Escarpment (Costello and Walker, 1972; Eynon and Walker, 1974; Chapman and Putnam, 1984; Karrow, 2005). AU2 may be stratigraphically equivalent to the Thorncliffe Formation (>25C ka yrs BP; Fig. 4.3), which is a sand-rich deltaic unit well exposed at the Scarborough Bluffs in Toronto, and identified below the Oak Ridges Moraine (Fig. 4.1; Miall, 1985; Eyles and Clark, 1988; Russell et al., 2003; Meyer and Eyles, 2007). The absence of till in MW26_09 and MW20_06 (Figs. 4.7, 4.8) makes relative dating and correlation of AU2 at the borehole locations uncertain; however the vertical facies succession of AU2 delineated in MW20_06 (Fig. 4.8) is similar to that of SUII of Meyer and Eyles (2007) identified in a borehole near MW4_09 (Figs. 4.2, 4.8).

AU3 is a till unit interpreted to be equivalent to the Newmarket Till, which records advance of the LIS from the north into the study area during the Port Bruce Stadial (c. 14C ka yrs BP; Fig. 4.3; Barnett, 1992; Boyce and Eyles, 2000; Karrow, 2005; Meyer and Eyles, 2007). AU3 is interpreted here to be equivalent to SU IV identified by Meyer and Eyles (2007). The variable matrix textures of diamict facies (AU3a-e: Figs.

4.7, 4.12) are interpreted to reflect incorporation of materials from the substrate over which the ice advanced, whereby sandy diamict matrix records overriding and incorporation of proglacial outwash sediment (AU3a,c,e) and finer-grained diamict matrix records incorporation of glaciolacustrine sediment in the subglacial traction zone (AU3b,d; Evans et al., 2006). The irregular upper surface of AU3 may represent a buried drumlinized surface similar to that identified on the buried surface of the Northern (Newmarket) Till by Boyce and Eyles (2000) in the Pickering area (east of Toronto), or hummocky moraine which is common at modern ice margins (Kjær and Krüger, 2001). It is worth noting that Boyce and Eyles (2000) also delineated five diamict units within the Northern Till; however, regional correlation of these diamict components is uncertain and requires additional detailed work.

The concave-up geometry of the lower bounding surface and the broad lateral extent of AU4 suggests the formation of a broad outwash channel system that drained meltwater down the Escarpment slope (Fig. 4.13), probably after the LIS retreated from the Paris and Galt Moraines (Figs. 4.1, 4.3) during the early Mackinaw Interstadial (c. 13.4C ka yrs BP; Barnett, 1992; Meyer and Eyles, 2007). AU4 is delineated in the northern part of the MSMC site (A-A’), Princess Anne (C-C’), and northern part of the Limehouse-Lindsay Court site (D-D’; Fig. 4.13), and appears to occupy a bedrock trough that trends from the Georgetown-Acton bedrock valley into the Georgetown-Huttonville bedrock valley (Figs. 4.1D, 4.2, 4.13). AU4 appears to be located in a similar geographic position and to have a similar orientation as the modern Silver Creek (and part of Black Creek), and the glaciofluvial system in which it was deposited likely drained meltwater through the Acton re-entrant (Figs. 4.1D, 4.2, 4.13) east toward the area now occupied by the Credit River (Figs. 4.1D, 4.2). However, the direction of meltwater flow is uncertain in the absence of any paleocurrent indicators. The fining-upward and coarsening-upward components of AU4 are interpreted to record allogenic processes such as changes in the supply of coarse-grained sediment and meltwater discharge as well as autogenic processes such as lateral migration channels and bedforms (Beerbower, 1964; Eynon and Walker, 1974; Maizels, 1979; Miall, 2010). AU4 is most likely equivalent to SUV of Meyer and Eyles (2007) and may be equivalent to EAs1-3 of Slomka and Eyles (2013) delineated at Limehouse (Fig. 4.2).

AU5 is interpreted to record a sandy delta front and glaciolacustrine depositional environment, supplied with rainout debris from floating ice. Its stratigraphic position below the till of AU6 suggests AU5 formed prior to advance of the Halton ice, and likely formed during the late Mackinaw to early Port Bruce Stadial (c. 13C ka yrs BP; Fig. 4.3; Barnett, 1992). AU5 likely represents deposits of the early or paleo-'Peel Ponds', which include ephemeral lakes ponded at the margin of the Ontario lobe (Fig. 4.3; Barnett, 1992). An advancing ice margin out of the Ontario basin (from the southeast) would likely block outlets (the AU4 channel system?) and dam meltwater at the base of the Escarpment, possibly in the Acton re-entrant (Figs. 4.1, 4.3; Costello and Walker, 1972; Barnett, 1992; Karrow, 2005; Slomka and Eyles, 2013). The architecture of AU5 (AU5a-c; Fig. 4.12) suggests fluctuating water levels and dynamic depositional conditions within the paleolake, which is common in modern glaciolacustrine settings, and likely reflects fluctuating ice margin positions during overall ice advance (Gustavson and Boothroyd, 1987; Matthews et al., 2000; Blass et al., 2003). The finest-grained component (AU5a) is located in a topographic low on the surface of AU4 in the Georgetown-Huttonville bedrock valley (Figs. 4.1D, 4.13), which suggests ponding of meltwater was concentrated (and deepest?) in the bedrock valley. The precise location of meltwater and sediment input points is uncertain, but likely sources include the ice margin to the southeast, meltwater channels from the Escarpment to the west, and the area occupied by the ORM to the north (Figs. 4.1, 4.3). AU5 is probably equivalent to the lower sediments of SUVI of Meyer and Eyles (2007) and EA4 of Slomka and Eyles (2013) recorded in the Limehouse area (Fig. 4.2).

AU6 is probably equivalent to the Halton Till (and the upper part of SUVI of Meyer and Eyles, 2007), which has been mapped throughout the western part of the Ontario basin in southern Ontario (Fig. 4.1; Barnett, 1992; Karrow, 2005), and records advance of ice over the study area during the Port Huron Stadial (c. 13C ka yrs BP; Fig. 4.3; Barnett, 1992). The internal architecture of AU6 (Figs. 4.7, 4.12) suggests the Halton ice margin (AU6a) fluctuated in its position, allowing deposition of a sheet of sands (AU6b); however the extent of retreat of the ice margin is uncertain. Diamicts and outwash of AU6c are interpreted to record a second minor advance of the ice margin over the MSMC area. The Halton Till forms a thin cover of drift that directly overlies bedrock on the Escarpment slope (Fig. 4.1A,B), and may represent only the first advance phase of Halton ice (AU6a).

AU7 forms a wedge-shaped unit in the Cedarvale (B-B') site (Figs. 4.2, 4.13) and the geometry and spatial relationship of its architectural components (AU7a-c; Fig. 4.11) suggests a thick accumulation of deltaic sands was deposited in a lake basin in the northern part of the valley (MW23_07, 20_06, 25_07; Fig. 4.8). This lake was probably formed as a result of blocking of the ‘paleo-Credit River’ and other outlets by the Ontario ice lobe. Sand was probably supplied from a sandy braided river-delta plain depositional system (Figs. 4.2, 4.8, 4.13) that served as a sediment source in the Princess Anne area (AU7c). The stratigraphic position and elevation of AU7c (C-C’) and the sandy component of the Halton Till (AU6b; A-A’; Figs. 4.7, 4.12, 4.13) suggests these sandy architectural components may be time-equivalent, and that sediments of AU6b may have supplied outwash sediment to the sandy delta of AU7. Thick successions of sand-rich deposits are located at a similar stratigraphic position as AU7 in the Glen Williams area (2 km north of Georgetown; Karrow, 2005) and further work is needed to determine the stratigraphic and genetic relationship between these various sand bodies.

Ice marginal retreat from the study area is recorded by gravels of AU8, which truncate sands of AU7 (C-C’) and overlie gravels of AU4 in the northern part of MSMC (A-A’) and Limehouse-Lindsay Court (D-D’; Figs. 4.2, 4.12, 4.13). Retreat of the Ontario lobe to the east would open outlets and drain lakes ponded at the base of the Escarpment (in which AU7 was deposited; Karrow, 2005). AU8 is interpreted to record deposition in a proglacial outwash channel that transported gravels down the Escarpment from the northwestern part of the study area (MW5_11) toward the southeast (A-A’; Fig. 4.13). The absence of Halton Till (AU6) overlying AU8 suggests it was deposited during deglaciation of the study area, probably during the mid to late Port Huron Stadial (c. 12.5C ka yrs BP?; Barnett, 1992). Shale-rich diamicts and gravels of AU9 (which directly overlie AU8 at C-C'; Figs. 4.2, 4.13), may record deposition of sediment from a source area in which shales of Queenston Formation are exposed. Queenston Formation shale is exposed at surface in Terra Cotta (10 km north of Georgetown) and in a section of the Credit River valley in the northern part of Georgetown (adjacent to 26_07; Fig. 4.1D; Karrow, 2005). It is possible that AU9 may be equivalent to EA6 of Slomka and Eyles (2013), which also contains abundant weathered Queenston shale. An alternate interpretation is that AU9 may be a lateral facies variation of AU6a or AU6c, and records advance of the Halton ice margin; however, the architecture of AU9 and AU6 are substantially different which suggests they are not equivalent.

AU10 overlies AU4, AU8, and AU9 (Fig. 4.13), and is interpreted to have formed after the Mackinaw Interstadial and possibly after Halton ice had retreated from the study area (c. <12C ka yrs BP?; Barnett, 1992). The absence of Halton Till (AU6) in D-D' suggests that it was removed by fluvial erosional processes on the Escarpment slope. However, previously mapped surficial Quaternary sediments in this area (Figs. 4.1A, B) record Halton Till at surface; clearly, further investigation of subsurface sediments in the Acton re-entrant and on the Escarpment slope is needed to better understand the spatial relationship, relative age, and depositional history of sediments of AU10, and their relationship to the Halton Till. The heterogeneous facies assemblage of AU10 probably records mass wasting of exposed bedrock slopes on the Escarpment and deposition of sands and gravels in high energy outwash streams that likely drained meltwater from the LIS (located to the north of the study area) into the Acton re-entrant (Fig. 4.1D).

The subsurface sedimentary architecture of the southern part of the Cedarvale valley (B-B'; Fig. 4.13) is recorded in four boreholes (Fig. 4.8) located at the confluence of Silver and Black Creeks, and in an underfit U-shaped stream valley (Fig. 4.13; CVC, 2001, 2009). The boreholes are located in the western part of the Georgetown-Huttonville bedrock valley (Fig. 4.1D) and the absence of till (AU3 and AU6) and other older AUs at these borehole locations suggests that AU11 was deposited after ice retreated from the Georgetown area (c. 12C ka yrs BP; Fig. 4.7). The lower bounding surface of AU11 is interpreted to record incision of older units and entrenchment of a fluvial system, probably as a result of lowered base levels caused by ice margin retreat (enhanced by isostatic rebound?; Bryan et al., 1987). The oldest architectural component of AU11 (AU11a) is interpreted here to record aggradation of cobble and boulder bedload which was likely supplied from areas draining the retreating Simcoe lobe in the north (Fig. 4.3). Younger architectural components (AU11b and AU11c) likely record progressive retreat of the ice margin (resulting in decreased supply of coarse-grained sediment and discharge) and transition to a slackwater depositional setting, in which silts, clays and fine-grained sands (upper part of AU11b, c) were deposited. Lateral migration of the river system (the 'paleo' Black and Silver Creeks) and flood events in the Cedarvale valley likely resulted in minor scour of older sediments and deposition of thin gravel beds (AU11b,c; Fig. 4.8). Damming of Silver Creek (in the area of 8th Line and 15 Side Road; Fig. 4.2) in the early nineteenth century ponded water in the Cedarvale valley (called 'Wilbur Lake'; CVC, 2001) and may have allowed deposition of fine-grained material in the upper part of AU11b; subsequent draining of the dam in the early twentieth century

Fig. 4.13. Conceptual fence-diagram of the ‘nested’ subsurface sedimentary architecture of the Georgetown area, based on sedimentary logs recorded from boreholes utilized in this study. A. Fence diagram of architectural units (AUs) bounded by sixth-order surfaces. The location of Black and Silver Creeks is indicated by a dashed line. Refer to Fig. 4.2 for borehole and transect locations. B. ‘Nested’ architectural framework of the Georgetown area including architectural elements (fourth-order surfaces), architectural components (fifth-order surfaces), architectural units (sixth-order surfaces), and the Quaternary basin fill (seventh-order surfaces). Grey shapes on D-D’ represent the location of outsized boulders. Refer to Fig. 4.2 for borehole and transect locations, Figs. 7-10 for AUs delineated in sedimentary logs, and Figs. 4.11 and 4.12 for the detailed internal architecture and interpretation of AUs.

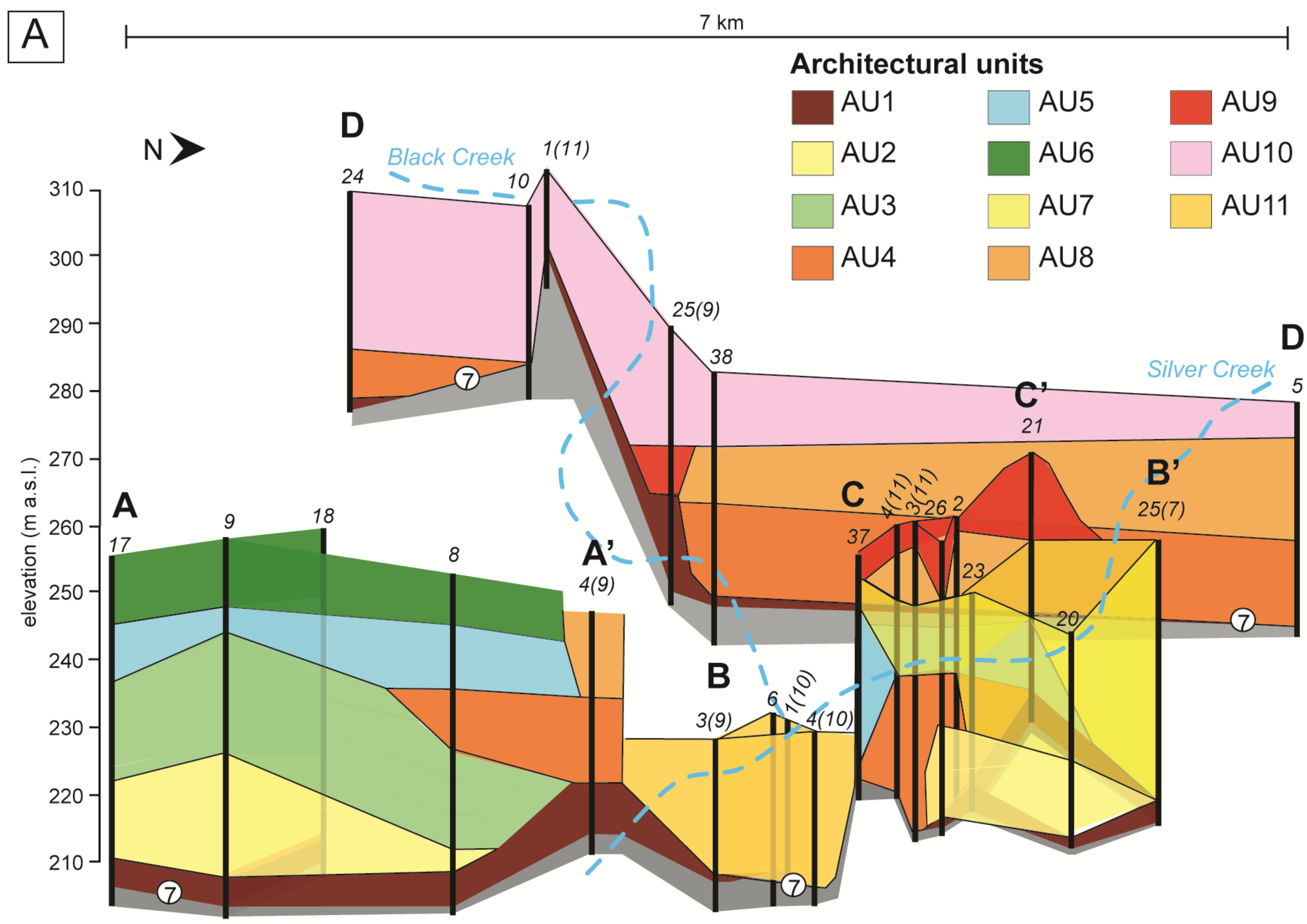
A
7 km
Architectural units
AU1
AU2
AU3
AU4
AU5
AU6
AU7
AU8
AU9
AU10
AU11
N
D
D'
C
C'
B
B'
A
A'
Black Creek
Silver Creek
elevation (m a.s.l.)

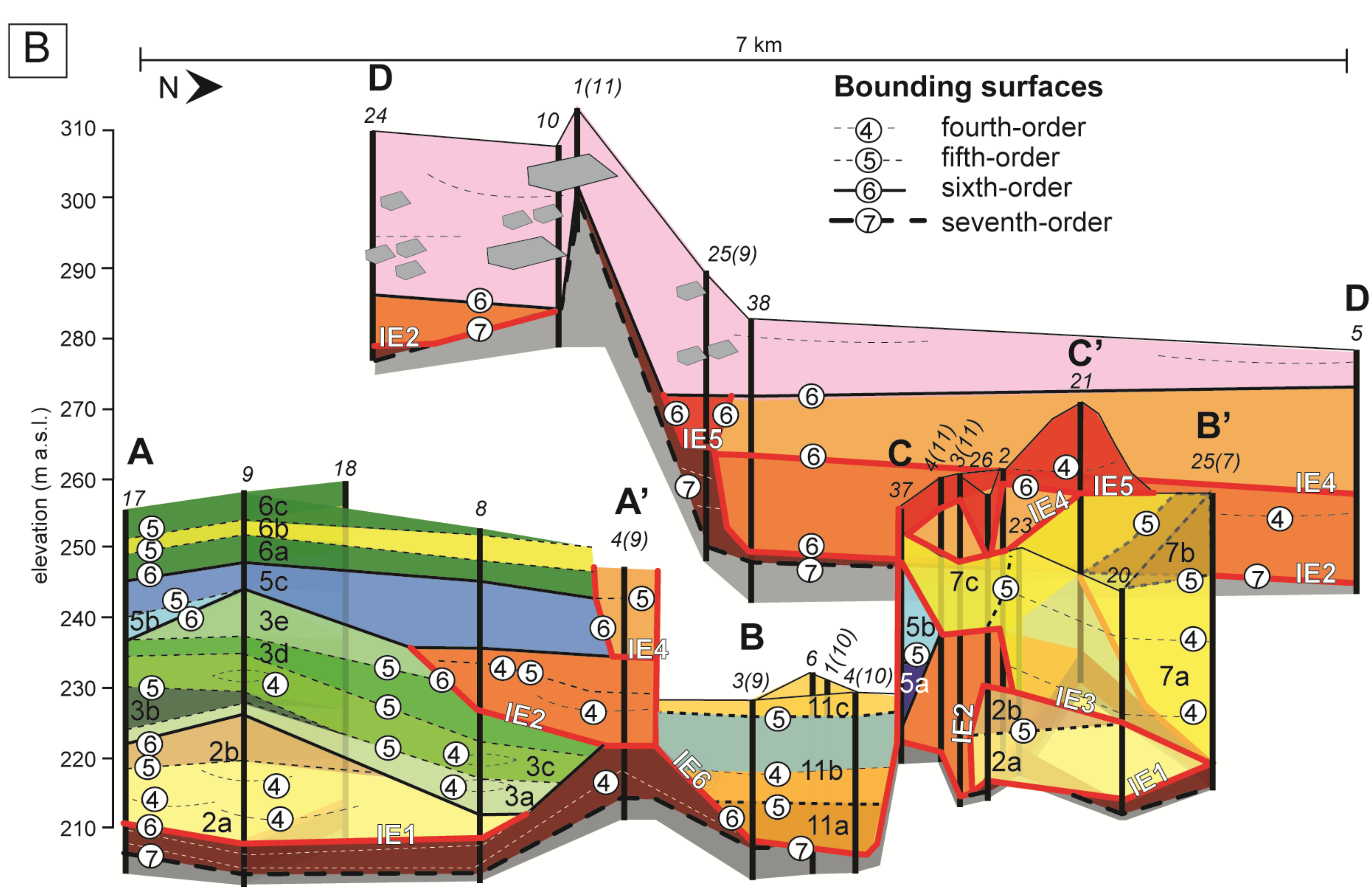
B
7 km
Bounding surfaces
fourth-order
fifth-order
sixth-order
seventh-order
N
D
D'
C
C'
B
B'
A
A'
IE1
IE2
IE3
IE4
IE5
IE6
elevation (m a.s.l.)

(CVC, 2001) probably caused scouring of the fine-grained sediments and deposition of gravels in AU11c (Fig. 4.8).

4.5.2 Hydrostratigraphy

Georgetown contains three municipal well fields located in the Cedarvale valley (B-B'), Princess Anne (C-C'), and Lindsay Court (D-D') sites (Fig. 4.2). Establishing the detailed sedimentology and architecture of subsurface stratigraphic units is fundamental for understanding aquifer and aquitard heterogeneity and connectivity (Howard and Beck, 1986; Gerber et al., 2001; Meriano and Eyles, 2009), and accurate prediction and modeling of small-scale (local) groundwater flow and its connection to the regional groundwater flow system (Anderson, 1989; Anderson et al., 1999; Klingbeil et al., 1999).

The subsurface architecture of the northern part of Georgetown (at the locations of boreholes analysed in this study; Fig. 4.2, 4.7-4.10) is dominated by glaciofluvial and deltaic units (Fig. 4.11), which truncate and completely remove the 'regional' till stratigraphy (AU3 and AU6); however, these till units are preserved in the southern part of the study area (A-A'; Fig. 4.13; Meyer and Eyles, 2007). At least six glaciofluvial incision events (IE1-6) are identified in the Georgetown area, recorded by the lower bounding surfaces of AU2, AU4, AUs7-9, and AU11 (Fig. 4.13B). Understanding the spatial relationship of incision events is important because they truncate fine-grained till and glaciolacustrine units that form confining layers for aquifers and increase the geologic (and possibly hydraulic?) connection between coarse-grained units that otherwise may not be connected (Slomka and Eyles, 2013). The incision events (IEs) identified in the Georgetown area are interpreted to have formed as a result of allogenic processes including those associated with an advancing ice margin and initiation of an outwash plain (IE1) and retreat of the ice margin and lowering of base level (IEs2-6), possibly enhanced by post-glacial isostatic rebound (IEs 5, 6). The lower bounding surface of the Newmarket Till sheet (AU3) may also be considered to record ‘incision’ where it truncates underlying sediments of AU2 (Fig. 4.13).

The area between 8th Line and 15 Side Road (A-A’; Fig. 4.2) is identified as an area of future urban development (Town of Halton Hills, 2013) and contains two subsurface units that host prospective aquifers. The weathered bedrock surface (AU1) hosts an aquifer that is utilized for private wells, and has previously been interpreted to be directly confined by the Halton Till (CVC, 2001); however, the diamict of AU1, as delineated in this study, is overlain by sands and gravels of AU2 and AU4, and it may be susceptible to contamination from surface point sources in areas where the Newmarket and Halton Tills have been removed (e.g. MW4_09). AU2 is regarded as the primary aquifer unit in the MSMC area (Lotimer, 2014, *personal communication*), and is stratigraphically positioned between two fine-grained units of AU1 and AU3 (Figs. 4.11-4.13). AU2 forms a prospective confined aquifer in the MSMC area; however, it is truncated by the overlying till complex of AU3 and is confined to a relatively narrow part of the bedrock valley (Fig. 4.1D). Close to the Niagara Escarpment (between the 5th Line and 6th Line area; Fig. 4.2), this aquifer has a high transmissivity and high potential yield (boreholes of Meyer and Eyles, 2007); however, as the valley extends toward Silver Creek, the sediments become much finer-grained and have a lower transmissivity

(Lotimer, 2014; *personal communication)*. This constrains the yield of the aquifer in this area (A-A') to less than what is normally required for a successful municipal groundwater supply (based on previously conducted pumping tests; Lotimer, 2014; *personal communication*). Sands of AU2 located along the northern margin of the MSMC site (A-A'; Figs. 2, 13) do not appear to be geologically connected to coarse-grained units in the Cedarvale valley; however, geologic and hydraulic connections may be present in areas where the older stratigraphy is incised and removed (by AUs 4, 8, 11; boreholes of Meyer and Eyles, 2007).

Incision events 3-5 (Fig. 4.13), as delineated in this study, appear to form vertical and horizontal geologic connections between shallow and deep coarse-grained units (AUs 2, 4, 7-11) in the Princess Anne (C-C'), Lindsay Court (D-D'), and Cedarvale (B-B') areas. Wells in the Princess Anne area are screened in, and produce water from, gravels of AU4 (Fig. 4.9). Previously conducted pumping tests at MW4_11 (Fig. 4.2) suggest gravels of AU4 form an unconfined aquifer in this area (Lotimer, 2014*; personal communication*). The sands and gravels of AU7 and AU8, and diamicts and gravels of AU9, allow recharge of groundwater to AU4, but the absence of fine-grained units (e.g. till) overlying these units may compromise the integrity and water quality of AU4; however, previous testing of water in AU4 (at MW4_11) determined the water to be potable (Lotimer, 2014; *personal communication*). Although the Princess Anne and Lindsay Court wells appear to be completed in the same aquifer system (AU4), there is no obvious direct hydraulic response when pumping from either well field (Lotimer, 2014; *personal communication*), and previously conducted pumping tests in the

Cedarvale well field do not indicate any hydraulic connectivity between the Cedarvale wells and aquifer and the Princess Anne and Lindsay Court wells and aquifer (Lotimer, 2014; *personal communication*). Elevated bedrock topography in the area of MW21_06 (Figs. 4.1D, 4.2, 4.13), and the lateral spatial relationship of fine-grained sediments of AU5 and AU11b,c (Fig. 4.13B) may form a hydraulic boundary between the three well fields; hence, incision event 6, involving the entrenchment of the gravelly fluvial system (AU11a) and subsequent deposition of fine-grained sediments (AU11b,c), resulted in a sedimentary architecture that hosts a confined prospective aquifer (Cedarvale aquifer; Fig. 4.2). The lateral extent of cemented gravels in AU4 and AU8 may also contribute to a vertical hydraulic barrrier between the aquifers and surface water sources; however, further work is needed to understand the 3-dimensional geometry of AU5, and the genetic origin of the cement, and its spatial extent and significance to groundwater flow in these areas. Furthermore, previous aquifer tests on gravels in AU11a suggest a groundwater source from the Limehouse area (Acton re-entrant), and further investigation of the subsurface sedimentary architecture is required to determine the stratigraphic relationship between gravels of AU10 in the Acton re-entrant (at MW24_09) and AU11a in the Cedarvale valley.

The sedimentary architecture of subsurface units in the Georgetown area, as delineated in this study, provides insight to the 2-dimensional sedimentary heterogeneity and geometry of till units (AU3 and AU6), which are considered to form relatively impermeable units (and form confining layers) in MSMC (A-A'; Figs. 4.7, 4.13). The lower till complex (AU3; Newmarket Till) consists of alternating sheet-like, coarse-

(AU3a,c,e) and fine-grained (AU3b,d) diamict architectural components that contain interbeds of coarse-grained sand and gravel (Fig. 4.7, 4.12). The coarse-grained sand and gravel lenses and sand-rich diamict in AU3c may serve as conductive zones within the AU3 till complex, and may facilitate fluid transport horizontally through the till body and into the underlying sandy aquifer below (AU2; Gerber and Howard, 1996; Gerber et al., 2001; Boyce and Eyles, 2000; Meriano and Eyles, 2009). The upper till complex (AU6; Halton Till) is composed of a tripartite succession of diamict and sand architectural components (Figs. 4.7, 4.12). The lower diamict component (AU6a) is architecturally homogenous (i.e. has an absence of coarse-grained interbeds) and likely forms a confining layer. The upper diamict component (AU6c) contains several sand and gravel interbeds that may facilitate a hydraulic connection from the surface to the underlying sand component (AU6b), and sandy parts of AU5 below (Fig. 4.13; Howard and Beck, 1986; Gerber and Howard, 1996; Gerber et al., 2001). Truncation of the till units (AU3 and AU6) by incision events 2 and 4 (along the northern part of the MSMC site; A-A'; Figs. 4.2, 4.13) may result in horizontal hydraulic connections between the coarser-grained components of the till architecture (AU6c, e) and AU4, and the formation of unconfined conditions in AU4 (MW4_09; A-A'; Fig. 4.13).

4.5.3 Significance of AEA to subsurface mapping

The application of concepts of AEA, including unit and bounding surface hierarchies (Fig. 4.6), for the analysis of subsurface sedimentary architectures from sediments recovered in fully cored boreholes, as presented here, provides insight to the depositional history and hydrostratigraphy of the Georgetown area. Not all levels of unit hierarchies could be delineated in all boreholes (Figs. 4.7- 4.10; 4.13); however, the bounding surface hierarchy allowed the organization of sedimentary heterogeneity in a ‘nested’ architectural framework, which allows communication of the detailed sedimentary complexity (architectural elements and components) delineated in closely spaced boreholes, and maintains the ‘big picture’ framework of larger-scale units (architectural units) on a more regional scale (Fig. 4.13). The nested architectural model, as presented here, may facilitate a ‘magnifying glass’ approach to geologic modeling whereby high-resolution heterogeneity in an area of interest may be represented by small-scale units (architectural elements; fourth-order surfaces) and connected to larger-scale mappable units (architectural components and units) by fifth- and sixth-order surfaces with increasing distance from the study area (the practical applications of the nested architectural model will be explored in future studies). The delineation of architectural components (fifth-order surfaces), as demonstrated here, may facilitate integration of sedimentological data with geophysical, geochemical, thermal, and hydrogeological data (e.g. Klingbeil et al., 1999; Bridge and Tye, 2000; Gerber et al., 2001; Conant et al., 2004; Hansen et al., 2009) and serve as field-derived ‘geometric objects’ which may be assigned quantitative values (e.g. hydraulic conductivity or transmissivity; Anderson, 1989; Klingbeil et al., 1999) and utilized for computer object-based modeling (e.g. Deutsch and Tran, 2002).

The concept of a ‘predesigned’ landscape in southern Ontario appears to apply to the Georgetown area, whereby surface water features, Quaternary outwash channels, and bedrock valleys have similar orientations and locations, and generally follow the orientation of regional tectonic lineaments (Eyles et al. 1993, 1997). The location of buried bedrock valleys does, in part, coincide with the location of modern stream systems and subsurface coarse-grained glaciofluvial and deltaic units delineated in the Georgetown area (discussed above). Hence, the location of modern stream systems may be utilized as a first approximation of the location of coarse-grained outwash units and bedrock valleys that may host aquifers, recharge zones, or migration pathways for groundwater and contaminants (Fig. 4.13). The utilization of geophysical data can significantly enhance the cost-effectiveness of detailed subsurface stratigraphic and architectural investigations, and may provide additional data that cannot be readily obtained from the analysis of core samples such as the identification of 'fuzzy contacts' or to supplement sections of poor core recovery (Boyce and Eyles, 2000; Bridge and Tye, 2000). Further work is needed to better understand the 3-dimensional architecture and internal heterogeneity of till complexes, which serve as regional aquitard units in the Georgetown area, and the hydrogeological and paleoenvironmental significance of glaciofluvial incision events and valley fill stratigraphy.

4.6 CONCLUSIONS

This study demonstrates that architectural element analysis can be effectively applied to the detailed sedimentological and architectural analysis of sediments recovered from fully cored boreholes. AEA of sediments recovered from twenty-four fully cored boreholes in the Georgetown area facilitated the delineation of a hierarchy of subsurface sedimentary units based on detailed analysis of facies types, their vertical succession, and the nature of facies contacts. Eleven architectural units were characterized and delineated, and their internal architecture (components) provided insight to the depositional history of the Georgetown area. The geometry and spatial relationship of coarse-grained units that host prospective aquifers and recharge zones revealed complex spatial relationships, and at least six different glaciofluvial incision events, which truncate and remove older units, were identified; these incision events may form important geologic and hydraulic connections between otherwise confined aquifers. The architectural framework of the Georgetown area, as delineated in this study, also provides insight into the heterogeneity of till sheets, which may have significant implications for aquitard integrity and the distribution of groundwater recharge zones to deeper subsurface units. The method of AEA utilized in this study for the analysis of fully cored boreholes (creating a nested architectural framework) can be applied to the investigation of subsurface glacial sedimentary architectures elsewhere, specifically in areas with limited or an absence of outcrop exposures, and may provide insight to 3-dimensional subsurface geologic and hydrostratigraphic mapping in other previously glaciated areas.

Acknowledgements

This work was supported by an NSERC-PGS scholarship and Geological Society of America student research grant awarded to JS and an NSERC Discovery Grant awarded to CE. The authors thank the Regional Municipality of Halton for providing financial support, and the Region of Halton and SLR Consulting are thanked for providing access to borehole cores. The authors acknowledge field assistance from various former members of the Glacial Sedimentology Lab at McMaster University, and helpful and insightful discussion with Andrew Brennan. Tim Lotimer and Dr. Joseph I. Boyce provided helpful comments and suggestions on a previous version of the manuscript.

REFERENCES

Aitken, J. F. Sedimentology of Late Devensian glaciofluvial outwash in the Don Valley, Grampian Region. Scottish Journal of Geology, **34**(2): 97-117.

Anderson, M.P. 1989. Hydrogeologic facies models to delineate large-scale spatial trends in glacial and glaciofluvial sediments. Geological Society of American Bulletin, **101**, 510-511.

Anderson, M.P., Aiken, J.S., Webb., E.K., and Mickelson, D.M. 1999. Sedimentology and hydrogeology of two braded stream deposits. Sed. Geol., **129**, 187-199.

Ashmore, P. 1991. Channel morphology and bed load pulses in braided, gravel-bed streams. Geografiska Annaler, **73A**(1): 37-52.

Barnett, P.J. 1992. Chapter 21: Quaternary Geology of Ontario. In Geology of Ontario. Ontario Geological Survey, Special Volume 4, pp.1082.

Bhattacharya, J.P. and Walker, R.G. 1992. Deltas. *In* Facies models, response to sea level change. *Edited by* R.G. Walker and N.P. James. Geological Association of Canada., St. Johns, Newfoundland. pp. 157-178.

Bhattacharya, J.P. and Posamentier, H.W. 1994. Sequence stratigraphy and allostratigraphic Applications in the Alberta Foreland basin. In Geological Atlas of the Western Canada Sedimentary basin. (G.D. Mossop and I. Shetsen). Online: http://www.ags.gov.ab.ca/AGS_PUB/ATLAS_WWW/A_CH25/CH_25_F.HTM (accessed 2014-06-10)

Boulton, G.S. (1996). Theory of glacial erosion, transport and deposition as a consequence of subglacial sediment deformation. Journal of Glaciology, **42**, 43-62.

Boyce, J.I., and Eyles, N. 2000. Architectural element analysis applied to glacial deposits: Internal geometry of a late Pleistocene till sheet, Ontario, Canada. Geological Society of America Bulletin, **112**: 98-118.

Blair, T. C. and McPherson, J.G. 1994. Alluvial fans and their natural distinction from rivers based on morphology, hydraulic processes, sedimentary processes, and facies assemblages. Journal of Sedimentary Research, **A64**(3): 450-489.

Blass, F. S. A. and Ariztegui, D. 2003. 60 years of glaciolacustrine sedimentation in Steinsee (Sustenpass, Switzerland) compared with historic events and instrumental meteorological data. Eclogae geol. Helv., **96**(1): 59-71

Blikra, L.H. and Nemec, W. 1998. Postglacial colluvium in western Norway: depositional processes, facies and palaeoclimatic record. Sedimentology, **45**: 909-959.

Bridge, J. S. and Tye, R.S. 2000. Interpreting the dimensions of ancient fluvial channel bars, channels, and channel belts from wireline-logs and cores. American Association of Petroleum Geologists Bulletin, 84(8): 1205-1228.

Brogly, P.J., Martini, I.P. and Middleton, G.V. 1998. The Queenston Formation: shale dominated, mixed terrigenous-carbonate deposits of Upper Ordovician, semiarid, muddy shores in Ontario, Canada. Canadian Journal of Earth Sciences, **35**: 702-719.

Brookfield, M.E. and Martini, I.P. 1999. Facies architecture and sequence stratigraphy in glacially influenced basins: basic problems and water-level/glacier input-point controls (with an example from the Quaternary of Ontario, Canada). Sedimentary Geology, **123**: 183-187.

Bryan, R.B. and Campbell, I.A. 1980. Sediment entrainment and transport during local rainstorms in the Steveville Badlands, Alberta. Catena, **7**: 51-65.

Calvo-Cases, A. and Harvey, A.M. 1996. Morphology and development of selected badlands in southeast Spain: implications of climatic change. Earth Surface Processes and Landforms, **21**: 725-735.

Cant, D. J. 1977. Development of a facies model for sandy braided river sedimentation: comparison of the South Saskatchewan River and the Batter Point Formation. Canadian Society of Petroleum Geologists, Special Publications, Memoir **5**: 627-639.

Cant, D. J. and Walker, R.G. 1978. Fluvial processes and facies sequences in the sandy braided South Saskatchewan River, Canada. Sedimentology, **25**(5): 625-648.

Catuneanu, O., Abreu, V., Bhattacharya, J.P., Blum M.D., Dalrymple, R.W., Eriksson P.G., Fielding, C.R., Fisher, W.L., Galloway, W.E., Gibling, M.R., Giles, K.A., Holbrook, J.M., Jordan, R., Kendall, C.G.St.C., Macurda, B., Martinsen, O.J., Miall, A.D., Neal, J.E., Nummedal, D., Pomar, L., Posamentier, H.W., Pratt, B.R., Sarg, J.F., Shanley, K.W., Steel, R.J., Strasser, A., Tucker, M.E., and Winker, C. 2009. Towards the standardization of sequence stratigraphy. Earth-Science Reviews, **92**: 1-33.

Chapman, L.J. and Putnam, D.F. (1984). The Physiography of Southern Ontario, 3rd Edition; Ontario Geological Survey, Special Volume 2, 270p. Accompanied by Map P.2715 (coloured), scale 1:600 000.

Conant, Jr., B., Cherry, J. A., and Gillham, R.W. 2004. A PCE groundwater plume discharging to a river: influence of the streambed and near-river zone on contaminant distributions. Journal of Contaminant Hydrology, **73**: 249-279.

Credit Valley Conservation 2001. Silver Creek Subwatershed Study, Background Report. Online: http://www.creditvalleyca.ca/watershed-science/our-watershed/subwatershed-studies/subwatershed-11-silver-creek/ (accessed 2014-07-07).

Credit Valley Conservation 2009. Black Creek Subwatershed Study (Subwatershed 10), Background Report. Online: http://www.creditvalleyca.ca/watershed-science/our-watershed/subwatershed-studies/subwatershed-10-black-creek/ (accessed 2014-07-07).

Costello, W. R. and Walker, R. G. 1972. Pleistocene sedimentology, Credit River, southern Ontario: A new component of the braided river model. Journal of Sedimentary Petrology, **42**(2): 389- 400.

Davis, J.M., Lohmann, R.C., Phillips, F.M., Wilson, J.L. and Love, D.W. 1993. Architecture of the Sierra Ladrones Formation, central New Mexico: Depositional controls on the permeability correlation structure. Geological Society of America Bulletin, **105**: 998-1007.

Deutsch, C.V. and Tran, T.T. 2002. FLUVSIM: a program for object-based stochastic modeling of fluvial depositional systems. Computers & Geosciences, **28**: 525-535.

Dredge, L.A. and Tholeifson, L.H. 1987. The Middle Wisconsinan history of the Laurentide Ice Sheet. Géographie physique et Quaternaire, **41**(2): 215-235.

Dreimanis, A. and Gibbard, P. 2005. Stratigraphy and sedimentation of the stratotype sections of the Catfish Creek Drift Formation between Bradtville and Plum Point, north shore, Lake Erie, southwestern Ontario, Canada. Boreas, **34**: 101-122.

Eriksson, P. G., Reczko, B.F.F., Boshoff, A. J. and Schreiber, U.M. 1995. Architectural elements from Lower Proterozoic braid-delta and high-energy tidal flat deposits in the Magaliesberg Formation, Transvaal Supergroup, South Africa. Sedimentary Geology, **97**: 99-117.

Evans, D.J.A. 2005. Glacial landsystems. *Edited by* D.J.A. Evans. Arnold: London, 544 pp.

Evans, D.J.A., Phillips, E.R., Hiemstra, J.F. and Auton, C.A. 2006. Subglacial till: Formation, sedimentary characteristics and classification. Earth-Science Reviews, **78**: 115-176.

Eyles, N. 1979. Facies of supraglacial sedimentation on Icelandic and Alpine temperate glaciers. Canadian Journal of Earth Sciences, **16**: 1341-1361.

Eyles, C.H. and Eyles N. 1983. Sedimentation in a large lake: A reinterpretation of the late Pleistocene stratigraphy of Scarborough Bluffs, Ontario, Canada. Geology, **11**: 146-152

Eyles, N., Eyles C.H., and Miall, A.D. 1983. Lithofacies types and vertical profile models; an alternative approach to the description and environmental interpretation of glacial diamict and diamictite sequences. Sedimentology, **30**: 393- 410

Eyles, N. and Clark, B.M. 1988. Storm-influenced deltas and ice scouring in a late Pleistocene glacial lake. Geological Society of America Bulletin, **100**: 793-809.

Eyles, N. and Eyles C.H. 1992. Glacial depositional systems. *In* Facies models, response to sea level change. *Edited by* R.G. Walker and N.P. James. Geological Association of Canada, St. Johns, Newfoundland. pp. 73-100.

Eyles, N., Boyce, J. and Mohajer, A.A. 1993. The bedrock surface of the western Lake Ontario region: Evidence of reactivated basement structures? Géographie physique et Quaternaire, **47**(3): 269-283.

Eyles, N., Arnaud, E., Scheidegger, A. E. and Eyles, C. H. 1997. Bedrock jointing and geomorphology in southwestern Ontario, Canada: an example of tectonic predesign. Geomorphology, **19**:17-34.

Eynon, G. and Walker, R.G. 1974. Facies relationships in Pleistocene outwash gravels, southern Ontario: a model for bar growth in braided rivers. Sedimentology, **21**: 43-70.

Gao, C., Shirota, J., Kelly, R. I., Brunton, F.R., and van Haaften, S. 2006. Bedrock topography and overburden thickness mapping, southern Ontario; Ontario Geological Survey, Miscellaneous Release--Data 207. ISBN 1-4249-2550-9. Available online: http://www.mndmf.gov.on.ca/mines/ogs_earth_e.asp (accessed 2014-04-07).

Gao, C. 2011. Buried bedrock valleys and glacial and subglacial meltwater erosion in southern Ontario, Canada. Canadian Journal of Earth Sciences, **48**: 801-818.

Geological Survey 2010. Surficial geology of Southern Ontario; Ontario Geological Survey, Miscellaneous Release Data 128-REV. ISBN 978-1-4435-2482-7 [MRD128-REV]. Available online: http://www.mndmf.gov.on.ca/mines/ogs_earth_e.asp (accessed 2014 04-07)

Gerber, R.E. and Howard, K.W.F. 1996. Evidence for recent groundwater flow through Late Wisconsin till near Toronto, Ontario. Canadian Geotechnical Journal, **33**: 538-555.

Gerber, R.E., Boyce, J.I. and Howard, K.W.F. 2001. Evaluation of heterogeneity and field-scale groundwater flow regime in a leaky till aquitard. Hydrogeology Journal, **9**: 60-78.

Ghazi, S. and Mountney, N.P. 2009. Facies and architectural element analysis of a meandering fluvial succession: The Permian Warchha Sandstone, Salt Range, Pakistan. Sedimentary Geology, **221**: 99-126.

Government of Ontario, 2005. Places to Grow Act. *ServiceOntario eLaws.* Online: http://www.elaws.gov.on.ca/html/statutes/english/elaws_statutes_05p13_e.htm (accessed 2014-07-07).

Government of Ontario, 2006. Clean Water Act. *ServiceOntario eLaws.* Online: http://www.elaws.gov.on.ca/html/statutes/english/elaws_statutes_06c22_e.htm (accessed 2014-07-07).

Gustavson, T.C. and Boothroyd, J.C. 1987. A depositional model for outwash, sediment sources, and hydrologic characteristics, Malaspina Glacier, Alaska: A modern analog of the southeastern margin of the Laurentide Ice Sheet. Geological Society of America Bulletin, **99**: 187-200.

Germanoski, D. and Schumm, S.A. 1993. Changes in braided river morphology resulting from aggradation and degradation. The Journal of Geology, **101**(4): 451-466.

Halton Region, 2013. Annual Drinking Water Quality Report, Georgetown Drinking Water System. Online: http://www.halton.ca/cms/one.aspx?pageId=14097 (accessed 2014-07-07).

Hansen, L. Beylicj, A. Burki, V., Eilertsen, R.S., Fredin, O., Larsen, E., Lyså, A., Nesje, A., Stalsberg, K. 2009. Stratigraphic architecture and infill history of a deglaciated bedrock valley based on georadar, seismic profiling and drilling. Sedimentology, **56**: 1751-1773.

Heinz, J., Kleineidam, S., Teutsch, G. and Aigner, T. 2003. Heterogeneity patterns of Quaternary glaciofluvial gravel bodies (SW-Germany): application to hydrogeology. Sedimentary Geology, **158**: 1-23.

Hjellbakk, A. 1997. Facies and fluvial architecture of a high-energy braided river: the Upper Preterozoic Seglodden Member, Varanger Peninsula, northern Norway. Sedimentary Geolology, **114**: 131- 161.

Howard, K.W.F. and Beck, P. 1986. Hydrochemical interpretation of groundwater flow systems in Quaternary sediments of southern Ontario. Canadian Journal of Earth Sciences, **23**: 938-947.

Johnson, M. D., Armstrong, D.K., Sanford, B.V., Telford, P.G., and Rutka, M.A. Chapter 20: Paleozoic and Mesozoic Geology of Ontario. In Geology of Ontario. Ontario Geological Survey, Special Volume 4, pp.907.

Karrow, P.F. 1974. Till stratigraphy in parts of southwestern Ontario. Geological Society of America Bulletin, **85**: 761-768.

Karrow, P.F. 2005. Quaternary Geology Brampton Area. Ontario Geological Survey, Report 257.

Karrow, P.F., McAndrews, J.H., Miller, B.B., Morgan, A.V., Seymour, K.L. and White, O.L. 2001. Illinoian to Late Wisconsin stratigraphy at Woodbridge, Ontario. Canadian Journal of Earth Sciences, **38**: 921-942.

Kasanin-Grubin, M. 2013. Clay mineralogy as a crucial factor in badland hillslope processes. Catena, **106**: 54-67.

Kjær, K.H. and Krüger, J. 2001. The final phase of dead-ice moraine development: processes and sediment architecture, Kötlujökul, Iceland. Sedimentology, **48**: 935-952.

Klingbeil, R., Kleineidam, S., Asprion, U., Aigner, T. and Teutsch, G. 1999. Relation lithofacies to hydrofacies: outcrop-based hydrogeological characterisation of Quaternary gravel deposits. Sedimentary Geology, **129**(3-4): 299-310.

Krüger, J. and Kjær, K.H. 2000. De-icing progression of ice-cored moraines in a humid, subpolar climate, Kötlujökull, Iceland. The Holocene, **10**(6): 737-747.

Logan, C., Russell, H.A.J., and Sharpe, D.R. 2001. Regional three-dimensional stratigraphic modelling of the Oak Ridges Moraine area, southern Ontario; Geological Survey of Canada, Current Research 2001-D1, 19 p.

Maizels, J. 1979. Proglacial aggradation and changes in braided channel patterns during a period of glacier advance: an alpine example. Geografiska Annaler. Series A, Physical Geography, **61**(1/2): 87-101

Maizels, J. 1993. Lithofacies variations within sandur deposits: the role of runoff regime, flow dynamics and sediment supply characteristics. Sedimentary Geology, **85**: 299-325.

Maizels, J. 1997. Jökulhlaup deposits in proglacial areas. Quaternary Science Reviews, **16**: 793-819.

Marren, P.M. 2005. Magnitude and frequency in proglacial rivers: a geomorphological and sedimentological perspective. Earth-Science Reviews, **70**: 203-251.

Marren, P.M., Russell, A.J., and Rushmer, E.L. 2009. Sedimentology of a sandur formed by multiple jökulhlaups, Kverkfjöll, Iceland. Sedimentary Geology, **213**: 77-88.

Martin, C.A.L. and Turner, B.R. 1998. Origins of massive-type sandstones in braided river systems. Earth-Science Reviews, **44**: 15-38.

Matthews, J.A., Dahl, S.O., Nesje, A., Berrisford, M.S., and Andersson, C. 2000. Holocene glacier variations in central Jotunheimen, southern Norway based on distal glaciolacustrine sediment cores. Quaternary Science Reviews, **19**: 1625-1647.

McPherson, J.G., Shanmugam, G., and Moiola, R.J. 1987. Fan-deltas and braid deltas: varieties of coarse-grained deltas. Geological Society of America, **99**: 331-340.

Meriano, M. and Eyles, N. 2009. Quantitative assessment of the hydraulic role of subglaciofluvial interbeds in promoting deposition of deformation till (Northern Till, Ontario). Quaternary Science Reviews, **28**: 608-620.

Meyer, P.A. and Eyles, C. H. 2007. Nature and origin of sediments infilling poorly defined buried bedrock valleys adjacent to the Niagara Escarpment, southern Ontario, Canadian Journal of Earth Sciences, **44**: 89- 105.

Miall, A.D. 1977. A review of the braided-river depositional environment. Earth-Science Reviews, **13**: 1-62

Miall, A.D. 1985. Architectural-element analysis: A new method of facies analysis applied to fluvial deposits. Earth-Science Reviews, **22**: 261-308

Miall, A.D. 1988. Architectural elements and bounding surfaces in fluvial deposits: anatomy of the Kayenta Formation (Lower Jurassic), southwest Colorado. Sedimentary Geology, **55**: 233-262.

Miall, A.D. 1992. Alluvial models. *In* Facies models, response to sea level change. *Edited by* R.G. Walker and N.P. James. Geological Association of Canada, St. Johns, Newfoundland. pp. 119-142.

Miall, A.D. 1994. Reconstructing fluvial macroform architecture from two-dimensional outcrops: exmaples from the Castlegate Sandstone, Book Cliffs, Utah. Journal of Sedimentary Research, **B64**(2): 146-158.

Miall, A.D. 2010. Alluvial Deposits. In Facies Models 4. Edited by Noel P. James and Robert W. Dalrymple. Geological Association of Canada, St. John's, Newfoundland, pp. 105-137

Miall, A.D. 2014. Fluvial depositional systems. Springer International Publishing, Switzerland, 316 p.

Mott, R.J. and Matthews, J.V. 1990. The last interglaciation in Canada. Géographie physique et Quaternaire, vol. **44**(3): 245-248.

Mottershead, D.N. 1971. Coastal head deposits between Start Point and Hope Cove, Devon. Field Studies, **3**: 433-453.

Mountney, N., Howell, J., Flint, S. and Jerram, D. 1999. Relating eolian bounding-surface geometries to the bed forms that generated them: Etjo Formation, Cretaceous, Namibia. Geology, **27**:159-162

NACSN 2005. North American Stratigraphic Code. AAPG Bulletin, **89**(11), 1547 1591.Ontario

Nadal-Romero, E., Regüés, D., Martí-Bono, C., and Serrano-Muela, P. 2007. Badland dynamics in the Central Pyrenees: temporal and spatial patters of weathering processes. Earth Surface Processes and Landforms, **32**: 888-904.

Nemec, W. and Kazanci, N. 1999. Quaternary colluvium in west-central Anatolia: sedimentary facies and palaeoclimatic significance. Sedimentology, **46**: 139-170.

Olariu, C. and Bhattacharya, J. 2006. Terminal distributary channels and delta front architecture of river-dominated delta systems. Journal of Sedimentary Research, **76**: 212-233.

Paterson, J. T. and Cheel, R.J. 1997. The depositional history of the Bloomington Complex, an ice-contact deposit in the Oak Ridges Moraine, southern Ontario, Canada. Quaternary Science Reviews, **16**: 705-719.

Regional Municipality of Halton, 2011. Sustainable Halton Water & Wastewater Master Plan. Online: http://www.halton.ca/planning_sustainability/environmental_assessments__eas_/a_stud es/sustainable_halton_water_wastewater_master_plan/ (accessed 2014-07 07).

Reesink, A.J.H. and Bridge, J.S. 2007. Influence of superimposed bedforms and flow unsteadiness on formation of cross strata in dunes and unit bars. Sedimentary Geology, **202**: 281-296.

Russell, H.A.J., Arnott, R.W.C. and Sharpe, D.R. 2003. Evidence for rapid sedimentation in a tunnel channel, Oak Ridges Moraine, southern Ontario, Canada. Sedimentary Geology, **10**, 33-55.

Russell, H.A.J., Arnott, R.W.C. and Sharpe, D.R. 2004. Stratigraphic architecture and sediment facies of the Western Oak Ridges Moraine, Humber River Watershed, southern Ontario. Géographie physique et Quaternaire, **58**(2-3), 241-267.

Russell, H.A.J., Hinton, M.J., van der Kamp, G., and Sharpe, D.R. 2004. An overview of the architecture, sedimentology and hydrogeology of buried-valley aquifers in Canada. *In* Proceedings of the 57th Canadian Geotechnical Conference and the 5th joint CGS-IAH Conference; 2004; pages 2B (26-33) (GSC Cont.# 2004085)

SEPM 2014. Allostratigraphy. Online: http://www.sepmstrata.org/Terminology.aspx?id=allostratigraphy (accessed 2014-07-07).

Sharpe, D.R., Dyke, L.D., Hinton, M.J., Pullan, S.E., Russell, H.A.J., Brennand, T.A., Barnett, P.J., and Pugin, A. 1996. Groundwater prospects in the Oak Ridges Moraine area, southern Ontario: application of regional geological models. *In* Current Research 1996-E; Geological Survey of Canada, p. 181-190.

Sharpe, D.R. Hinton, M.J., Russell, H.A.J., and Desbarats, A.J. 2002. The need for basin analysis in regional hydrogeological studies: Oak Ridges Moraine, southern Ontario. Geoscience Canada, **29**(1): 3-20

Sharpe, D.R., Pugin, A., Pullan, S.E. and Gorrell, G. 2003. Application of seismic stratigraphy and sedimentology to regional hydrogeological investigations: an example from Oak Ridges Moraine, southern Ontario, Canada. Canadian Journal of Earth Sciences, **40**: 711-730.

Sharpe, D., Pugin, A., Pullan, S. and Shaw, J. 2004. Regional unconformities and the sedimentary architecture of the Oak Ridges Moraine area, southern Ontario. Canadian Journal of Earth Sciences, **41**: 183-198.

Skelly, R.L., Bristow, C.S., and Ethridge, F.G. 2003. Architecture of channel-belt deposits in an aggrading shallow braided river: the lower Niobrara River, northeast Nebraska. Sedimentary Geology, **158**: 249-270.

Slomka, J.M. and Eyles, C.H. (2013). Characterizing heterogeneity in a glaciofluvial deposit using architectural elements, Limehouse, Ontario, Canada. Canadian Journal of Earth Sciences, **50**: 911-929.

Straw, A. 1968. Late Pleistocne glacial erosion along the Niagara Escarpment of southern Ontario. Geological Society of America Bulletin, **79**: 889-910.

Terasmae, J. 1980. Some problems of late Wisconsin history and geochronology in southeastern Ontario. Canadian Journal of Earth Sciences, **17**: 361-381.

Town of Halton Hills 2013. The Vision Georgetown Project. Online: http://www.haltonhills.ca/visiongeorgetown/index.php (accessed 2014-07-07).

Vail, P.R., Mitchum, R.M., Jr., and Thompson, S., III 1977. Seismic stratigraphy and global changes of seal level, Part 3: relative changes of sea level from coastal onlap. In M26: Seismic Stratigraphy- Applications to Hydrocarbon Exploration, American Association of Petroleum Geologists Special Volumes, **A165**: 63-81.

Walker, R.G. 1992. Facies, facies models and modern stratigraphic concepts. *In* Facies models, response to sea level change. *Edited by* R.G. Walker and N.P. James. Geological Association of Canada, St. Johns, Newfoundland. pp. 1-14.

Willman, H.B. and Frye, J.C. 1970. Pleistocene Stratigraphy of Illinois. Illinois State Geolological Survey Bulletin, **94**, pp. 204

Yuvaraj, S.V. 2011. Use of architectural-element analysis to interpret the depositional environment and reservoir characteristics of the Pictures Cliffs Sandstone, northern San Juan Basin, Colorado. M.Sc. Thesis. Bowling Green State University, U.S.A.

CHAPTER 5: CONCLUSIONS AND RECOMMENDATIONS FOR FUTURE WORK

5.1 SUMMARY AND CONCLUSIONS

The main objective of this research is to understand the sedimentary complexity of glacial deposits and explore how the underlying concepts of architectural element analysis (AEA) can be utilized to deconstruct glacial deposits into their basic geometric building blocks, which compose the sedimentary architecture. This will significantly enhance understanding of the spatial and temporal relationships between component parts of the glacial depositional system and will facilitate paleoenvironmental reconstructions of ancient glacial successions. In previously glaciated regions, such as southern Ontario and Illinois, there is an increasing demand to understand the nature and geometry of subsurface Quaternary successions as the population of communities dependent on groundwater for potable water supplies grow and plan for future development (Kempton et al. 1982; Gerber and Howard, 1996; Howard et al. 2003; Sharpe et al. 2003; Herzog et al., 2003). In other areas underlain by glacial deposits, such as Alberta, understanding the subsurface heterogeneity of glacial successions for irrigation and land-use planning is critical (Hendry, 1982; França and Potter, 1991; Government of Alberta, 2014), and the potential for glacial deposits to host significant hydrocarbon reservoirs is gaining interest, specifically in areas of possible hydrocarbon-groundwater interactions (Bachu, 1997; Andriashek and Atkinson, 2007; Ahmad et al., 2009; Huuse et al., 2012). These ongoing and growing areas of concern demonstrate that understanding of the sedimentological heterogeneity and 3-dimensional geometry of subsurface glacial successions is imperative.

The sedimentary complexity inherent in glacial successions makes delineation of the geometry of sedimentary packages difficult; this is compounded by the lack of an objective methodology to systematically characterize and organize the heterogeneity of glacial deposits at different scales of resolution. Architectural element analysis facilitates delineation of sedimentary geometry based on detailed analysis of facies types and contacts, the grouping of facies associations, and understanding autogenic and allogenic controls on their deposition; however, AEA has scarcely, and only recently, been utilized for the analysis of glaciogenic deposits (Boyce and Eyles, 2000; Marren et al., 2009; Slomka and Eyles, 2013).

This thesis research explores the validity of AEA for the characterization of glacial sedimentary architectures and addresses and provides insight to the aforementioned concerns by: 1) investigating the applicability of AEA to the characterization of the internal heterogeneity of a thick till complex (aquitard), which was conducted through detailed analysis of facies and facies contacts in sediments exposed in outcrop (Chapter 2); 2) testing the validity and full potential of AEA for the characterization of the sedimentary architecture of a modern glacial landscape (Chapter 3), and 3) exploring the utility of fundamental principles of AEA (bounding surface and unit hierarchies) for deconstructing a glacial succession into architectural units, which involved detailed analysis of sediments recovered in fully-cored boreholes (Chapter 4).

This thesis clearly demonstrates the applicability and effectiveness of AEA as a powerful tool for the analysis of glacial sedimentary architectures delineated in outcrop, at modern glacial landscapes, and from sediments recovered in boreholes. Tills are commonly considered to have two contrasting types of internal organization, and are either relatively homogenous or highly heterogeneous, and the processes involved in their formation are not well understood. This is largely because of a lack of sedimentological evidence available to substantiate theoretical models of till formation and the inaccessibility of subglacial depositional environments for direct observation and documentation of subglacial processes at modern ice margins. However, detailed analysis of a thick till succession exposed in outcrop utilizing AEA (Chapter 2), provides insight to the organization of till heterogeneity at different scales (from small-scale facies to larger mappable units; Fig. 5.1). This research identifies five different 'building blocks' that make up the small-scale till architecture; these are grouped to form larger-scale architectural units that can be mapped across the local study area. The till architecture suggests a negative feedback response of allogenic controls, including: meltwater accumulation on a low permeability bed, ice-bed decoupling, draining of meltwater and deposition of sands in subglacial conduits, and ice-bed recoupling (Chapter 2).

The complexity of modern glacial landscapes is commonly characterized and classified using landsystem analysis; however, this form of analysis does not provide a tool for systematic organization and arrangement of different parts of the landsystem, and translation of this information to subsurface sediments. This research demonstrates the robustness of the integration of AEA with landsystem analysis for the delineation of the sedimentary architecture of a modern glacial landscape at Sólheimajökull in Iceland (Chapter 3). Surface features are delineated by fourth-order surfaces, and packaging of genetically-related surface features allow characterization landsystem components, which make up the large-scale architecture of a landsystem tract (depositional environment; Fig. 5.1). This research utilized landsystem components from different landsystem tracts (and the spatial arrangement of fifth-order bounding surfaces) to identify eight allostratigraphic units. These allostratigraphic units provided insight to the depositional history and evolution of the Sólheimajökull landsystem. The sedimentary architecture delineated at Sólheimajökull (Chapter 3) facilitated the construction of three architectural models which represent the sedimentary architecture in ice-marginal, proglacial, and ice-distal locations in the landsystem which may be utilized for subsurface investigations of sedimentary architectures in other glaciated terrains.

The fundamental principles on which AEA is based are also found to be highly effective for delineating the subsurface sedimentary architecture of deeply buried Quaternary sediments recovered in boreholes (Chapter 4). The principles of bounding surface and unit hierarchies of AEA were applied to the analysis of glacial sediments recovered from fully-cored boreholes in the Georgetown area, Ontario, which is dependent on groundwater as a potable water source. Sixth-order surfaces delineate large-scale mappable units (architectural units; Fig. 5.1) which record different depositional environments. The internal heterogeneity of architectural units is characterized by grouping genetically-related facies associations (architectural elements) bounded by major discontinuities (fifth-order surfaces), which make up architectural components (Fig. 5.1). This research demonstrates the significance of understanding the detailed architecture of subsurface glacial deposits for paleoenvironmental reconstruction and understanding of the depositional history of the Georgetown area. AEA is a particularly useful tool as it facilitates the identification of the geometry and interconnectivity of coarse-grained units (aquifer and recharge zones) and fine-grained units (aquitards; Chapters 2-4). It is essential to understand the complex spatial relationship and geometry of these coarse- and fine-grained units, specifically in areas such as Georgetown (Ontario; Chapter 4), where confining (aquitard) layers are discontinuous and coarse-grained glaciofluvial units incise and truncate (and in places completely remove) older stratigraphic units including regionally extensive till sheets (Chapters 3, 4). Glaciofluvial incision is a common erosional process at modern ice margins (Chapter 3), and the location, lateral extent, and geometry of incision events are important to understand because they may create hydraulic connections between units that would otherwise be disconnected (Chapter 4). AEA, as utilized in this research, facilitates the construction of an architectural framework which may be utilized to refine hydrostratigraphic models and provide insight to hydrogeological responses of aquifers hosted in coarse-grained glacial deposits (Chapter 4).

Overall, this research (Chapters 2-4) demonstrates that fifth-order bounding surfaces are key constituents of the sedimentary architecture of depositional systems as the spatial arrangement of these surfaces delineates sediment packages at a scale that effectively characterizes the sedimentary architecture and detailed heterogeneity (Chapters 2-4), facilitates paleoenvironmental reconstruction and understanding of depositional histories (Chapters 2-4), and provides insight to the geological controls on the hydrogeological behaviour of aquifers (Chapter 4). The spatial arrangement of fifth-order bounding surfaces, and the spatial relationship of sediments they contain, may help in the definition of time-equivalent units (allostratigraphy) in glacial successions (Chapter 3); this is important for understanding the depositional history of a glaciated basin and may facilitate predictive mapping of the subsurface glacial architecture in areas with limited borehole data and a paucity of outcrop (Chapter 4). This research also demonstrates that sixth-order surfaces can cross-cut lithostratigraphic unit boundaries (Chapter 4). This is significant for the delineation of different glaciofluvial units (commonly ‘lumped’ as single lithostratigraphic units), which incise and cross cut each other and older stratigraphies (including till sheets), resulting in complex subsurface spatial relationships and geometries (Chapters 3, 4). Of utmost importance, this research highlights the significance of AEA’s inherently ‘built-in’ tool for genetic interpretation (derived from previous work of Allen, 1968 and others, and facies models; Chapter 1), which allows understanding of autogenic and allogenic controls on the deposition of glacial deposits and evolution of the sedimentary architecture, and provides a robust methodology for paleoenvironmental reconstruction, which may be utilized for analysis of sediments exposied in outrop, core, and at modern ice margins, and applied to sediments deposited in different depositional environments (Chapters 2-4).

Fig. 5.1 Hierarchies of bounding surfaces and units as delineated in this research through analysis of glacial sediments at a modern glacial landscape (Chapter 3), exposed in outcrop (Chapter 2), and recovered in fully-cored boreholes (Chapter 4).

	Modern glacial landscape		Outcrop		Fully-cored boreholes	
Field site	*Solheimajokull, southern Iceland*		*Tiskilwa till, Rattlesnake Hollow Illinois, U.S.A.*		*Geogetown, Ontario Canada*	
Hierarchies	***bounding surfaces***	***units***	***bounding surfaces***	***units***	***bounding surfaces***	***units***
	—	—	1	till layer or laminae (<1 cm thick)	—	—
	—	—	2	sand and gravel stringer	—	—
	—	—	3	depositional slice of till (bed-scale)	—	—
	4	surface feature	4	architectural element	4	architectural element
	5	landsystem component	5	element association	5	architectural component
	6	landsystem tract	6	till complex	6	architectural unit
	7	landsystem	—	—	7	Late Quaternary basin fill

5.2 FUTURE WORK

The research contained within this thesis presents a ‘glimmer’ of the potential of AEA for characterizing the sedimentary architecture within glacial deposits. This is an exciting area of research that requires additional exploration, particularly at modern ice margins which provide a ‘living laboratory’ for real-time observation of depositional processes, ice margin fluctuations, and landscape evolution. It is important to study and record the detailed sedimentology, landforms, and depositional and erosional processes at modern ice margins, specifically those which are experiencing rapid retreat, in order to document their evolution and preserve a record of these events for future studies. The Sólheimajökull architectural model, presented in this research, would benefit from continued research at this site (specifically to document the geomorphic impact of rapid ice margin retreat) and data collection should extend beyond the geographic limits utilized in this study in order capture a more complete record of the landsystem architecture. Documentation of these processes and deposits in a digital geospatial format (accompanied by hand drawn field sketches and notes) is most effective and easily translatable for other research purposes. With the increasing development of robust geographic information systems (GIS) and 3-dimensional computer modeling software, accessibility of GIS software in the form of handheld mobile systems, and the need for quantitative and spatial field-based data (for applications such as land use planning and groundwater investigations), comes the need for digital data collection, database management, and a platform to facilitate geospatial data exchange between researchers (e.g. National Snow & Ice Data Centre, and the Nordic Data Grid Facility). The costs associated with travel required for fieldwork at modern ice margins and licenses for robust computer software are quite high; however, the development of free geospatial applications such as Google Earth © allows important field reconnaissance to be conducted prior to travel. Investigations based on remote-sensing of historical and recent imagery of modern ice margins, and high-resolution terrain data (e.g. LiDAR), have great future potential for delineating sedimentary architectures, and will provide interesting and cost-effective research avenues in the area of 'glacial architectural element analysis'.

Modern ice margins provide modern analogues which can be utilized to understand glacial depositional and erosional processes and the environmental controls involved in the formation of sedimentary architectures that characterize deeply buried Quaternary glacial successions. However, subglacial depositional environments are difficult to access at modern ice margins and hence the formation of tills is still poorly understood. Characterizing the heterogeneity of till sheets from sediments exposed in outcrop is imperative for understanding their depositional history, and there is great need for more detailed sedimentological data to support theoretical models of till formation. With increasing population growth in areas that are dependent on groundwater for a source of potable water, such as many communities in southern Ontario, the methodology of 'glacial architectural element analysis' will be crucial. Integration of other data types, such as geophysical and hydrogeological data, will undoubtedly help to refine and improve the accuracy of sedimentary architectural models and provide insight to the significance of different aspects of architectural elements for hydrogeological purposes. In the Georgetown area, it would be beneficial to continue this subsurface architectural work by integrating geophysical data from wireline logs and surface geophysical surveys (specifically in areas where fully-cored boreholes are absent), with detailed analysis of sediments recovered from new fully cored boreholes. Additionally, this work would benefit from the integration of landform analysis to refine the near-surface elements of the architectural model.

A detailed study of the local-scale hydrogeology of the Georgetown area (e.g. geochemical tracer tests, a field plan for a series of pumping tests, thermal data from surface water) would likely provide insight into the local-scale connectivity and geometry of coarse-grained and fine-grained units. Architectural components (fifth-order surfaces) and architectural units (sixth-order surfaces; Fig. 5.1) are ‘geometric objects’ that may facilitate the translation of geologic data (presented here) to a format that is useful for hydrogeological applications and computer object-based modeling (see Klingbeil et al., 1999; Deutsch and Tran, 2002) by assigning quantitative values to objects (e.g. hydraulic conductivity; Anderson, 1989), constrained by the surface hierarchy. The nested architectural framework, as presented in this thesis, preserves the detailed sedimentary complexity (architectural elements, or surface features; Fig. 5.1) within the large-scale geologic framework (Chapter 4). This nested framework facilitates a ‘magnifying glass’ approach, whereby investigation of local-scale heterogeneity may be represented by high-resolution units (architectural elements) and connected to larger-scale mappable units (architectural units or element associations; Fig. 5.1) by higher-order bounding surfaces (fifth- to seventh-order) with increasing distance from the area of interest. This is an exciting area of future research that will undoubtedly require collaboration of workers in different fields of expertise.

The methodology of AEA for the analysis of glacial sedimentary architectures, as developed and utilized in this thesis, and results obtained in this research can be applied as a framework to understand the heterogeneity and architecture of glacial successions in similar study areas in southern Ontario and Illinois, and previously glaciated regions and modern glacial landscapes elsewhere. AEA, as demonstrated here, may provide insight to the hydrostratigraphy and spatial relationship of aquifers and aquitards, facilitate the translation of field-based geologic data to a format useful for hydrogeologic investigations (e.g. object- and surface-based models, and translation to quantitative data), and enhance the accuracy of regional three-dimensional geologic and hydrogeologic models.

REFERENCES

Ahmad, J., Schmitt, D.R., Rokosh, C.D., and Pawlowicz, J.G. (2009). High-resolution seismicand resistivity profiling of a buried Quaternary subglacial valley: Northern Alberta, Canada. Geological Society of America Bulletin, 121(11-12): 1570-1583.

Allen, J.R.L. (1968). The nature and origin of bedform hierarchies. Sedimentology, 10: 161-182.

Andriashek. L. D. and Atkinson, N. (2007). Buried channels and glacial-drift aquifers in the Fort McMurray Region, Northeast Alberta. Alberta Energy and Utilities Board, AlbertaGeological Survey, Earth Sciences Report 2007-01.

Boyce, J.I. and Eyles, N. (2000). Architectural element analysis applied to glacial deposits: Internal geometry of a late Pleistocene till sheet, Ontario, Canada. Geological Society of America Bulletin, 112: 98-118.

Bachu, S. (1997). Flow of formation waters, aquifer characteristics, and their relation to hydrocarbon accumulations, Northern Alberta Basin, AAPG Bulletin, 81(5): 712 733.

França, A. B. and Potter, P. E. (1991) Stratigraphy and reservoir potential of glacial deposits of the Iararé Group (Carboniferous-Permian), Paraná Basin, Brazil. AAPG Bulletin, 75(1): 62-85.

Gerber, R.E. and Howard, K.W.F. (1996). Evidence for recent groundwater flow through Late Wisconsinan till near Toronto, Ontario. Canadian Geotechnical Journal, 33: 538-555.

Government of Alberta (2014). The Alberta Land Use Framework. Online: https://landuse.alberta.ca/Pages/default.aspx (accessed 2014-07-14).

Hendry, J. M. (1982). Hydraulic conductivity of a glacial till in Alberta. Ground Water, 20 (2): 162-169.

Herzog, B.L., Larson, D.R., Abert, C.C., Wilson, S.D., and Roadcap, G.S. (2003). Hydrostratigraphic modeling of a complex, glacial-drift aquifer system for importation into MODFLOW. Ground Water, 41(1): 57-65.

Howard, K.W.F., Eyles, N., Smart, P.J., Boyce, J.I., Gerber, R.E., Salvatori, S.L., and Doughty, M. (1996). The Oak Ridges Moraine of southern Ontario: a ground water resource at risk. Geoscience Canada, 22(3): 101-120.

Huuse, M., Le Heron, D. P., Dixon, R., Redfern, J., Moscariello, A., and Craig, J. (2012). Glaciogenic reservoirs and hydrocarbon systems: an introduction. Geological Society of London, Special Publications, 368: 1-28.

Kempton, J. P., Morse, W.J., and Visocky, A.P. (1982). Hydrogeologic evaluation of sand and gravel aquifers for municipal groundwater supplies in east-central Illinois. Illinois Department of Energy and Natural Resources- Champaign, IL. State Geological Survey Division and State Water Survey Division, Cooperative Groundwater Report 8, 59 p.

Marren, P. M., Russell, A. J., and Ruschmer, E.L. (2009). Sedimentology of a sandur formed by multiple jökulhlaups, Kverkfjöll, Iceland. Sedimentary Geology, 213: 77-88.

Sharpe, D.R., Pugin, A., Pullan, S.E., and Gorrell, G. (2003). Application of seismic stratigraphy and sedimentology to regional hydrogeological investigations: an example from Oak Ridges Moraine, southern Ontario, Canada. Canadian Geotechnical Journal, 40: 711-730.

Slomka, J.M. and Eyles, C.H. (2013). Characterizing heterogeneity in a glaciofluvial deposit using architectural elements, Limehouse, Ontario, Canada. Canadian Journal of Earth Sciences, 50: 911-929.

APPENDIX

Fig. A1. Annotated field photographs of sediments and landsystem tracts, annotated with bounding surfaces, recorded at Sólheimajökull, Iceland.

A. Chute channel on the fan terrace component (jökulhlaup landsystem tract) between transects 7 and 8. The photo is taken approximately 200 m north of transect 8.

B. Fifth-order bounding surface separating the fan terrace component and trunk channel of the channelized boulder terrace component (jökulhlaup landsystem tract) between transects 7 and 8. The location of the photo in ‘A’ is indicated in the top right corner. The photo is taken approximately 150 m north of transect 8.

C. Fourth-order bounding surface separating the boulder field and chutes and trunk channel of the channelized boulder terrace component (jökulhlaup landsystem tract) at transect 8. The location of the photo in ‘B’ is indicated in the centre-right of the photo. The photo is taken at the location of transect 8.

D. A sixth-order bounding surface separates the till plain component (ice contact landsystem tract), jökulhlaup landsystem tract (boulder field of the channelized boulder terrace component), and glaciofluvial landsystem tract (terraced channel fill component). The photo is taken approximately 100 m south of the location of transect 8.

E. Circular depression and linear ridges in the boulder field of the channelized boulder field component.

F. Fifth-order bounding surfaces separate individual terraced channel fill components (glaciofluvial landsystem tract). The location of the photos in ‘D’ and ‘H’ are indicated in the left and centre of the photo, respectively. The photo is taken at the location of transect 8.

G. A sixth-order surface separates the ice contact and glaciofluvial landsystem tracts. Fourth-order surfaces delineate bars and channels. The location of the sedimentary log ‘I’ is labeled by ‘L1’ in the top-left corner of the photo. The photo is taken at the location of transects 4 and 5.

H. A sixth-order bounding surface separates the ice contact landsystem tract (till plain component) from the glaciofluvial landsystem tract. Fourth-order surfaces separate channels and bars in the Jökulsá valley. A terraced channel fill component (fifth-order surface; glaciofluvial landsystem tract) and the jökulhlaup landsystem tract (sixth-order surface) can be seen in the distance. The location of the sedimentary log in ‘J’ is labeled by ‘L2’ in the left-centre of the photo. The photo is taken approximately 250 m south of transect 9.

I. Photo of three diamict beds (i, ii) exposed in an outcrop section incised into a drumlin of the till plain component along a terrace wall of the glaciofluvial landsystem tract. A sedimentary log (L1) is superimposed on the photo. Refer to ‘G’ and Fig. 3.3 for the location of L1.

J. Photo of sediments exposed in an outcrop section incised into a moraine of the till plain component along a terrace wall of the Jökulsá valley. A sedimentary log (L2) , the 2-dimensional geometry of diamicts and coarse-grained interbeds (ice contact landsystem tract) and gravels (glaciofluvial landsystem tract), and bounding surfaces are annotated on the photo. Refer to ‘H’ and Fig. 3.3for the location of L2.

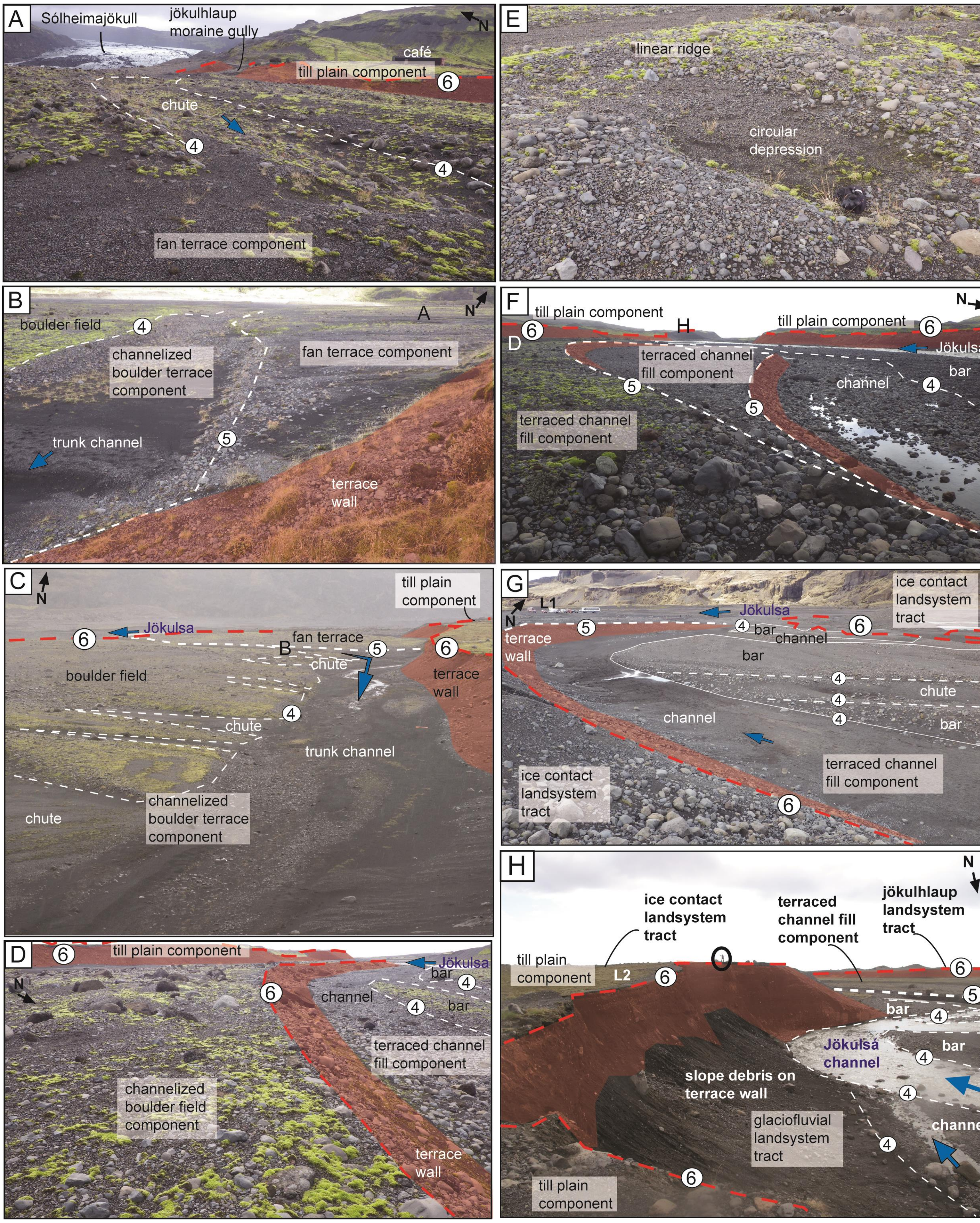
A
Sólheimajökull
jökulhlaup moraine gully
N
café
till plain component
6
chute
4
4
fan terrace component
E
linear ridge
circular depression
B
boulder field
4
A
N
channelized boulder terrace component
fan terrace component
trunk channel
5
terrace wall
F
till plain component
H
till plain component
N
6
6
D
Jökulsa
terraced channel fill component
bar
channel
4
5
5
terraced channel fill component
C
N
till plain component
6
Jökulsa
fan terrace
B
5
6
chute
boulder field
terrace wall
4
chute
trunk channel
chute
channelized boulder terrace component
G
ice contact landsystem tract
N
L1
Jökulsa
5
4
bar
channel
6
terrace wall
bar
4
4
chute
4
bar
channel
terraced channel fill component
ice contact landsystem tract
6
D
6
till plain component
N
Jökulsa
bar
4
6
channel
4
bar
terraced channel fill component
channelized boulder field component
terrace wall
H
N
ice contact landsystem tract
terraced channel fill component
jökulhlaup landsystem tract
till plain component
L2
6
6
5
bar
4
Jökulsá channel
bar
4
slope debris on terrace wall
4
channel
glaciofluvial landsystem tract
4
6
till plain component

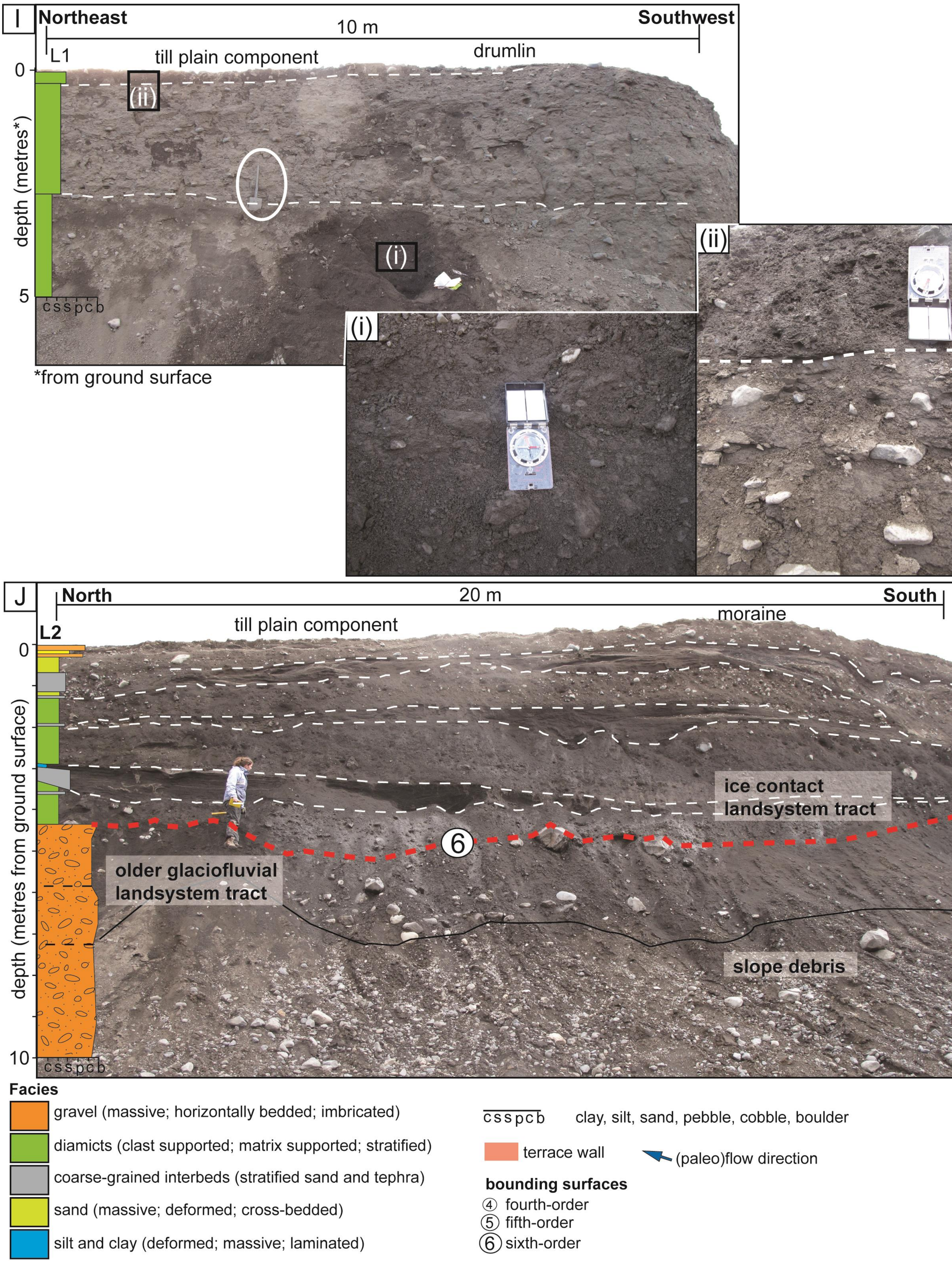
I
Northeast
Southwest
10 m
L1
till plain component
drumlin
(ii)
(i)
0
5
depth (metres*)
c s s p c b
*from ground surface
(i)
(ii)
J
North
South
20 m
moraine
till plain component
L2
0
10
depth (metres from ground surface)
ice contact landsystem tract
6
older glaciofluvial landsystem tract
slope debris
c s s p c b
Facies
gravel (massive; horizontally bedded; imbricated)
diamicts (clast supported; matrix supported; stratified)
coarse-grained interbeds (stratified sand and tephra)
sand (massive; deformed; cross-bedded)
silt and clay (deformed; massive; laminated)
c s s p c b
clay, silt, sand, pebble, cobble, boulder
terrace wall
(paleo)flow direction
bounding surfaces
4 fourth-order
5 fifth-order
6 sixth-order